ON-LINE MEASUREMENT AND CONTROL OF PARISON DIMENSIONS IN EXTRUSION BLOW MOLDING

by

(c) Robert DiRaddo

A Thesis Submitted to the Faculty of Graduate Studies and Research in Partial Fulfillment of the Requirements for the Degree of Doctor of Philosophy

Department of Chemical Engineering
McGill University
Montreal, Canada

March 1989

ISBN 0-315-57197-7

On-line measurement and control of Parison dimensions in blow molding

ABSTRACT

Extrusion blow molding is utilized in the production of plastic hollow containers. The predominant stage in the process sequence is the formation of the preform, known as the parison. Parison extrusions through an annular die are subject to varying degrees of swell and sag along the length. Different parts also require varying amounts of polymer depending on part design. This demands variations in the wall thickness along the length of the parison.

Control of the thickness profile is necessary to minimize resin usage while maintaining the required product characteristics. Presently, parison thickness distribution is controlled by open loop parison programmers. These programmers require cumbersome trial and error procedures to ascertain the necessary die gap set point profile. Unexpected disturbances entering the system are not compensated for.

This work concerns the design and development of an on-line computerized parison thickness profile measurement technique for the purpose of implementing closed loop control of the parison thickness profile. A video camera is used in the measurement.

The thickness measurement was evaluated by comparing it to data from the conventional pinch-off mold technique. The control strategy employed is a simple on-line adaptive control scheme. Programmed set point profiles, such as constant, linear and oscillatory are controlled to within a 5 % error. Disturbances of the system are compensated by the adaptive controller.

RESUME

Le moulage par soufflage est un procédé utilise pour l'élaboration de containers en plastique creux. L'étape prédominante du cycle de fabrication est l'extrusion d'une tube, appellée " paraison ". L'extrusion de cette paraison au travers d'une filière annulaire fait apparaître des variations de gonflement et d'étirement le long de l'extrudat. De même, suivant leurs formes, certaines parties de pièces moulées exigent une quantité de polymère plus ou moins importante. Cela impose des variations d'épaisseur sur toute la longeur de la tube.

Le contrôle de l'épaisseur du profil est nécessaire si l'on veut minimiser les depenses en résine tout en respectant les caractéristiques du produit conçu. Actuellement, les épaisseurs de paraison sont contrôlées par des programmes en boucle ouverte qui nécessitent des essais encombrants et des procédures de tatonnement permettant de s'assurer le profil exacte d'ouverture de filière exigé, les perturbations exterieurs qui entrent dans le systéme n'étant pas compensées.

Ce travail présente la conception et le developpement d'une technique de mesure du profil d'épaisseur d'une paraison en cours d'extrusion, devant déboucher sur la réalisation de son contrôle en boucle fermée.

La mesure d'épaisseur est effectuée par comparaison avec des mesures obtenues par la technique conventionnelle de moule " pinch-off ". La stratégie de contrôle employée est celle d'un schéma de contrôle adaptif en ligne simple. Les variables

préprogrammées, telles les constantes linéaires et oscillatoires, sont contrôlées avec moins de 5 % d'erreur. Les perturbations du système sont compensées par un contrôle adaptif.

ACKNOWLEDGEMENTS

I would like to thank my supervisors, Professor and Chairman M.R. Kamal and Professor W.I. Patterson for their advice and guidance throughout the course of this work. I also express my gratitude to the remainder of the staff of the Department of Chemical Engineering at McGill University, specifically the Machine and Electronic Workshops.

I am grateful to Novacor Chemicals of Calgary, Alberta and Union Carbide of Canada, Pointe aux Trembles, for the use of their equipment in conducting the experimental portion of this work. I would also like to thank Don Parks for his supervisory contribution to the project as well as the staff of the Novacor Technical Centre for various specific contributions.

Financial support from Xerox Canada, McGill University, Novacor Chemicals, The Natural Sciences and Engineering Research Council of Canada and Le Ministere de l'Education du Gouvernement du Quebec is also acknowledged. I would also like to express my gratitude to my fellow colleagues for their aid in this work, with specific mention being given to M. Samara and D. Abu Fara.

Finally, I would like to thank my family for their support and encouragement.

TABLE OF CONTENTS

LIST OF FIGURES

LIST OF TABLES

CHAPTER 1

INTRODUCTION

Extrusion blow molding is the process of choice for the production of hollow containers such as bottles and drums. Container manufacturing by blow molding has lower energy and labour costs than competing processes. The trend of utilizing blow molding is further demonstrated by the rapid growth and diversification of the plastics container industry in recent years (1,2). Contemporary developments are leading to the use of extrusion blow molding for the production of automobile parts (3) because of increased resin savings and greater part assembly versatility.

Extrusion blow molding entails the extrusion of a polymer melt through an annular die to produce a hollow cylindrical preform called a " parison ". The parison dimensions are highly dependent on the swell and sag characteristics of the resin and the process. The parison is subsequently inflated to take the shape of an enclosing mold and the final part is cooled (4).

The control of thickness distribution in the final product is important for obtaining bottles that have the required physical characteristics while maintaining the minimum acceptable overall weight. The physical characteristics include strength, resistance to cracking and the ability to withstand inflation

during the bottle formation. Excessive bottle weight results in material loss and an increase in cooling time. The increase in cooling time results in an increase in cycle time and consequently decreased production.

Control of parison length is important so as to minimize flash, which is the excessive molten polymer pinched by the mold, yet ensuring proper bottle formation. Parison diameter profile control is important as it contributes to the thickness profile.

The product dimensions are ultimately dependent on the parison dimensions. Therefore, control of the final product dimensions is contingent upon control of the parison dimensions and particularly parison thickness distribution, as the length and diameter profiles are highly dependent on the thickness profile. General Electric (5) is currently working on commercially available software for predicting final part thicknesses from parison thicknesses. Models for axial expansion are probably utilized in this estimation (6).

Thickness profiles are important, as different locations along the product length require different amounts of polymer. The handle and body of a bottle would require more material than the neck and bottom of the same bottle. This profile variation of material along the parison length is usually determined by a process known as parison programming. Parison programming employs a preset varying die gap profile during the extrusion, to obtain the desired parison thickness profile (1).

Current practice involves open loop parison programming for

controlling the parison profile thicknesses. However, closed loop feedback control would be preferable because dimension variations, in the form of process noise, enter the system through unexpected disturbances, such as material property changes, temperature drift, resin feed impurities and uneven flow in the hydraulic system.

Multivariable, closed loop control, based on on-line measurement of the parison profile dimensions, and employing the die gap profile as the manipulated variable would be most desirable. The widest range of control and the fastest response of the parison thickness profile, are obtained by using the die gap profile as the manipulated variable. Another possible manipulated variable of interest is the ram velocity profile during extrusion.

Closed loop control requires the employment of a dimension measurement technique that supplies the necessary feedback signal to the controller. A review and critique of the dimension measurement alternatives studied is given in Appendix 2. The alternative chosen for this study is an image processsing apparatus that yields parison length and diameter profiles. The technique involves an estimation procedure for obtaining parison thickness profiles.

1.1 OBJECTIVES

The objectives of the present work are outlined below.

1. To design, construct and operate an image processing apparatus for non-contact measurement of the evolution of parison length versus time and diameter profile versus time and to employ these measurements in order to estimate parison thickness profiles as a function of time.
2. To obtain deterministic and stochastic models of the parison thickness profile by employing the die gap profile as the manipulated variable and to use these results of dynamic studies to develop a suitable strategy and model for closed loop control of parison thickness profiles.
3. To construct a closed loop feedback system for controlling parison thickness profiles by manipulating the die gap profile during the extrusion.
4. To implement the above control system and to test its response to selected programmed set point profiles and to selected imposed disturbances.

CHAPTER 2

TECHNICAL BACKGROUND

This chapter will review relevant technical information regarding three different topics. Initially, the blow molding process and its constituent stages will be described. This will be followed by a study of extrudate die swell and sag behaviour. Finally, some general techniques for extrudate dimension measurement and control will be discussed.

2.1. EXTRUSION BLOW MOLDING

2.1.1 PROCESS DESCRIPTION

Extrusion blow molding processes are based on either continuous or intermittent modes of extruder operation (1).

The continuous process employs a screw pump that conveys and melts the feed resin. This operation is generally used for high volume and small part production. Continuous extrusion utilizes multiple die heads, molds and/or clamping units. The continuous process is also employed for heat sensitive resins, such as PVC, as it is necessary to limit residence time within the barrel in order to avoid resin degradation.

Intermittent operation is generally used for quality control tests and large parts, where part removal must be done manually.

The general process is depicted in Figure 2.1. The accumulator or screw retracts to allow the required amount of resin into the barrel. The screw then acts as a ram, and forces the melt out through an annular die to form the parison. The machine employed in this study operates on the intermittent principle.

The extrusion blow molding process consists of four stages.

1. Plastication
2. Parison Formation
3. Clamping and Inflation
4. Cooling

Typical times required for the various stages are given in Table 2.1. Plastication, inflation, exhaust and cooling are conducted simultaneously. The total cycle time is approximately thirty seconds.

A comprehensive study of the constant extrusion gap blow molding process was performed by Kalyon (6). A general review of the process and its assorted stages was reported by Ryan (2).

2.1.1.1 PROCESS VARIATIONS There are several variations on extrusion blow molding, depending on the specific product or process requirements. The injection blow molding process is generally utilized for high volume small size products, where precision neck finish is critical (2). This process gives exact control of thickness distribution along the parison. However, higher capital costs are generally involved with injection blow molding.

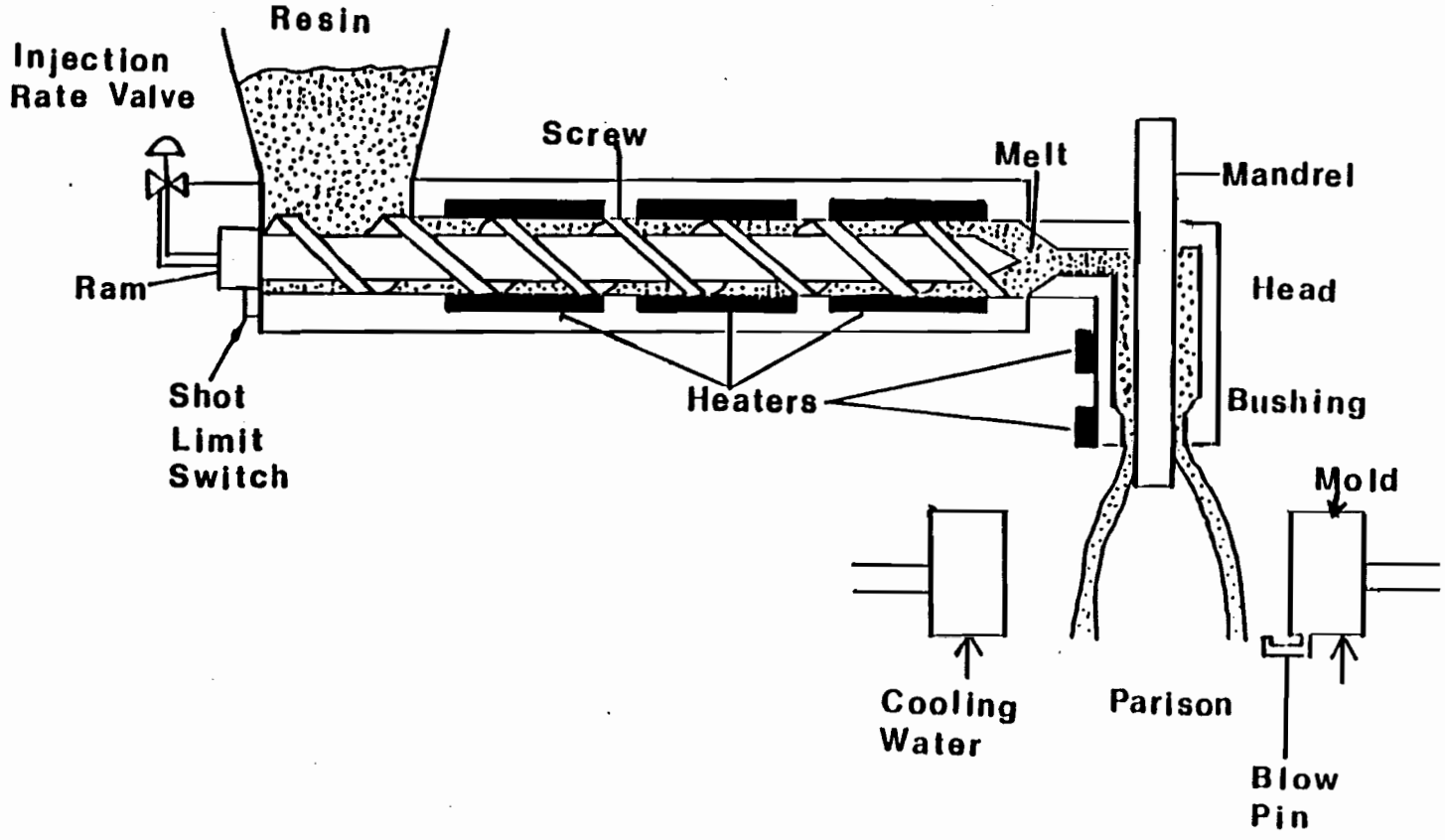

Figure 2.1: General Extrusion Blow Holding Process

TABLE 2.1

TYPICAL EXTRUSION BLOW MOLDING TIMING SEQUENCE

PROCESS	TIME (SEC)
PARISON FORMATION	1.5
CLAMPING	1.0
PARISON INFLATION	2.0
BLOW PRESSURE APPLICATION	10
EXHAUST	3.0
PLASTICATION	5.0
COOLING	20

Molten resin is injected around a blowing mandrel by employing an injection molding machine. The mandrel and parison are subsequently rotated and positioned in the blowing section of the process, where they are placed inside a mold with the desired cavity shape. Inflation, cooling and ejection follow.

The stretch-blow molding process is generally utilized for products that require superior barrier and impact properties. The parison is mechanically stretched in the axial direction by a rod, to increase the degree of axial orientation. This process is generally used for manufacturing polyethylene terephthalate (PET) softdrink bottles (2,6).

Coextrusion is used for the production of multilayer containers. Elaborate die designs are required for the multilayer parison extrusion. An instance of a multilayer extrusion could be an inner layer for barrier protection, the middle layer as an adhesive and a low cost outer layer with good mechanical strength (2,6).

Peters and Rothman (7) discuss the blow-molding of irregular shaped parts with multiple parting lines. These parts have a reverse fold or inward wall projection. The molding of these parts is accomplished by locating a moveable mold section, midway between the mold halves. The parison flows around this part during inflation, thus producing the inward fold.

2.1.1.2 BLOW MOLDING RESINS Blow molding is most commonly used with polyolefins (1,2,6). High density polyethylene (HDPE) is the most frequently used resin in extrusion blow molding because of its high melt strength, combination of physical properties and relatively low cost. Polyethylene terephthalate (PET) is utilized in the production of softdrink bottles because of its high resistance to gas permeation. Other materials are employed depending on the specific application. Polypropylene, for example, is employed for hot fill applications while polyamide and polyvinyl chloride for chemical resistance and low density polyethylene for low cost products (1,2,6). Coextrusion of several layers of different materials allows for flexiblity in achieving various property requirements.

2.1.2 PLASTICATION

The screw or ram retracts during plastication to accumulate an amount of resin, specified by the shot size, in the barrel. The retraction and rotation of the screw, in conjunction with the heaters placed on the barrel, mix and melt the resin pellets, to obtain a homogeneous melt (Figure 2.2).

The solids conveying zone encompasses the feed hopper and the barrel portion where only solid pellets remain. Solid and molten resin coexist in the melting zone of the barrel, while only molten resin should be found in the metering zone (1,2,6).

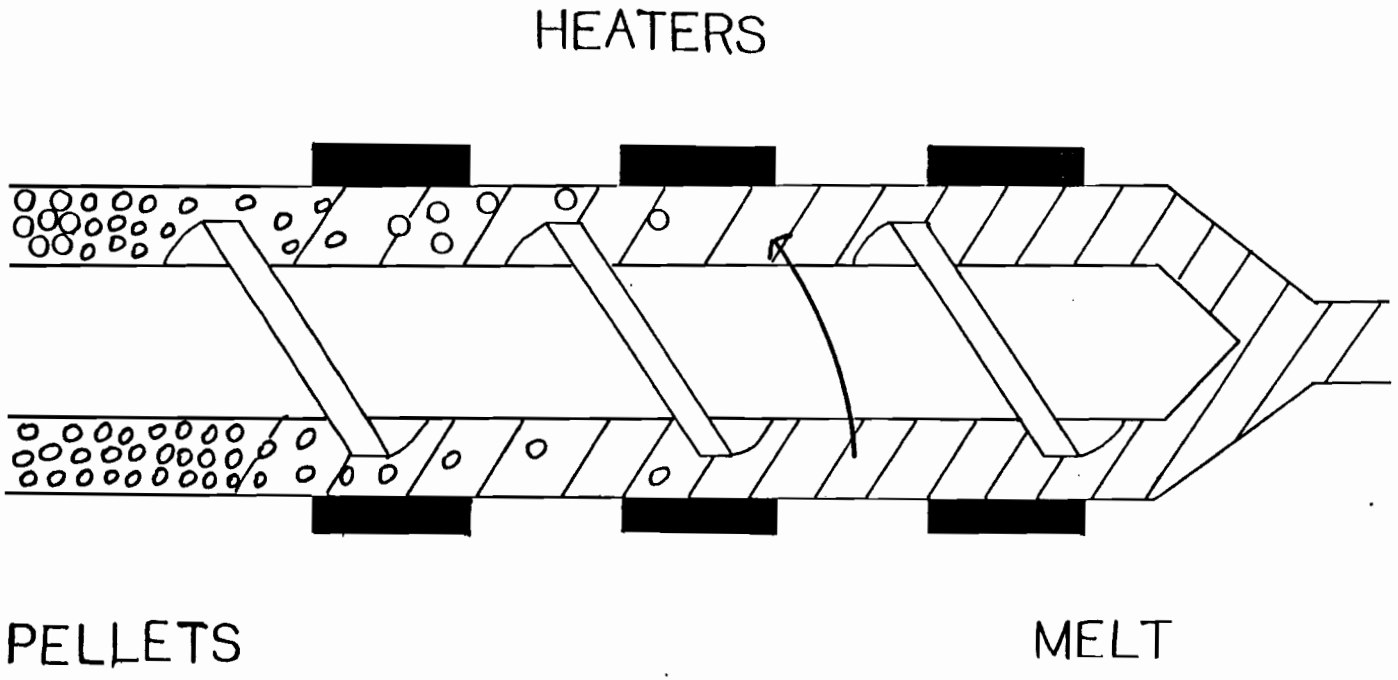

Figure 2.2: Plastication Stage

2.1.3 PARISON FORMATION

The molten polymer is forced vertically through an annular die by the application of hydraulic pressure to the ram (Figure 2.3). The velocity of the extrusion is controlled by the appropriate injection valve. Extrusion through the die results in the formation of a hollow cylindrical tube of sufficient length and wall thickness to allow for its capture and pinch-off by the mold. The parison diameter and thickness are significantly greater than at the die exit, as a result of extrudate swell, and tend to vary along the length of the parison. The die head assembly consists of a stationary outer bushing and a vertically moveable inner mandrel. The die gap is determined by the distance between the mandrel and the bushing. The molten polymer is extruded through the die gap. The parison thickness is dependent on the die gap and, to a lesser degree, the other machine variables (1,2,6).

2.1.4 CLAMPING AND INFLATION

The parison is captured by two moveable mold halves mounted to a clamp assembly (Figure 2.4). The assembly consists of platens and an actuating hydraulic cylinder mechanism. A pin directs pressurized air into the parison, so as to inflate it to take the shape of the mold. The melt is consequently forced to deform and make contact with the mold.

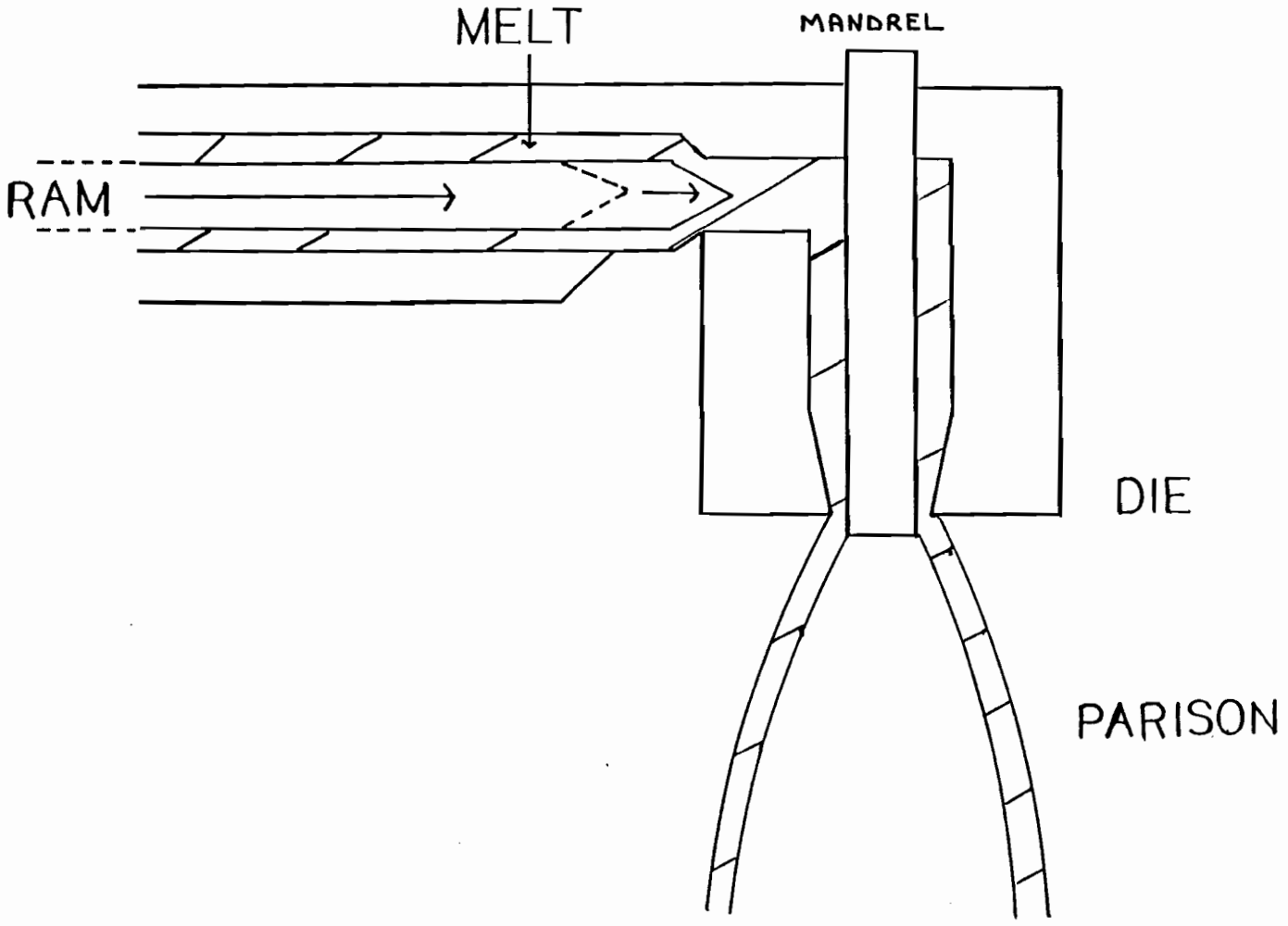

Figure 2.3: Annular Die Extrusion Stage

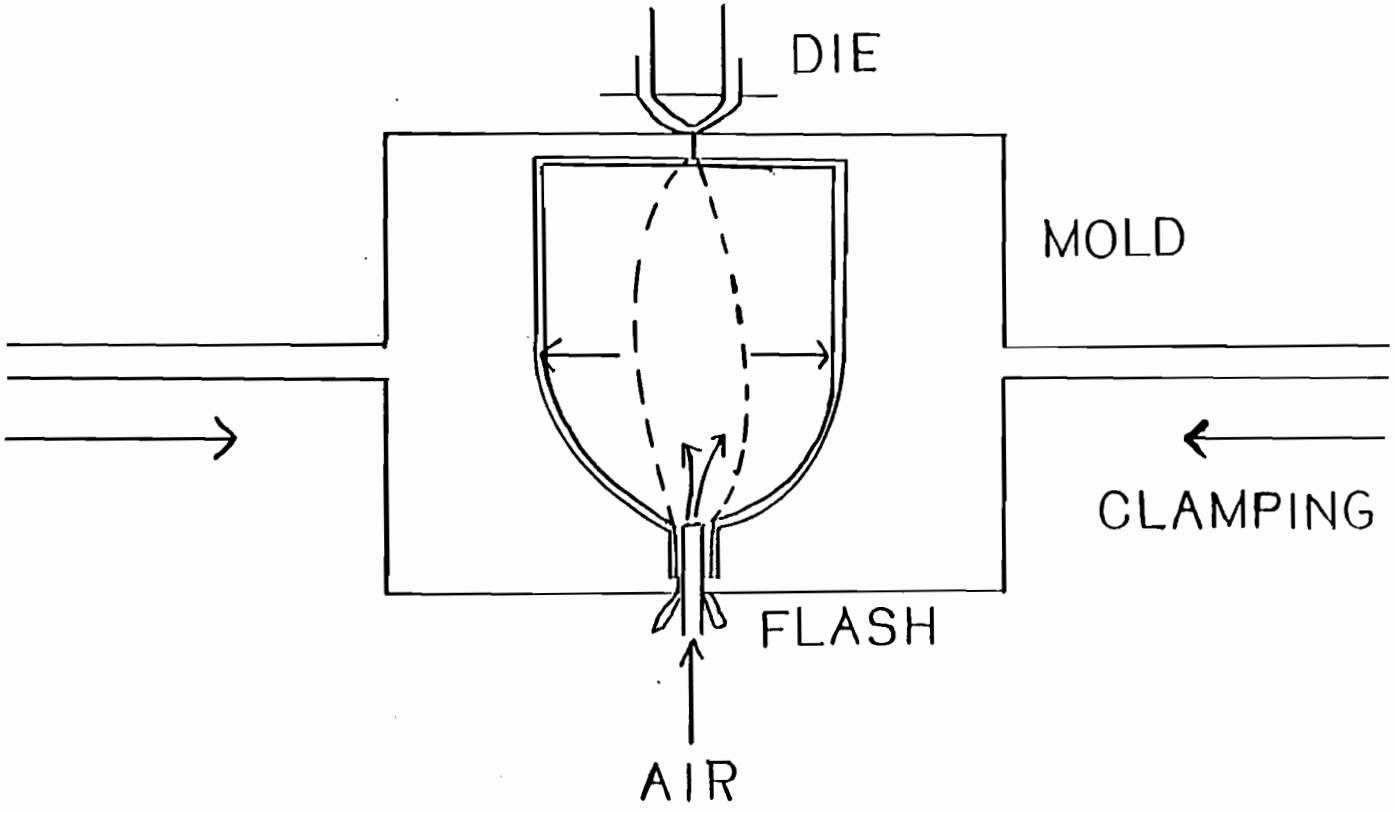

Figure 2.4: Clamping and Inflation Stage

The air pressure is maintained to ensure proper bottle formation. The air is then exhausted.

The pin can be located on the mold such that the air pressure is applied from underneath the parison, or it can puncture the parison as a needle from the side. Other fluids aside from air, such as carbon dioxide and nitrogen, have been used for inflation. These fluids decrease the cooling time considerably but increase operating costs (1,2,6).

Preblow, employing a stream of air projected up into the parison while extruding, can be utilized to provide support for the parison, increase melt strength and consequently limit sagging and necking (8).

2.1.5 COOLING

The part is cooled and solidified in the final chosen shape (Figure 2.5). The longest segment of the cycle time is the cooling stage. Polymers are poor heat conductors; therefore, they cool down slowly. Reducing the cooling time increases productivity. Therefore, high heat transfer rates between the mold and the polymer are desirable. This can be realized by using metal molds with high thermal conductivity, increasing the cooling rate in the mold and increasing the air pressure to achieve good part-mold contact. Usually, the molds are cooled with a refrigeration system. The design of the cooling channels in the mold should be optimized in order to obtain the most

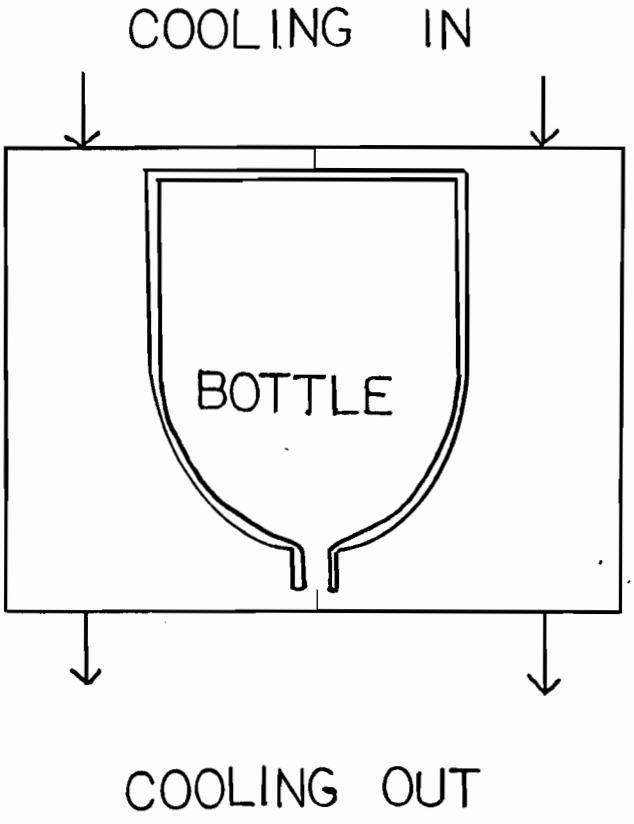

Figure 2.5: Cooling Stage

efficient cooling (1,2,6).

Once the part is sufficiently rigid, the mold opens and a knockout system frees the finished product from the machine. The cycle is then repeated.

2.1.6 FINISHING STEPS

Part ejection can either be forward or downward between the mold halves. A stripping plate, moved by pneumatics, is generally used for part removal. The container is hit such that the chances of damage are small. Small parts can be removed by air jets. Very large parts are generally removed manually.

Once ejected, the containers fall onto a conveyor belt that moves them to a finishing station. The parts are then trimmed for flash removal. The trimming can be done manually or automatically.

Since polyethylene is non-polar, the surface of the container must be activated before decorating. Direct flame or heat from a chemical source oxidizes the surface and makes it receptive to bonding by inks and adhesives (2).

Smoluk (9) and Strojinc (10) have reviewed recent advances in blow molding automation. Automation systems for part removal, leak detection, trimming, adhesive labelling and bottle conveying have been developed. Robotic arms are utilized for moving the part from station to station. Unblown parisons are detected and removed from the conveying line.

2.1.7 PARISON PROGRAMMING

Control of parison dimensions is important to control the weight and thickness distribution of the finished product. Extrusion blow molding machines are generally equipped with parison programmers. Currently, commercial parison programmers employ open loop thickness profile control as well as closed loop metal temperature and pressure controls at selected barrel and die head locations.

Parison programming is currently based on open loop control; i.e., no corrective feedback signal is employed. Finding an acceptable set point profile requires expensive and time consuming trial and error procedures to obtain the desired parison material distribution. The profile can be generated by either employing a constant die gap with a varying flow rate or by varying the die gap with a constant flow rate (1,2,6).

The die gap is varied during extrusion by varying the position of the mandrel relative to the bushing. The mandrel position is detected by a transducer and is varied with a hydraulic system and servovalve. The distance of mandrel travel and the speed of the movement, enacted by the action of the servovalve, are calculated by the programmer.

2.1.7.1 PROGRAM POINTS Each parison profile is set by a series of program points that define the die gap for specified ram positions during the extrusion. The points correspond to equally sized zones of the total stroke. As the extrusion stroke advances, the gap changes according to the value set for that corresponding zone of the stroke.

Interpolation is employed for transition from point to point. An increase in the number of profile points results in a decrease in the amount of polymer needed.

2.1.7.2 RECENT DEVELOPMENTS Two industrial establishments are at the forefront of parison programming developments. Hunkar Laboratories (11) have released an open loop parison programmer that contains a 34 point interpolation profile. Hunkar also furnishes a type of parison length control. The length is measured with a photocell arrangement. The manipulated variable is the shot size. A servovalve system is incorporated into the accumulator to enact the shot size manipulation.

Barber-Colman (12) produces the MACO VI parison programmer. This unit has a 49 point interpolation program for profiling. Moog (13) also supplies traditional parison programmers.

2.1.7.3 OVALIZATION Ovalization entails controlled changes in the die gap size and shape, by horizontal movement of selected bushing sectors in conjunction with vertical movement of the mandrel.

Standard round tooling can yield uneven product distributions. Voelz and Gleason (14) discuss the utilization of radial parison programming with flexible dies. A dynamic flexible die ring is deformed to a profile set by a Programmable Wall Distribution System. Servovalves and position transducers attached to the die ring affect ovalization.

The profile obtained is controlled by the predeformation of the die ring. Ovalized tooling allows for three dimensional parison programming and therefore can promote uniform product thickness, as well as other more complex three dimensional profiles.

2.2 EXTRUDATE DIE SWELL AND SAG

2.2.1 ORIGINS OF SWELL

Molten polymer extruded through an annular die or capillary has an extrudate cross sectional area appreciably larger than the area of the die exit. The swell can be characterized in different ways as discussed in Section 2.2.3.

A portion of the swell can be attributed to the rearrangement from the parabolic velocity profile in the die to the plug flow profile outside the die (15,16). The remainder of the swell is viscoelastic swell, attributable to the tendency of polymeric melts to recover back when external forces, such as flow in a constrained die, are removed. The ability to recoil is

a direct result of the viscoelasticity and fading memory of polymer melts.

Cotten (17,18) has observed that viscoelastic swell consists of two components: an instantaneous, very fast recovery that results from the solid-like elastic recoil of the quasi-network and a much slower relaxation, that results from the gradual disorientation of the molecular chains that were aligned in the direction of flow. Cotten suggests that both these mechanisms originate from the extensional deformation imposed by the die entrance. This view is in disagreement with the general belief that the swell is also related to the shear deformation.

Shear stresses cause the orientation of molecular segments in the flow direction. Such orientation is associated with a higher energy state and less random configuration. When the shearing disappears at the exit, the external force disappears and the molecular chains tend to return to a more random, lower energy state. A unit of volume of oriented melt within the die becomes shorter in length and larger in cross sectional area upon exit from the die. The result is called extrudate swell (19).

2.2.2 PARAMETERS AFFECTING SWELL

2.2.2.1 EFFECT OF SHEAR RATE The degree of swell increases with an increase in the amount of deformation (20,21,22). Higher shear rates result in more orientation of the molecular chains and subsequently higher swell. The deformations that occur in

the die are due to both extensional and shear effects (23). The extensional deformation is caused by the elongation and stretching that occurs in the converging and diverging parts of the die, respectively. Shear deformation is the result of the radial velocity gradients between the mandrel and the bushing.

Swell is dependent on the time allowed for recovery and consequently the distance beyond the die exit (6). The polymer continues to swell, after the initial instantaneous swell, until an ultimate long time (equilibrium) value is reached. It is important to note that in extrusion blow molding, whereas shear rate increases with increased extrusion velocity, recovery time is decreased under the same conditions. The swelling of the parison is terminated at the point of mold closing. Therefore, higher swells associated with higher shear rates are at least partly offset by the shorter recovery times.

2.2.2.2 EFFECT OF TEMPERATURE Discrepancies exist in the literature regarding the effect of temperature on die swell. Several studies (24-28) have found that swell decreases, as temperature rises. With respect to extrusion blow molding, as the temperature rises, the viscosity decreases, the elastic strain related to the flow resistance decreases and consequently the swell decreases.

However, some studies (29,30) report that swell increases with a temperature increase. A temperature increase results in a decrease in extrusion time, as there is less resistance to flow,

and subsequently an increase in ram velocity and shear rate. Therefore, an increase in swell is expected. It is therefore anticipated that the effects of temperature are specific to the resin, process and equipment being utilized.

2.2.2.3 EFFECT OF LENGTH TO DIAMETER RATIOS Swelling decreases as the length to diameter ratio of the die increases, approaching a constant value at large L/D ratios, such that the effect of the extensional deformation is minimized (21). The extensional elastic strain associated with the die entrance begins to decay in the flow channel until a steady equilibrium value, corresponding to the shear deformation, remains.

2.2.2.4 EFFECT OF DIE CONFIGURATION Parisons flowing through converging dies swell considerably more than those that flow through diverging dies (31). Swell increases slightly with increasing converging angle and decreasing diverging angle.

2.2.2.5 EFFECT OF FILLERS The addition of fillers reduces the amount of extrudate swell (18). It is possible that the fillers cause the molecular chains to retain their orientation upon exiting from the die, thereby inhibiting swell.

2.2.2.6 EFFECT OF MOLECULAR STRUCTURE It is generally accepted that the higher molecular weights and broader molecular weight distributions are associated with higher swells (32). However,

the converse has also been reported (33,34). This is probably attributable to the slower recovery rates that might occur at higher molecular weights.

2.2.3 SWELL DEFINITIONS

Several swell parameters can be defined, depending on the specific case under consideration.

Capillary swell, B_C, is defined as

$$B_C = D_E / D_C \qquad (2.1)$$

where D_E is the extrudate diameter and D_C is the capillary exit diameter.

In the case of extrusion blow molding, annular flow is involved (Figure 2.6), and different definitions are required.

The diameter swell, B_1, is defined as,

$$B_1 = D_P / D_O \qquad (2.2)$$

where D_P is the parison outer diameter and D_O is the outer diameter at the exit of the die. The thickness swell, B_2, is defined as

$$B_2 = h_i / h_o \qquad (2.3)$$

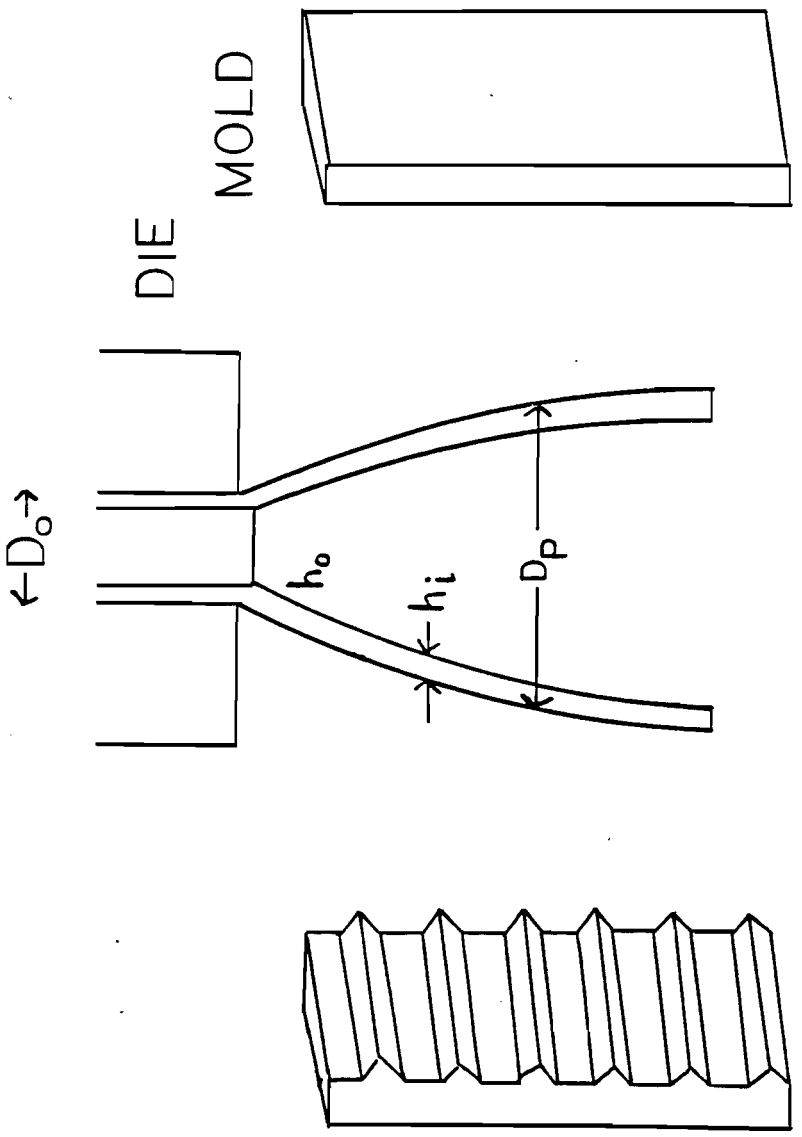

$$B_1 = D_P / D_o$$

$$B_2 = h_i / h_o$$

Figure 2.6: Parison Formation

where h_i is the parison thickness and h_o is the die gap.

The weight swell, B_3, is defined for an axial segment of the parison as:

$$B_3 = \frac{4\ W(i)}{\pi\rho(D_o^2 - D_i^2)L(i)} \qquad (2.4)$$

where W(i) is the weight of segment i, ρ is the melt density, D_o is the outer die diameter, D_i is the inner die diameter and L(i) is the length of the segment. Assuming constant melt density and validity of the slit approximation (D(i) >> h(i)), the three swell parameters are then related by

$$B_3 = (B_1)(B_2) \qquad (2.5)$$

Kalyon (6) has shown experimentally that this approximation is valid, for typical blow molding conditions, yielding a maximum error of 2 %.

The weight distribution, W(i), can be obtained by employing a pinch-off mold developed by Sheptak and Beyer (35). This mold consists of several blades placed one inch apart (Figure 2.6). The blades divide the parison into pillow-shaped segments and hold them until the parison freezes. The segments are then cut apart and weighed, so as to obtain the weight distribution. The outer diameter distribution along the parison length can be estimated from pinch-off mold experiments by the equation

$$D_p = \frac{2\ w\ (\rho_s/\rho)^{1/3}}{\pi} \qquad (2.6)$$

where w is the width of the segment and ρ_s is the solid extrudate density. However, Kalyon (6), has shown that this method yields inaccurate values of parison diameter. His results also indicate that an optical determination of outer parison diameter is more accurate. This conclusion is in agreement with the results of the present study, as will be shown later.

2.2.4 EXTRUDATE SWELL PREDICTION

2.2.4.1 DIE SWELL RELATED TO RECOVERABLE STRAIN The models utilized for die swell prediction generally employ the observation that die swell is directly related to the recoverable strain, S_R. The recoverable strain is defined as

$$S_R = \tau J_E \qquad (2.7)$$

where τ is the applied shear stress and J_E is the steady state shear compliance. This equation is applicable only to the linear viscoelastic range of low shear rates and is not reliable at higher shear rates. The recoverable strain, S_R, can also be obtained at low shear rates from

$$S_R = N_1 / (2 \tau) \qquad (2.8)$$

where N_1 is the first normal stress difference.

Several models have been developed relating the capillary

swell, B_C, to the recoverable strain, S_R. Vlachopolous, et al. (36), Utracki et al. (37), Garcia-Rejon(38) and Kalyón(6) reviewed and studied these models. Experimental results show that the proposed relationships are useful to some extent as a first approximation. These models assume the swell to be instantaneous, whereas in actuality it is time dependent. The models also assume linear viscoelastic behaviour, which is not necessarily valid, since practical applications are always outside this linear range.

2.2.5 SAG

A parison suspended in air tends to sag due to its own weight. The degree of sag is directly related to the extensional stress growth function, Γ_+, and the parison suspension time. Sag becomes a major problem in the production of large parts and in slow extrusions (39).

Sag tends to increase with an increase in temperature, a decrease in extrusion speed, an increase in parison length and a decrease in the resin melt viscosity. An increase in temperature corresponds to a decrease in melt extensional viscosity. A decrease in extrusion speed and an increase in parison length result in an increase in extrusion time and consequently an increase in the parison suspension time. However, in this study, resins of high melt strength were employed and the suspension time was less than two seconds. Therefore, the effect of sag is

negligible (38), (Appendix 3).

2.2.6 PARISON BEHAVIOUR

Sheptak and Beyer (35) were the first to study parison behaviour by utilizing a pinch-off mold (Figure 2.6). Their primary findings were that the parison weight distributions were dependent on both swell and sag. Several subsequent studies (40-45) also employed a pinch-off mold, in attempting to discover the combined effects of swell and sag on the parison weight distributions.

Ajroldi (45) considered that, in intermittent blow molding, the polymer melt in the first extruded segment undergoes relaxation in the die whereas the following segments begin to relax after leaving the die. Ajroldi also discussed the dynamics of the parison by considering elastic recovery under a tensile stress. The total strain was assumed to consist of the recoverable strain and the creep strain. The individual components were treated as Hencky strains.

Cogswell (46) proposed a relationship correlating weight swell to capillary swell by the following equation.

$$B_1(t)B_2(t) = 0.242 + 0.727\ (B_C)^2 \qquad (2.9)$$

This equation must be used with caution since capillary data are generally obtained from completely annealed samples and the

weight swells were obtained at short times after the extrusion, so as to coincide with the mold closing. Cogswell et al.(47) also suggested a mathematical model of the parison formation stage by incorporating simultaneously the impacts of swell and sag. The results were found to be in reasonable agreement with the limited experimental data available.

Garcia-Rejon(38) employed an annular die in conjunction with a capillary rheometer and two isothermal chambers to study the combined effects of swell and sag. The findings indicated that for high density polyethylene resins, the effect of sag was distinguishable only after the parisons were suspended for eight minutes. The individual transient diameter and thickness swells were fit to the equation.

$$B_S = B_{S\infty} - (B_{S\infty} - B_{SO})\exp(t/\delta_S) \qquad (2.10)$$

The subscript S takes on a value of one for diameter swell and a value of two for thickness swell. The subscript, ∞, represents the equilibrium long time swell value. Time is designated by t and δ_S is a characteristic relaxation time. A simple model for estimating parison length as a function of time was developed based on these studies.

Kalyon et al.(48) and Kamal et al.(49) extended the work of Ajroldi by showing that parison behaviour can be predicted, provided that the transient diameter, $B_1(t)$, and thickness $B_2(t)$ swells are determined under conditions where sag is minimized.

This was achieved by extruding the polymer into an oil bath of the same temperature and density as the melt. The parison cross sectional areas were determined by employing weight distribution and creep compliance data. Kalyon and Kamal (50) and Dutta and Ryan (51) carried out extensive investigations of the parison formation stage by employing both photographic and pinch-off mold techniques.

Ryan (2) has reviewed work regarding the numerical simulation of the parison formation. An accurate complete mathematical simulation of the parison formation stage is yet unavailable due to the complex nature of the phenomena involved, including free surface and transient aspects.

2.3 EXTRUDATE DIMENSION MEASUREMENT AND CONTROL

Measurement of extrudate dimensions has generally involved some form of optical and/or pinch-off technique. Kalyon and Kamal (50) used a combination of high speed photography and a pinch-off mold to measure parison dimensions. Garcia-Rejon (38) and Orbey (31) measured annular die extrudate dimensions, in an oil bath, as functions of time by employing a photographic technique. Basu and Rauwendaal (52) and Huang and Campbell (53) employed a video camera arrangement for measuring total parison length and diameter profiles during extrusion of an annular extrudate from a melt indexer. The above techniques could not be used directly for closed loop control of parison dimensions as

they lack the necessary feedback signal.

Several attempts (19,54-60) have been made to measure on-line capillary extrudate swell by utilizing a light source, such as a laser beam, in conjunction with a photodiode array. Dennis-Germuska, Taylor and Wright (60) enacted thickness control on an extrudate of low density polyethylene by manipulating the screw speed, die heater setting and take-up rate. A masterbatch was added to the extrudate in order to produce a black extrudate with well defined edges. The extrudate was cooled in a bath before thickness measurement with the laser-photodiode arrangement.

Stevenson (61,62) measured and controlled profile extrudate dimensions by manipulating screw speed and die temperature. A pneumatic type system was used for measurement of the extrudate profile dimensions. Nuclear (63) and Infra-Red gauges (64), operating on the absorption principle, have been used for measuring film and bottle thicknesses, respectively. These systems are inapplicable for the case of parison thickness profile measurement because of problems associated with the appropriate location of the sensors.

Ultrasonic gauges (65), in conjunction with a liquid couplant, have been used for on-line pipe thickness measurement. The principle of operation is that of signal reflection. Buchscheidt et al. (66) utilized a series of ultrasonic gauges, with special measuring heads placed flush inside a mold, for blow molded part thickness measurement. The two major problems associated with ultrasonic gauges are the need for liquid

coupling between the part and the instrument and sensor damage at the high temperatures. Buchscheidt and coworkers claim that these problems are surmounted by the use of special measuring heads. However, the principle of operation and experimental data were not reported. Moreover, these authors did not comment on the ability of the sensor to measure thicknesses of curved sections. This is a key requirement in employing ultrasound for bottle thickness measurement.

A more detailed review of relevant dimension measurement techniques is given in Appendix 2.

CHAPTER 3

EXPERIMENTAL

This chapter summarizes the important properties of the blow molding resins employed in this study and outlines the experimental techniques employed to obtain these data. Also, it provides a description of the experimental apparatus comprising the image processing system, the blow molding machine itself and the computer interface with the blow molding machine.

3.1 MATERIALS

Two high density polyethylene (HDPE) resins, designated here as Resins A and B, were employed in this work. They were supplied by Novacor Chemicals. Both resins exhibit high swell. Resin B swells at a relatively greater rate and to a greater degree than Resin A.

3.1.1 MATERIAL PROPERTIES

The solid and melt densities and melt indices of the resins are presented in Table 3.1. The melt densities at 200 ^{o}C and 1 atmosphere were obtained by using the Instron Capillary Rheometer Model 3211 (67). The number, weight and z average molecular weights and the polydispersity, represented by the ratio of the weight average to the number average molecular weights, are also

TABLE 3.1

RESIN PROPERTIES

PROPERTY	RESIN A	RESIN B
SOLID DENSITY (Kg/m^3)	957	956
MELT DENSITY (Kg/m^3)	760	760
MELT INDEX (Kg/10 min)	0.0003	0.0005
MOLECULAR WEIGHT		
NUMBER AVERAGE (M_N)	34100	30700
WEIGHT AVERAGE (M_W)	527000	468000
Z AVERAGE (M_Z)	3090000	3157000
POLYDISPERSITY (M_W/M_N)	15.5	15.3

presented in Table 3.1. The molecular weight data were obtained by gel permeation chromatography (GPC). All of the above data were supplied by Novacor Chemicals.

3.1.2 RHEOLOGICAL PROPERTIES

The rheological data for Resins A and B were obtained with three separate rheometers. The Instron Capillary Rheometer Model 3211 (67) was employed at high shear rates. The Rheometrics System 4 Mechanical Spectrometer (68) was used at low shear rates and in the dynamic mode. The Rheometrics RER 9000 Extensional Rheometer (69) was utilized for elongational measurements.

The capillary rheometer results were obtained at 200°C or 225°C, depending on the specific test. The shear rheometer data were obtained at 200°C, and the extensional rheometer data were obtained at 150°C. Oil flashing prevented use of higher temperatures with the extensional rheometer.

Capillary flow rheometry involves extrusion of a polymer melt through a capillary die while monitoring the forces applied to the melt. Force transducer sensitivity considerations determine the lower shear rate range, whereas the onset of melt fracture establishes the higher shear rate limit.

When the Mechanical Spectrometer is used, the polymers are kept under a nitrogen atmosphere, in order to avoid oxidative degradation of the melts and maintain stability at 200°C. Edge effects, stemming from flow instabilities at the edges, limit

operation at high shear rates (54). The cone and plate geometry was utilized for all the Mechanical Spectrometer measurements. The cone angle was 0.04 radians and the plate diameter was 50 mm.

The extensional measurements involve fastening a cylindrical polymer sample, and deforming it in a vertical upward direction. The force applied to the sample is then measured. Detailed procedures for operation of the capillary, cone and plate and extensional rheometers are described elsewhere (54, 67-69).

3.1.2.1 VISCOSITY-SHEAR RATE RELATIONSHIP

The viscosity versus shear rate data at 200°C, for the two resins are presented in Figure 3.1 (poise=0.1 Pa-s). The high shear rate data were obtained with the capillary rheometer. The data were treated to take account of the Bagley and Rabinowitsch corrections (54). The low shear rate data were obtained with the Mechanical Spectrometer.

The two resins tend to behave differently in the low shear rate range. Resin A has a higher low shear rate limiting viscosity than Resin B. The higher viscosity for Resin A in the low shear rate range contributes to lower sag for Resin A. The uniaxial elongational viscosity is three times the shear viscosity in the linear viscoelastic range (54).

The extensional rheometer, operating at a strain rate of 0.1 sec^{-1}, was utilized to obtain elongational viscosity data for the

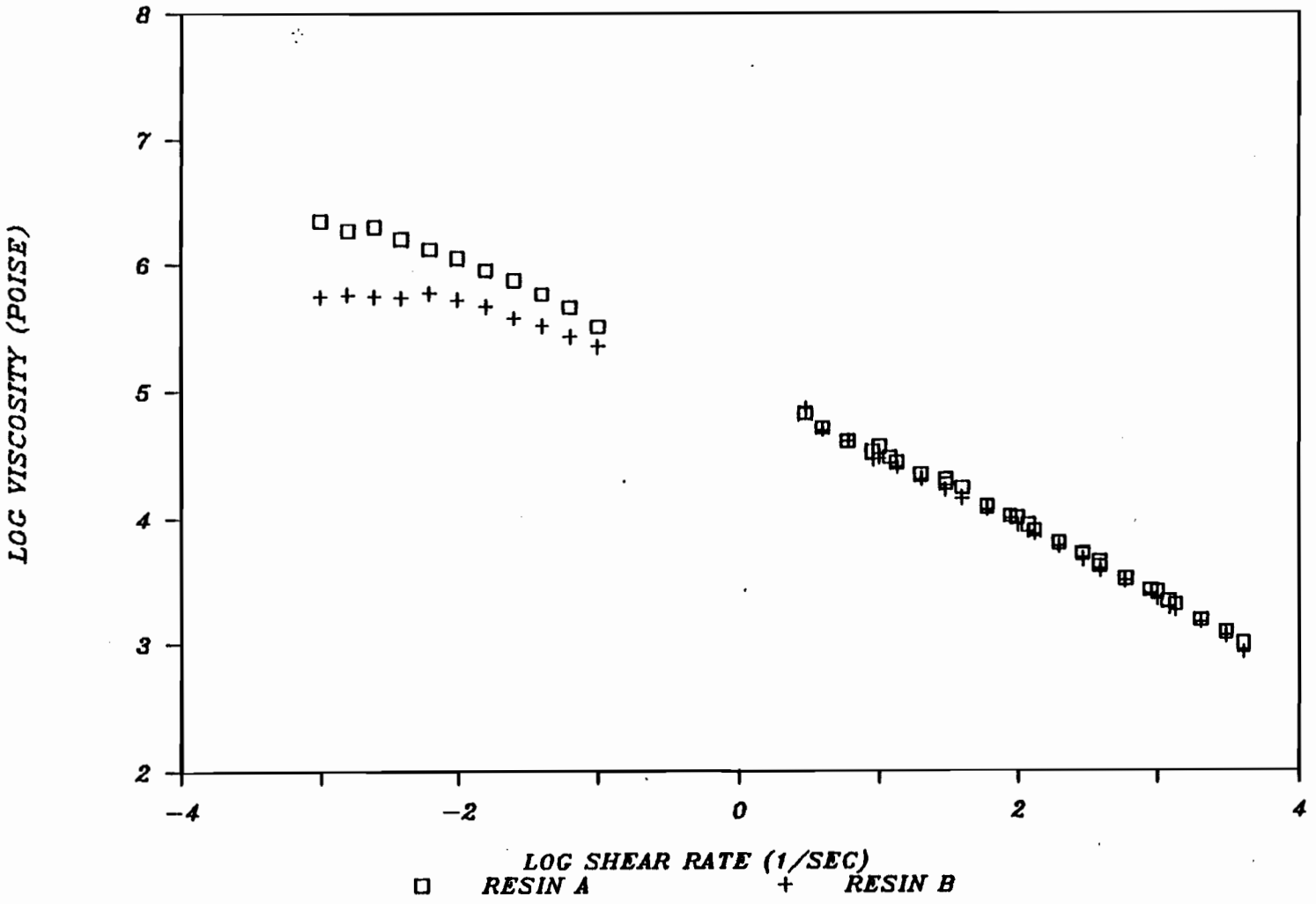

Figure 3.1: Shear Viscosity of Resins A and B at 200°C

two resins (Figure 3.2). The higher elongational viscosity for Resin A contributes to lower sag.

The resins behave similarly in the high shear rate range, of Figure 3.1, with Resin A having only a slightly greater viscosity than Resin B. The higher viscosities for Resin A indicate higher extrusion pressures for a specified extrusion rate.

The effect of temperature on the viscosity-shear rate behaviour of Resins A and B is shown in Figures 3.3 and 3.4, respectively. The sensitivity of the curve to temperature is roughly equal for both resins. The effect of temperature becomes small at the high shear rates. These data were obtained exclusively with the capillary rheometer, at temperatures of 200°C and 225°C.

3.1.2.2 TIME AND STRAIN SWEEP

Time sweeps were performed with the Mechanical Spectrometer at 200 °C and 0.05 rad/sec, to ascertain the thermal stability of the resins for a sufficient period of time (dyne=10^{-5} N). Time sweeps for Resins A and B are presented in Figure 3.5. The rate of oscillatory deformation was 0.05 rad/sec, and the total sweep time was 90 minutes. The storage, G', and loss, G'', moduli were calculated as a function of time. No degradation was indicated for the 90 minute time period.

Strain sweeps were also performed with the Mechanical Spectrometer at 200°C and a rate of 10 rad/sec, in order to

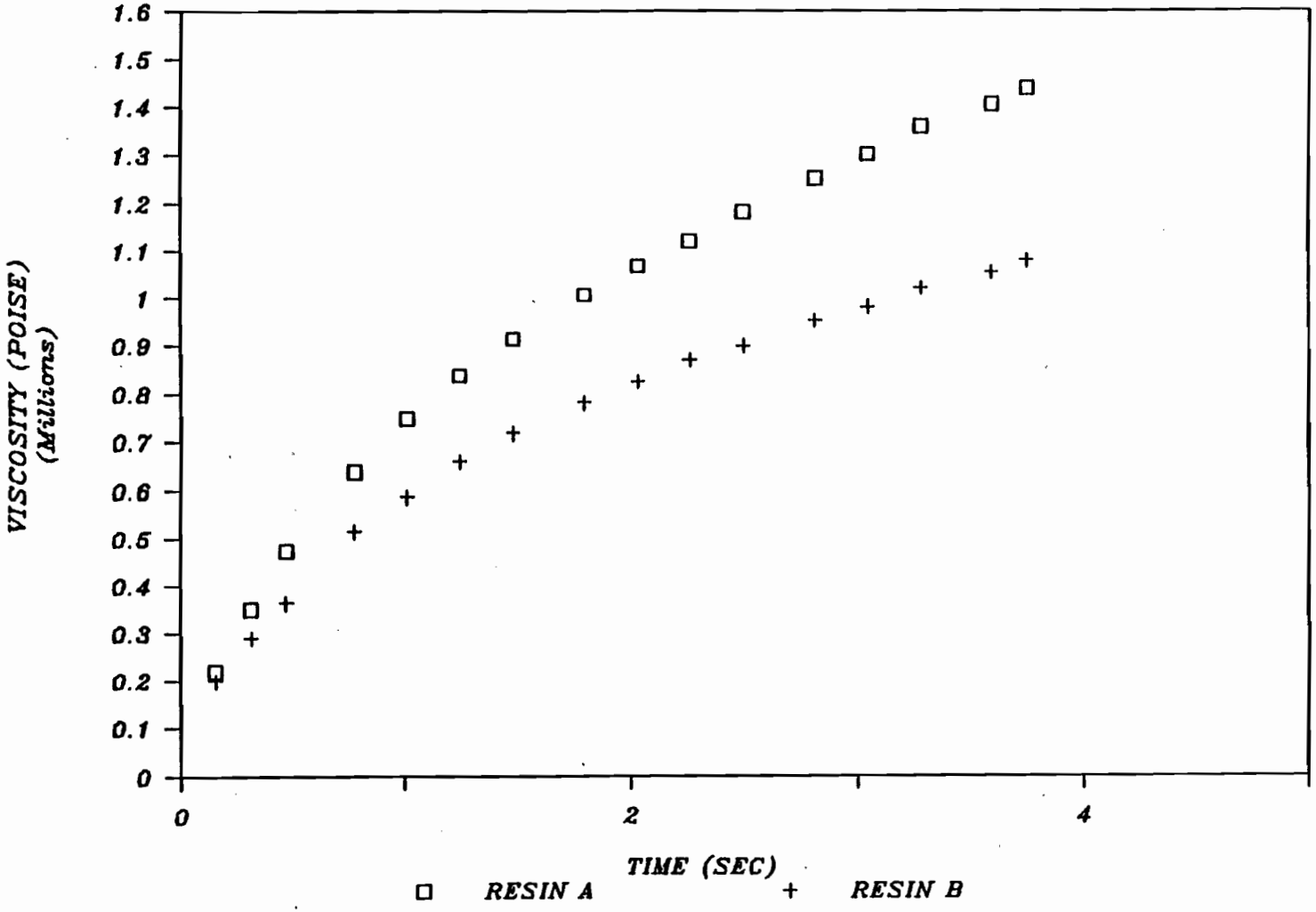

Figure 3.2: Elongational Viscosity of Resins A and B at 150 ^{o}C and 0.1 sec^{-1} Strain Rate.

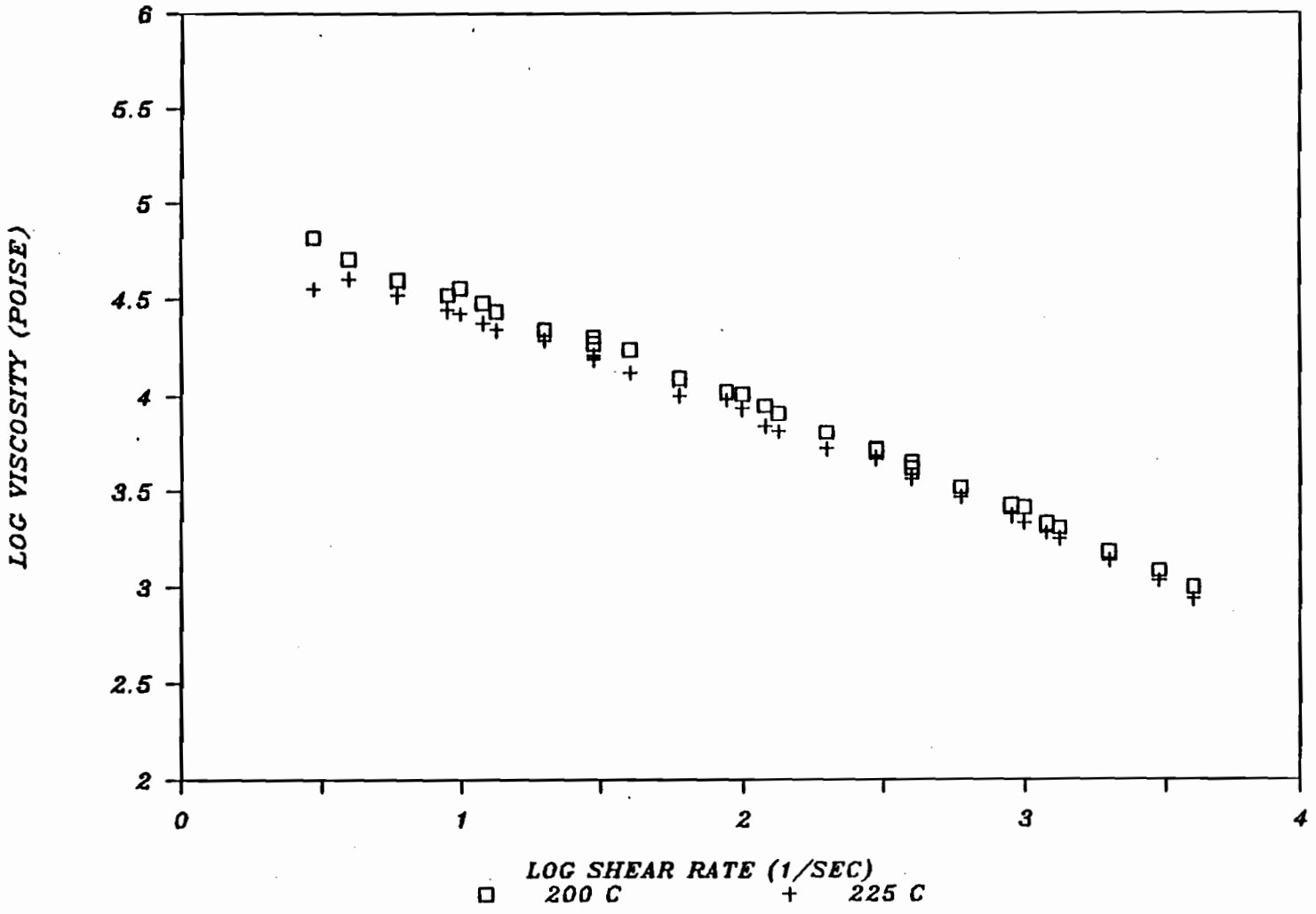

Figure 3.3: Shear Viscosity of Resin A at 200°C and 225°C

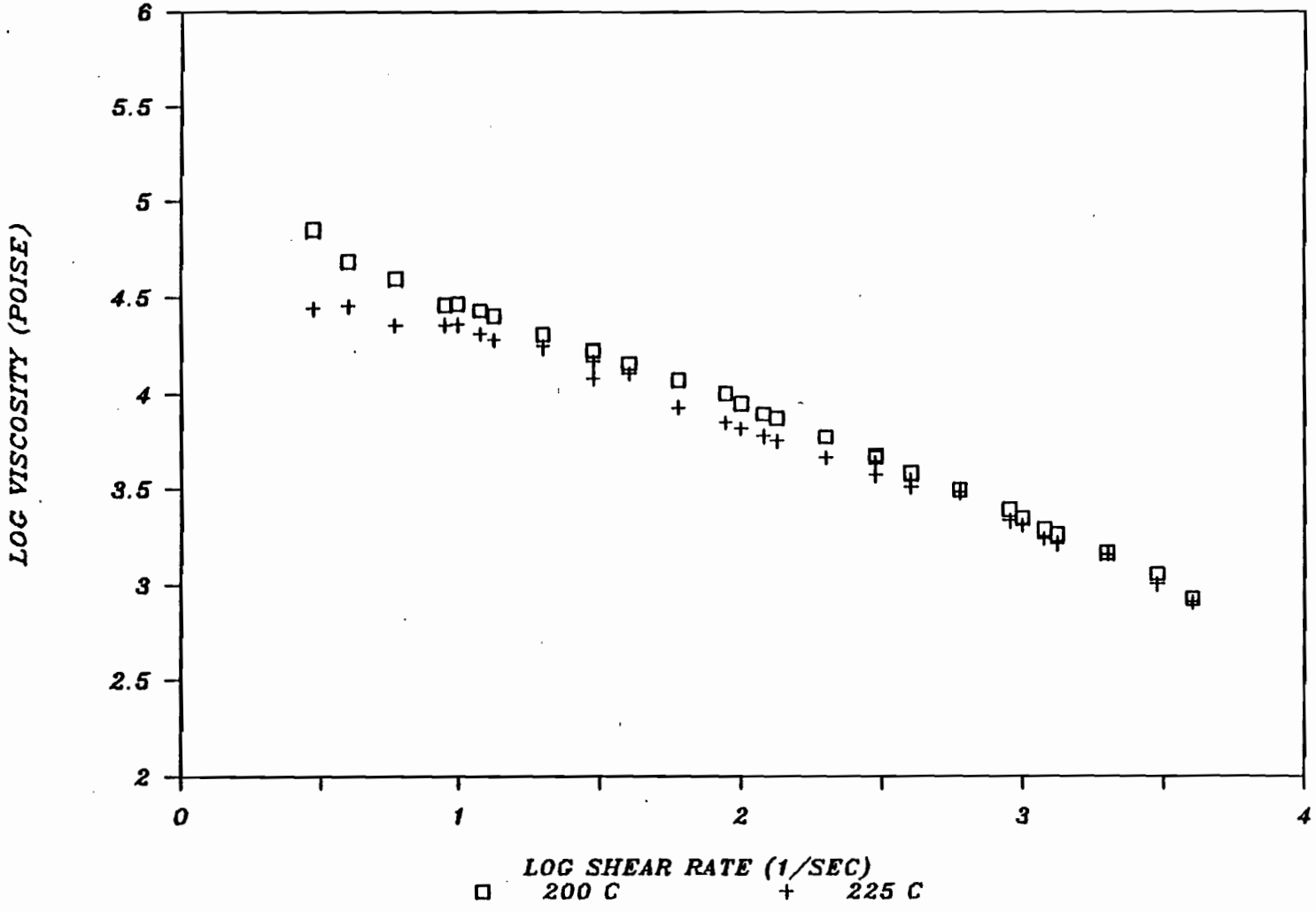

Figure 3.4: Shear Viscosity of Resin B at 200°C and 225°C.

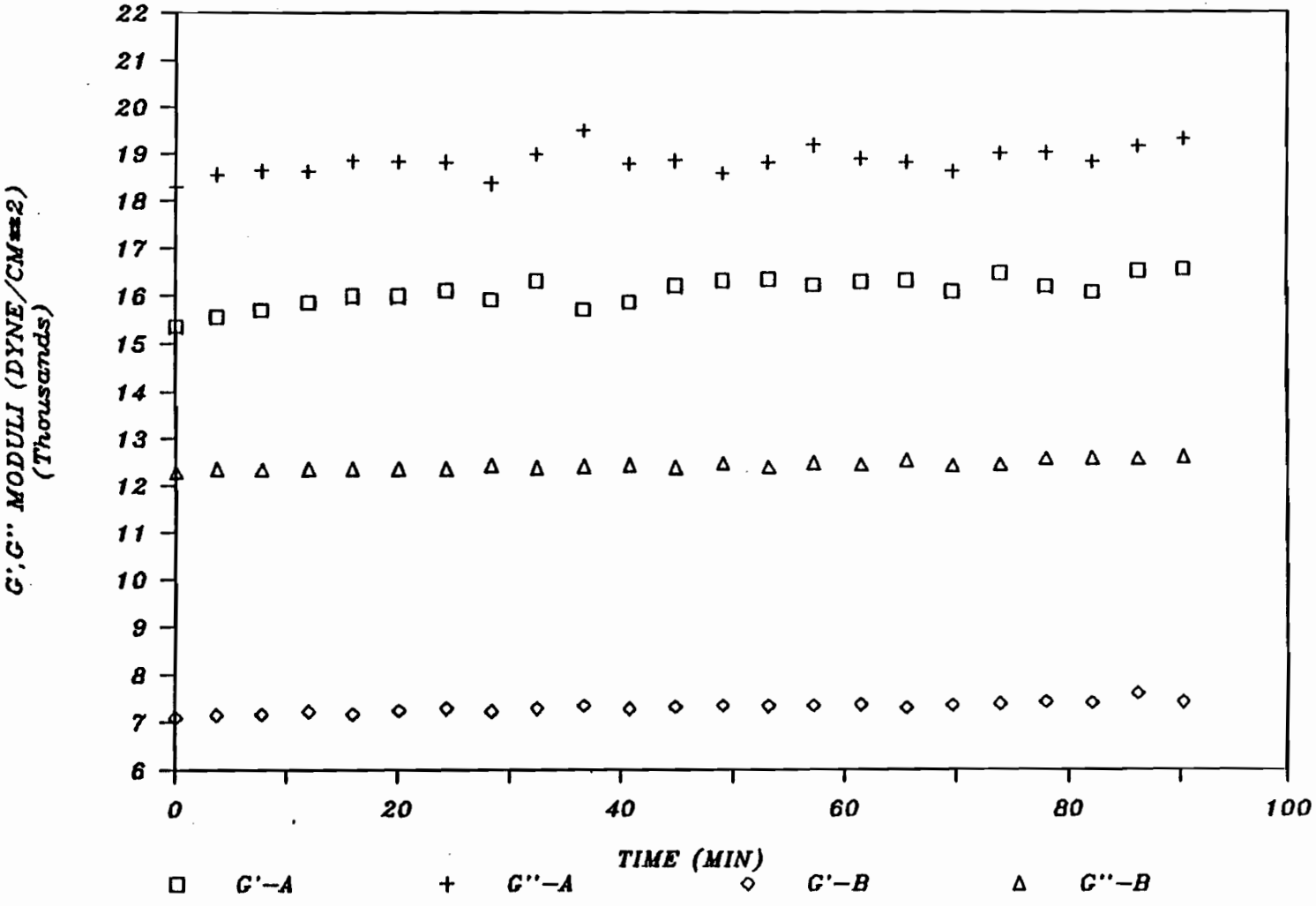

Figure 3.5: Time Sweeps for Resins A and B at 200°C and 0.05 rad/sec

determine the onset of non-linear viscoelastic behaviour (Figure 3.6). The storage and loss moduli are monitored as a function of increasing percent strain. Non-linear viscoelasticity is indicated when the storage and loss moduli are no longer independent of the amplitude of the deformation. This occurs at about 20 percent strain.

3.1.2.3 STORAGE AND LOSS MODULI

Mechanical spectrometer frequency sweeps at 200°C yield information regarding the variation of storage and loss moduli with frequency. The storage modulus is indicative of the elasticity of the resin, while the loss modulus is indicative of the viscous component. Resin A (Figure 3.7) tends to have higher storage and loss moduli than Resin B (Figure 3.8). The difference is more pronounced in the low frequency range.

3.1.2.4 FIRST NORMAL STRESS DIFFERENCE

The dependence of first normal stress difference on shear rate, at 200 °C for Resins A and B, is shown in Figure 3.9. These data were also obtained with the Mechanical Spectrometer (54).

The values for Resin A are greater than for Resin B. It is widely accepted that first normal stress difference is a measure of elasticity. Based on the swell theories mentioned in Chapter

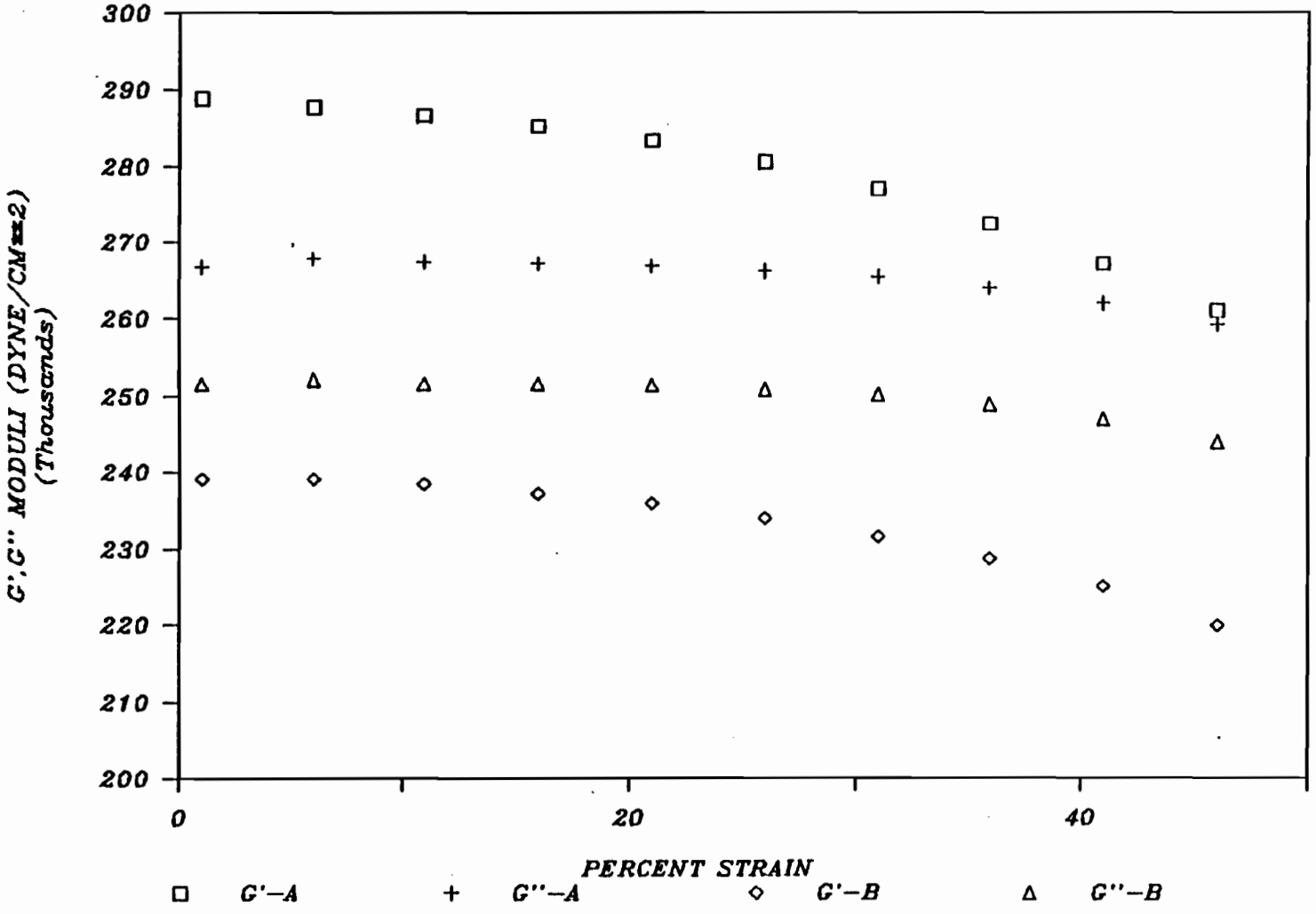

Figure 3.6: Strain Sweeps for Resins A and B at 200°C and 10 rad/sec

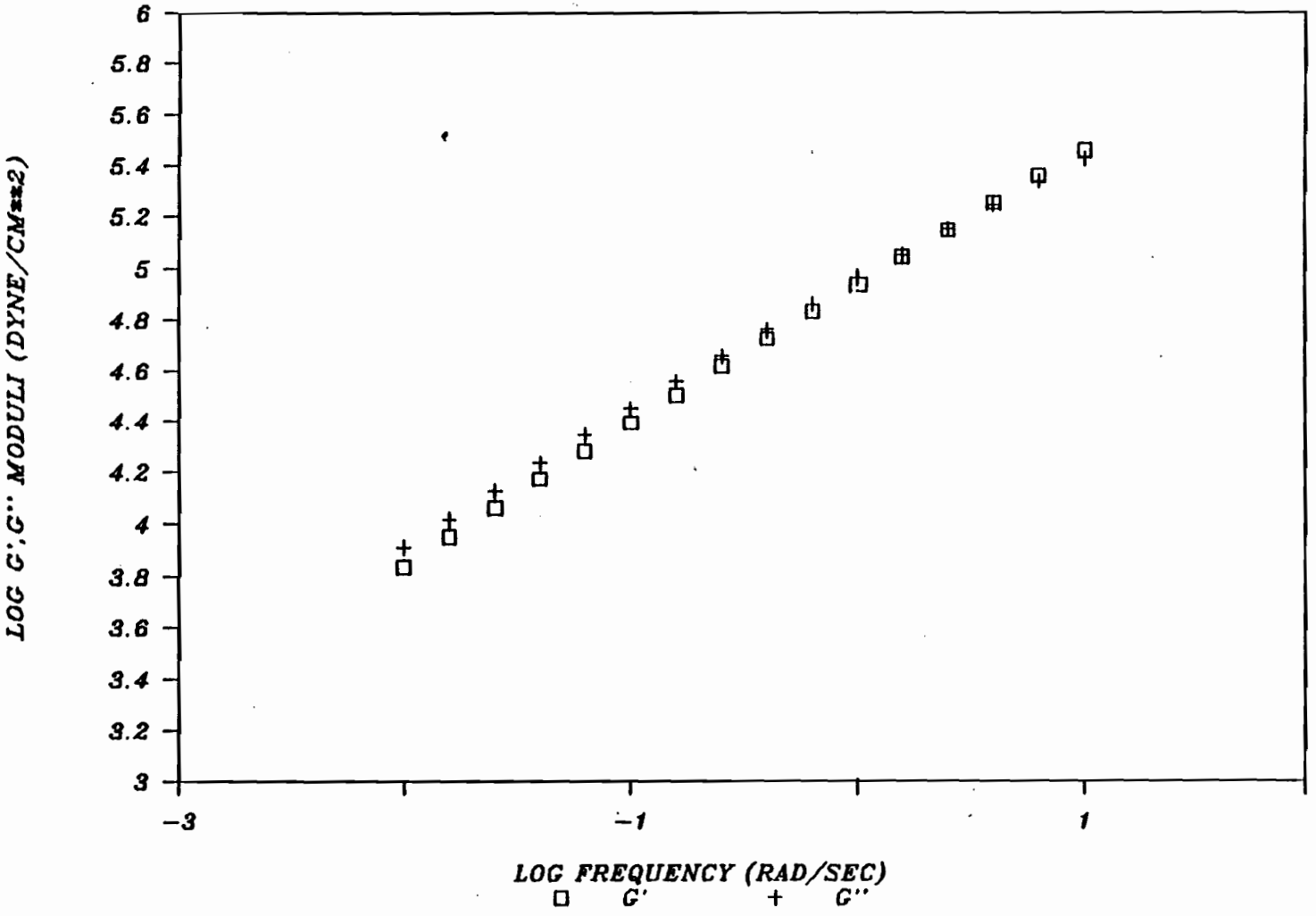

Figure 3.7: Storage and Loss Moduli for Resin A at 200°C.

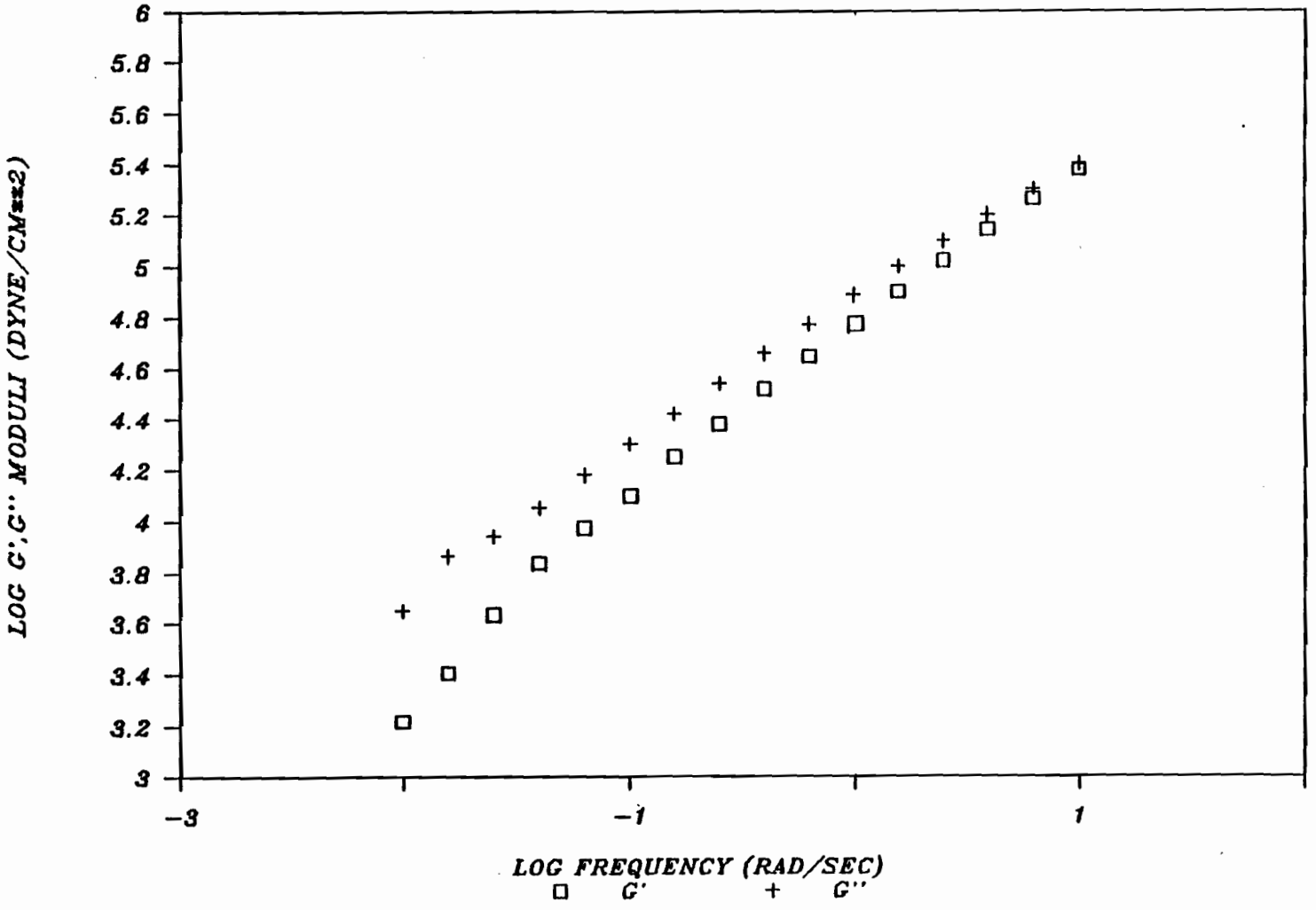

Figure 3.8: Storage and Loss Moduli for Resin B at 200°C.

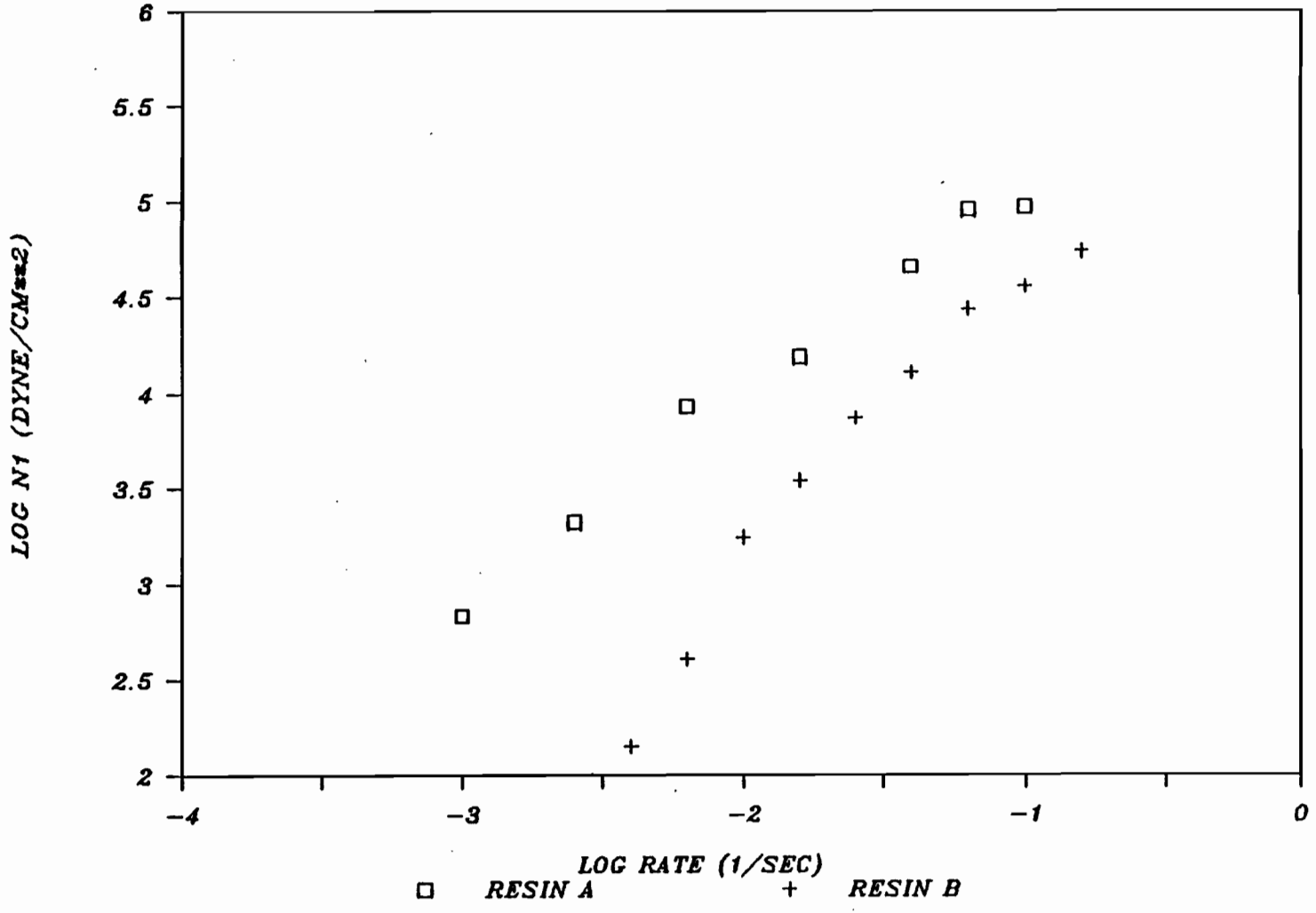

Figure 3.9: First Normal Stress Difference for Resins A and B at 200 °C.

2, Resin A is expected to swell to a greater extent than Resin B. However, it is important to recall that these models are valid only in the low shear rate range of linear viscoelasticity. The models are not likely to apply in the high shear rate range associated with extrusion blow molding. Edge effects preclude measurements at high shear rate data with the cone and plate rheometer.

3.1.2.5 STRESS RELAXATION

Stress relaxation entails the application of a constant deformation rate until time zero, whereupon the deformation is removed. The stress is then monitored for a sufficient period of time, until a steady stress is attained (54).

The stress relaxation behaviour of Resins A and B after shear deformation, applied by the Mechanical Spectrometer, at a rate of .106 sec^{-1}, is shown in Figure 3.10. The stress relaxation to an extensional deformation, applied by the Rheometrics Extensional Rheometer, at a rate of 0.1 sec-1, is presented in Figure 3.11.

Resin B relaxes at a relatively faster rate than Resin A for both deformation types. Therefore, it would be expected that Resin B should swell at a faster rate than Resin A. Both modes of relaxation are considered, since the deformations associated with the extrusion of a polymer melt through an annular die are likely to consist of both shear and extensional components. The

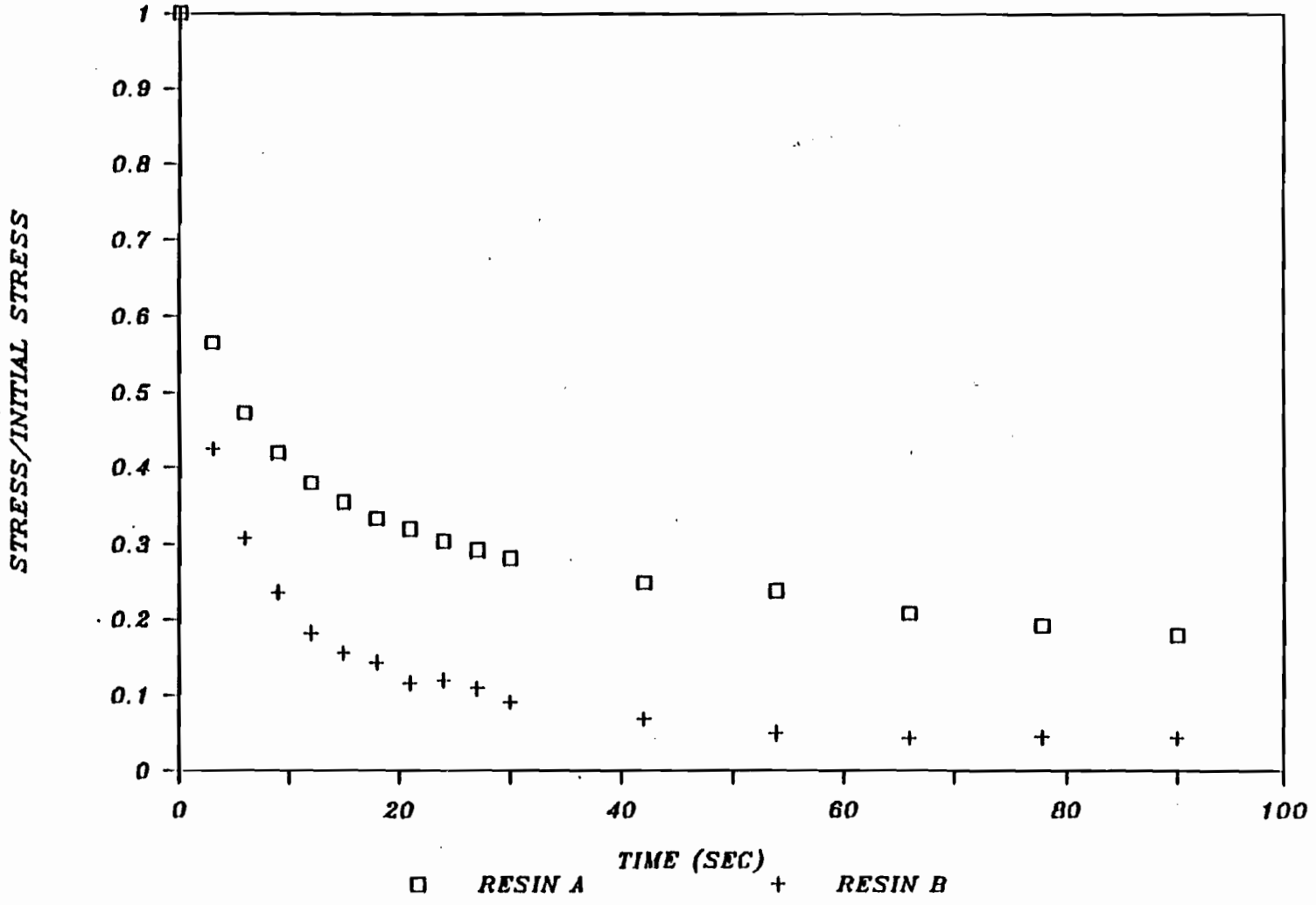

Figure 3.10: Stress Relaxation Upon Cessation of Steady Shear for Resins A and B to a Shear Deformation of 0.106 sec^{-1} at 200°C.

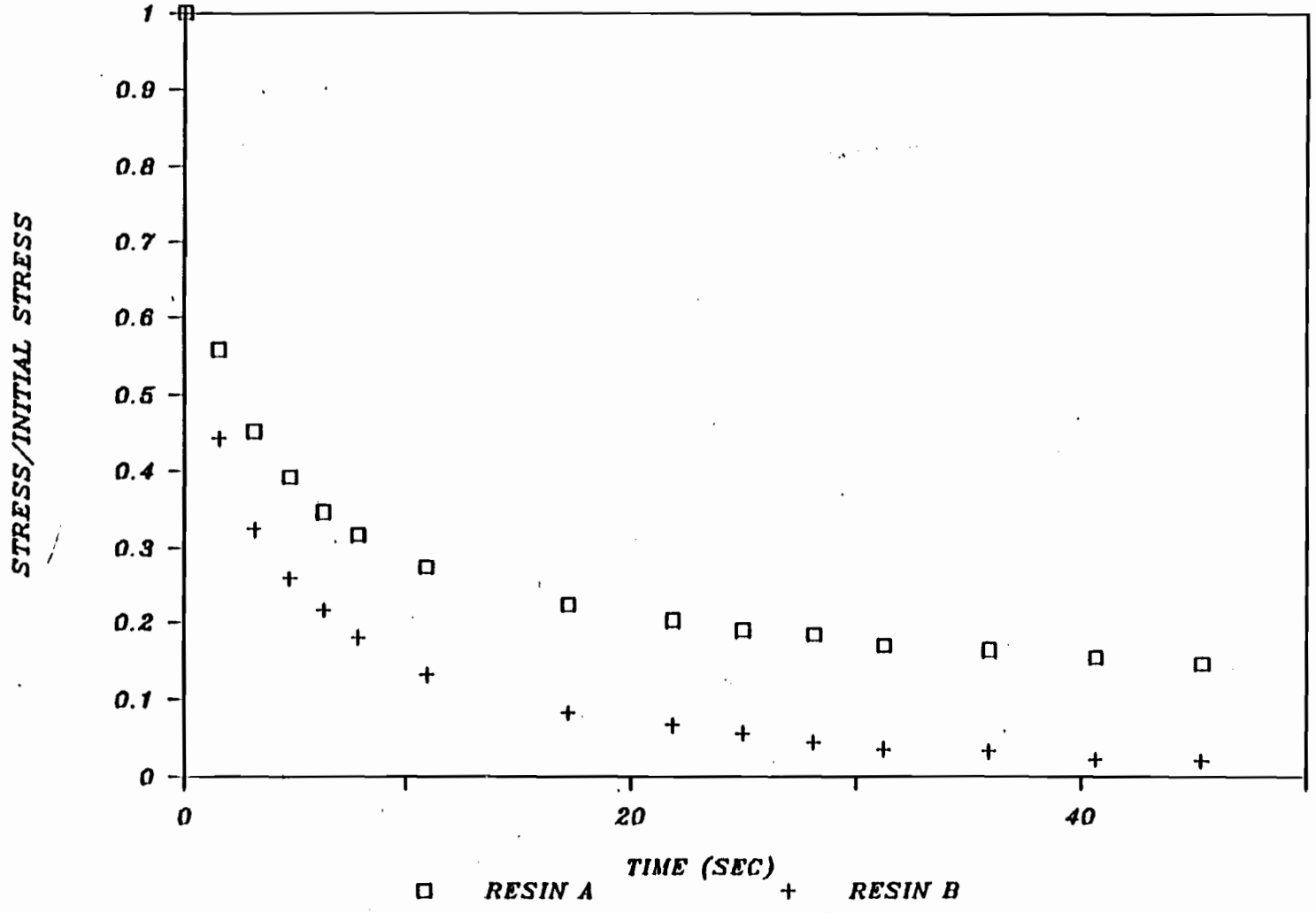

Figure 3.11: Stress Relaxation Upon Cessation of an Extensional Deformation of 0.1 sec^{-1} at 150°C for Resins A and B.

dominant contribution to the deformation is likely to be the shear component, because of the high shear rates involved (assuming long L/D ratios).

3.1.2.6 STRAIN RECOVERY

The strain recovery experiment involves the application of a constant stress by means of closed loop control on torque. The stress is suddenly removed, and the recoverable strain is monitored until a steady value is reached (54).

The strain recovery to a shear deformation, applied by the Mechanical Spectrometer, is shown in Figure 3.12. An instantaneous recoverable strain, shown by the intercept at time zero, is inherent in the shear experiment. The strain recovery after extensional deformation is presented in Figure 3.13. The initial deformation stress for both types was 5×10^4 Pascals.

The recoverable strains obtained from the extensional rheometer are comparable for Resins A and B, with the values for Resin A being slightly greater than for Resin B. However, the recoverable strain obtained with the shear rheometer is significantly greater for Resin B than for Resin A. It is

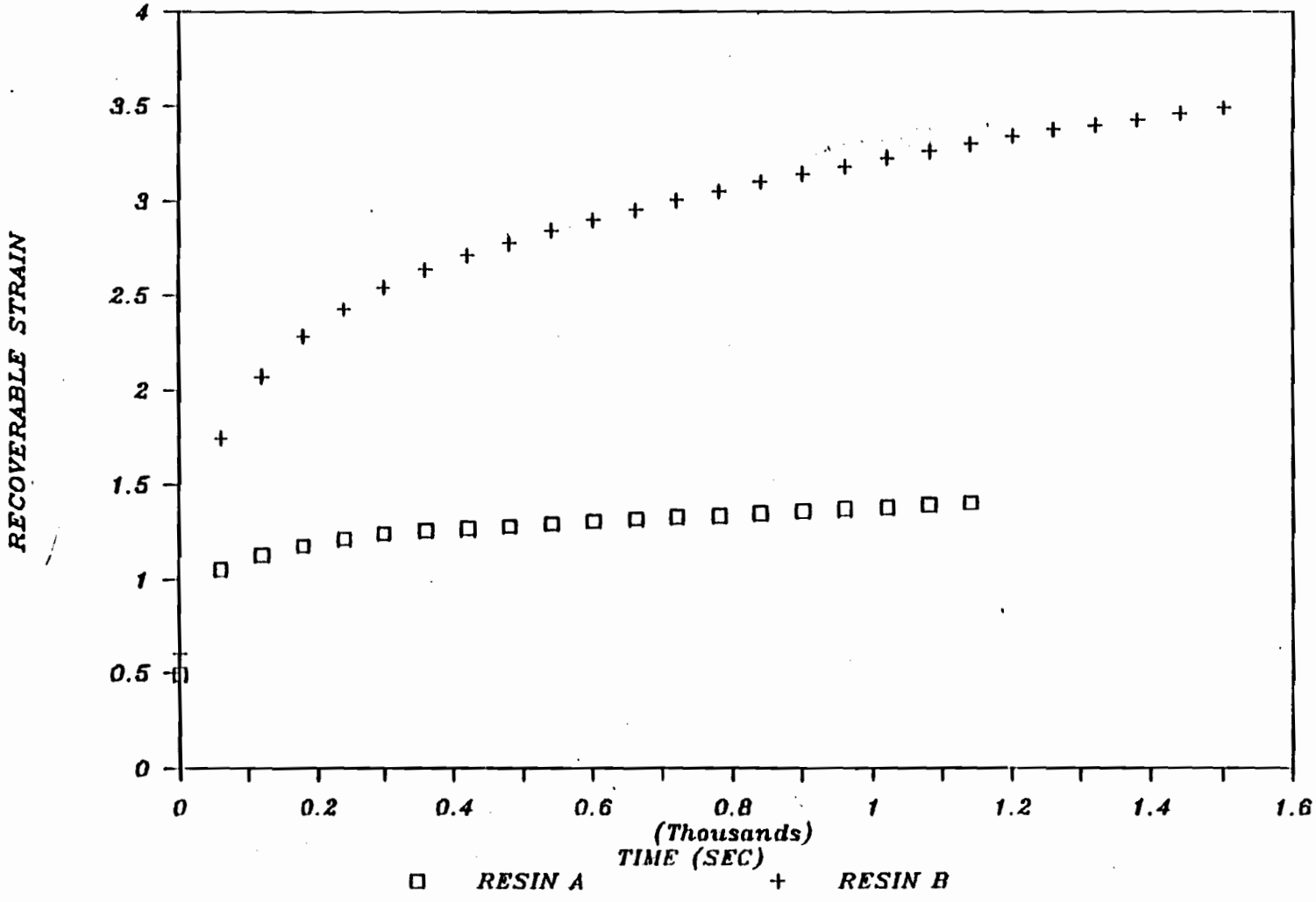

Figure 3.12: Strain Recovery from an Initial Shear Deformation Stress of 50000 Pa at 200°C for Resins A and B.

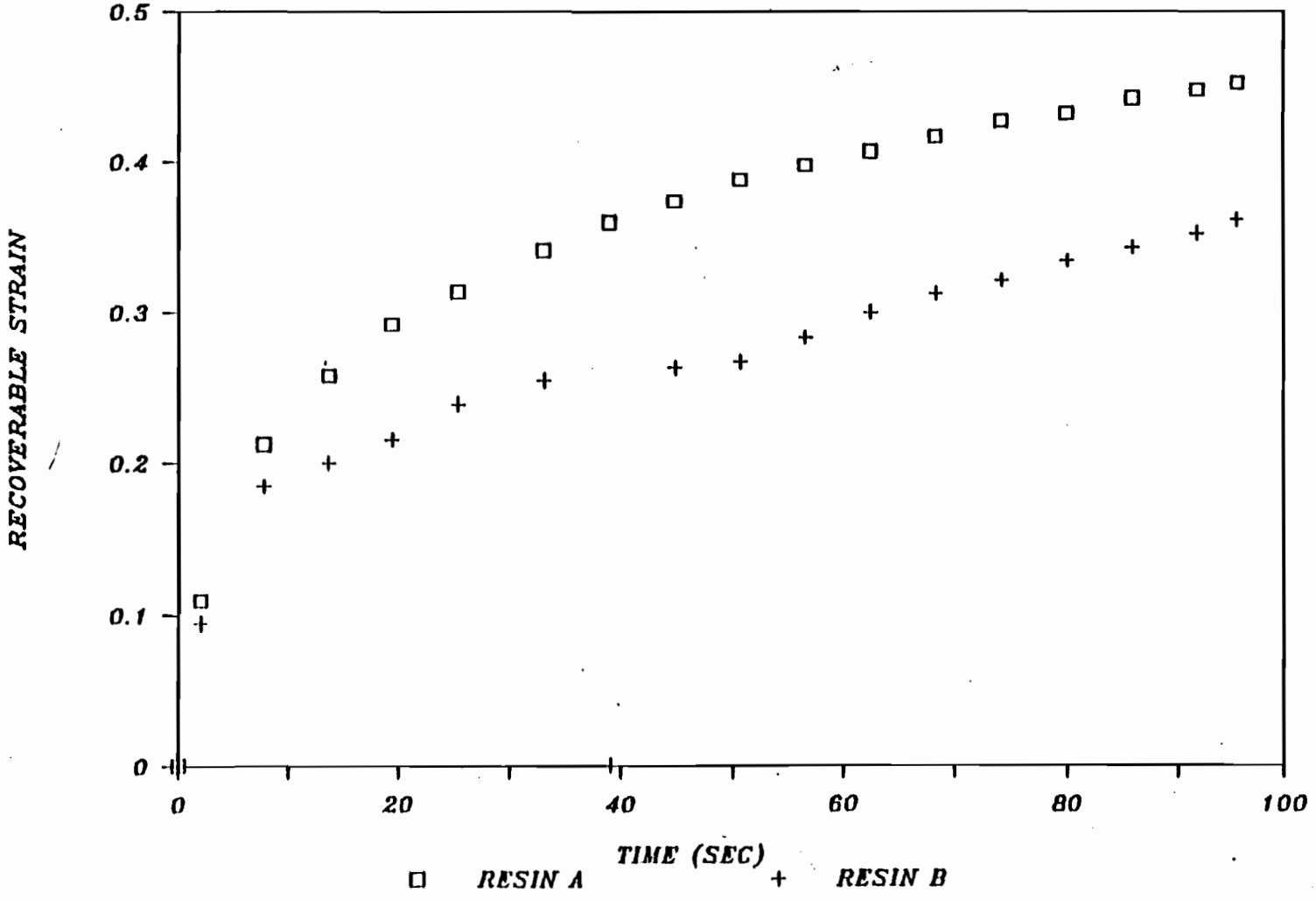

Figure 3.13: Strain Recovery from an Initial Extensional Deformation Stress of 50000 Pa at 150°C for Resins A and B.

expected that Resin B would swell at a relatively greater rate than Resin A.

3.2 BLOW MOLDING ARRANGEMENT

On-line parison profile dimension measurements are essential to provide the necessary feedback signals for closed loop control. The apparatus, designed and constructed in this work, measured and yielded estimates of profile dimensions after the extrusion. In the process mode, the data acquisition system is employed in conjunction with a video camera-frame grabber system (Figure 3.14).

Light from a high wattage light source illuminates the parison. A black background is necessary to ensure sufficient contrast between the parison and its surroundings. The video camera captures the image of the parison.

The frame grabber board digitizes the analog signal output from the camera and buffers it, to allow for analysis by the computer. A synchronization signal from the frame grabber determins the instant of picture taking. The board also transmits a signal to an external monitor so that the scene can be viewed and processed.

The blow molding machine was instrumented to yield continuous measurements of ram velocity (V_r), ram position (x_r), gap size (h_o) and melt pressure (P_h) during extrusion. These parameters were monitored with the analog-to-digital (A-D) section of the data acquisition system. Instants during the

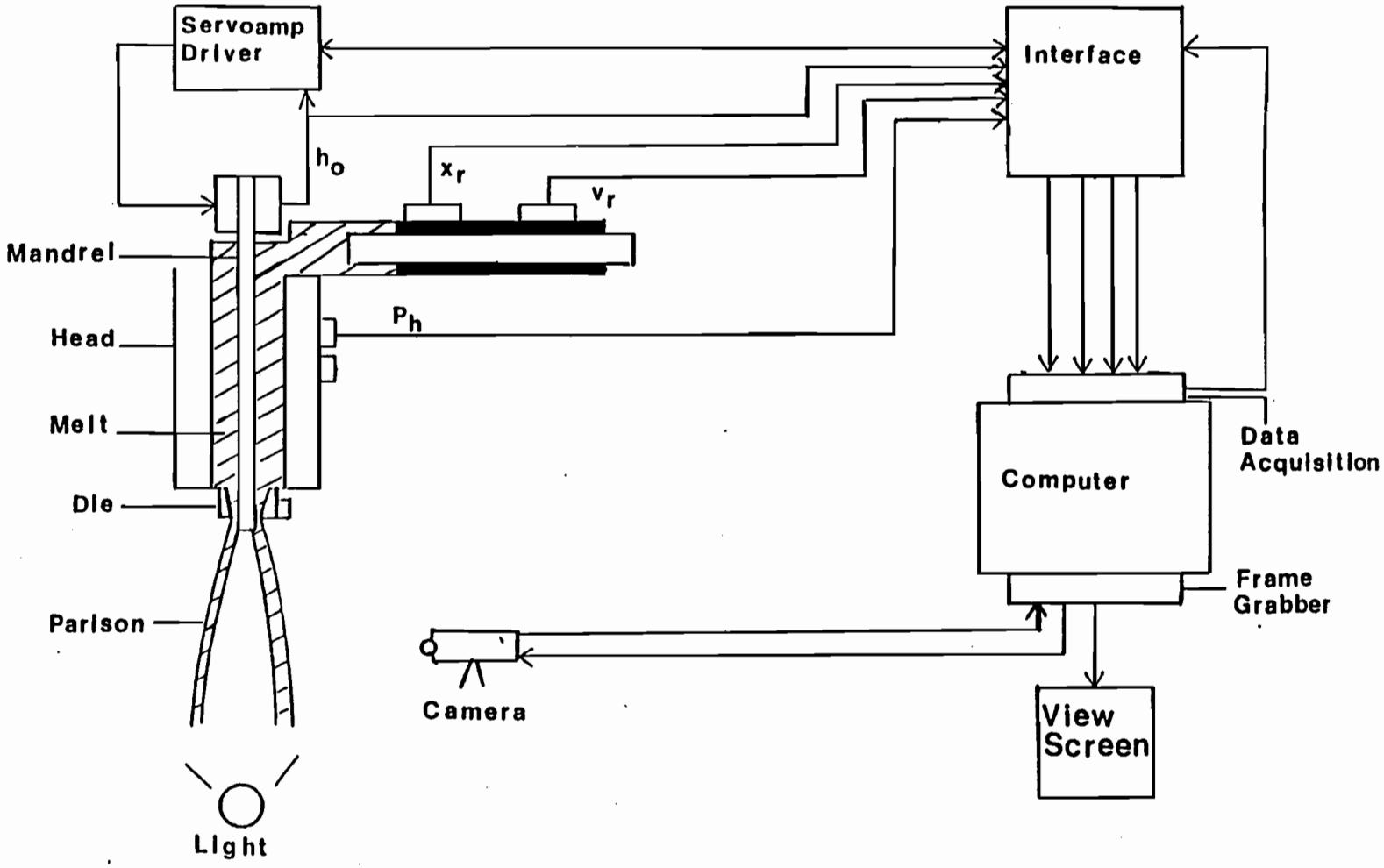

Figure 3.14: Blow Molding Machine-Data Acquisition System

extrusion, for triggering parison photographing, were selected by monitoring the ram travel, and hence the quantity of extrudate. The digital-to-analog (D-A) section of the board was employed to input various gap profiles during the extrusion.

A compatible (IBM-XT) personal computer was employed for data acquisition and video image processing. The computer was also used to calculate the dimension profiles, based on the techniques outlined in Chapter 4, and to achieve the desired control, as outlined in Chapter 5.

3.2.1 VIDEO IMAGE PROCESSING

3.2.1.1 PIXEL OPERATION Incident energy on crystalline silicon causes electrons to move to a higher energy state, whereby the crystals become more conductive. Positively charged electron-hole pairs are left behind by this electron elevation. Solid state image scanners operate on the principle of generation of charge carrier patterns in illuminated silicon crystals (19,70).

The light intensity incident on the silicon crystal is obtained by measuring the concentration of electron-hole pairs. This is most easily achieved by measuring the current which passes between the electrodes from an externally applied electric field.

The field of view is discretized into a two dimensional array of light sensitive picture elements or pixels. Each individual pixel outputs an analog signal directly proportional

to the incident light intensity. Charge output reaches saturation at a certain light intensity (Figure 3.15). The slope of the initial line is the sensitivity of the photodiode.

3.2.1.2 VIDEO CAMERA The image of the parison is focussed onto a matrix array of 384 (H) x 491 (V) pixels. The individual pixel cell size is 0.023 mm (0.000023 m) (H) x 0.0134 mm (0.0000134 m) (V). The array of pixels is located in a Charged Coupled Device (CCD) camera (Figure 3.16). CCD cameras offer several advantages over traditional Vidicon cameras. These include greater accuracy, broader spectral range, smaller size, lower power requirements and solid state ruggedness (19). The CCD camera shifts the charge pattern from point to point across the silicon surface, between depletion regions of positive hole pairs, until it reaches the output terminal (71).

The CCD image scan operates in a line by line, left to right and top to bottom sequence. Interlacing, which entails shifting between even and odd lines for consecutive image scans, is used to obtain a less apparent flicker of a continuous image. Interlacing allows an image updating rate of 66 Hz.

The camera utilized in this work was a Sony XC-38 CCD Video Camera Module (72). The camera lens was a biconvex 16mm (0.016m) focal length type. An Infra-Red filter, supplied with the camera, was mounted to block the IR radiation emitted by the hot parison.

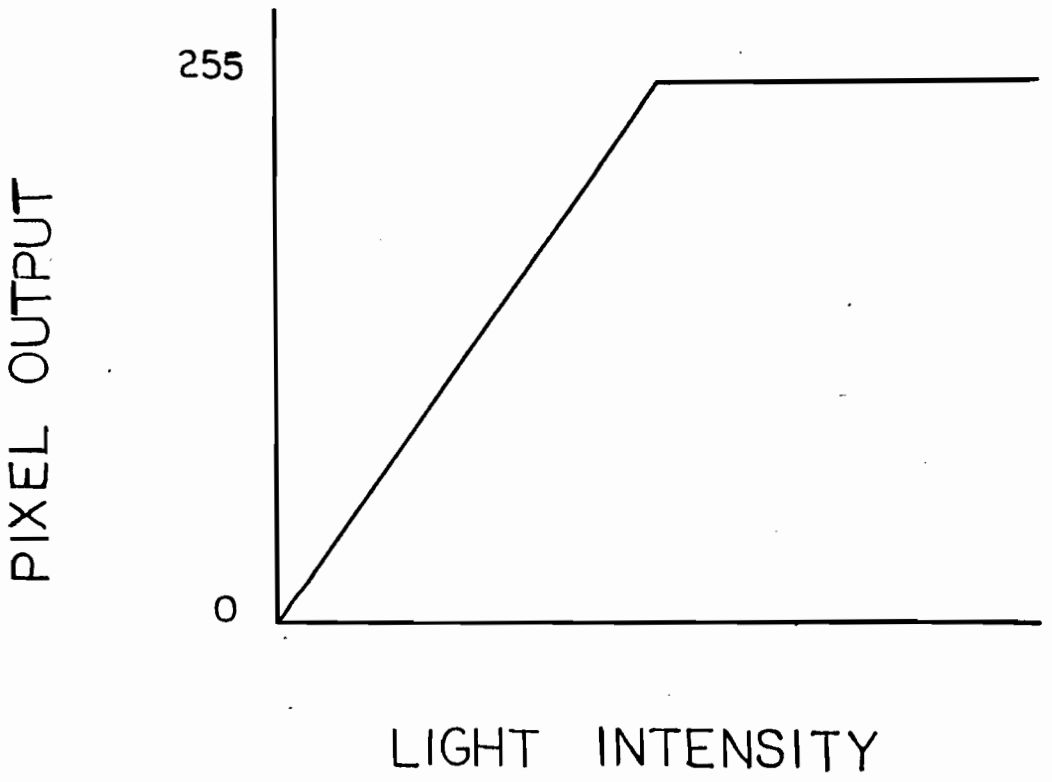

Figure 3.15: Typical Pixel Output Versus Incident Light Intensity.

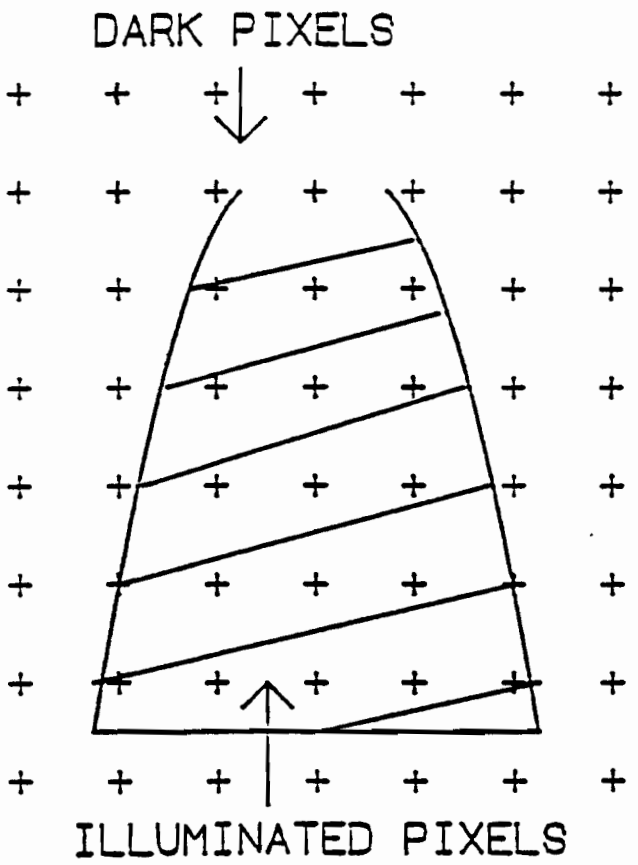

Figure 3.16: Matrix Array of Pixels in Video Camera

A Sony XC-38 Genlock unit is employed to interface the camera serial analog output RS-170 video signal to the horizontal and vertical synchronization signals. The RS-170 video format constitutes the timing and voltage level requirements for standard commercial video signals. Horizontal syncs are utilized to reset the scan to the next horizontal pixel line. Longer duration vertical syncs are employed to reset the scan to the next image (73). These synchronization pulses are necessary to allow the monitor and camera to identify where the sequence is in frame data.

3.2.1.3 ILLUMINATION SCENE Obstructions in the field of view prevented direct photographing of the complete parison. Therefore, a mirror was placed at an angle beneath the parison, in order to obtain an unobstructed view of the whole parison (Figure 3.17). This mirror arrangement required elaborate optical calculations to determine parison dimensions, as discussed in Chapter 4.

Two 250 watt light bulbs were placed behind the parison so that the field of view was flooded with light. This is known as rear illumination (73). A black background, obtained with a black matte finish cardboard, was necessary to enhance the contrast between the parison and the surroundings. High contrast is essential for adequate image resolution (74).

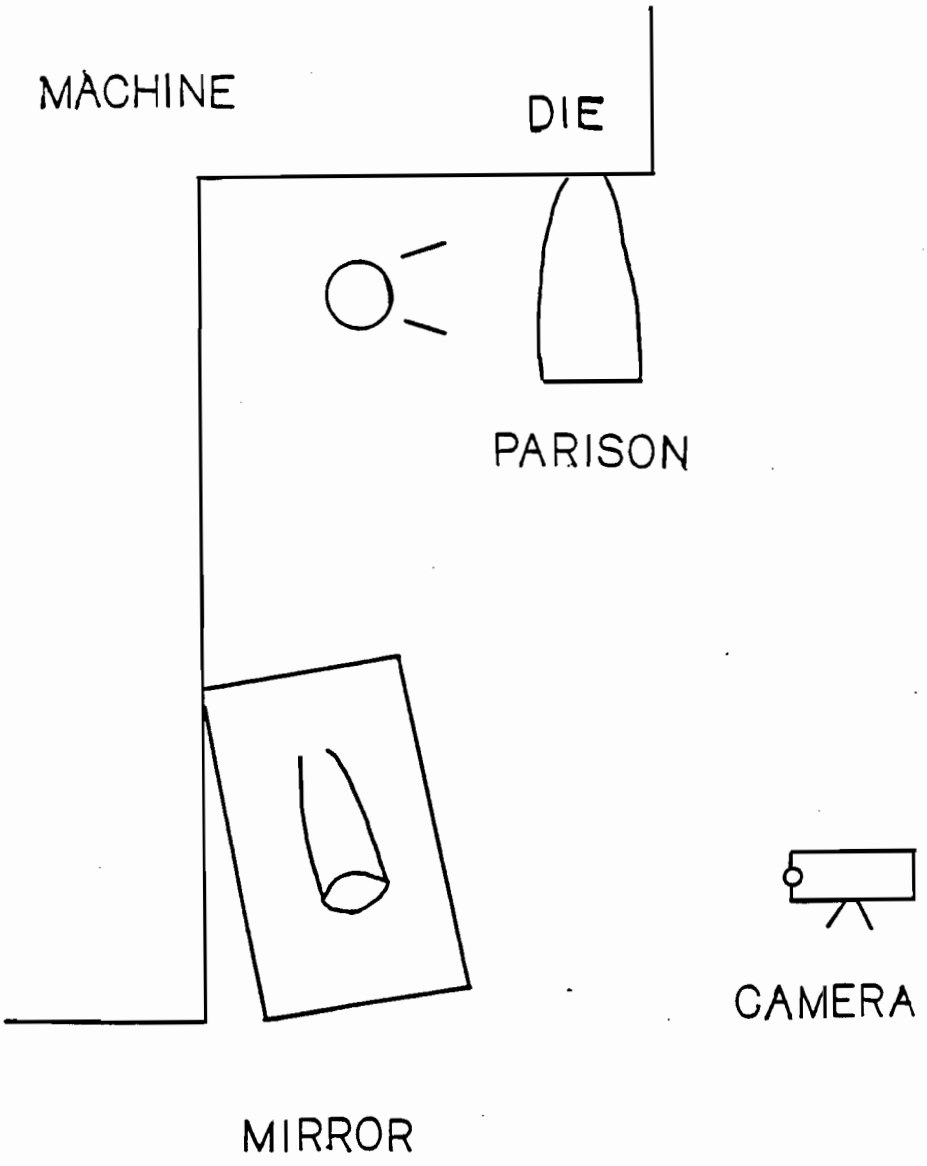

Figure 3.17: Placement of the Mirror at an Angle Beneath the Parison.

Edge detection of a column or row of pixels and the application of the corresponding expansion factors, determined by scenic calibration, yield an accurate estimate of parison length or diameter, respectively. Edge detection involves identification, by software, of the pixel, along the row or column, at which the light intensity increases or decreases sharply (72,74). Edge detection involves scanning a series of pixels to determine which pixels exceed a certain output. An edge is obtained when ten consecutive pixels exceed the threshold. Two edges, along a row or pixel, are necessary for adequate edge detection.

3.2.1.4 FRAME GRABBER BOARD The frame grabber module was used as an interface and storage buffer from the CCD video camera to the host computer. The image stored in the frame memory could be accessed by the microcomputer for image processing and anaysis.

The MATROX PIP 1024 (75), was employed in this work. The system accepts standard RS-170 video signals at a rate of 33 frames/second. The video image is stored in a 512 x 512 x 8 bit frame memory, located on the module itself. The board outputs a RS-170 video signal for image display on an external monitor. The module also provides the necessary horizontal and vertical syncs.

The board digitizes the input series of analog signals, to eight bits of accuracy. This provides a digitization range of 256 possible grey levels. A value of zero corresponds to a

totally black level and a value of 255 corresponds to a saturated white level. Intermediate levels represent varying degrees of grey. This process is known as quantization. Individual pixels can be randomly accessed in one microsecond. This corresponds to 0.25 seconds for the entire frame.

3.2.1.5 MONITOR The monitor used in this work is the Video 100 Monochrome Monitor. Its input is compatible with the RS-170 video signal. Markings on the monitor were used for field of view alignment and reproducibility.

3.2.2 BLOW MOLDING MACHINE

The extrusion blow molding machine used in this study was located at the Novacor Technical Centre in Calgary, Canada. The Impco Molding Machine B13, could be run in both the manual and automatic mode (76).

The clamping mechanism of the machine, consisting of platens and hydraulic oil pipes, blocked the view of the parison. Therefore, the mirror arrangement, mentioned in the previous section was required. The hydraulic pipe was covered in black, since it was a shiny metallic silver colour. It was not possible to operate the video arrangement simultaneously with a clamping mold, such as a pinch-off mold, as the closing clamping mechanism would interfere with the black metallic hydraulic pipe cover.

3.2.2.1 DIE TOOLING The die tooling utilized in this study is shown in Figure 3.18. The tooling is of the converging type with a mandrel converging angle of 63.5 ^{o} with the vertical. The die gap is a direct function of the vertical position of the moveable mandrel. A depth gage on the mandrel is employed to relate the values of absolute gap to the mandrel vertical position and subsequently to the corresponding voltage signal. The die outer diameter is constant at 3.32 cm (0.0332 m), whereas the die inner diameter is dependent on the value of the die gap.

3.2.2.2 MOOG PARISON PROGRAMMER The extrusion blow molding machine is equipped with a Moog Parison Programmer (13). The programmer is equipped with a 20 point gap interpolation set point profile. A typical set point profile, ranging from the top to the bottom of the parison is shown in Figure 3.19. This device operates as an open loop controller. It is normally disconnected when the apparatus developed in this work was in operation.

It is possible to manually control the shot size and the die gap from the control panel. A description of the automatic control of the gap set point profile, is available from the manual of operation (13).

3.2.2.3 PINCH-OFF MOLD A pinch-off mold similar to that employed by Sheptak and Beyer (35) was designed and constructed

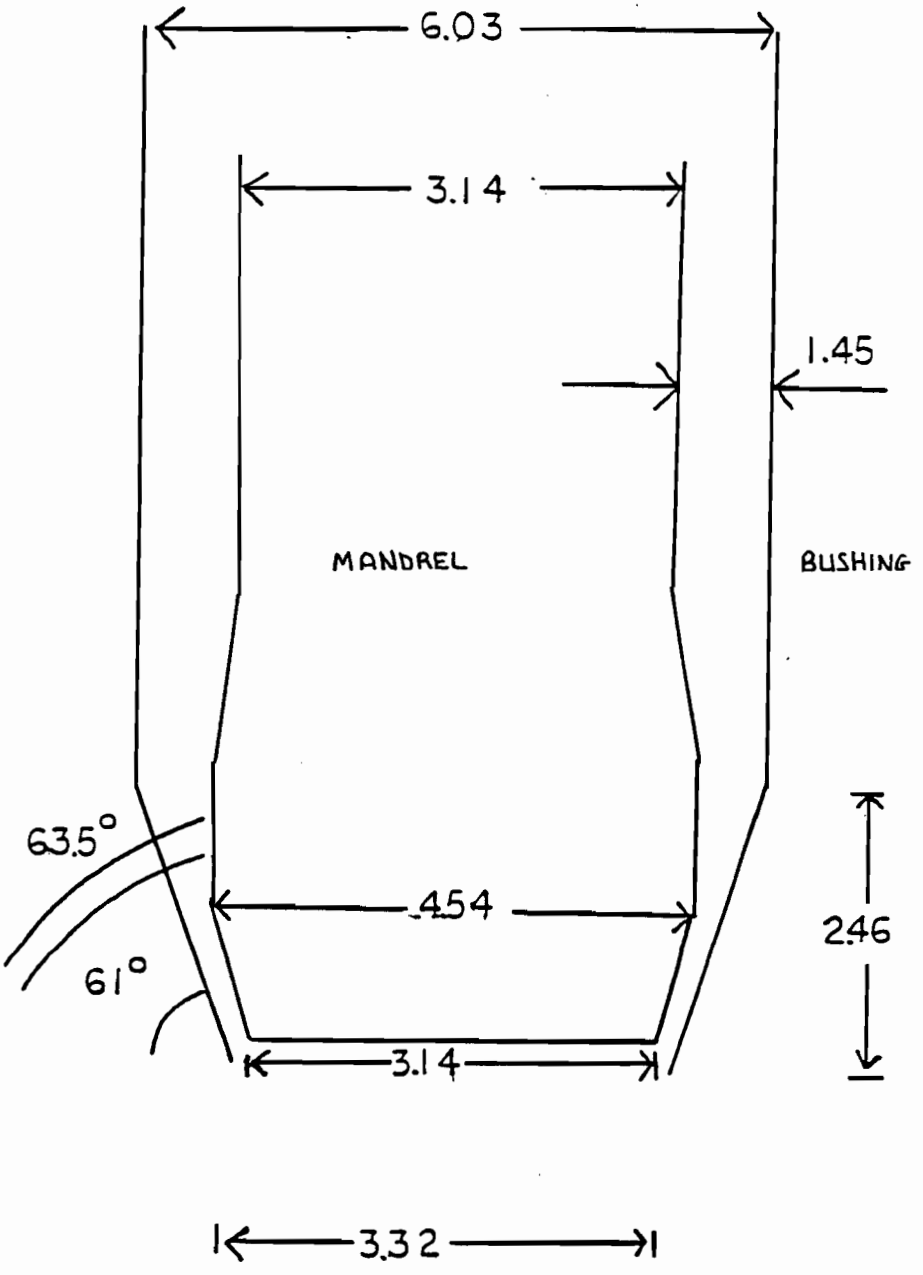

Figure 3.18: Die Tooling (cm)

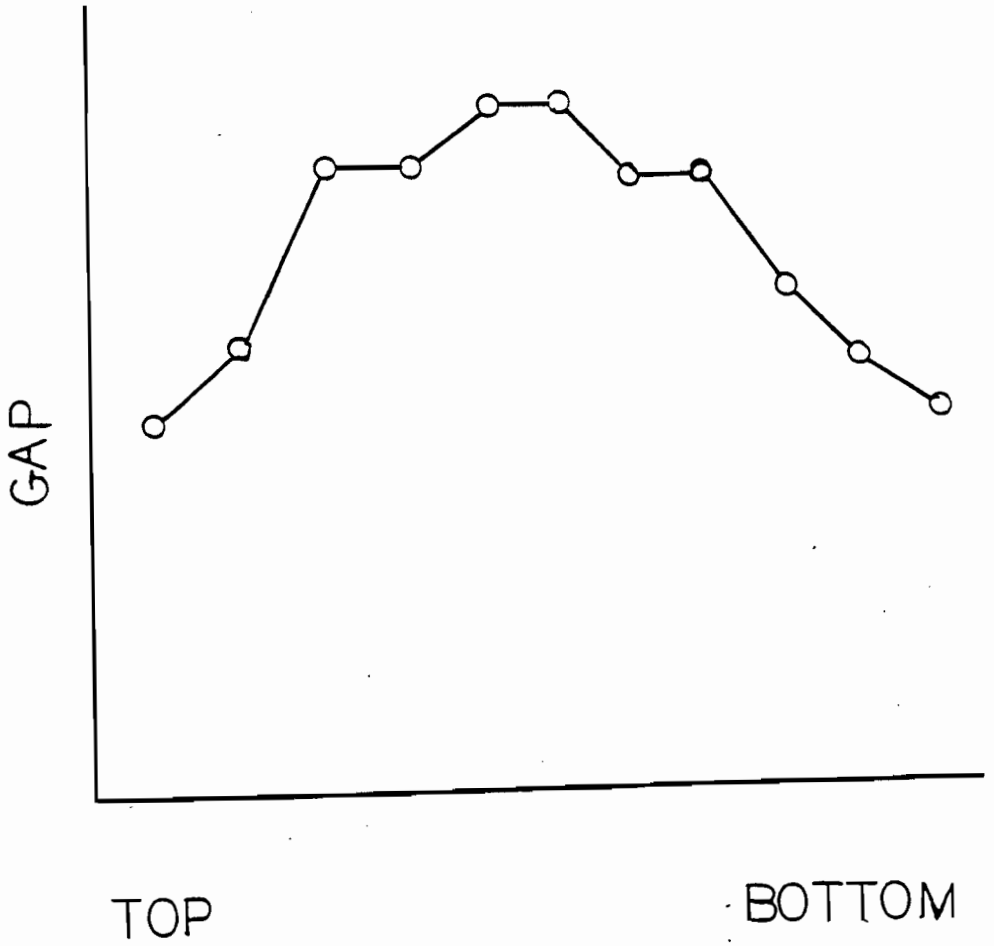

Figure 3.19: Typical Interpolated Thickness Set Point Profile for an Open Loop Parison Programmer.

for this study. The pinch-off mold was utilized for obtaining parison weight distributions. The aluminum mold has eighteen teeth and consequently seventeen pillow shaped segments. The pillows are one inch (.0254 m) long each. The final cooled part is a series of connected pillows representing the parison weight distribution. The parts are cut at the teeth locations and subsequently weighed. Cooling lines in the mold hasten part cooling.

3.2.3 COMPUTER INTERFACING

3.2.3.1 CLOCK A high resolution counter was required for the apparatus, because of the short extrusion times involved. The time of day clock on the multifunction board utilized has a resolution of one ten-thousandth of a second. The computer clock is accessed by reading four input ports.

3.2.3.2 TRANSDUCERS

3.2.3.2.1 PRESSURE TRANSDUCER AND MELT THERMOCOUPLE The die head pressure and melt temperature were monitored with a Dynisco TPT463E Pressure-Temperature Gage (77). The transducer is inserted in the die head itself, with the sensing diaphragm being flush with the inner surface. The maximum allowable pressure is 10000 psi (68948 kPa). The desired melt temperature is obtained by adjusting the zone heater settings.

3.2.3.2.2 VELOCITY TRANSDUCER The ram extrusion velocity was monitored with a Trans-Tek 112-001 Linear Velocity Transducer (78). The transducer operates on the principle of inducing a voltage by moving a magnet through a coil of wire, according to Faraday's and Lenz' Laws. The transducer is physically fixed to the moving ram, so as to move with it.

3.2.3.2.3 RAM POSITION TRANSDUCER A position transducer, supplied with the Moog Parison Programmer (13), is fixed to the ram. Ram position during the extrusion was monitored to determine the quantity of melt extruded during the extrusion.

3.2.3.2.4 GAP POSITION TRANSDUCER Another position transducer, also supplied with the Moog Parison Programmer, is fixed to the mandrel. Mandrel position was monitored so as to know the exact value of the gap at any time during the extrusion. The gap has upper and lower limits. The gap cannot exceed 1.75 mm (0.00175 m), otherwise parison adhesion to the bushing occurs. A gap lower than 0.70 mm (0.00070) is undesirable due to the resultant high head pressures, that can damage the pressure transducer.

3.2.3.3 GAP POSITIONING SERVOVALVE The Moog A076-103 servovalve (13) was utilized to control the flow of oil that subsequently controls the mandrel position and die gap. A negative current to the servovalve moves the mandrel downwards,

thus narrowing the gap, whereas a positive current moves the mandrel upwards, thus enlarging the gap. The servovalve functions in conjunction with the gap position transducer, to exactly set the gap.

3.2.3.4 DIGITAL-ANALOG DATA ACQUISITION BOARD The computer operates in the digital mode, whereas, the process requires analog signals. Therefore, conversions from analog to digital and digital to analog were essential for interfacing between the computer and the process.

A digital-analog data acquisition board was employed for this communication. The board chosen was the Data Translation DT2801 model (79). The module operates at a sampling rate of 13.7 kHz. This board is selected because of its relatively high sampling rate. The input gain is set at one for all the ports. The input voltages to the board must be in the 0-5 volt range. The A/D resolution is 12 bit. The D/A section of the board can output positive and negative signals depending on the requirement.

3.2.3.4.1 TRANSDUCER-BOARD INTERFACING The interface of the computer data acquisition system to the extrusion blow molding machine was designed as part of this work. The analog to digital interface is presented in Figure A4.1 The digital to analog interface is shown in Figure A4.2.

Signals representing the ram position and velocity, gap

position and head pressure enter the interface and are subsequently individually converted so that the input to the computer is in the 0-5 V range. A series of voltage dividers, inverters and amplification circuits are utilized to obtain this goal. A buffer, between the gap position transducer and the computer, is employed to limit the effect of high transducer impedance. A bias circuit is installed to set the zero level of the circuit by eliminating the inherent currents.

The machine, data acquisition board and op-amp power supply grounds must be connected at one point, to eliminate external ground loops from the system. In addition, each transducer return signal is connected through a 10 kohm resistor to the system ground, such that system noise is minimized.

The servoamp driver is required to exactly control the gap. The gap is maintained by means of closed loop control of the mandrel position, employing the servovalve output as the manipulated output. A hardware PID controller in the servovalve driver is used for this purpose. The driver is essential to overcome the effect of servoamp coil resistance variations. Zener diodes are employed in order to limit inadvertent oversignal conditions.

CHAPTER 4

THICKNESS PROFILE ESTIMATION

It is necessary to develop an estimation procedure for the thickness profile, as a direct measurement is not available with the sensor chosen. The proposed estimation procedure consists of two parts. The first part entails the development of a relationship between the length and diameter and the number of illuminated pixels, illuminated in the corresponding axis direction. The second part involves using swell relationships to estimate the thickness profile from measurement of melt flow rate during the extrusion, in conjunction with the diameter and length measurements.

4.1 SCENIC CALIBRATION

Length and diameter calculations were performed by employing expansion factors that were determined by calibration with white cylindrical standards of specified diameter and length. This involves obtaining a general expression relating the measured dimension, P, to the number of illuminated pixels deemed to be above threshold, N, by edge detection. Simplifying assumptions are made in the derivation of this expression, as the final expression is a semi-empirical fit.

Edge detection in the y direction must involve a scan for

the minimum top edge detected pixel and correspondingly, for the maximum bottom edge detected pixel. This is essential, in order to overcome the effect of any parison curling to the left or right.

The optical arrangement, with the mirror placed at angle beneath the parison, is shown in Figure 4.1. The mirror angle of tilt with the vertical is θ and the angle of reflection off the mirror is ϕ. P' is the parison dimension on the mirror and I is the image parison dimension before converging onto the matrix array by passing through a lens. Markings are placed on the viewing monitor to ensure that the field of view and the mirror angle of tilt are reproducible.

4.1.1 MIRROR TRANSFORMATION

The axis, be it length or diameter, must be transmitted from the die, to the mirror. The parison dimension, P, must be related to the reflection of the parison dimension on the mirror, P'. Subscripts x and y correspond to the horizontal and vertical directions, respectively. No subscript relates to the general case. This terminology will be used for various parameters throughout the chapter.

The distance from the field of view, at the die, to the field of view, on the mirror, is depicted as R' (Figure 4.2). The value of R' varies, depending on the specific location of the

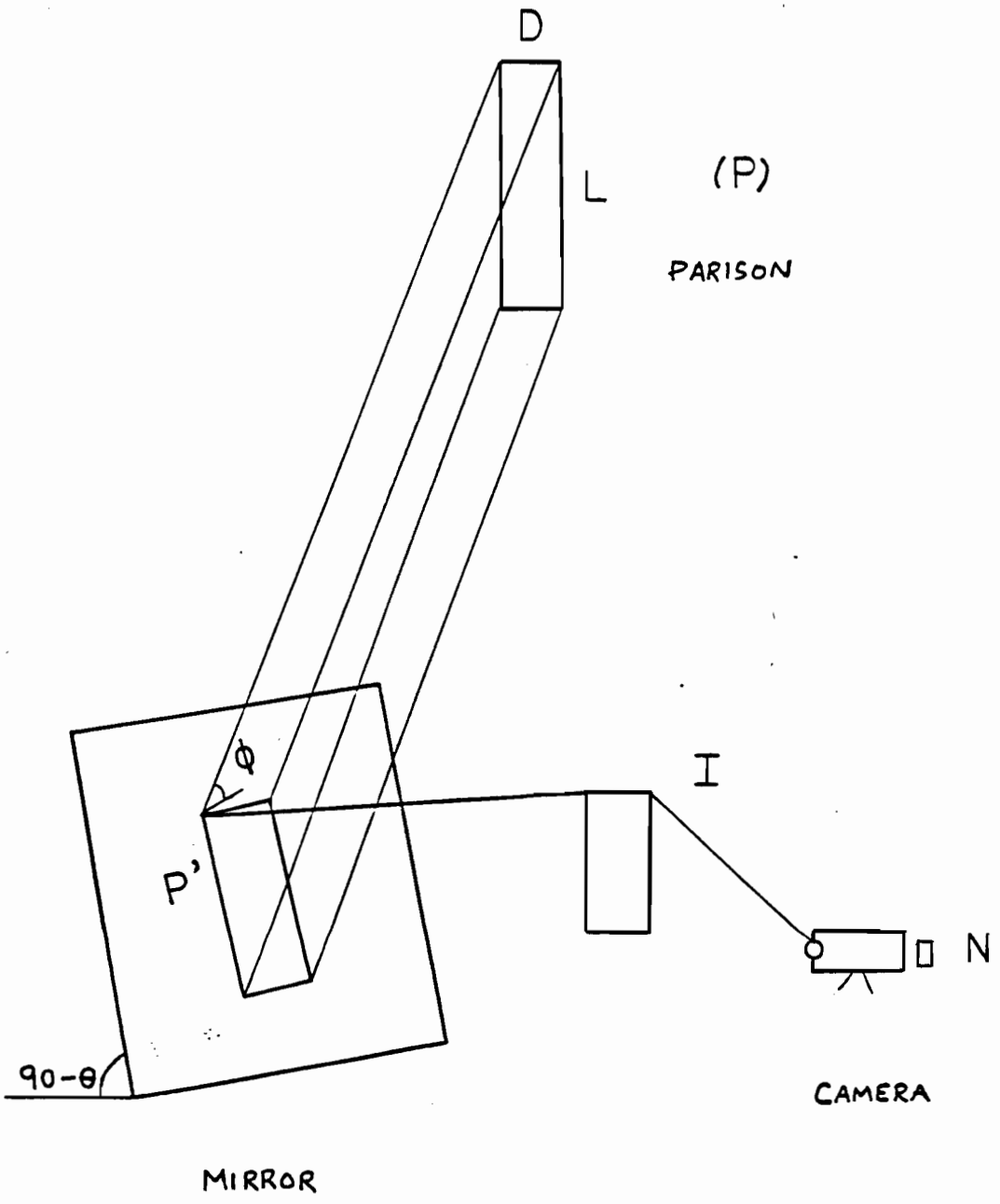

Figure 4.1: Overall Optical Arrangement

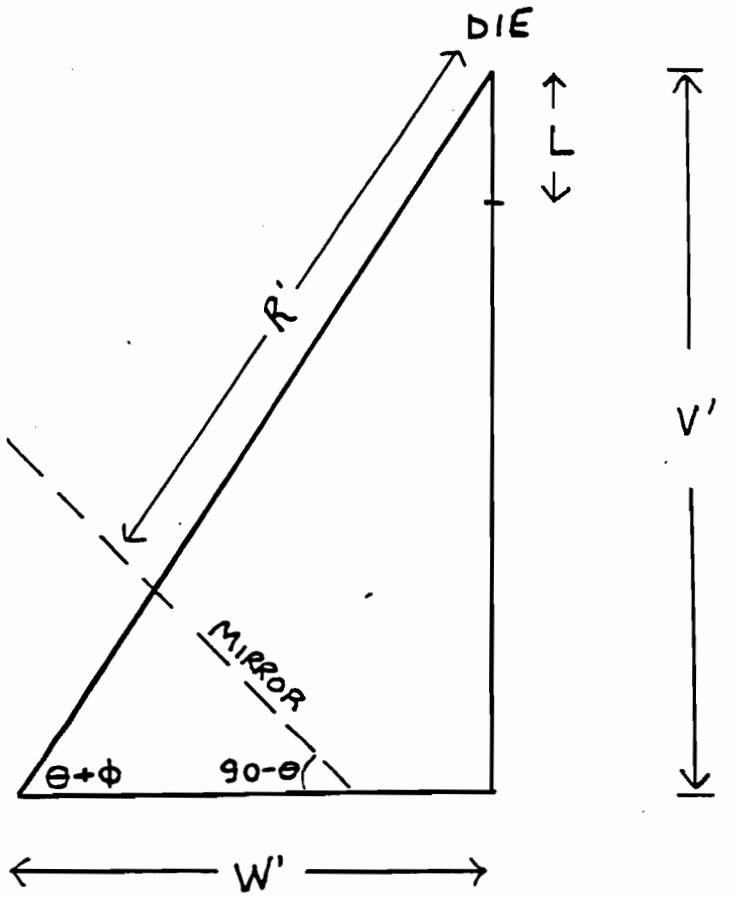

Figure 4.2: Specific Triangle from Overall Optical Configuration.

light ray generation in the die field of view.

According to the law of reflection (80), the angle of incidence equals the angle of reflection (Figure 4.3). The angle of tilt of the mirror, with the vertical, θ, is set at 60^{o}. The angle of reflection, ϕ, and, consequently, the value R', should be functions of the position of the light source at the die field of view.

It is shown below that the angle of reflection, along the field of view, in the diameter and length directions, remains relatively constant. The vertical distance between the camera and the die, straight down, V' (1.2 m), is much greater than both the distance, W' (0.2 m) defined in Figure 4.2, and the length of the parison, L. The reflection angle, ϕ, is given by

$$\tan(\theta + \phi) = \frac{V' - L}{W'} \qquad (4.1)$$

Therefore, the value of ϕ, will remain relatively constant over typical parison lengths of 30 cm (0.3 m). A good estimate for ϕ, is 18^{o}. This assumption is valid to within 2^{o}, for the worst case of the length axis and a 40 cm (0.40 m) separation between light ray sources.

The conclusion that all light rays from the field of view are parallel, in the specific x or y axis, stems from the assumption of constant reflection angle. This assumption of

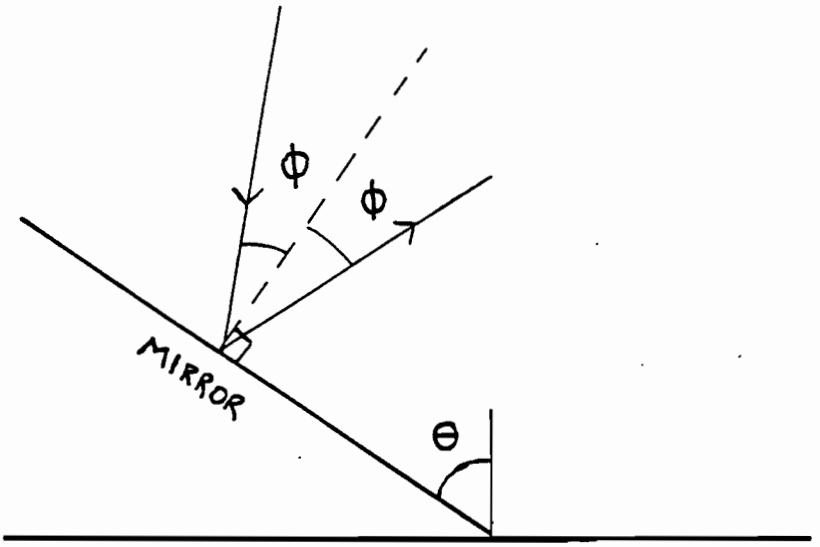

Figure 4.3: Law of Reflection

parallel light rays allows for the formation of the expanded triangle in Figure 4.4.a. The vertical distance between the two parallel lines is constant. The triangle has sides P, P' and P''. The value of P represents the axis dimension at the die, and the value P' represents the transformed axis dimension at the mirror.

The expanded triangle can be subdivided into two right angle triangles as shown in Figure 4.4.b. The axis dimension, P, is broken up into the individual triangle sides P_1 and P_2 such that

$$P = P_1 + P_2 \tag{4.2}$$

Simple trigonometry yields,

$$P_2 = P'\cos\theta \tag{4.3}$$

$$S = P'\sin\theta \tag{4.4}$$

$$S = \frac{P_1}{\tan(\theta + \phi)} \tag{4.5}$$

Substitution of Equation (4.5) into Equation (4.4) yields

$$P_1 = P'\sin\theta\tan(\theta + \phi) \tag{4.6}$$

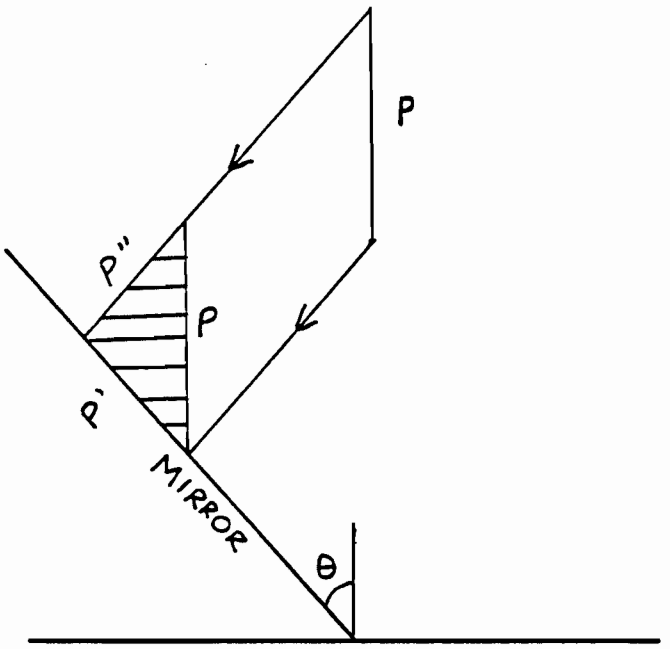

Figure 4.4a: Mirror Transformation of Field of View.

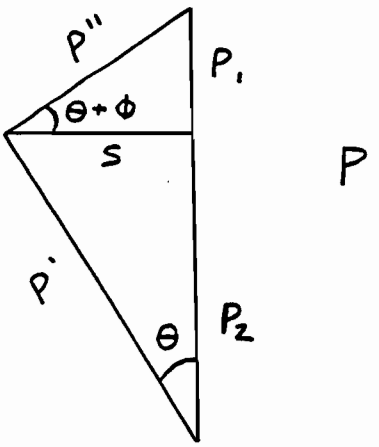

Figure 4.4b: Expansion of Shaded Triangle

Substitution of Equation (4.6) and (4.3) into (4.2) yields

$$P = P'[\sin\theta\tan(\theta + \phi) + \cos\theta] \qquad (4.7)$$

4.1.2 CAMERA FIELD OF VIEW

It is necessary now to transform the field of view of the mirror to the camera field of view (Figure 4.5a). The light rays maintain their parallel nature, as they are reflected off the mirror at equal reflection angles, ϕ. The image of the specific axis, is represented by I. The parison dimension in die area will be related to the image parison dimension. The enlargement of the shaded triangle results in Figure 4.5b. The image axis dimension, I, can be separated into two components, such that,

$$I = I_1 + I_2 \qquad (4.8)$$

Simple trigonometry yields:

$$I_2 = P'\cos\theta \qquad (4.9)$$

$$I_1 = P'\sin\theta\tan(\theta - \phi) \qquad (4.10)$$

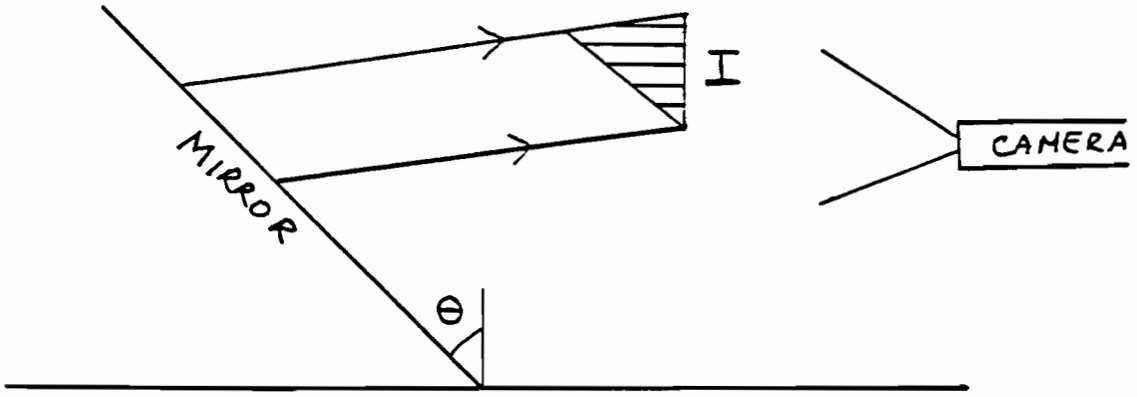

Figure 4.5a: Camera Transformation of Field of View.

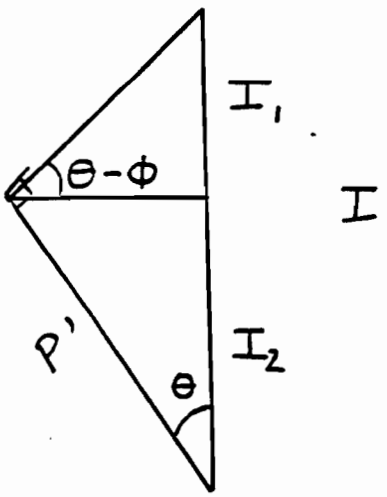

Figure 4.5b: Expansion of Shaded Triangle.

Therefore, substitution of Equations (4.10) and (4.9) into (4.8) yields

$$I = P'[\sin\theta\tan(\theta - \phi) + \cos\theta] \qquad (4.11)$$

Substitution of Equation (4.11) into Equation (4.7) yields

$$P = I \left\{ \frac{\sin\theta\tan(\theta + \phi) + \cos\theta}{\sin\theta\tan(\theta - \phi) + \cos\theta} \right\} \qquad (4.12)$$

Since the values of θ and ϕ are constant and specified by the optical arrangement, Equation (4.12) may be rewritten as follows.

$$P = (I)(F) \qquad (4.13)$$

where F is a trigonometric constant with a value of approximately 3.6, for $\theta = 60^{o}$ and $\phi = 18^{o}$.

4.1.3 ARRAY TRANSFORMATION

The camera field of view must now be transmitted to the matrix array of the CCD camera. Two situations arise, corresponding to the individual x and y axes.

The resolution of the array is defined as (73)

$$R = \frac{I}{N} \qquad (4.14)$$

where N represents the number of illuminated pixels.

The resolution is relatively constant for the case of diameter, as the parison tends to be centered in the field of view, along this axis. However, the resolution tends to vary along the parison length, as (i) it is not centered in the image field of view, and (ii) the final parison length is greater than the parison diameter, thus more likely to exhibit deviations in the reflection angle.

A typical lens demagnification of an image is shown in Figure 4.6. The distance from the object to the lens is O_c, whereas the distance from the camera image to the lens is i_c. The camera image height and the object height are i and I, respectively. The lens focal length is f. It is known that, for a thin converging lens (80),

$$\frac{1}{f} = \frac{1}{O_c} + \frac{1}{i_c} \qquad (4.15)$$

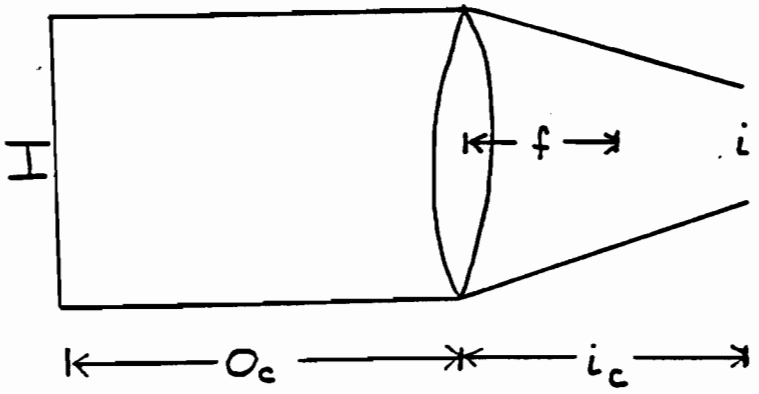

Figure 4.6: Lens Demagnification

The demagnification of the lens, M is

$$M = \frac{O_c}{i_c} = \frac{I}{i} \qquad (4.16)$$

Substitution and rearrangement yields

$$M = \frac{O_c}{f} - 1 \approx \frac{O_c}{f} \qquad (4.17)$$

It is known that for solid state image scanners (78),

$$M = \frac{R}{E} = \frac{I}{NE} = \frac{P}{FNE} \qquad (4.18)$$

where E is the pixel element spacing in the corresponding axis direction. Substitution into Equation (4.18) yields a value of 17 for M. This confirms the assumption of Equation (4.17). Therefore, substitution of Equation (4.18) into (4.17) and rearrangement yields

$$I = \frac{NEO_c}{f} \qquad (4.19)$$

The two axis directions will now be considered separately.

4.1.3.1 CASE 1: LENGTH It is necessary to relate the parison length, L, to the number of illuminated pixels in the corresponding axis direction. The transformation from the image to the camera is depicted in Figure 4.7, for the case of the y axis. It can be assumed that the image length is completely in the top half of the field of view of the camera. The complete length direction field of view, at the die, is (0.60 m). Typical parison lengths are generally less than 0.30 m. It can be seen from Figure 4.7, that O_{CY} varies with I_y such that

$$O_{CY} = [A_y^2 + (T_y - I_y)^2]^{1/2} \qquad (4.20)$$

where A_y represents the distance from the camera to the parison image. Substitution of Equation (4.20) into (4.19) and squaring both sides yields,

$$I_y^2 = (E_y N_y/f)^2[A_y^2 + (T_y - I_y)^2] \qquad (4.21)$$

Combining common power terms of I_y, results in a quadratic type equation.

$$0 = [(E_y N_y/f)^2 - 1]I_y^2 - [2T_y(E_y N_y/f)^2]I_y + (E_y N_y/f)^2(A_y^2 + T_y^2) \qquad (4.22)$$

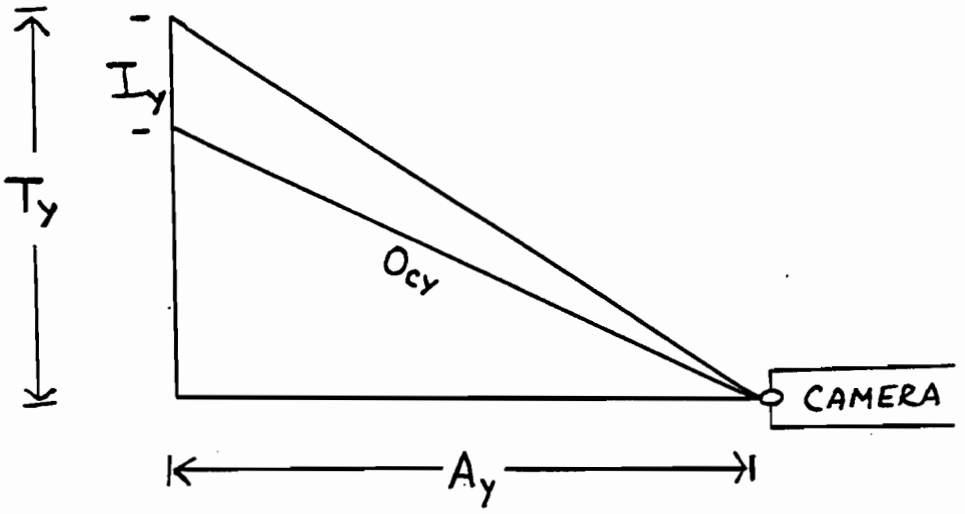

Figure 4.7: Array Transformation of Field of View: Length

For this specific solid state scanner

$$(EN/f)^2 \ll 1 \qquad (4.23)$$

Therefore

$$0 = I_y^2 + [2T_y(E_yN_y/f)^2]I_y - (E_yN_y/f)^2(A_y^2 + T_y^2) \qquad (4.24)$$

Solving for the quadratic yields

$$I_y = -T_y(E_yN_y/f)^2 + [T_y^2(E_yN_y/f)^4 + (E_yN_y/f)^2(A_y^2 + T_y^2)]^{1/2} \qquad (4.25)$$

It can be inferred, from Equation (4.23) that

$$(E_yN_y/f)^2(A_y^2 + T_y^2) \gg (E_yN_y/f)^4T_y^2 \qquad (4.26)$$

Therefore

$$I_y = -(T_yE_y^2/f^2)N_y^2 + ((E_y/f)(A_y^2 + T_y^2)^{1/2})N_y \qquad (4.27)$$

Substitution of Equation (4.13) into Equation (4.27) yields

$$L = -(T_yE_y^2F/f^2)N_y^2 + ((E_yF/f)(A_y^2 + T_y^2)^{1/2})N_y \qquad (4.28)$$

which is of the form,

$$L = a_0 N_y^2 + b_0 N_y + c_0 \qquad (4.29)$$

Equation (4.29) is employed to determine the scan locations for diameter. The coefficients of Equation (4.29) are obtained by employing white cylindrical standards in conjunction with a trial and error procedure that involves drawing lines , with software, on the monitor, at different pixel scan locations, X. This procedure determines the exact pixel location of the bottom of the cylinder.

Equation (4.29) cannot be used to measure absolute parison lengths, as the interior of the parison near the bottom causes the illumination of more pixels than the number corresponding to the true parison length. This " droop effect ", is directly related to the diameter at the bottom of the parison (Figure 4.8). This diameter is obtained by scanning for the maximum diameter in the bottom area of the parison, D_{max}.

The extra length illuminated in the mirror field of view is L'_b. The extra length in the die field of view is L_b. A similar trigonometric approach to that performed on the absolute length yields the following.

$$D_1 = L'_b \sin\theta \qquad (4.30)$$

$$D_2 = L'_b \cos\theta \tan(90 - \theta - \phi) \qquad (4.31)$$

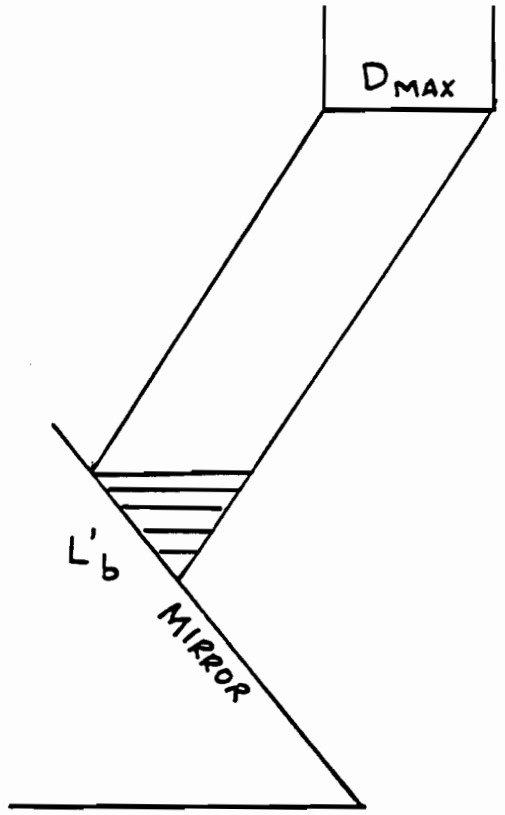

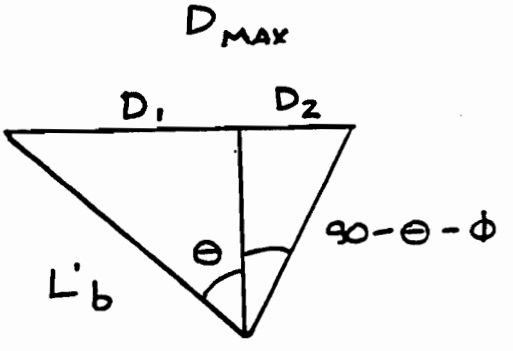

Figure 4.8: Droop Effect

$$D_{max} = L'_b[\sin\theta + \cos\theta\tan(90 - \theta - \phi)] \qquad (4.32)$$

Substitution of Equation (4.7) into (4.32) yields

$$L_b = D_{max}\left\{\frac{\sin\theta\tan(\theta + \phi) + \cos\theta}{\cos\theta\tan(90 - \theta - \phi) + \sin\theta}\right\} \qquad (4.33)$$

Introducing a constant trigonometric factor, F', such that

$$F' = \frac{\sin\theta\tan(\theta + \phi) + \cos\theta}{\cos\theta\tan(90 - \theta - \phi) + \sin\theta} \qquad (4.34)$$

yields

$$L_b = (F')(D_{max}) \qquad (4.35)$$

Substitution of Equation (4.28) into Equation (4.35) yields

$$-(T_y E_y^2 F/f^2)N_b^2 + (E_y F/f)(A_y^2 + T_y^2)^{1/2}N_b = F'D_{max} \qquad (4.36)$$

The assumption of linear resolution over L_b is acceptable since, L_b is much smaller than the parison length, L, and L_b is closer to the center of the camera field of view, thus avoiding the non-constant resolution over the length.

Therefore,

$$N_b = \frac{F' D_{max} f}{E_y F (A_y^2 + T_y^2)^{1/2}} \qquad (4.37)$$

The total number of illuminated pixels is depicted by N_t and the actual number of pixels corresponding to the length is represented by N_y.

Therefore,

$$N_y = N_t - N_b \qquad (4.38)$$

Substitution of Equations (4.38) and (4.37) into Equation (4.28), yields an equation of the form

$$L = a_1 N_t^2 + b_1 D_{max} N_t + c_1 D_{max}^2 + d_1 N_t + e_1 D_{max} + f_1 \qquad (4.39)$$

where

$$a_1 = - \frac{T_y E_y^2 F}{f^2} \qquad (4.40)$$

$$b_1 = \frac{2T_y E_y F'}{f(A_y^2 + T_y^2)^{1/2}} \qquad (4.41)$$

$$c_1 = -\frac{T_y F'^2}{F(A_y^2 + T_y^2)} \qquad (4.42)$$

$$d_1 = \frac{E_y F(A_y^2 + T_y^2)^{1/2}}{f} \qquad (4.43)$$

$$e_1 = -F' \qquad (4.44)$$

$$f_1 = 0 \qquad (4.45)$$

The last coefficient is required, since a multiple regression routine is used to obtain the best fit to Equation (4.39). Data are fit to this equation and the results are presented in Chapter 5. The terms DN_t and D^2 tend to be insignificant in comparison with the other terms. This is expected since

$$(A^2 + T^2)^{1/2} \gg T \qquad (4.46)$$

Therefore the final form of the equation for length prediction from the number of illuminated pixels is

$$L = a_2 N_t^2 + b_2 N_t + \beta c_2 D + d_2 \qquad (4.47)$$

where the subscript 2 implies that the constants are different from those in Equation (5.39).

The factor β is necessary in order to account for curl at the bottom of the parison. Parison curl is caused by the unsteady flow at the beginning of extrusion since the polymer melt in the die is allowed to relax for the period between cycles. Curling causes deviations from the cylindrical approximation in the first extruded segment. Thickness measurements are therefore unreliable in the first extruded segment.

The factor β depends on the resin, injection rate and gap and is generally in the range 0.95-1.0. The factors were obtained by using Equation (4.47) and equating lengths measured with the pinch-off mold to camera lengths measured with a one second delay after extrusion.

4.1.3.2 CASE 2: DIAMETER The same procedure can now be applied to the diameter axis direction. It is reasonable to assume that the camera bisects the parison, in the case of diameter visualization (Figure 4.9). The resolution is linear along the diameter, which is centered in the field of view.

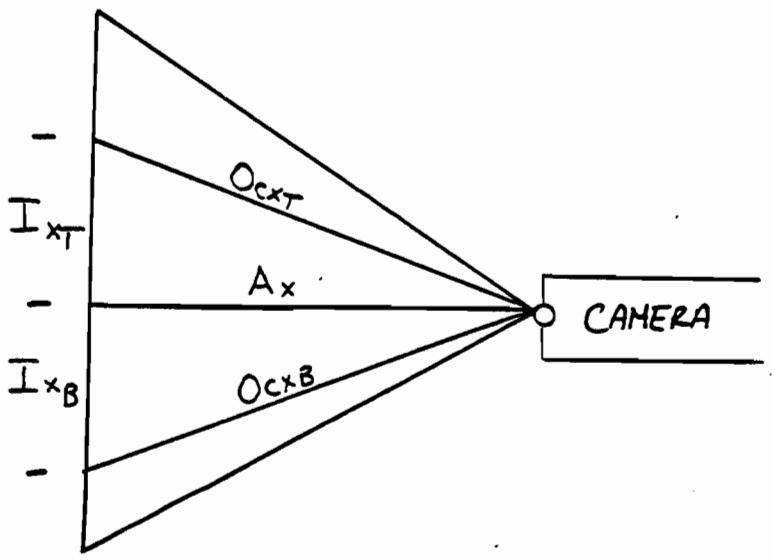

Figure 4.9: Array Transformation of Field of View: Diameter

Generally, the diameter of the parison is significantly smaller than the parison length. In the case of the top triangle,

$$I_{XT}^2 + A_X^2 = O_{CXT}^2 \qquad (4.48)$$

Substituting Equation (4.19) into Equation (4.48) and rearranging yields

$$0 = \left(\frac{N_{XT}^2 E_X^2}{f^2} - 1\right) I_{XT}^2 + \frac{N_T^2 E_X^2 A_X^2}{f^2} \qquad (4.49)$$

It has been established that

$$\left(\frac{NE}{f}\right)^2 \ll 1 \qquad (4.50)$$

Therefore

$$I_{XT} = \frac{N_{XT} E_X A_X}{f} \qquad (4.51)$$

Similarly for the bottom triangle,

$$I_{XB} = \frac{N_{XB} E_X A_X}{f} \qquad (4.52)$$

Addition of Equations (4.51) and (4.52) and subsequent substitution into Equation (4.13) yields

$$D = \left(\frac{E_X A_X F}{f} \right) N_X \qquad (4.53)$$

The value of A_X is directly dependent on the pixel diameter scan location, X, which is determined from Equation (4.29).

$$L = a_o X^2 + b_o X + c_o \qquad (4.29)$$

$$A_X = \{ A_{Xo}^2 + (a_o X^2 + b_o X + c_o)^2 \}^{1/2} \qquad (4.54)$$

A_{Xo} is a constant and represents the centerline distance from the camera to the image of the parison. Expansion of the terms and completion of the square of Equation (4.54) results in an equation of the form

$$A_X = a_3 X^2 + b_3 X + c_3 \qquad (4.55)$$

Substitution of Equation (4.55) into (4.53) yields

$$D = a_3 X^2 N_X + b_3 X N_X + c_3 N_X + d_3 \qquad (4.56)$$

The constants in Equations (4.29), (4.47) and (4.56) are estimated by fitting 100 data points, using a multiple regression

routine, as shown in Chapter 5. The correlation coefficient in each case is very close to unity. The purpose of the above procedure is to determine a form of the desired expression, so that the coefficients can be estimated by the appropriate equation fit.

4.2 THICKNESS PROFILE ESTIMATION

Now that the parison diameter profiles and total lengths can be estimated, the subsequent step involves the estimation of the thickness profile. Monitoring the ram travel during extrusion allows the parison to be divided into equiweight segments, (assuming constant density) of weight W(i). The segment nearest to the die corresponds to i=1, and downstream segments along the parison length correspond to higher values of i. If the segments are assumed to be cylindrical, then the weight of each segment is given by

$$W(i) = \pi\rho L(i)h(i)[D(i) - h(i)] \qquad (4.57)$$

where ρ is the melt density, h the segment thickness, L the segment length and D the segment outer diameter.

If

$$D(i) \gg h(i) \tag{4.58}$$

then

$$W(i) = \pi\rho L(i)h(i)D(i) \tag{4.59}$$

Assuming that the diameter and thickness swell vary exponentially with time and neglecting sag yields (38)

$$B_S = B_{S\infty} - (B_{S\infty} - B_{S0})\exp(t/\delta_S) \tag{4.60}$$

where $B_{S\infty}$ refers to equilibrium swell at long time and δ_S is a characteristic swell time. The subscript S refers to diameter when S = 1 and thickness when S = 2. For short extrusion times, much less than the characteristic time, one obtains

$$B_S = B_{S0}\exp(t/\delta_S) \tag{4.61}$$

The diameter and thickness swell along the length of the parison were defined in Chapter 2 as follows:

$$B_1(i) = D(i)/D_o \qquad (2.2)$$

$$B_2(i) = h(i)/h_o \qquad (2.3)$$

Substitution of Equations (2.2), (2.3) and (4.61) into (4.59) and rearranging yields

$$L(i) = \frac{W(i)\exp[-t(i)/\epsilon(i)]}{\pi\rho B_{12}(i)h_o(i)D_o} \qquad (4.62)$$

where

$$\epsilon(i) = \frac{\delta_1\delta_2}{(\delta_1 + \delta_2)} \qquad (4.63)$$

$$B_{12}(i) = (B_{1o})(B_{2o}) \qquad (4.64)$$

and the individual segment suspension times are t(i). The outer die diameter is constant throughout the extrusion.

A similar analysis can be performed for equilength segments (element 1 instead of i) yielding

$$W(1) = \pi\rho h_o(1)L(1)D_oB_{12}(1)\exp[t(1)/\epsilon(1)] \quad (4.65)$$

Note that both equiweight length segments and the equilength weight segments vary exponentially with time during the extrusion.

A set of constant gap extrusions, performed at (five) different die gaps, gives values for ϵ and B_{12} at each of these gaps. This set of extrusions is referred to as a gap scan. The total parison length is measured at the end of extrusion , L_E, and with a one second delay after the end of extrusion, L_D. Neglecting the effect of sag, the length varies exponentially with time according to

$$L_D = L_E\exp(-1/\epsilon_T) \quad (4.66)$$

Cotten (17,18), as indicated in Chapter 2, observed that swell consisted of instantaneous and much slower relaxation components. It is reasonable, therefore, to assume that the rate of relaxation of the total parison, ϵ_T, is the same as the rate of relaxation of the individual segments, $\epsilon(i)$, as a first approximation. This assumption is valid only if the contribution of relaxation of the top segment to the total parison length is small. Values of ϵ are thus obtained from

Equation (4.66).

The above approximation is not valid for the segment nearest to the die, as this is the region of the instantaneous relaxation. The majority of the relaxation occurs in this segment. However, since this area is normally pinched by the mold, the exclusion of this segment from the analysis does not interfere with the accuracy, in relation to the ultimate goal of bottle dimension profile control. Additionally, parison diameter measurements in the first segment are not dependable because of the high variation of diameter with scan location in this area of the parison.

The value of B_{12} is obtained from the equation

$$B_{12} = \frac{\Sigma W(i)\exp[-t(i)/\epsilon]}{\pi\rho L_E h_o D_o} \qquad (4.67)$$

Values for B_{12} and ϵ are obtained by linear interpolation, for gap values different from those in the gap scan, When a step in the gap occurs, the values for B_{12}, ϵ and h_o of the transition gap , V(i), are a time weighted average of the values, V_1 and V_2, at the two gap values in the step. Therefore,

$$V(i) = \frac{V_2*[t(i) - 0.05] + (V_1 + V_2)*(0.05)/2}{t(i)} \qquad (4.68)$$

where V(i) represents the traditional value of the parameter of interest (B_{12}, ϵ or h_o) during the step. The time for the step

is 0.05 seconds in all cases, independent of the step magnitude, direction or initial gap value.

Now, the length of the individual segments can be obtained by utilizing Equation (4.62). A noise factor, α, is utilized to account for variations that occur from experiment to experiment. System noise entering the process is more likely to affect the entire parison rather than the individual segments. A drift entering the process will remain for the entire extrusion, as the time of extrusion is relatively short in comparison to the cycle time. The factor α is defined as follows

$$\alpha = \frac{L_E}{\Sigma\, L(i)} \qquad (4.69)$$

where L_E is measured during the specific extrusion. The factor α, which is usually in the range 0.95 to 1.05, is required to specify the exact diameter scan locations during a given extrusion. When α deviates from the above range, the gap scan is repeated to obtain B_{12} and ϵ at each of the five gaps. The length segments are adjusted according to

$$L(i) = (\alpha)*[L(i)] \qquad (4.70)$$

The diameter profile, D(i), at the identified scan locations is now available. Substituting Equations (4.70) and (4.62) into (4.57) yields

$$\left\{\frac{\alpha \exp[-t(i)/\epsilon(i)]}{B_{12}(i)h_o(i)D_o}\right\}h(i)[D(i) - h(i)] - 1 = 0 \quad (4.71)$$

Solving the quadratic, for h(i), provides an estimate of the desired parison thickness profile.

CHAPTER 5

RESULTS AND DISCUSSION

This chapter consists of two parts. The first part deals with machine characteristics and parison dimension profile measurements. It seeks to obtain an understanding of the response of the blow molding machine to changes in operating variables. This part also demonstrates the validity and accuracy of the parison thickness profile estimation technique. The second part deals with dynamics and on-line control of parison thickness profiles. It includes a treatment of the dynamic responses of the thickness profile and evaluates the proposed control strategy.

Software was written for the various segments of the work. Fortran was the language of choice because of its speed, simplicity and compatibility to the vision, data acquisition and clock software available. The software for the individual experimental sets is not presented, but is available upon request.

Generally, the experiments were run at the following median conditions:

Melt Temperature: 200°C
Shot Size Setting: 4
Injection Valve Setting: 1.25
Gap: 1.25 mm

Variation on these values are reported as they occur.

5.1 MACHINE CHARACTERISTICS AND PARISON DIMENSION MEASUREMENTS

5.1.1 LENGTH AND DIAMETER VS NUMBER OF ILLUMINATED PIXELS

White acrylic cylinders were employed for scenic calibration. The standard dimensions were chosen in order to correspond to typical parison dimensions during extrusion. The cylinders were 40, 30, 20, 10 and 5 cm. in length. The diameters of the cylinders were 5.08, 7.62 and 10.16 cm.

The standards, simulating parisons, were placed with the diameter centered over the mandrel and flush with the bushing. The cylinders were suspended from this position, supported with copper wire, and were illuminated with the 250 W light sources. This procedure was employed with the blow molding machine in the off mode.

It was essential to reproduce the field of view at all times. The mirror angle of tilt was reproduced with markings on the floor and on the mirror vertical support on the blow molding machine. The angle of reflection was reproduced with markings on the viewing monitor, representing the center of the mandrel and the outer boundary of the field of view. A black cardboard border was placed on the field of view of the mirror to coincide with the monitor markings. The field of view alignment utilized the continuous mode of imaging, in software referred to as CONT.

The number of illuminated pixels, in the two directions (length and diameter) and at any specified scan location was

determined with edge detection software called EDGE. The number of illuminated pixels returned by the EDGE routine must be zero, when no standard is placed in the field of view. This is attained by employing a black matte background.

The coefficients for Equation (4.29) (Table 5.1) were fit by a trial and error procedure. The procedure consisted of drawing lines at various vertical locations on the monitor, until the line coincided with the bottom of the cylinder. The bottom of the cylinder was identified by the point where the droop effect commences. The diameter scan locations were obtained from Equation (4.56). Equations (4.47) and (4.56) were subsequently fit, using the EDGE routine. More than one hundred data points were fit to each of the three equations. The factor, β, is unity for the standards, as they do not curl inwards, in the way parisons do. The fit coefficients and the correlation coefficients, for each of the three equations, are presented in Table 5.1. The specific dimensions are in units of centimeters.

5.1.2 MACHINE VARIABLES

5.1.2.1 SIMPLE MACHINE RELATIONSHIPS

At the outset, it is desirable that the simple process variables, such as shot weight, hydraulic pressure, melt flowrate

TABLE 5.1

SCENIC CALIBRATION COEFFICIENTS

(Units in Centimeters)

EQUATION (4.29) $L\ (cm) = a_0 N_y^2 + b_0 N_y + c_0$

$a_0 = 0.000371$

$b_0 = 0.374$

$c_0 = -0.902$

$r^2 = 0.9877$

EQUATION (4.47) $L\ (cm) = a_2 N_t^2 + b_2 N_t + c_2 D + d_2$

$a_2 = -0.000428$

$b_2 = 0.411$

$c_2 = -3.50$

$d_2 = -5.06$

$r^2 = 0.9941$

EQUATION (4.56) $D\ (cm) = a_3 X^2 N_x + b_3 X N_x + c_3 N_x + d_3$

$a_3 = 0.00000420$

$b_3 = -0.00168$

$c_3 = 0.2408$

$d_3 = 0.2215$

$r^2 = 0.9785$

and ram velocity, be related to elementary machine operator settings. These machine settings are subsequently employed as the independent variables.

5.1.2.1.1 SHOT WEIGHT VS SHOT NUMBER The relation between the total shot weight and the shot number is shown in Figure 5.1. The shot number is a simple numeric setting on the parison programmer. The relationship is essentially linear, as expected.

5.1.2.1.2 HYDRAULIC PRESSURE VS VALVE SETTING Figure 5.2 illustrates the relationship between the hydraulic pressure and the injection valve setting. The gap was set at 1.25 mm for this experimental set, as the hydraulic pressure tends to vary with gap. The hydraulic pressure was read with an analog gauge.

5.1.2.1.3 MELT FRACTION VS FRACTION OF STROKE The development of parison weight during extrusion was measured by employing a pinch-off mold in conjunction with step applications every sixteenth of a stroke. The steps were applied as part of the SAMP program, which is used for data acquisition as described in Section 5.1.2.2. The transition segment is obtained by the linear interpolation of the weights of the adjacent segments, to yield an estimate of a weight value for that step location.

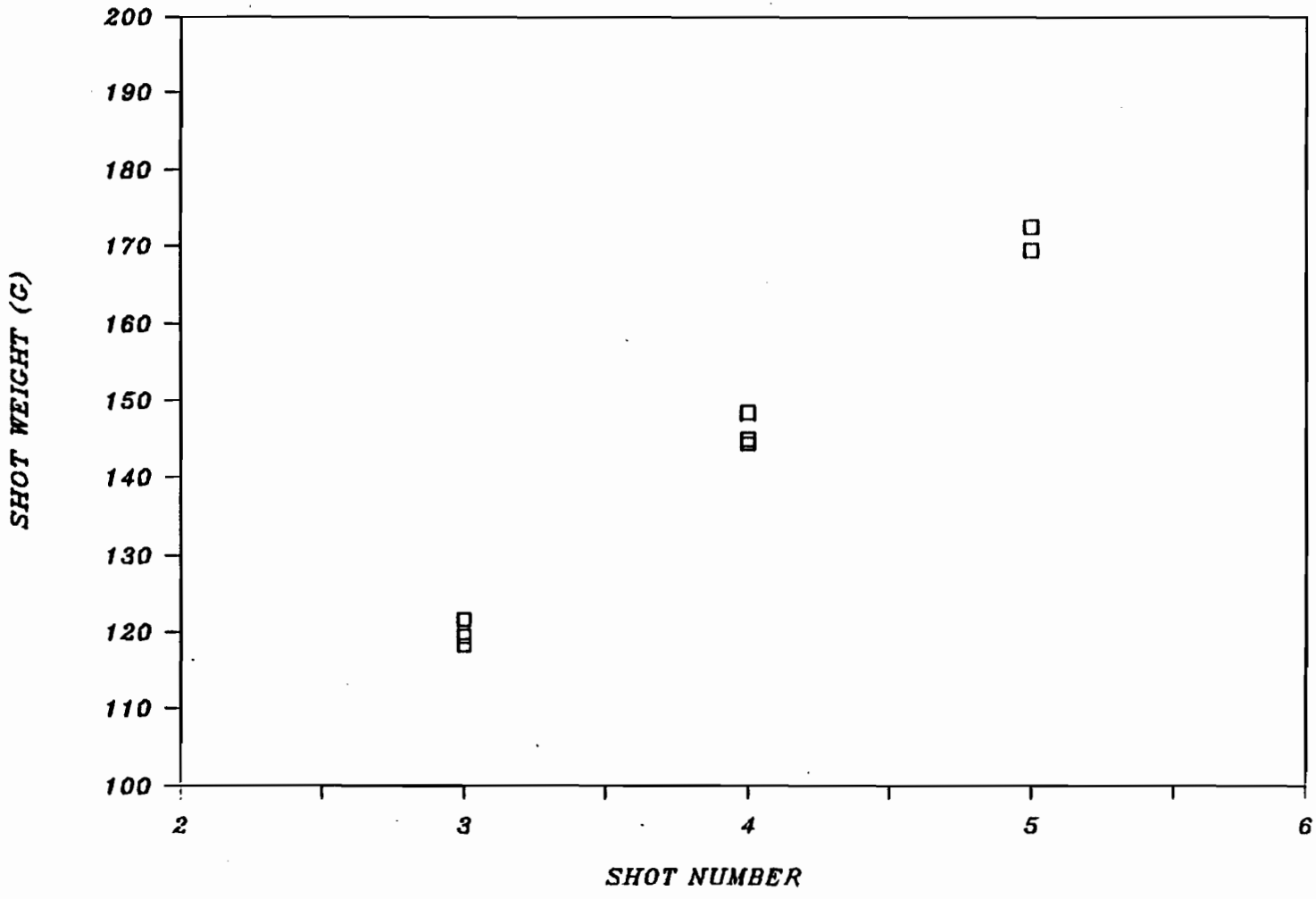

Figure 5.1: Shot Weight Versus Shot Number at 200°C, Injection Valve Setting 1.25 and 1.25 mm Gap.

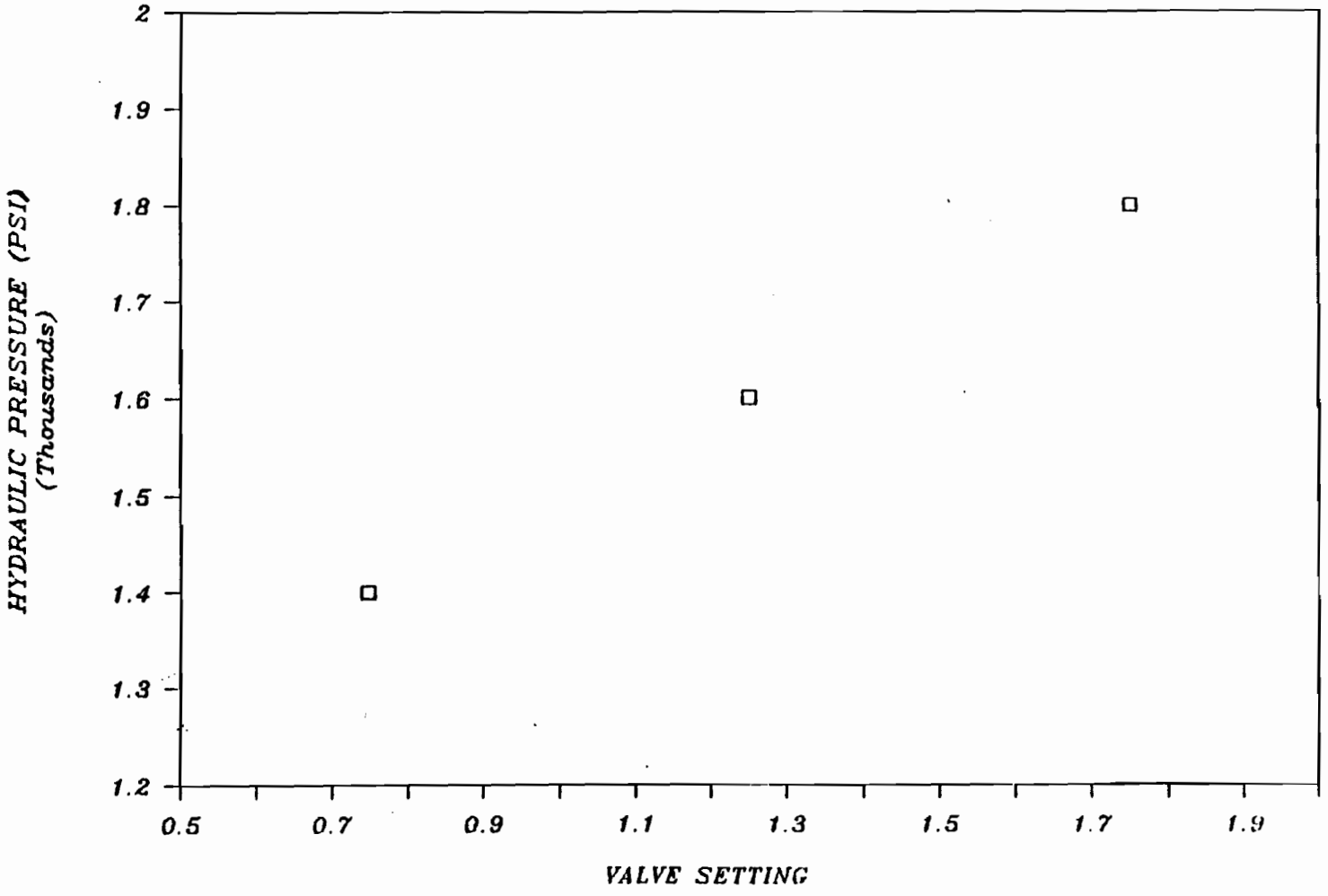

Figure 5.2: Hydraulic Pressure Versus Injection Valve Setting at 200°C, 1.25 mm Gap and Shot Number 4.

The relationship of parison weight versus fraction of stroke is shown in Figure 5.3. As expected, the relationship is linear with the intercept corresponding to the onset of extrusion. The delay is caused by compression of the polymer melt, by the ram, prior to the melt attaining enough pressure to flow out through the annular die. The flow begins in the second sixteenth of a stroke. However, as this segment tends to exhibit unsteady flow characteristics, it is neglected in the control studies.

5.1.2.1.4 RAM VELOCITY VS MACHINE VARIABLES Figure 5.4 illustrates the relationship between the average ram velocity and gap. The ram velocity increases with increasing annular gap, at constant injection valve setting. This is expected, since the resistance to flow decreases with increasing annular gap, to an ultimate steady value. Resin B tends to flow easier than Resin A, since it exhibits lower viscosities, as shown in Figure 3.1.

The relationship between ram velocity and injection valve setting is shown in Figure 5.5. The ram velocity increases with increasing injection valve setting. This is expected, since more hydraulic pressure is being applied to the ram.

Figure 5.6 shows the ram velocity versus melt temperature relationship. The ram velocity increases slightly with increasing melt temperature. This is expected, as the viscosity for polymer melts tends to decrease with increasing temperature.

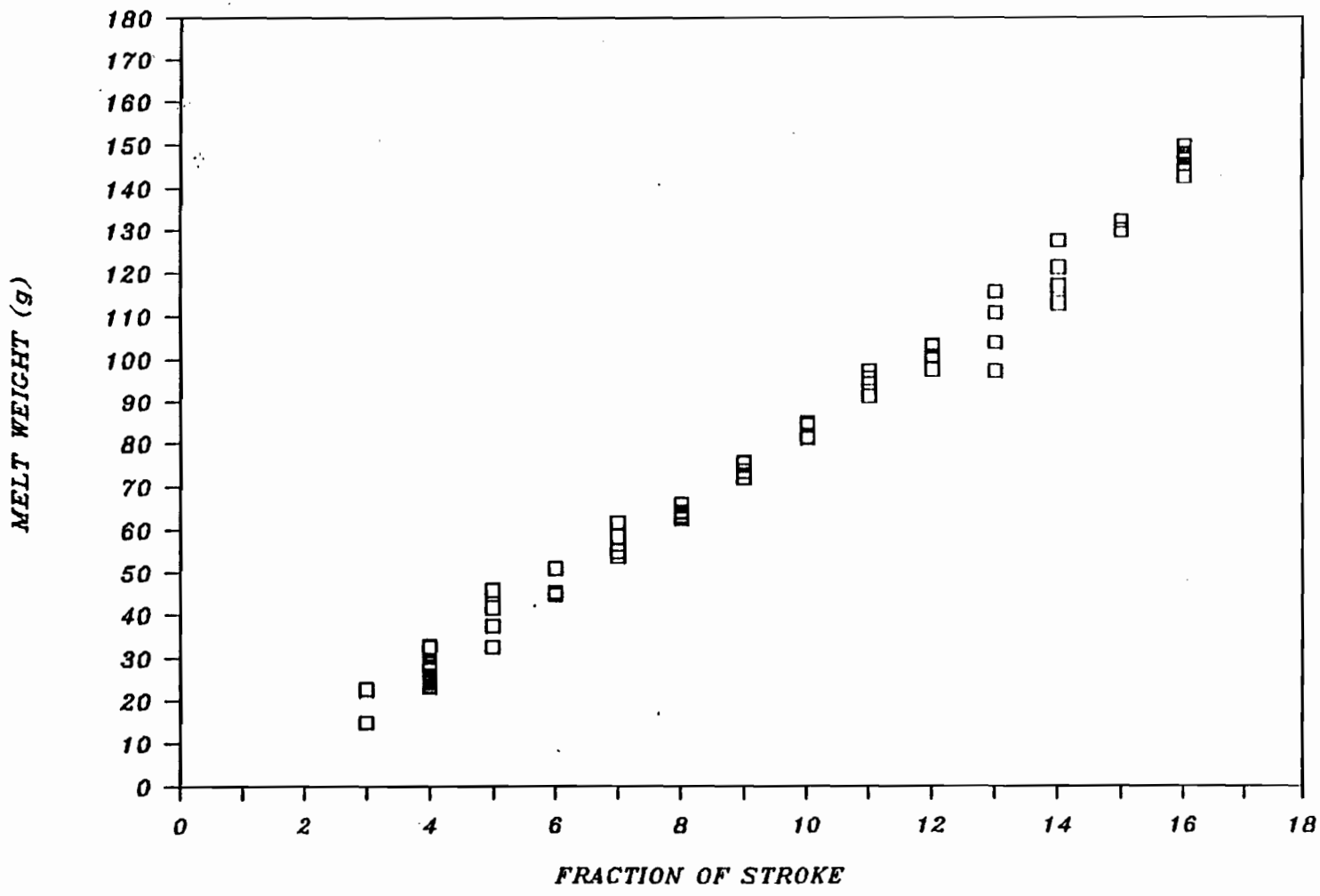

Figure 5.3: Parison Weight Versus Fraction of Stroke at 200°C, 1.25 mm Die Gap, Shot Number 4 and Injection Valve Setting 1.25.

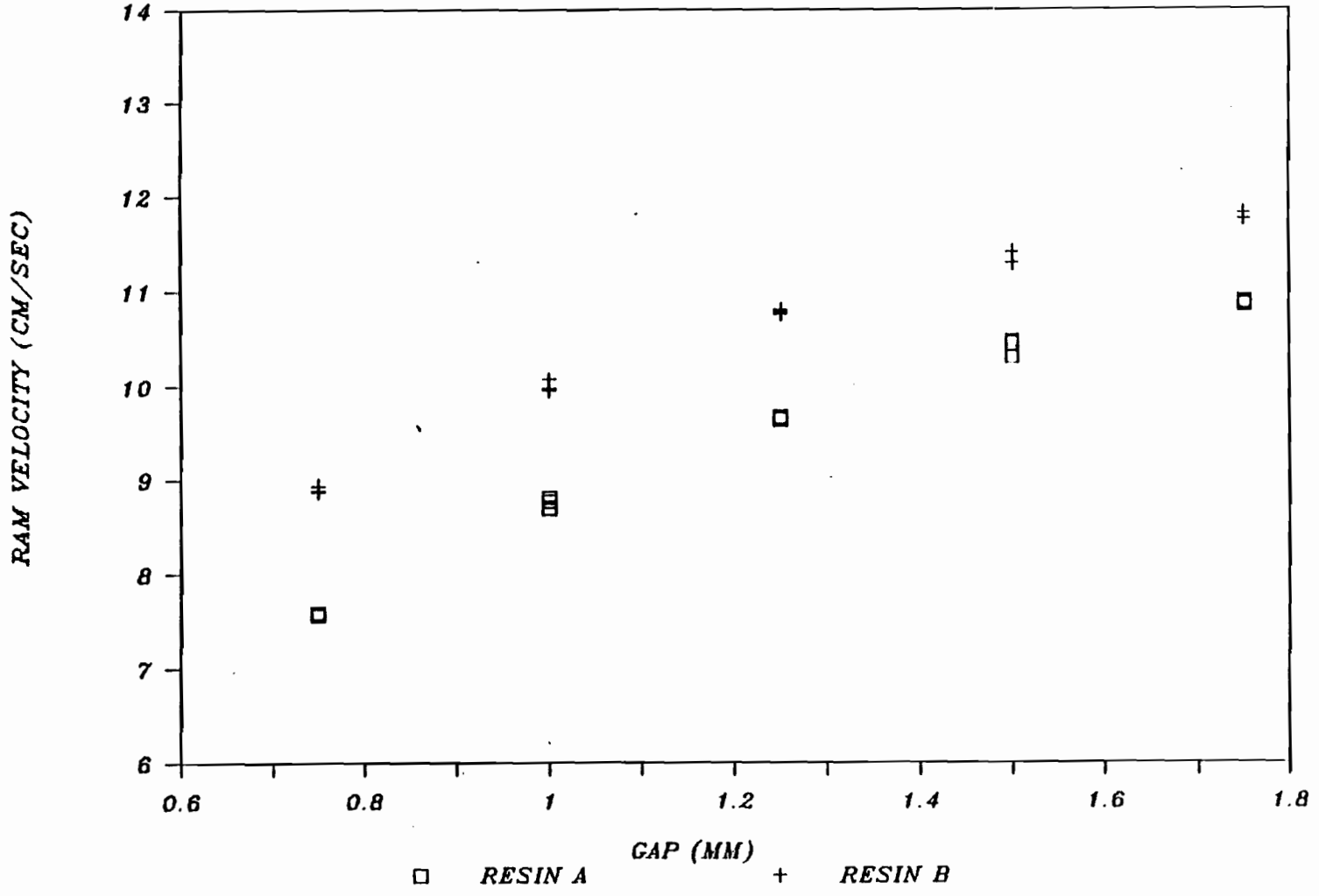

Figure 5.4: Average Ram Velocity Versus Die Gap at 200°C, Shot Number 4 and Injection Valve Setting 1.25.

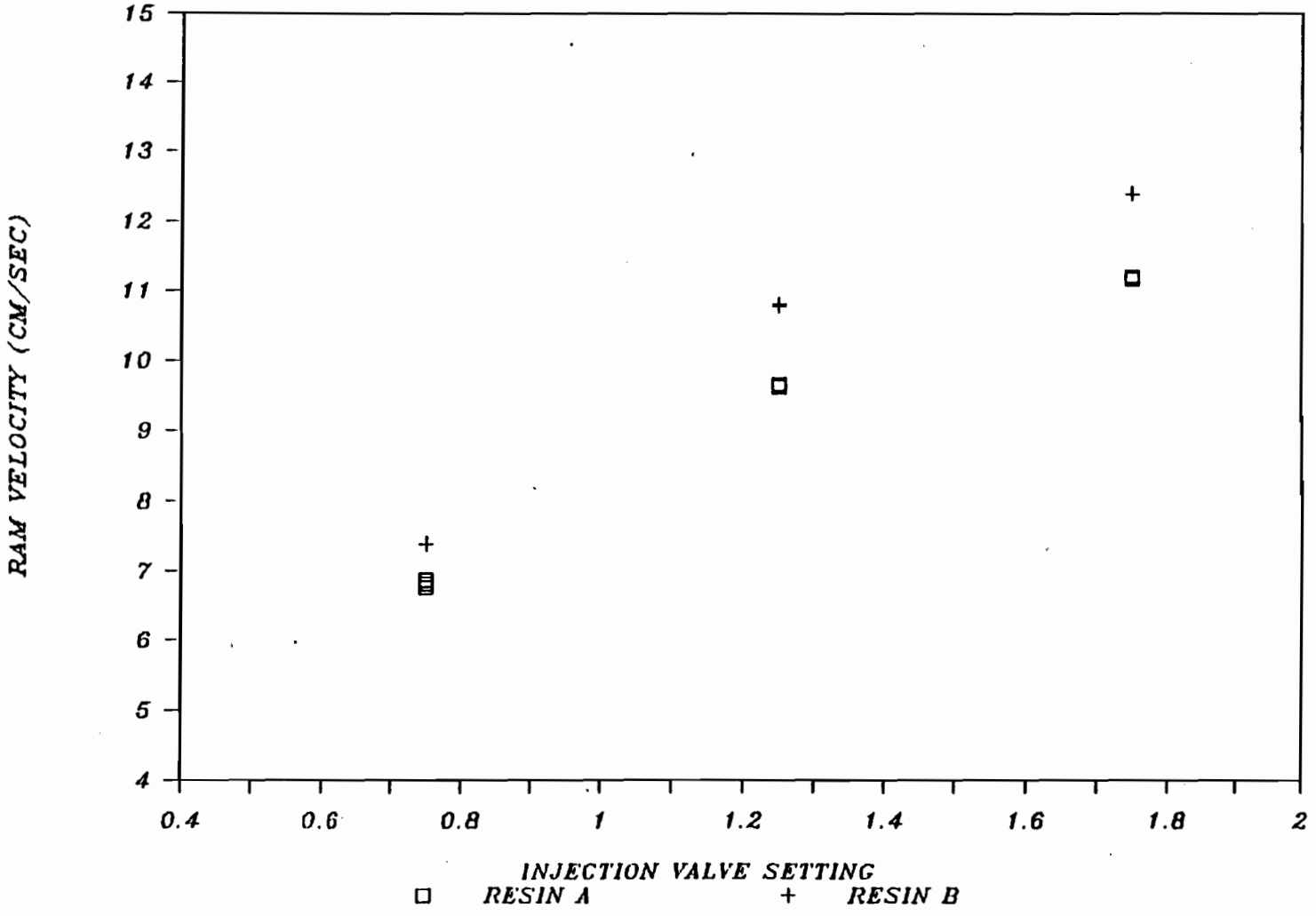

Figure 5.5: Average Ram Velocity Versus Injection Valve Setting at 200°C, Shot Number 4 and 1.25 mm Die Gap.

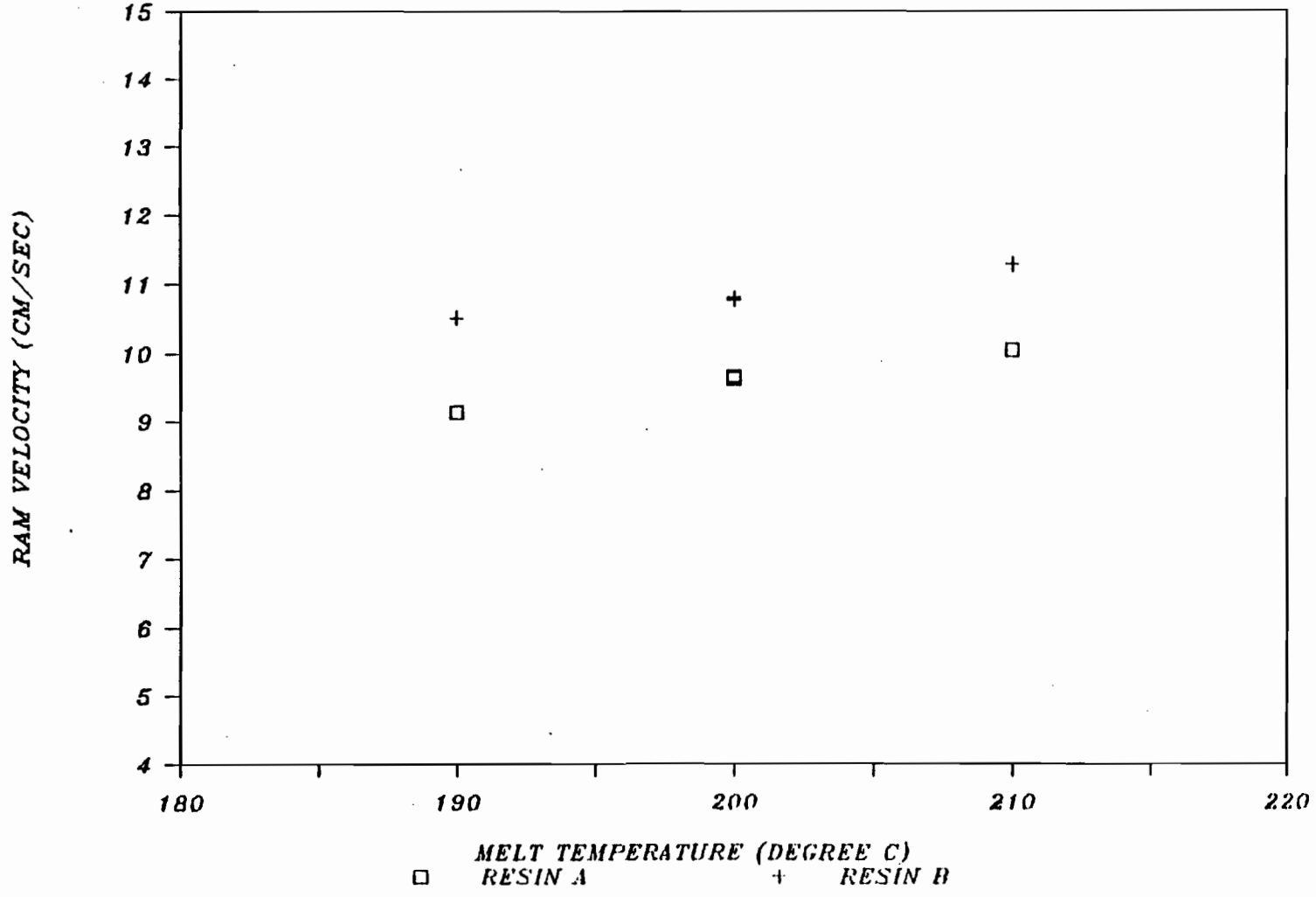

Figure 5.6: Average Ram Velocity Versus Melt Temperature at Shot Number 4, Injection Valve Setting 1.25 and 1.25 mm Die Gap.

5.1.2.1.5 HEAD PRESSURE VERSUS MACHINE VARIABLES Figure 5.7 shows the relationship between the average head pressure and gap. The head pressure decreases with increasing gap, as anticipated. Resin A exhibits slightly higher flow pressures than Resin B, for the same extrusion gap.

The head pressure increases with increasing valve setting, as illustrated in Figure 5.8. The increasing valve setting results in an increasing hydraulic pressure to the ram, and consequently increasing pressures throughout the flow field.

Head pressure versus melt temperature is shown in Figure 5.9. The effect of temperature on head pressure appears to be insignificant, in the range of melt temperatures considered in this work.

5.1.2.2 MACHINE VARIABLES EXTRUSION DYNAMICS

The response of the machine variables during extrusion was monitored with the help of the software SAMP. This program applies arbitrarily selected steps in the gap during the extrusion, and monitors transducer output.

5.1.2.2.1 GAP VS TIME The absolute value of the gap is calibrated with a depth gage, attached to the mandrel. Figure 5.10 illustrates the variation of gap versus time during a constant gap extrusion. It can be seen that the servoamp driver provides good control over the gap, throughout the extrusion.

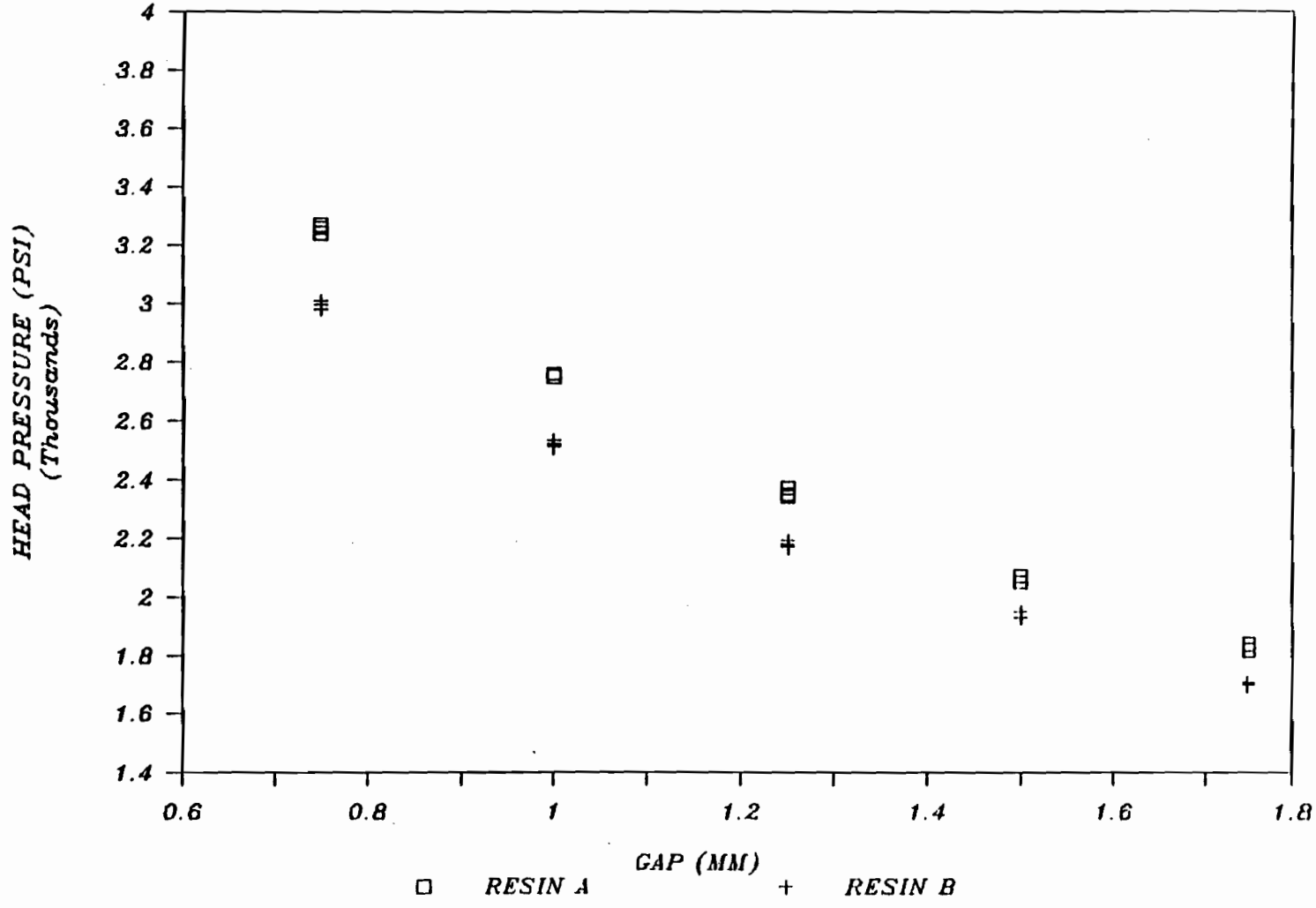

Figure 5.7: Average Head Pressure Versus Die Gap at 200°C, Shot Number 4 and Injection Valve Setting 1.25.

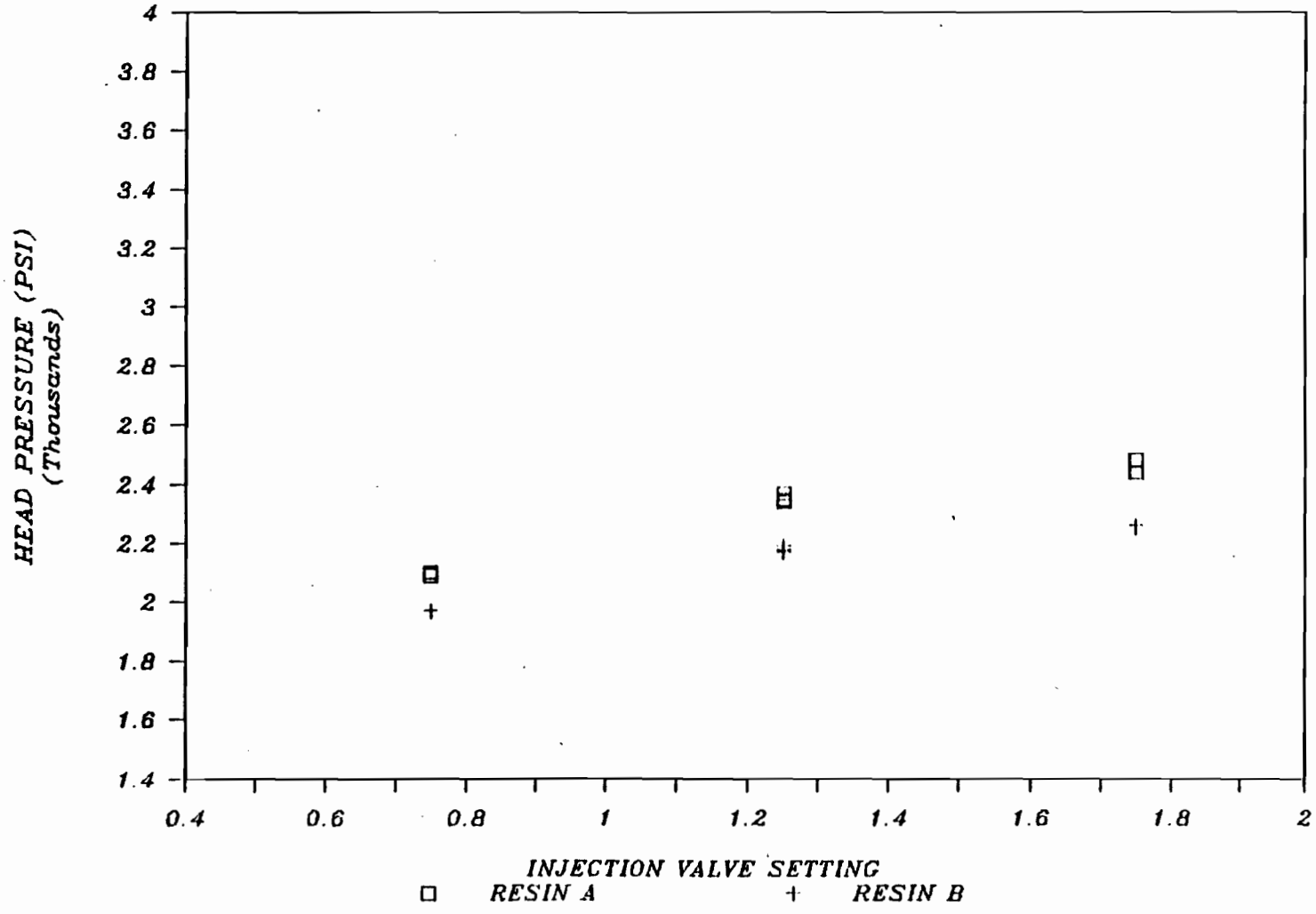

Figure 5.8: Average Head Pressure Versus Injection Valve Setting at 200°C, 1.25 mm Die Gap and Shot Number 4.

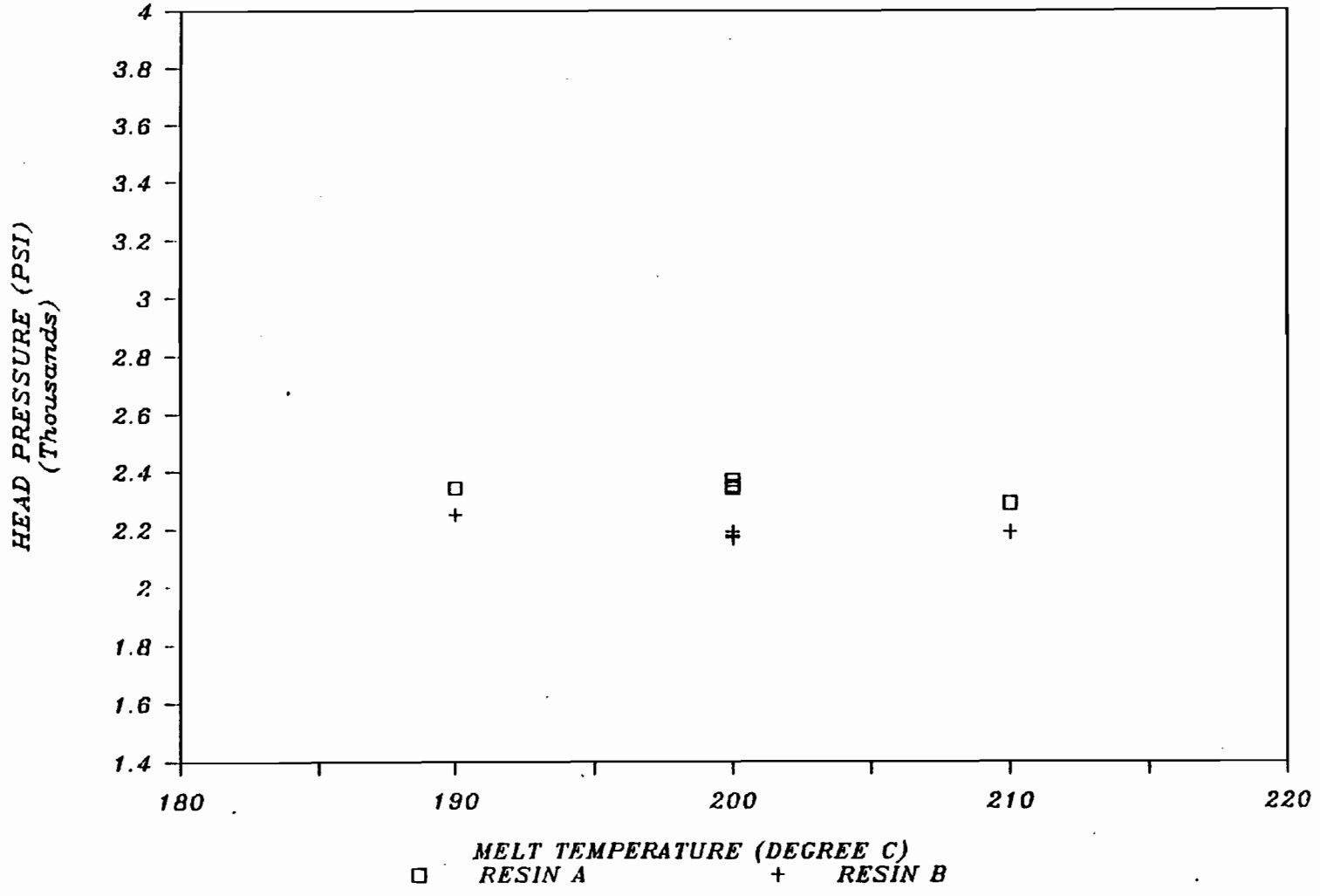

Figure 5.9: Average Head Pressure Versus Melt Temperature at Injection Valve Setting 1.25, 1.25 mm Die Gap and Shot Number 4.

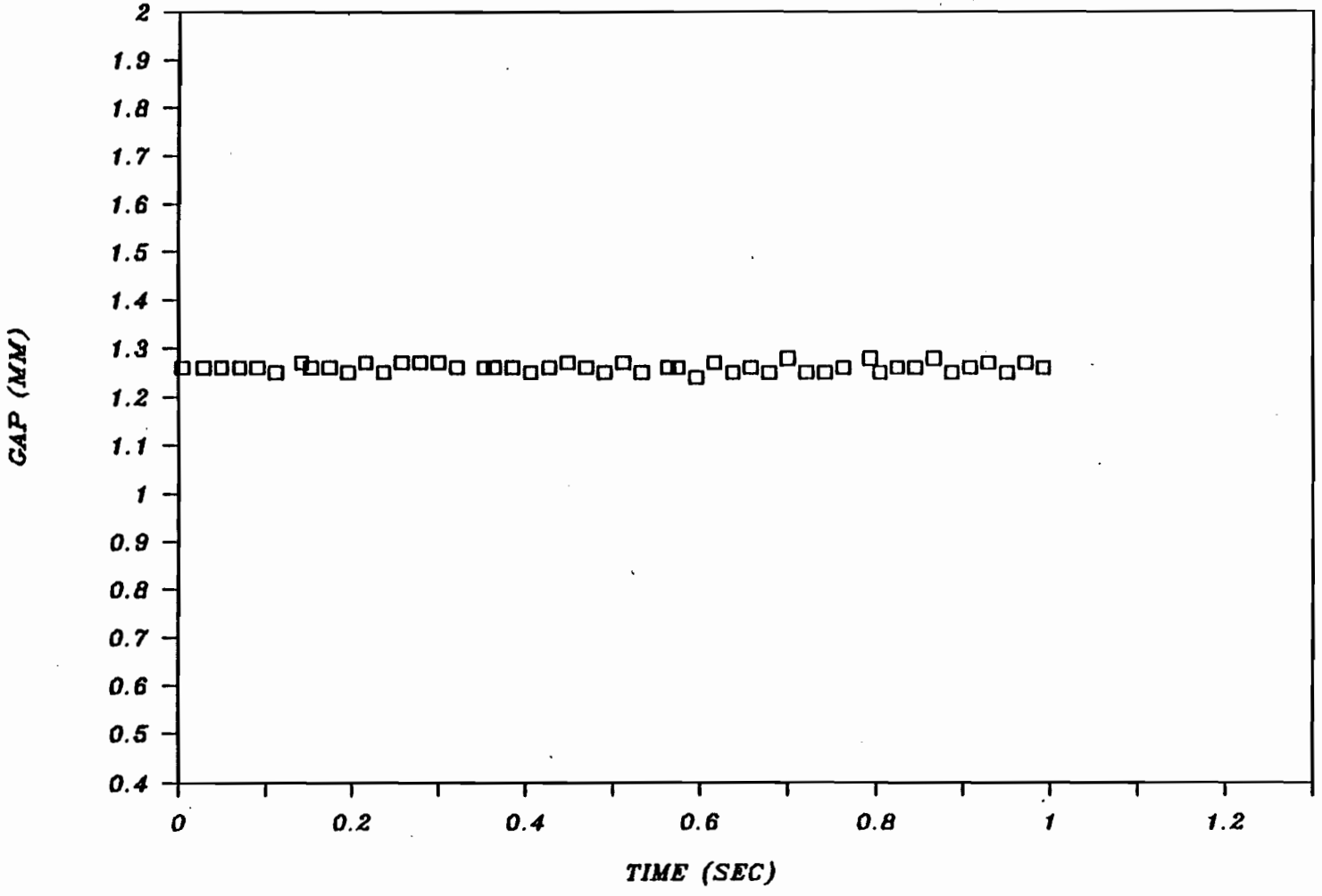

Figure 5.10: Die Gap Versus Time During Extrusion at 1.25 mm Constant Die Gap Setting.

Figures 5.11 and 5.12 refer to gap steps downwards and upwards, respectively, during the extrusion. The gap step takes 0.05 seconds, regardless of the step magnitude, direction or initial gap. The gaps reach the new steady state within three readings. Therefore, the most practical relation attainable for the variation of gap with time, during the transition, is a linear relationship.

The minimum discernible change for a gap, was 0.03 mm. This change was necessary for the fine adjustments required in control, yet it was not sufficient for inducing a visible change in the thickness measurement, in the dynamic step tests.

5.1.2.2.2 HEAD PRESSURE VS TIME The head pressure versus time, for a constant gap extrusion, is shown in Figure 5.13. The pressure increases steadily to a constant value in the unsteady, initial onset of extrusion. The head pressure versus time response to gap steps down and up in the extrusion, is illustrated in Figures 5.14 and 5.15, respectively. There is no significant delay in the process response to a gap step.

5.1.2.2.3 RAM VELOCITY VS TIME The ram velocity versus time, for a constant gap extrusion, is illustrated in Figure 5.16. The velocity decreases to the steady extrusion value, as the resistance to extrusion builds up in the onset flow region. The ram velocity versus time response to a gap step down and up in

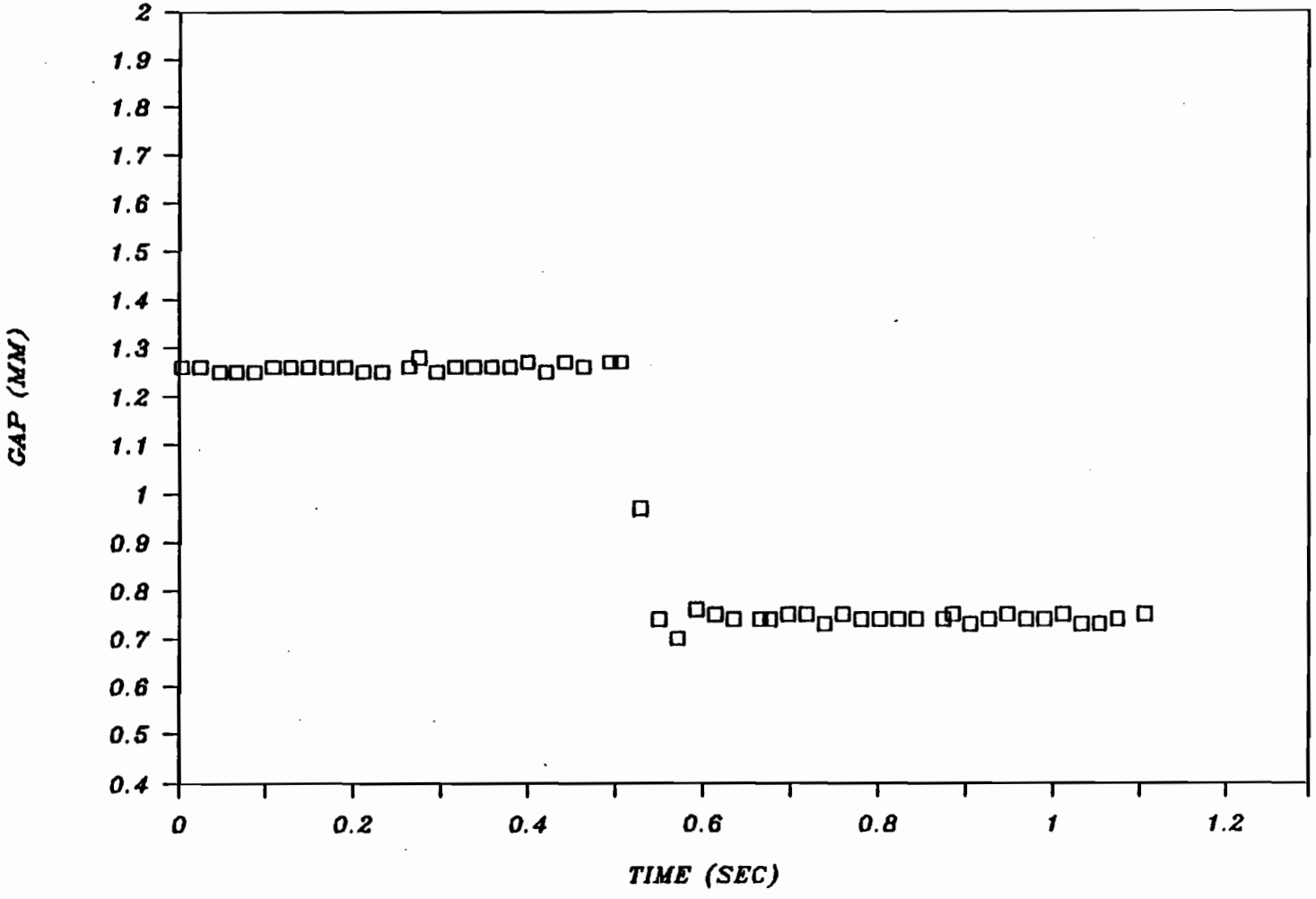

Figure 5.11: Die Gap Versus Time During Extrusion: Step Down 1.25mm-0.75mm Die Gap.

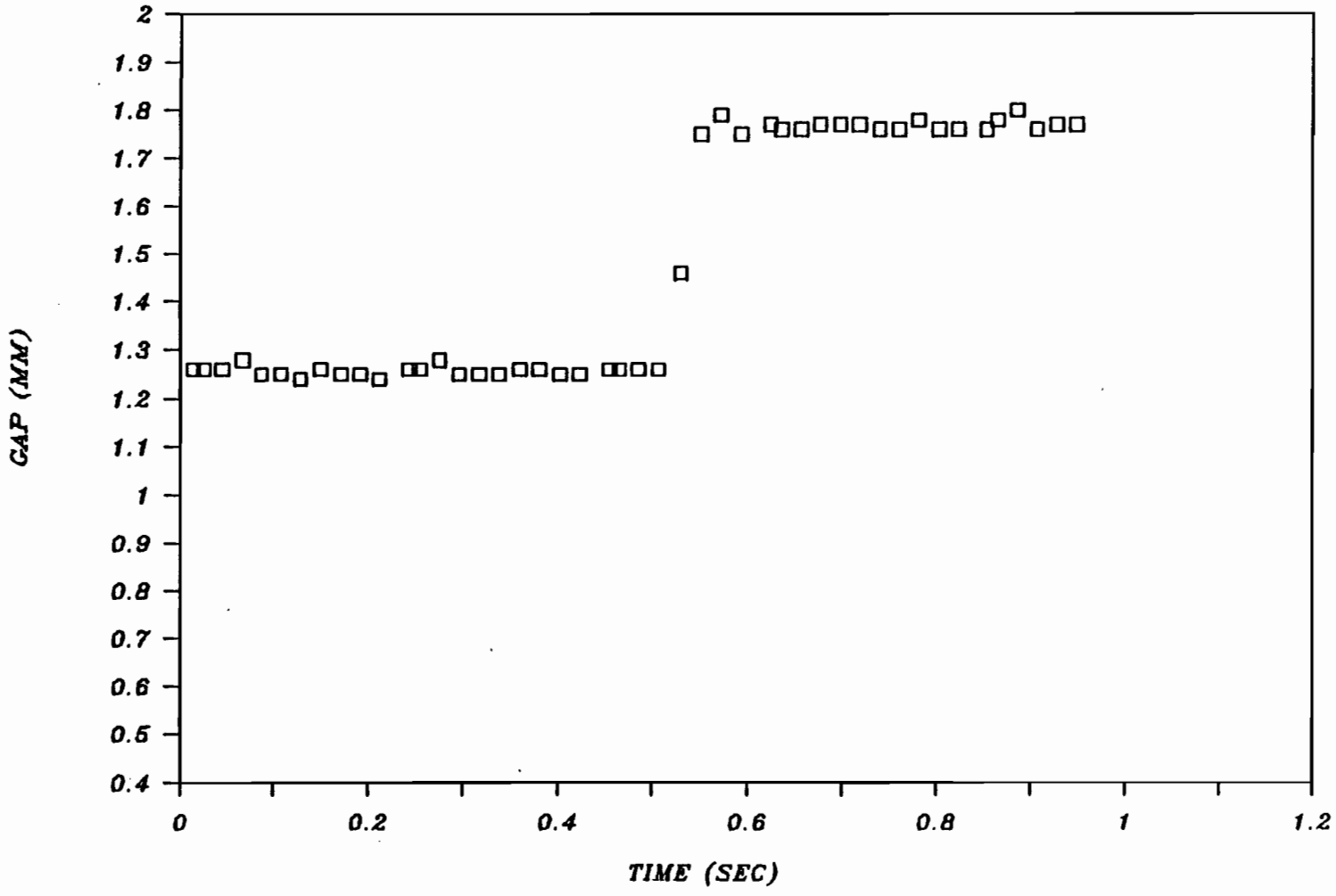

Figure 5.12: Die Gap Versus Time During Extrusion: Step Up 1.25 mm-1.75 mm Die Gap.

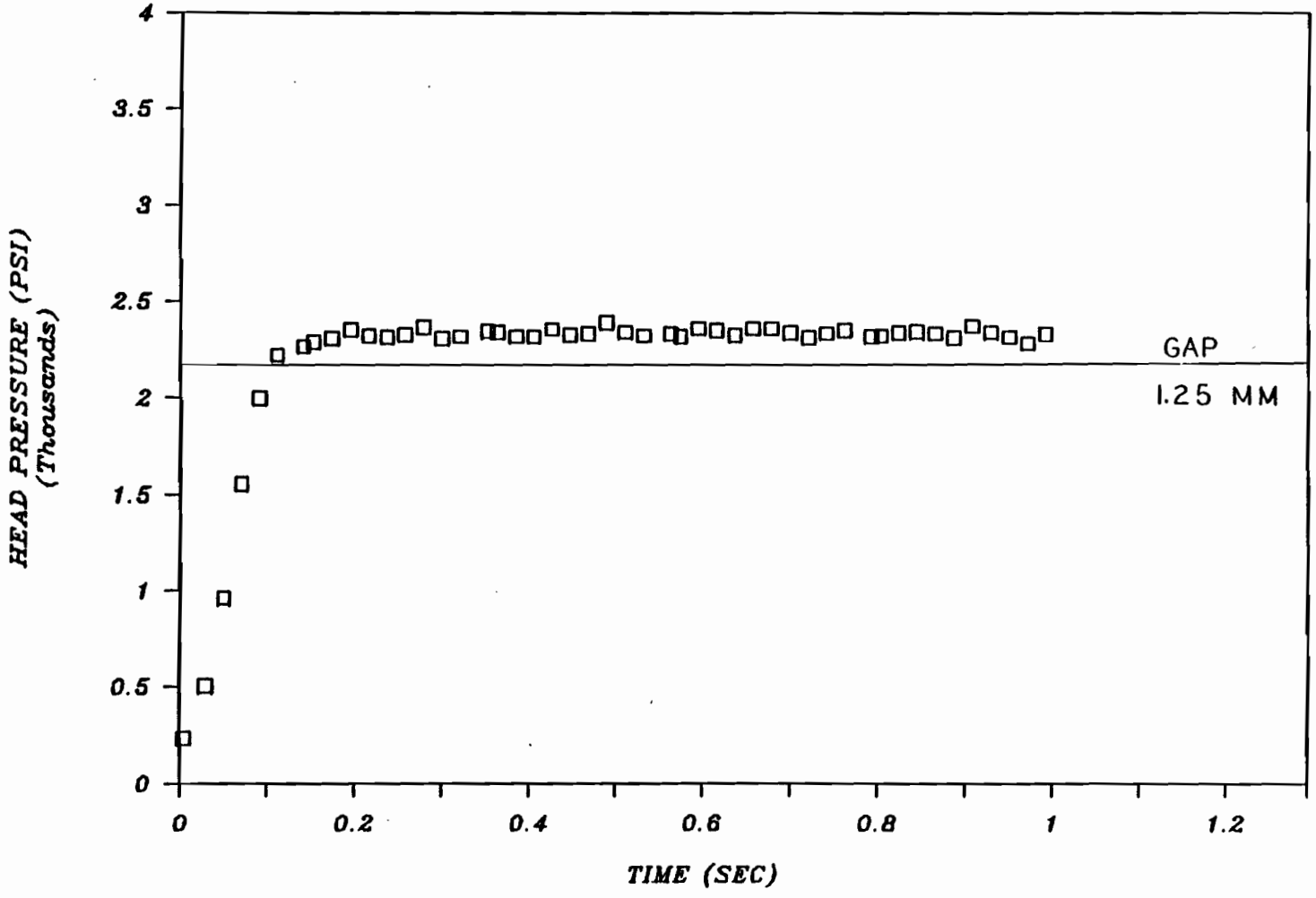

Figure 5.13: Head Pressure Versus Time Response to Constant Gap Profile of Figure 5.10.

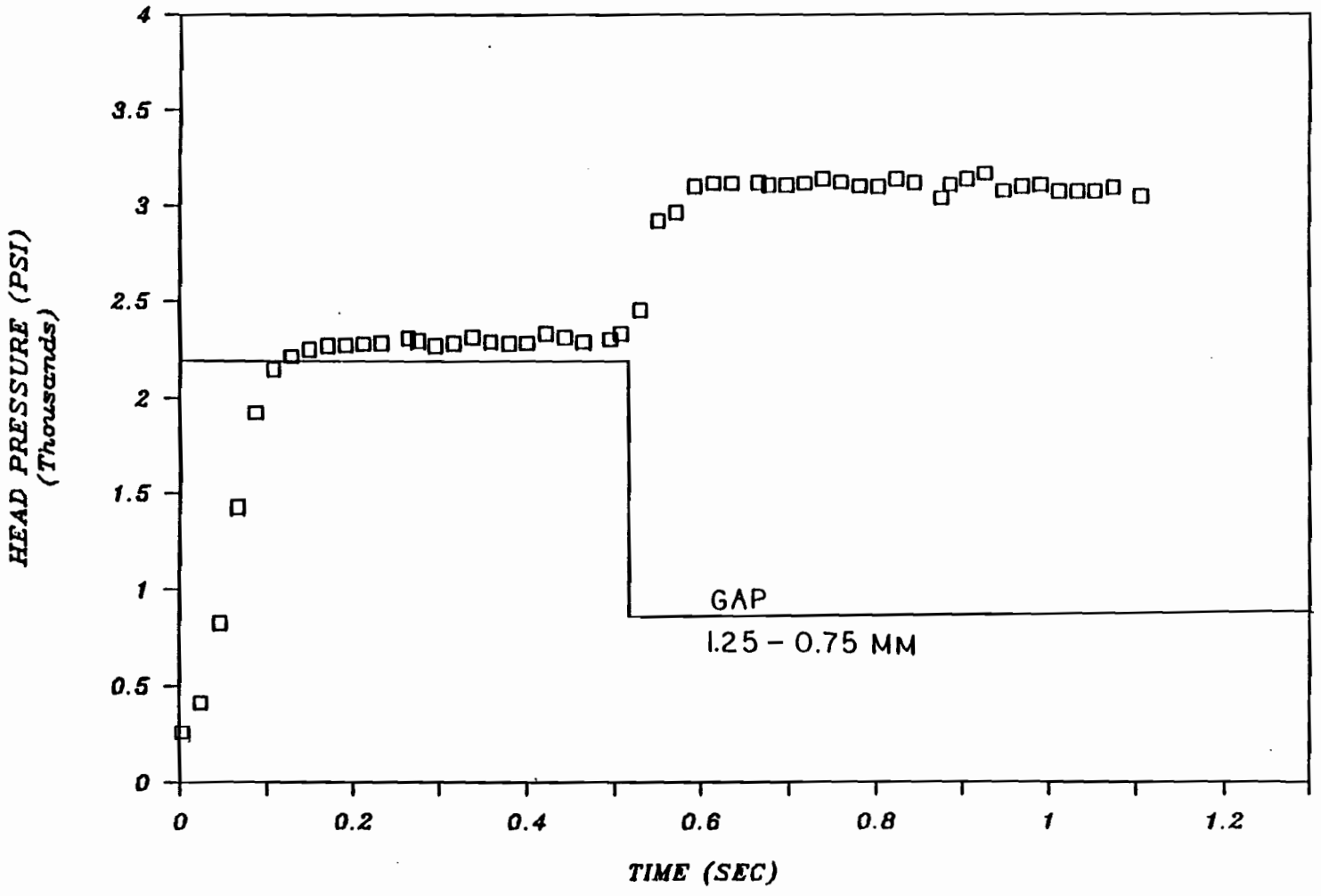

Figure 5.14: Head Pressure Versus Time Response to Gap Step Down of Figure 5.11.

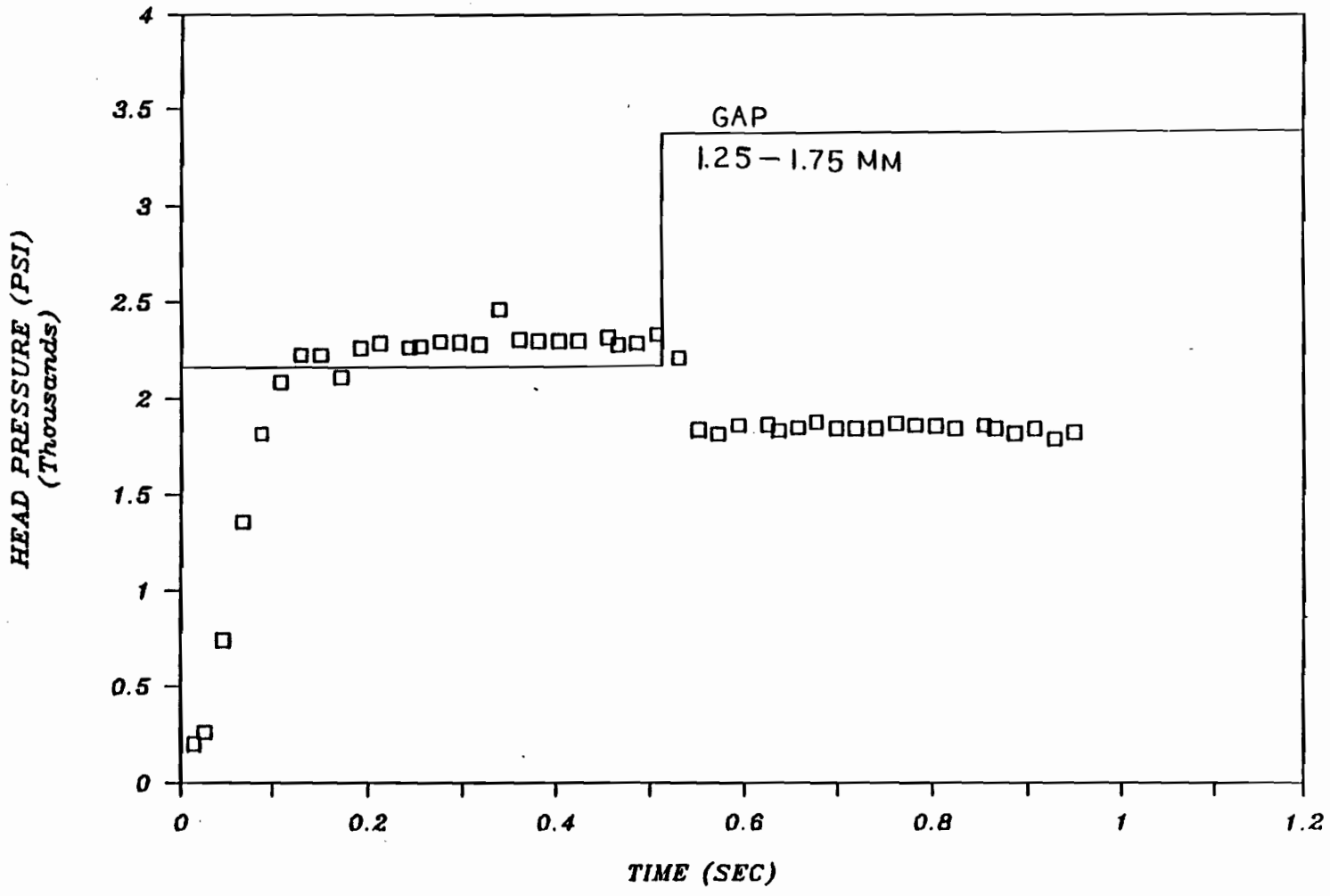

Figure 5.15: Head Pressure Versus Time Response to Gap Step Up of Figure 5.12.

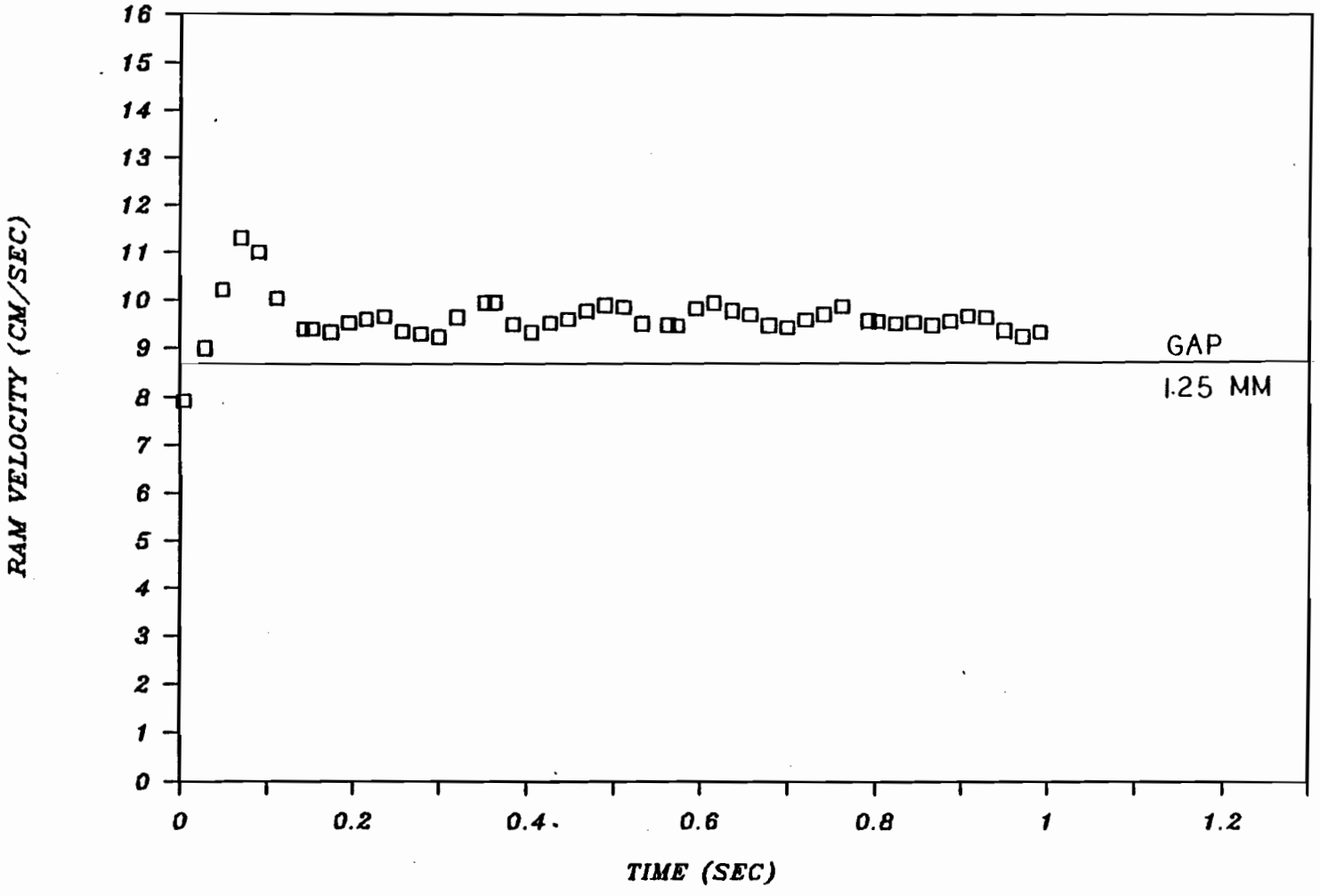

Figure 5.16: Ram Velocity Versus Time Response to Constant Gap Profile of Figure 5.10.

the extrusion, is shown in Figures 5.17 and 5.18 respectively.

5.1.3 PARISON LENGTH AND DIAMETER PROFILES

5.1.3.1 PARISON LENGTH VS FRACTION OF STROKE

Preliminary experiments were conducted to determine if the parison length versus time, during the extrusion, can be utilized in the thickness estimation. According to Equation (4.62), there is an exponential relationship between parison length and fraction of stroke.

$$L(i) = \frac{W(i)\exp[-t(i)/\epsilon(i)]}{w\rho B_{12}(i)h_o(i)D_o} \qquad (4.62)$$

Figure 5.19 illustrates the relationship between parison length and fraction of stroke. The data were obtained by utilizing the software LEN. Extrusion was carried out at the median values of gap 1.25 mm, melt temperature of 200°C and injection valve setting of 1.25. Parison photographs were taken at equispaced fractions of stroke, over several extrusions. Four images (maximum storage capacity) were procured from each extrusion.

The length could not be obtained with any dependable degree of accuracy, during the early fractions of stroke, since the resolution of the measurement was of the same order of magnitude as the length itself. Additionally, in this length range, a

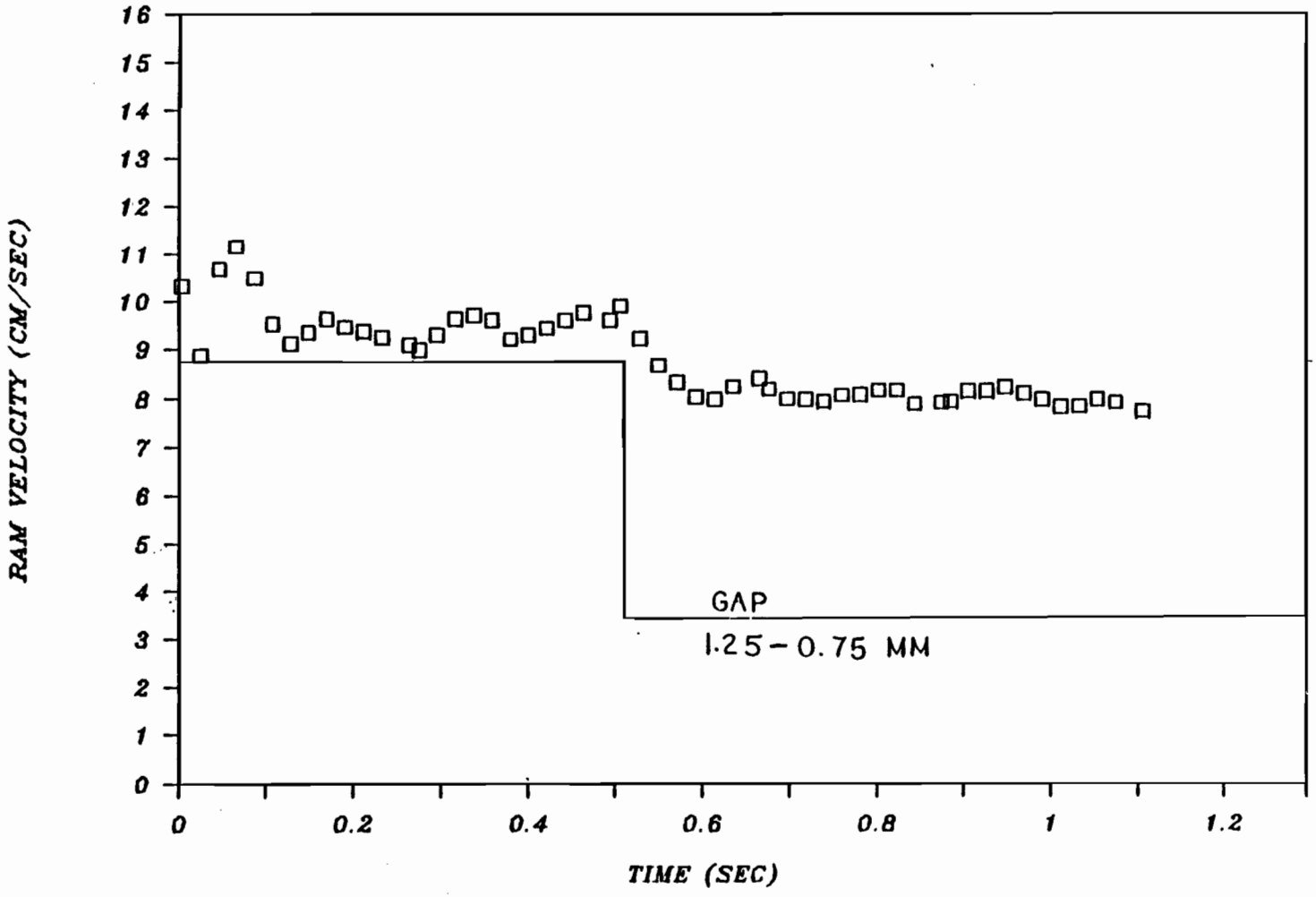

Figure 5.17: Ram Velocity Versus Time Response to Gap Step Down of Figure 5.11.

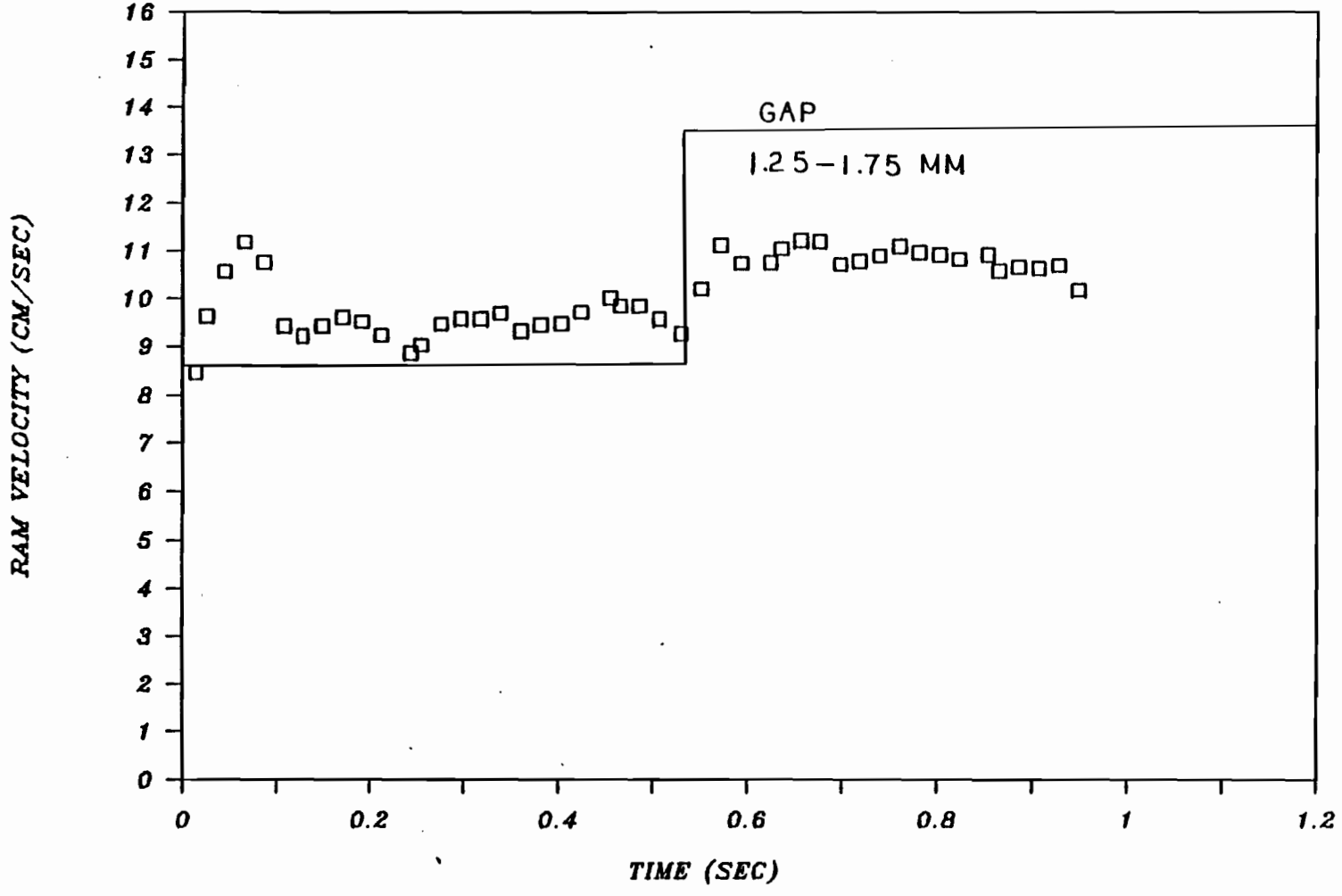

Figure 5.18: Ram Velocity Versus Time Response to Gap Step Up of Figure 5.12.

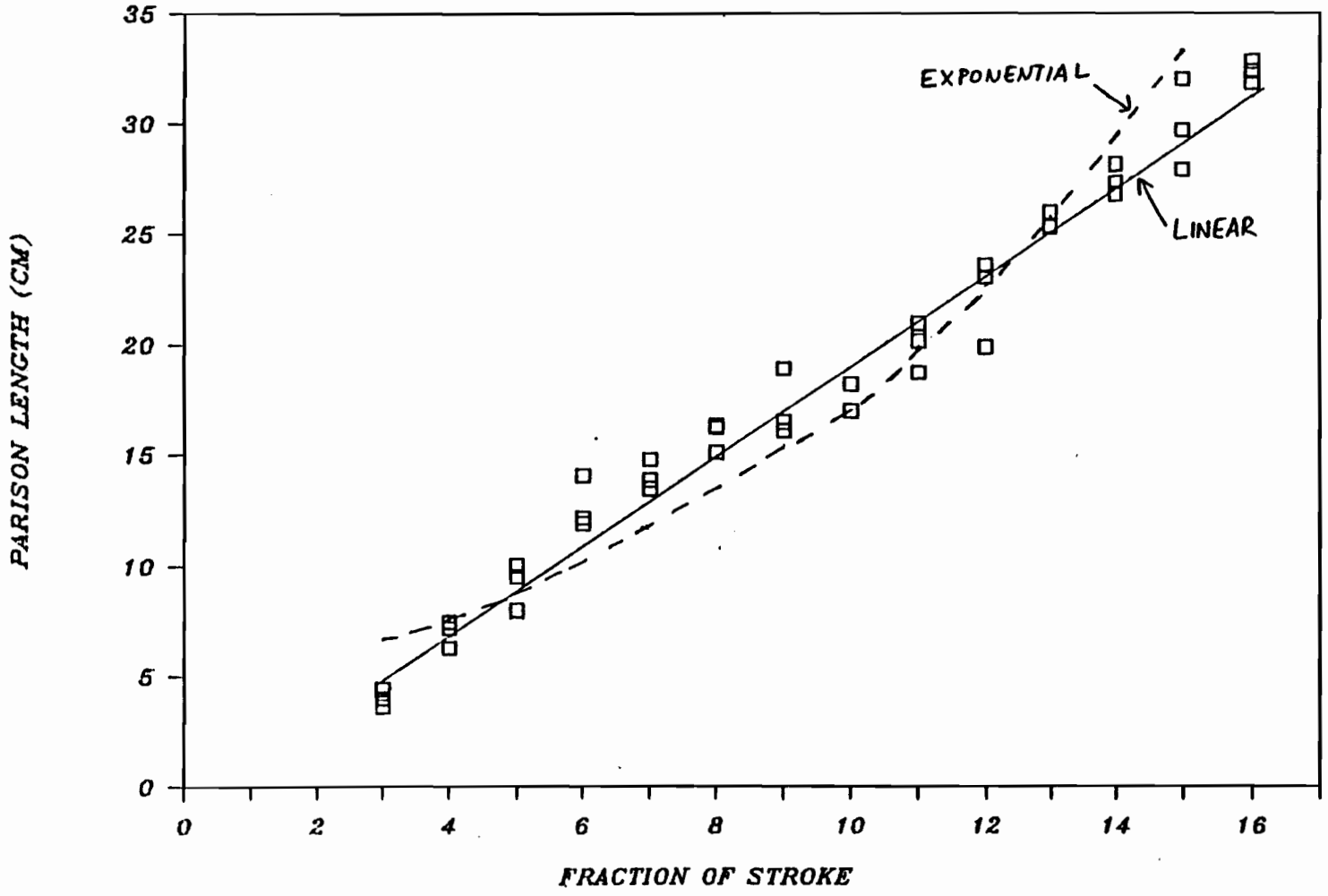

Figure 5.19: Parison Length Versus Fraction of Stroke (Exponential and Linear Fit Shown).

large fraction of the length measured corresponds to the droop effect.

The data were fit to both a simple linear and exponential relationship. The correlation coefficient of fit for the linear relationship was 0.977, whereas for the exponential relationship it was 0.887 (Figure 5.19). Therefore, the data appeared to follow the linear form better than the exponential form.

On the basis of the above, it can be concluded that the length resolution of the camera, within the time scale of the experiment, is not sufficient for detecting the exponential relaxation of the parison length, and subsequently the swell, as it is extruded. The exponential relationship would be dominant in the beginning of the extrusion, but again the length resolution is not suitable for accurate measurement during this period. Therefore, intermediate parison lengths cannot be utilized for thickness estimation. The estimation technique outlined in Chapter 4, utilizing the complete parison, must be employed.

It is also possible to conclude that sag is negligible during the extrusion, since the correlation does not deviate greatly from linearity.

5.1.3.2 CHARACTERISTIC SWELL TIME VS PARISON LENGTH

The thickness estimation technique presented in Chapter 4 assumes that the characteristic swell time (1/swell rate) of the complete parison, ϵ_T, equals the characteristic swell time of the individual segments, ϵ. This approximation is not valid for the last extruded segment, since the rate of relaxation of this segment is abnormally high. The other segments, however, undergo secondary relaxation which is significantly slower than that occuring at or near the die exit.

The characteristic swell time for various lengths of parison could be obtained by measuring the total lengths of the parison at the end of extrusion and after a one second delay, for various shot size extrusions. The value for the specific characteristic swell time was obtained with Equation (4.66).

$$L_D = L_E \exp(-1/\epsilon) \qquad (4.66)$$

The parameter, ϵ, is expected to decrease with parison length, as the relaxation of the last extruded segment becomes more predominant. The validity of the assumption that the swell rate of the complete parison is equal to the swell rate of the individual segments would be supported if the swell rate did not vary significantly with parison length. Figure 5.20 shows the relationship between the characteristic swell time and parison length at extrusion end.

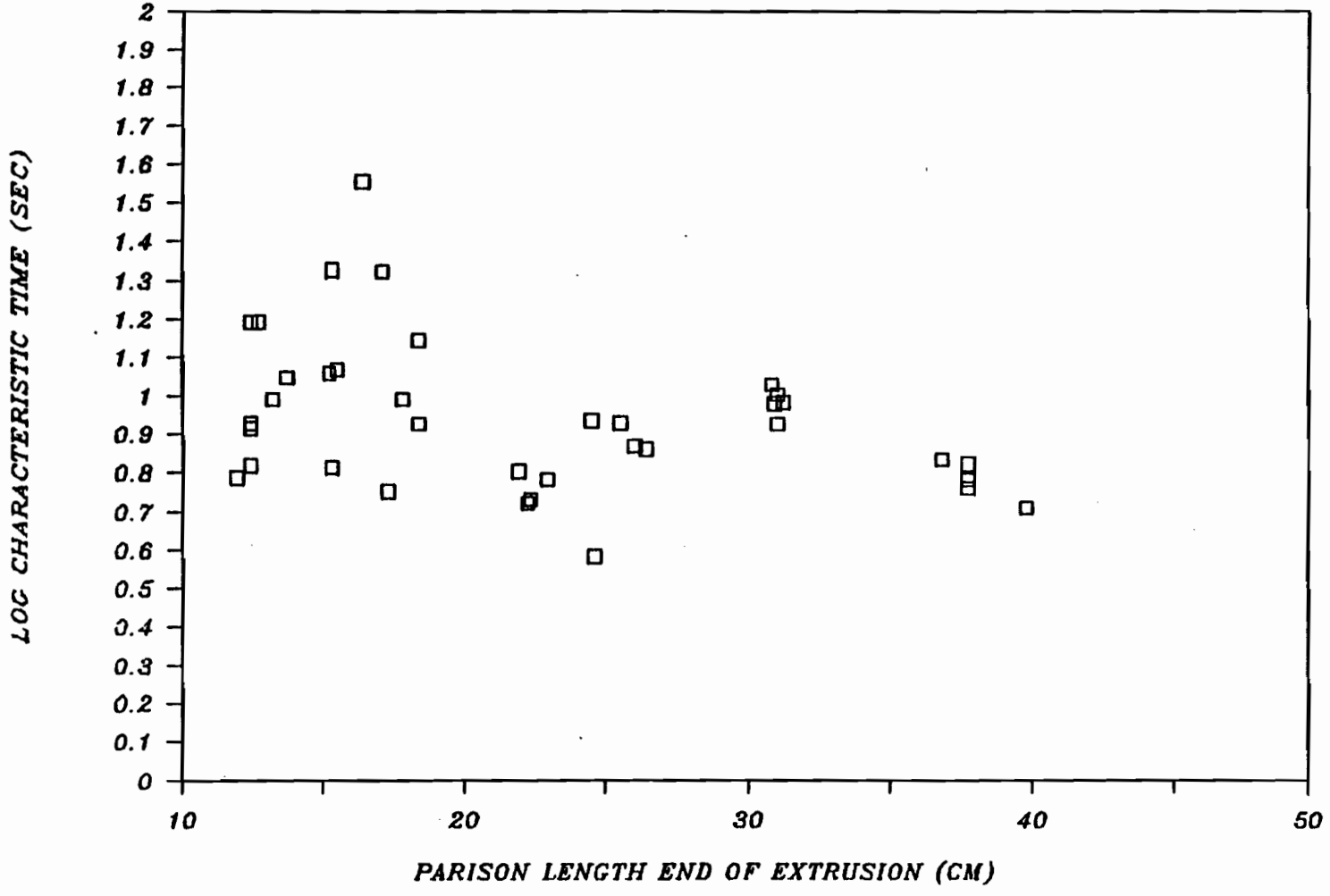

Figure 5.20: Characteristic Swell Time Versus Parison Length at Extrusion End.

The extrusions were run at the median parameters settings. The characteristic swell time data were obtained by the software SWELL. The parameter ϵ, does not vary significantly over the parison length range of 20-40 cm. However for parison lengths below 20 cm., reproducibilty of the measurement technique is not dependable. This is expected, because of the loss of length resolution in the low length range.

Therefore, with the data available, it is possible to assume that the swell rate for the whole parison approaches the swell rates for the individual segments, except for the segment closest to the die.

5.1.3.3 DIAMETER PROFILES

Figures 5.21, 5.22 and 5.23 illustrate the parison diameter profiles at extrusion gaps of 0.75, 1.25 and 1.75 mm, respectively. Equiweight diameter data were obtained with the software DYN. The top of the parison corresponds to segment number one, which is the last extruded segment. The first extruded segment corresponds to segment number fifteen which is the bottom of the parison. Resin B has a larger diameter swell than Resin A. The diameter profiles do not vary significantly with die gap. Therefore, the diameter profiles could not be employed as the controlled variables.

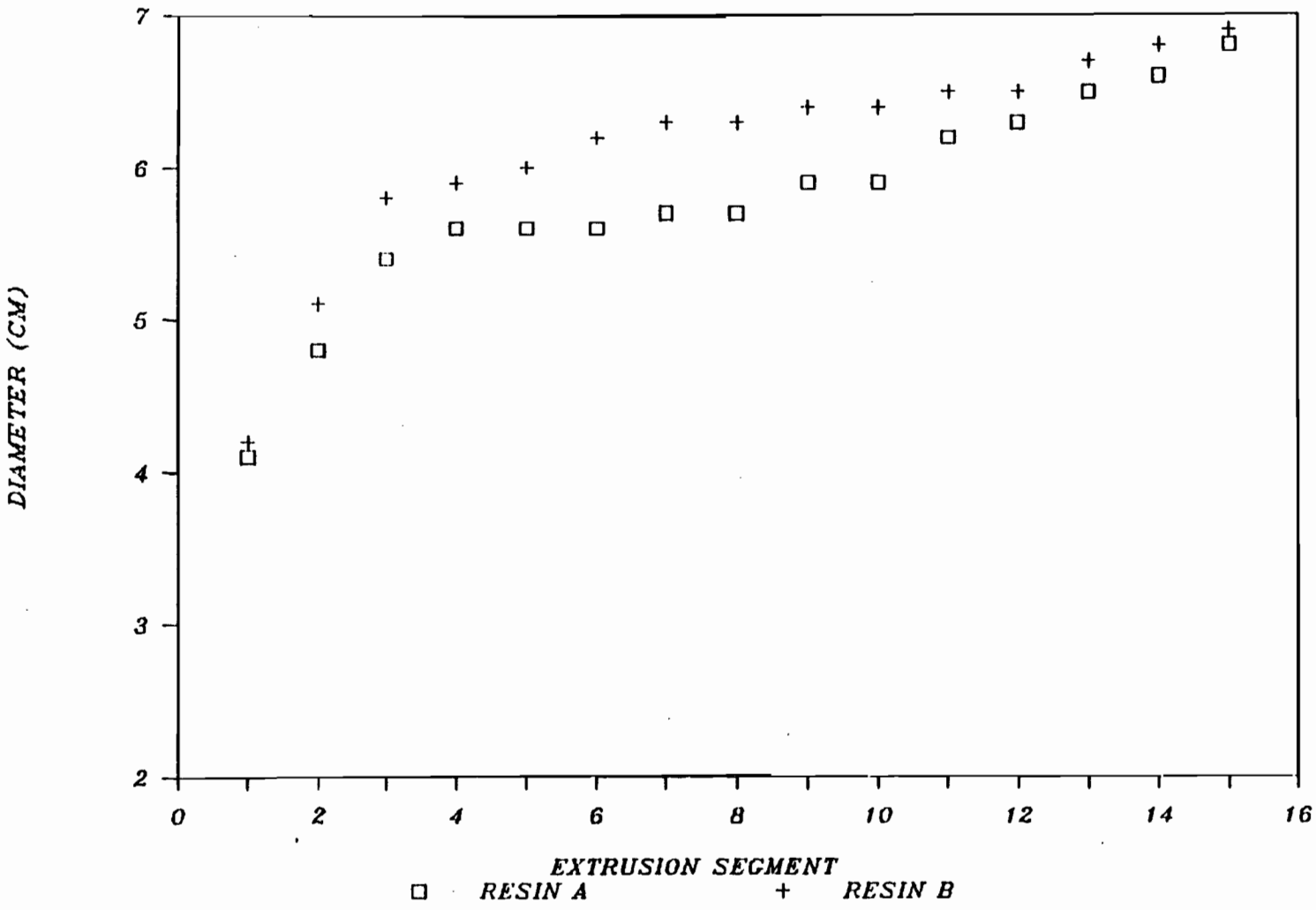

Figure 5.21: Parison Diameter Profile, for Resins A and B, at 0.75 mm Die Gap.

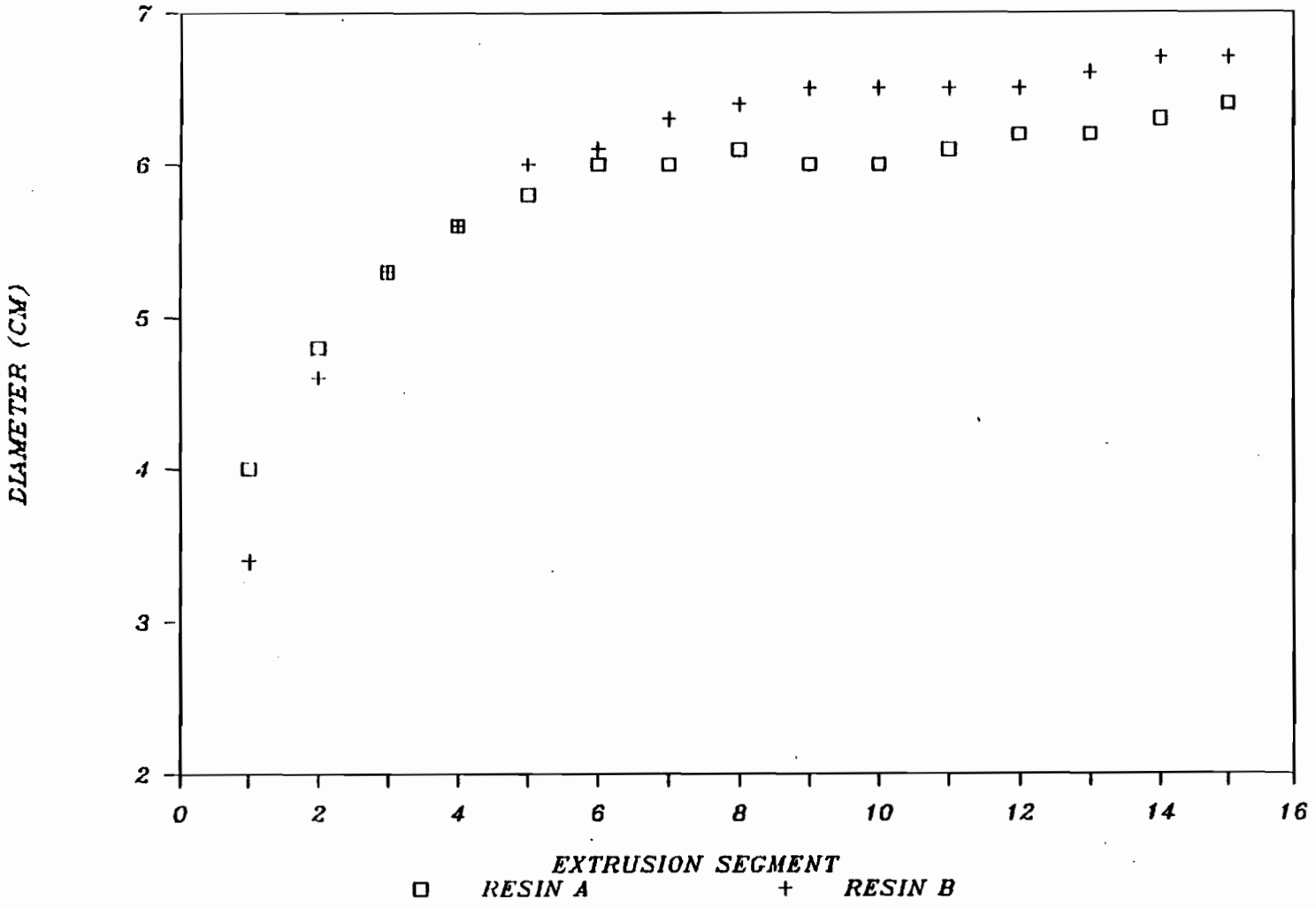

Figure 5.22: Parison Diameter Profile, for Resins A and B, at 1.25 mm Die Gap.

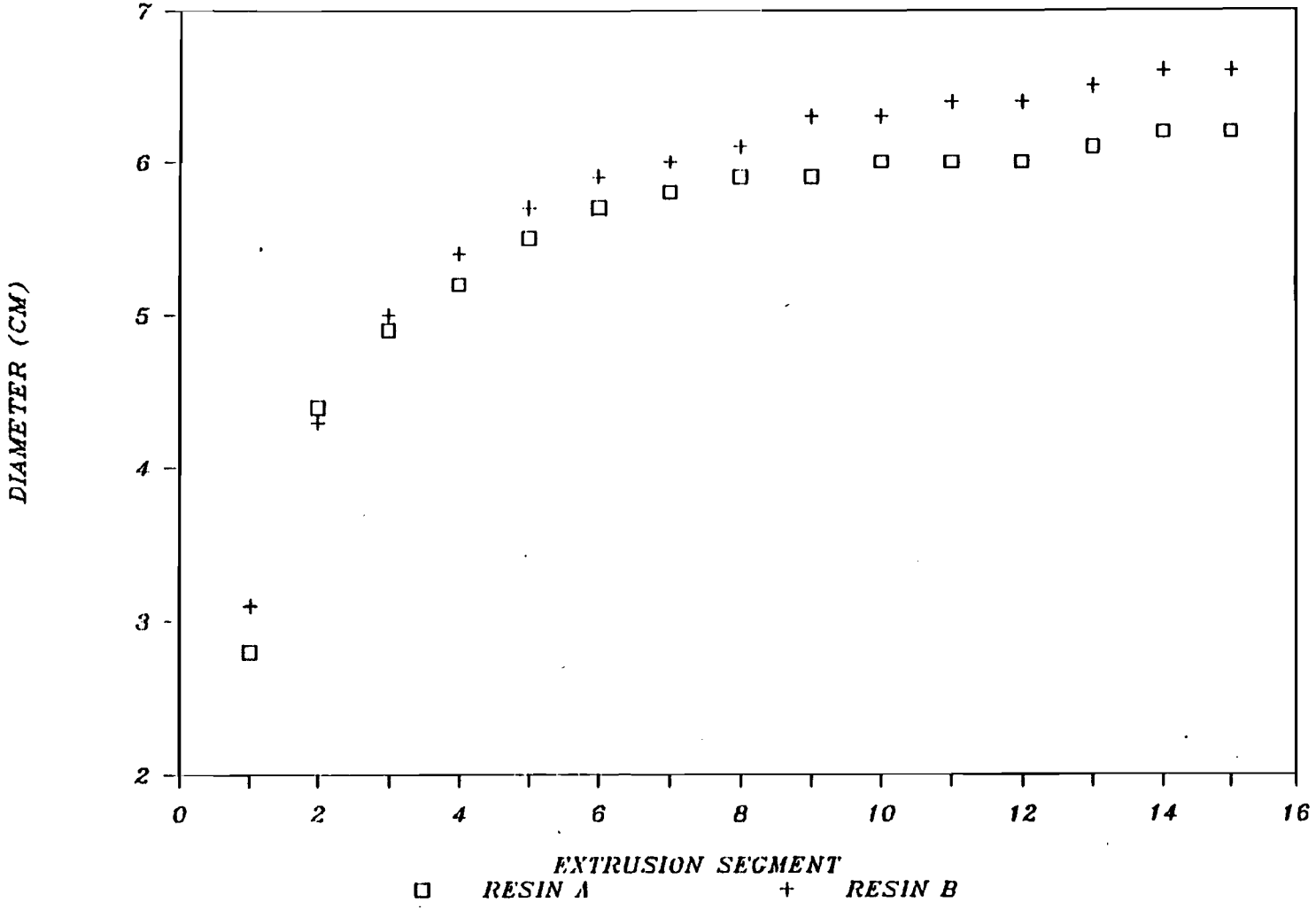

Figure 5.23: Parison Diameter Profile, for Resins A and B, at 1.75 mm Die Gap.

5.1.4 VIDEO CAMERA-PINCH OFF MOLD COMPARISON

5.1.4.1 DIAMETER PROFILES

Sheptak and Beyer (35) suggest the use of a pinch-off mold to estimate the distribution of outer parison diameters with the help of Equation (2.6).

$$D_P = \frac{2w(\rho_S/\rho)^{1/3}}{\pi} \qquad (2.6)$$

However, this equation is valid only for parisons thinner than half the distance between the two sides of the pillowed segment, in a closed pinch-off mold. The parison tends to spread out, in the case of thicker parisons, under the action of the closing mold, yielding overestimates of diameter. This tendency is illustrated in Figure 5.24. Equilength diameter data were obtained with the software PINCH. The diameter scan locations for the video camera coincided with the halfway point of each pinch segment.

5.1.4.2 THICKNESS PROFILES

The thickness profiles obtained from the on-line video camera estimation technique must be compared to an established measurement technique. This was essential in order to ensure that the on-line estimation routine was correct. The comparison

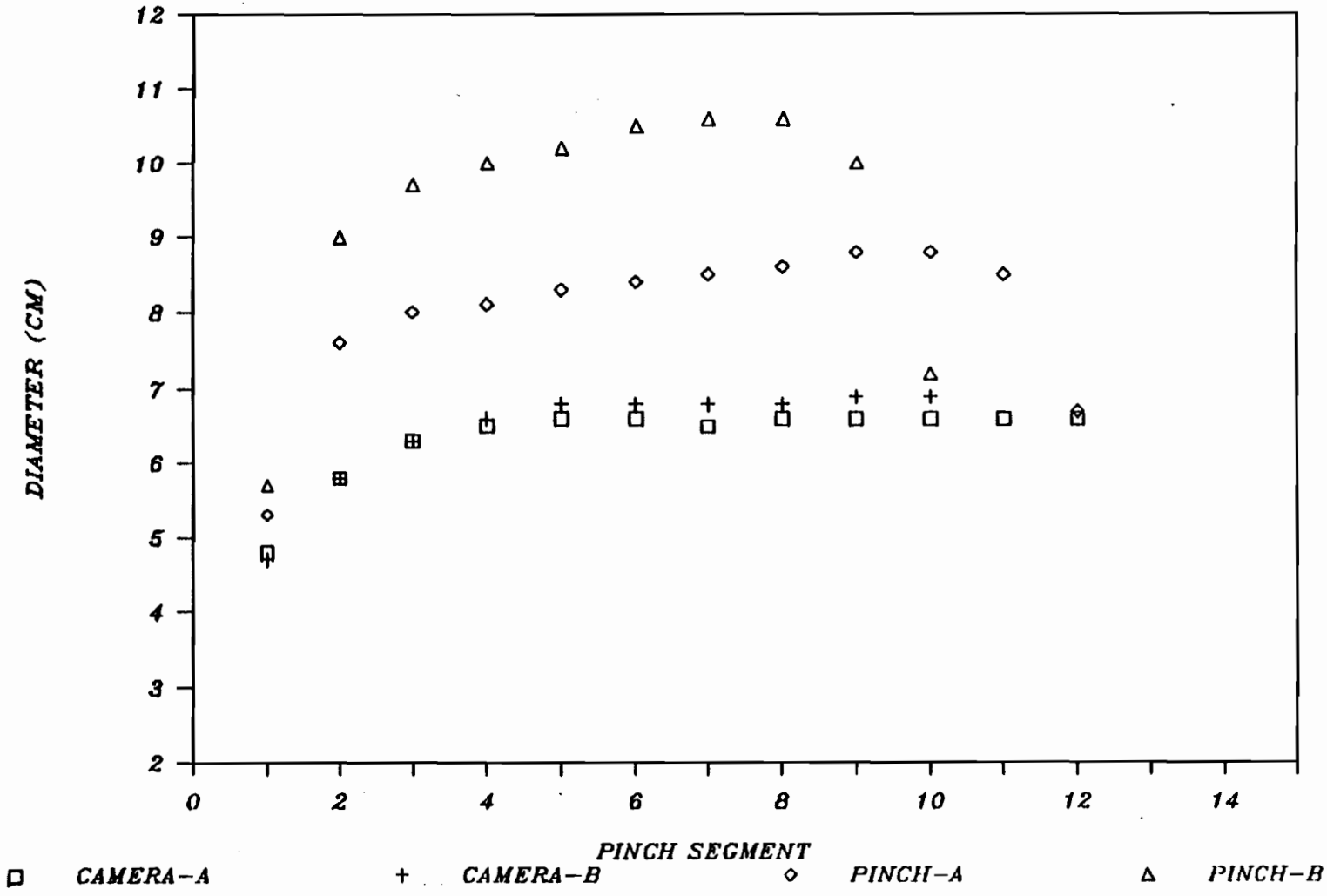

Figure 5.24: Parison Diameter Profile, for Resins A and B, Measured with Pinch-Off Mold and Video Camera.

is made, in this section, by displaying results at various extrusion gaps, with a step down and up halfway through the extrusion, at various melt temperatures, injection valve settings and shot numbers.

The pinch-off mold was employed in combination with the diameter profile obtained from the video camera and the software PINCH, to estimate the parison thickness profile. It is necessary to make the comparison at equispaced diameter scan locations, in order to obtain correspondence with the pinch-off mold segments.

The equilength on-line thicknesses were obtained with Equation (4.65), in conjunction with a gap scan and the software SWELL, for the determination of the swell factors, B_{12} and ϵ, and the software PINCH, for the outer diameter profiles.

$$W(1) = \pi\rho h_o(1)L(1)D_oB_{12}(1)\exp[t(1)/\epsilon(1)] \qquad (4.65)$$

Several replicates were performed for both the pinch off mold and the on-line measurements. The means of these replicates are presented. The individual segments were allowed to relax for the one second mold close time, in addition to the individual segment suspension time. The individual suspension times were obtained by interpolation based on the weight distribution, obtained from the pinch-off mold.

5.1.4.2.1 EFFECT OF GAP The comparison of the two thickness measurement techniques, for both resins, is presented in Figures 5.25, 5.26, 5.27, 5.28 and 5.29 for constant extrusion gaps of 0.75, 1.0, 1.25, 1.5 and 1.75 mm, respectively. The agreement is very good for all the gaps. The agreement tends to deviate slightly, for Resin B, at the highest gap of 1.75 mm, because of the increasing invalidity of Equation (4.58).

$$D(i) \gg h(i) \qquad (4.58)$$

As expected, the thickness increases with increasing gap. The thickness decreases along the length of the profile reaching a steady value. This result is in contradiction with the previous belief (31,38) that thickness tends to increase along the length of the parison. These results were verified with a micrometer and visual observation, by measuring the thickness at the top and the bottom of the parison. Again, the thickness at the top was greater than the thickness at the bottom of the parison.

The results can be explained by observing that the diameter swells at a much greater initial rate than the thickness. The swelling of the diameter tends to stretch the parison outward in the radial direction, thus decreasing the thickness. However, it is important to realize that, this result is specific to the resin chosen. Kalyon (6) observed similar results.

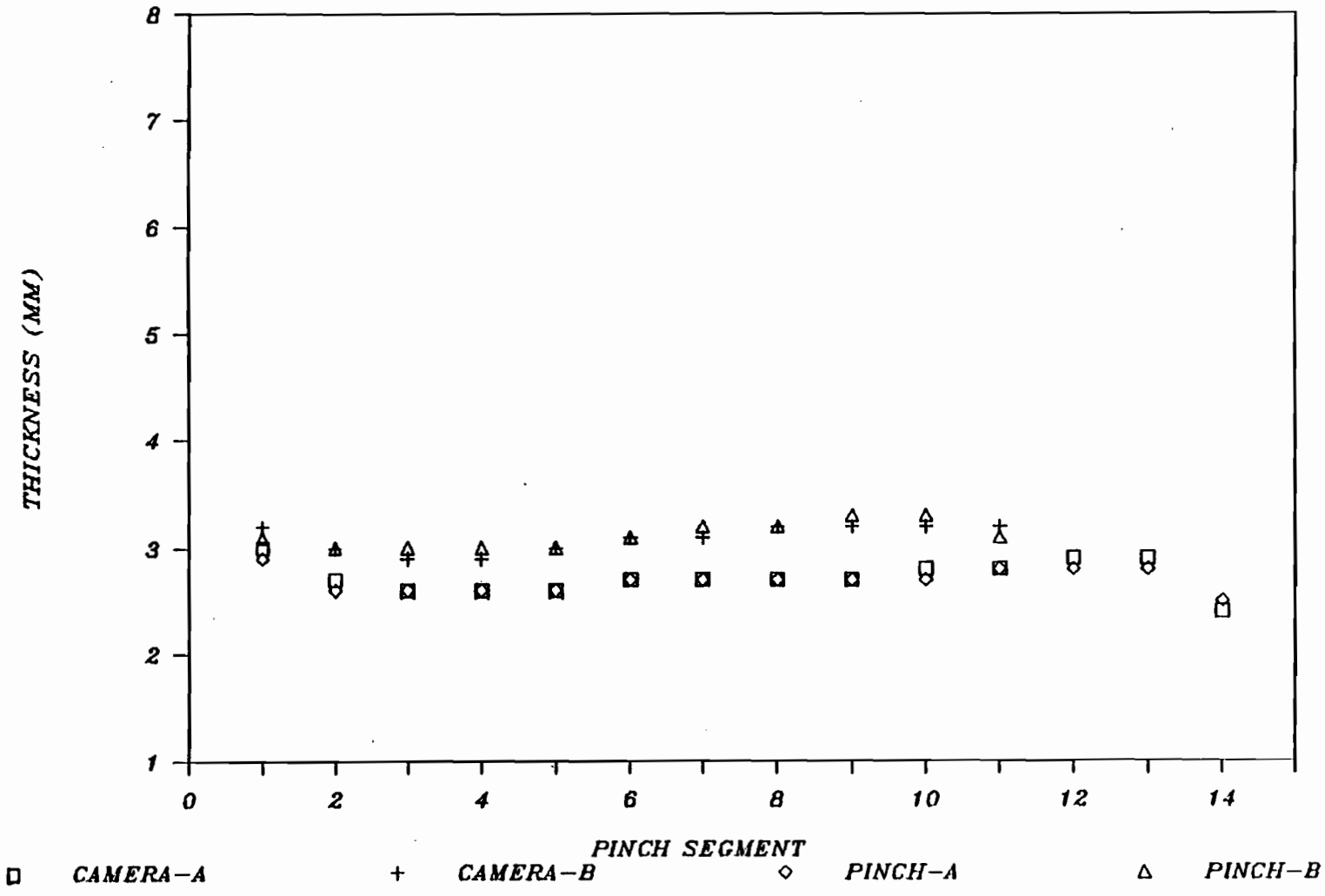

Figure 5.25: Parison Thickness Profiles, Measured with Pinch-Off Mold and Video Camera at 0.75 mm Constant Die Gap.

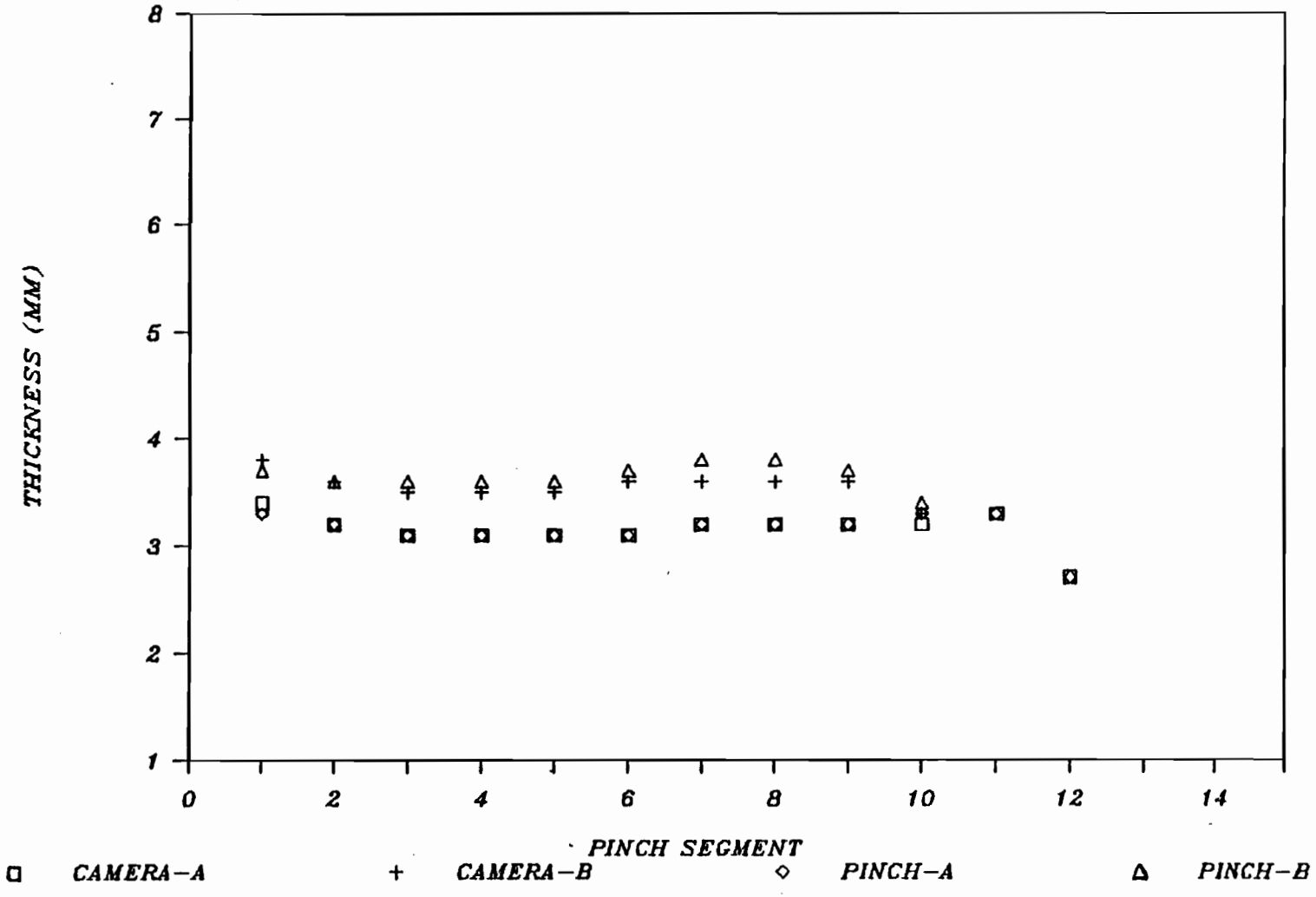

Figure 5.26: Parison Thickness Profiles Measured with Pinch-Off Mold and Video Camera at 1.0 mm Constant Die Gap .

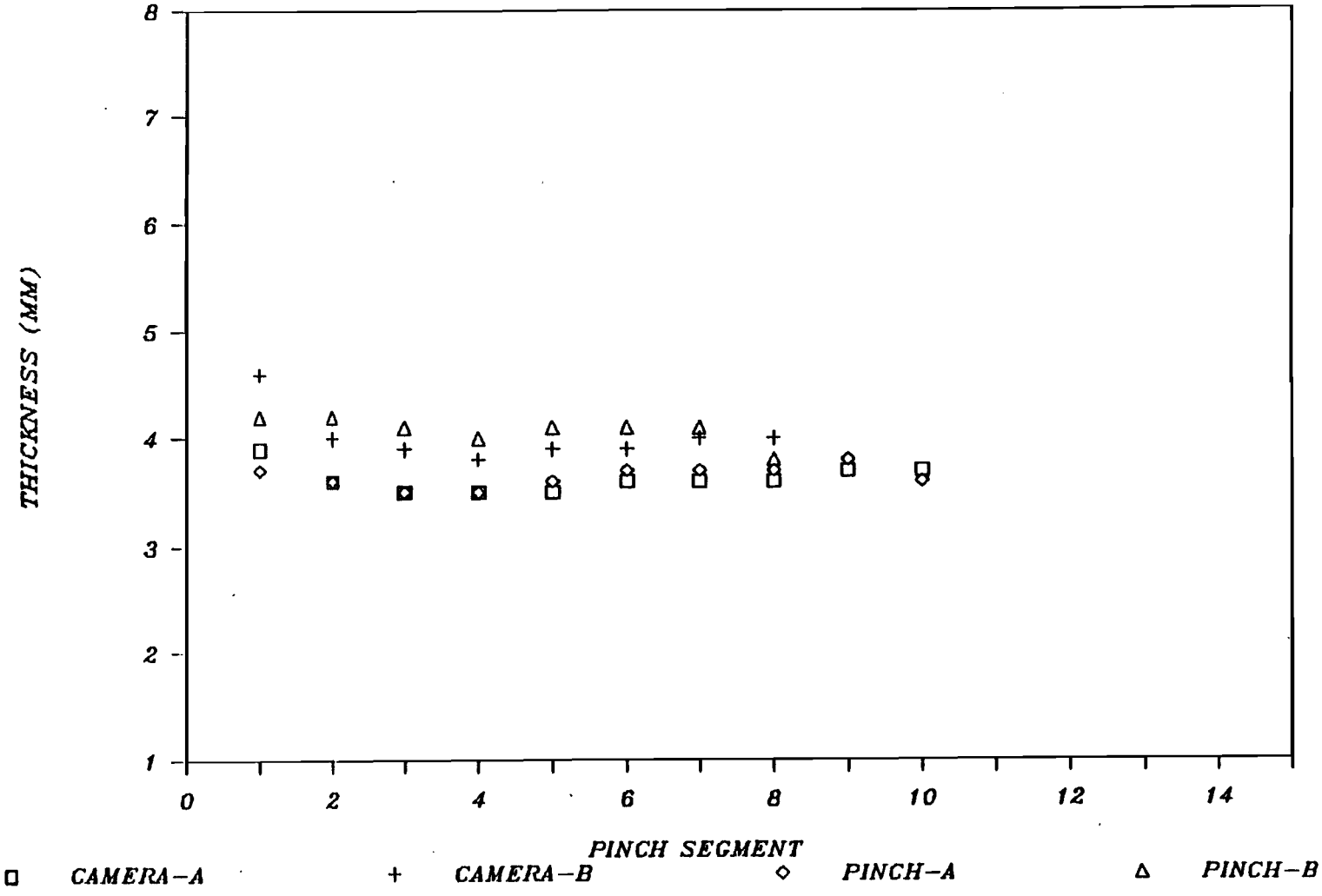

Figure 5.27: Parison Thickness Profiles, Measured with Pinch-Off Mold and Video Camera at 1.25 mm Constant Die Gap.

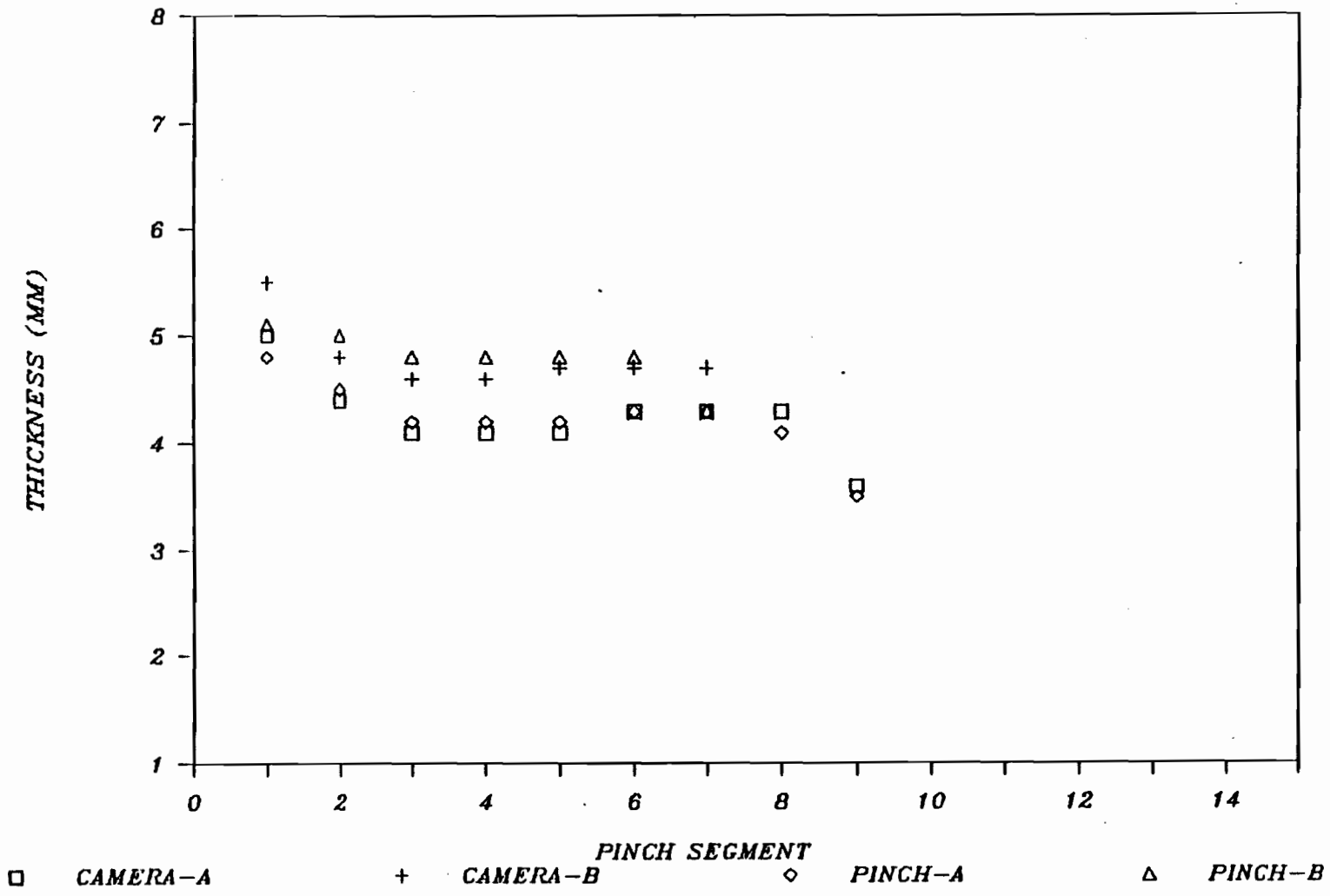

Figure 5.28: Parison Thickness Profiles, Measured with Pinch-Off Mold and Video Camera at 1.50 mm Die Gap.

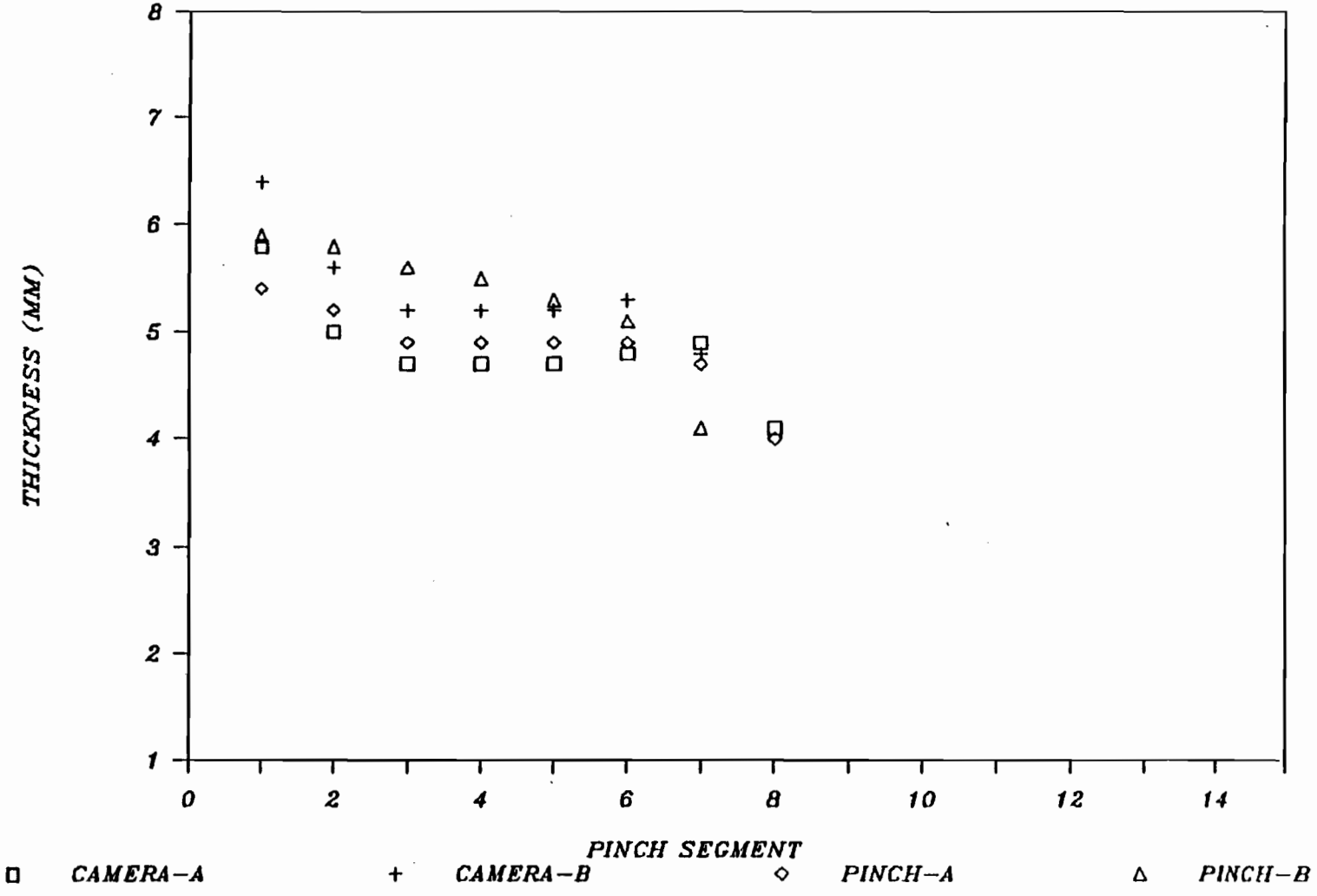

Figure 5.29: Parison Thickness Profiles, Measured with Pinch-Off Mold and Video Camera at 1.75 mm Die Gap.

5.1.4.2.2 EFFECT OF GAP STEP Figures 5.30 and 5.31 illustrate the effect on the thickness profile of steps down and up, respectively, in the gap, halfway through the extrusion. The transition to the new thickness is quick, requiring only one transition segment. This is an important point, as will be shown later in this work.

5.1.4.2.3 EFFECT OF MELT TEMPERATURE The effect of melt temperature on the thickness profile of Resin A is illustrated in Figures 5.32. The effect of melt temperature seems negligible for this range of the dependent variable. The agreement of the pinch-off mold with the on-line measurement is shown in Figures 5.33 and 5.34 for melt temperatures of 190 and 210°C, respectively.

5.1.4.2.4 EFFECT OF SHOT NUMBER The effect of shot size on the thickness profile of Resin A is illustrated in Figures 5.35. Increased shot numbers result in an increase in the number of pinch segments, as expected. The agreement of the pinch-off mold with the on-line measurement is shown in Figures 5.36 and 5.37 for shot numbers of 3 and 5 respectively.

5.1.4.2.5 EFFECT OF INJECTION VALVE SETTING The effect of injection valve setting on the thickness profile of Resin A is shown in Figure 5.38. There seems to be little effect of the

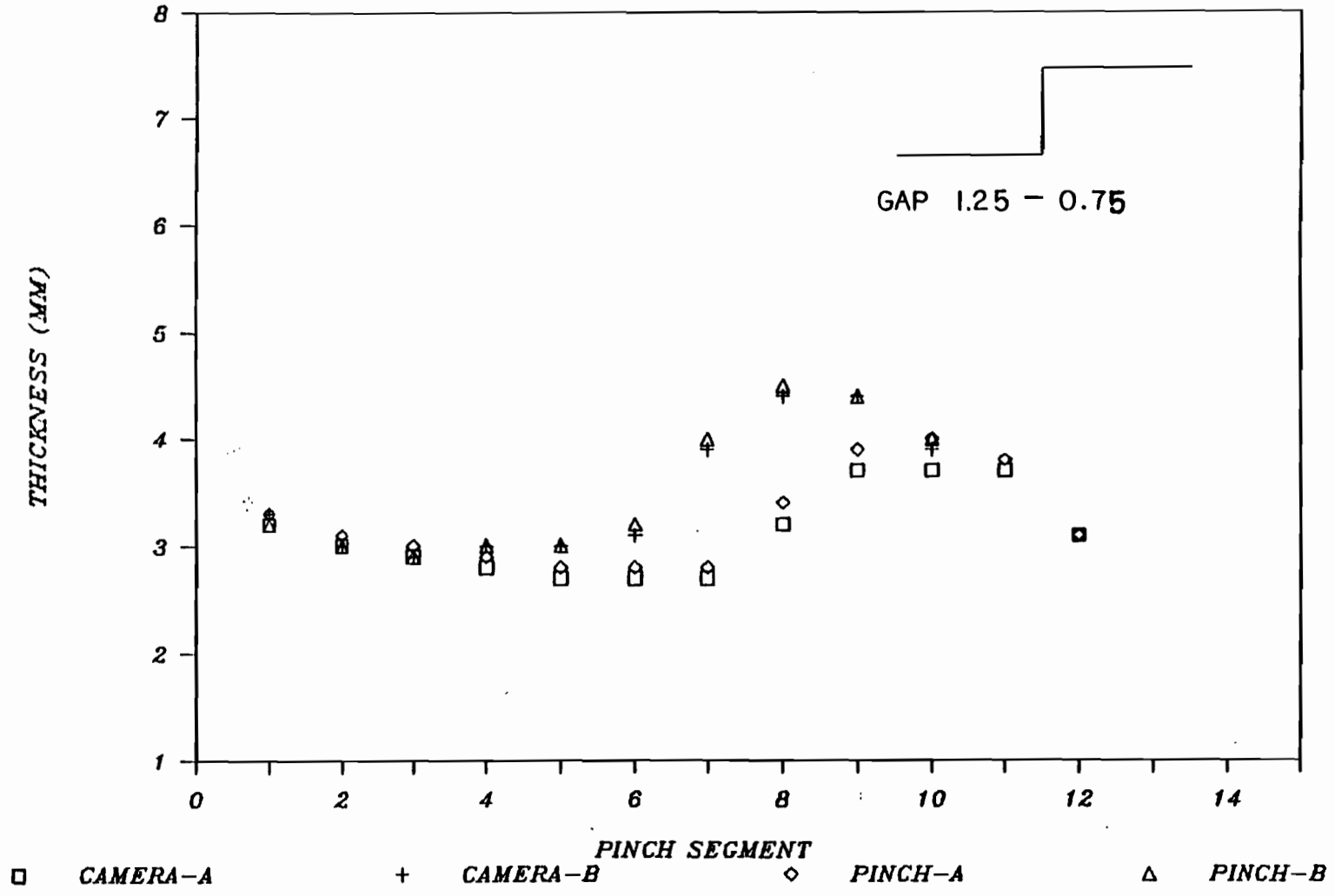

Figure 5.30: Parison Thickness Profiles, Measured with Pinch-Off Mold and Video Camera at Gap Step Down 1.25mm-0.75mm.

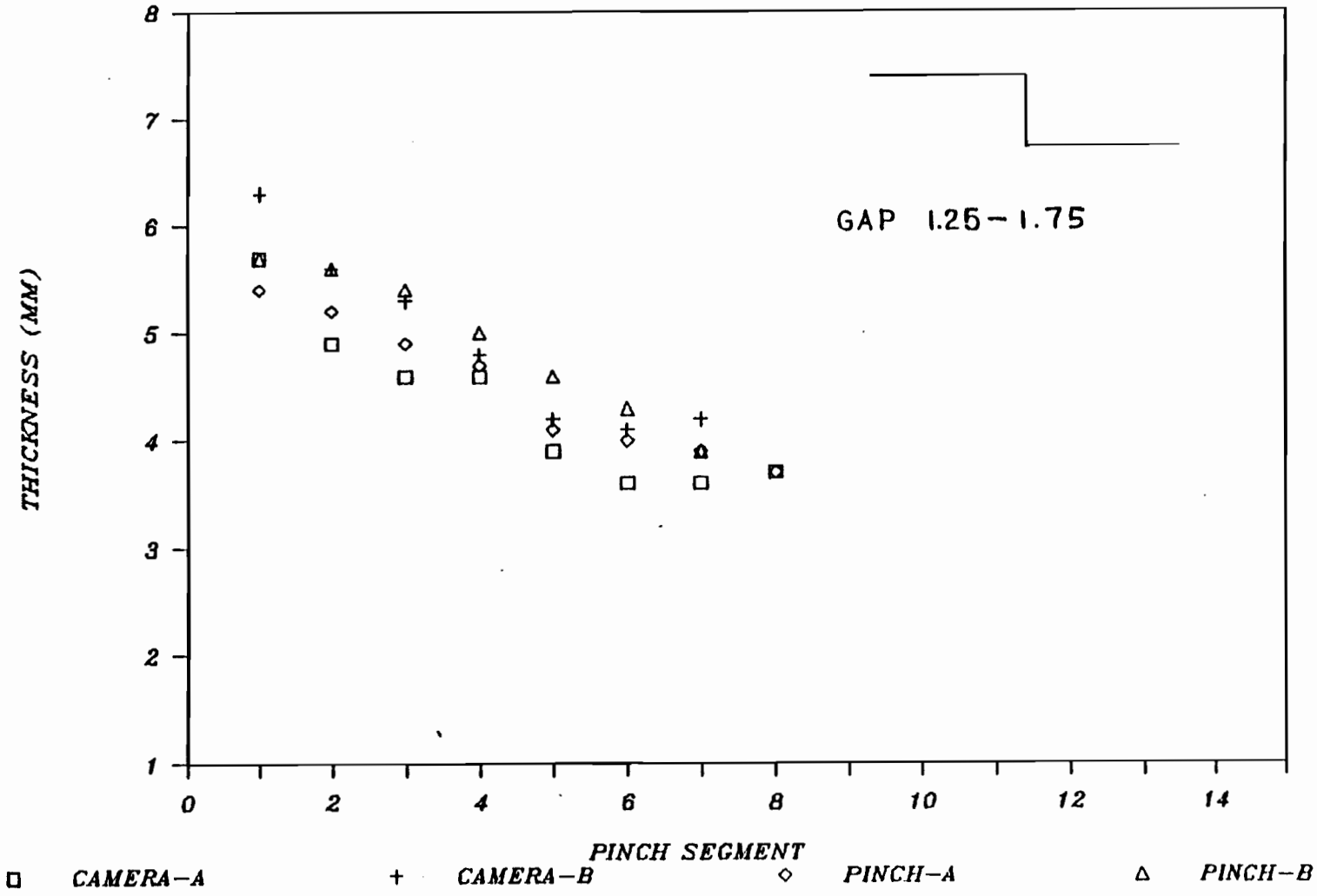

Figure 5.31: Parison Thickness Profiles, Measured with Pinch-Off Mold and Video Camera at Gap Step Up 1.25mm-1.75mm.

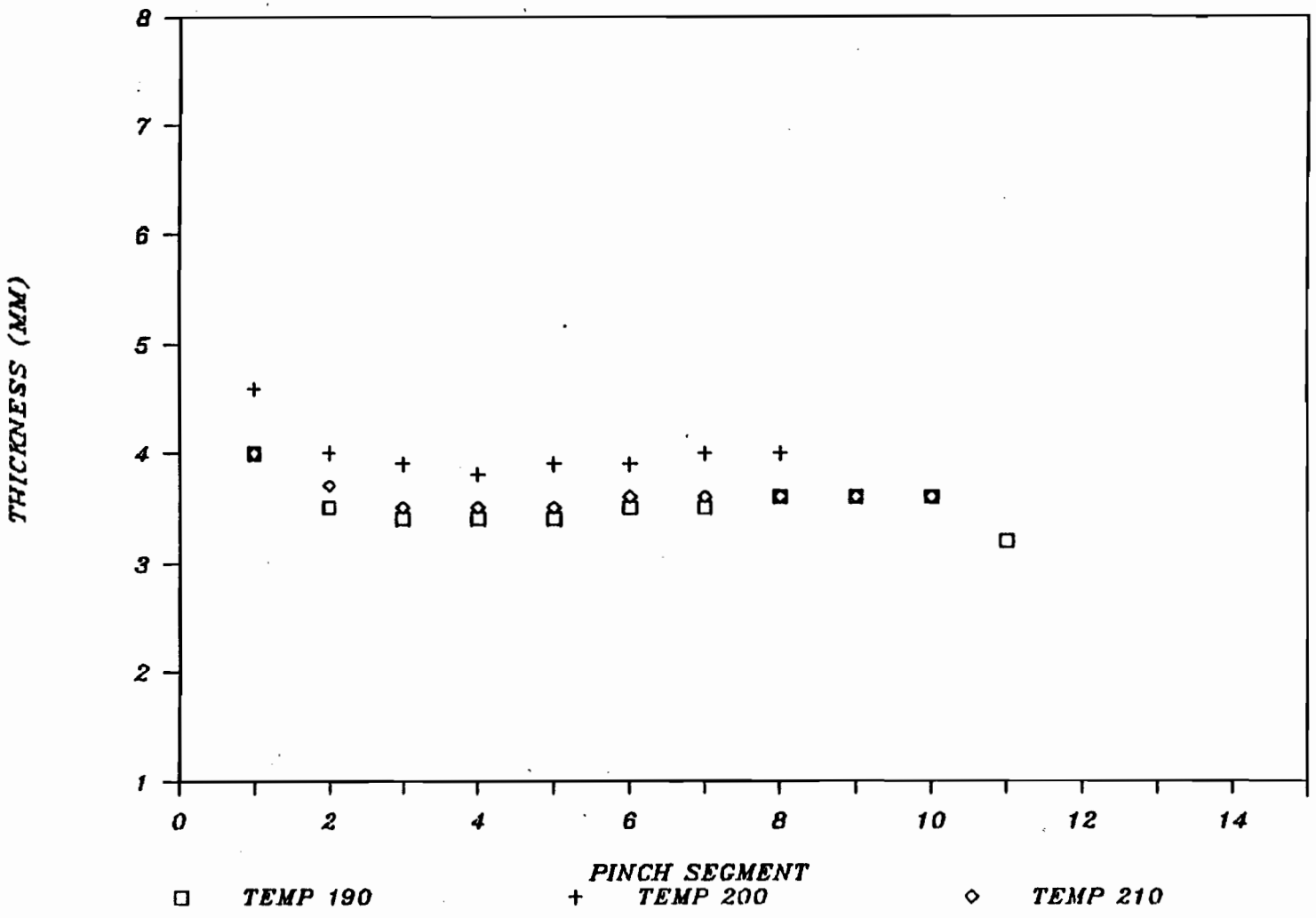

Figure 5.32: Effect of Melt Temperature on Parison Thickness Profile, for Resin A.

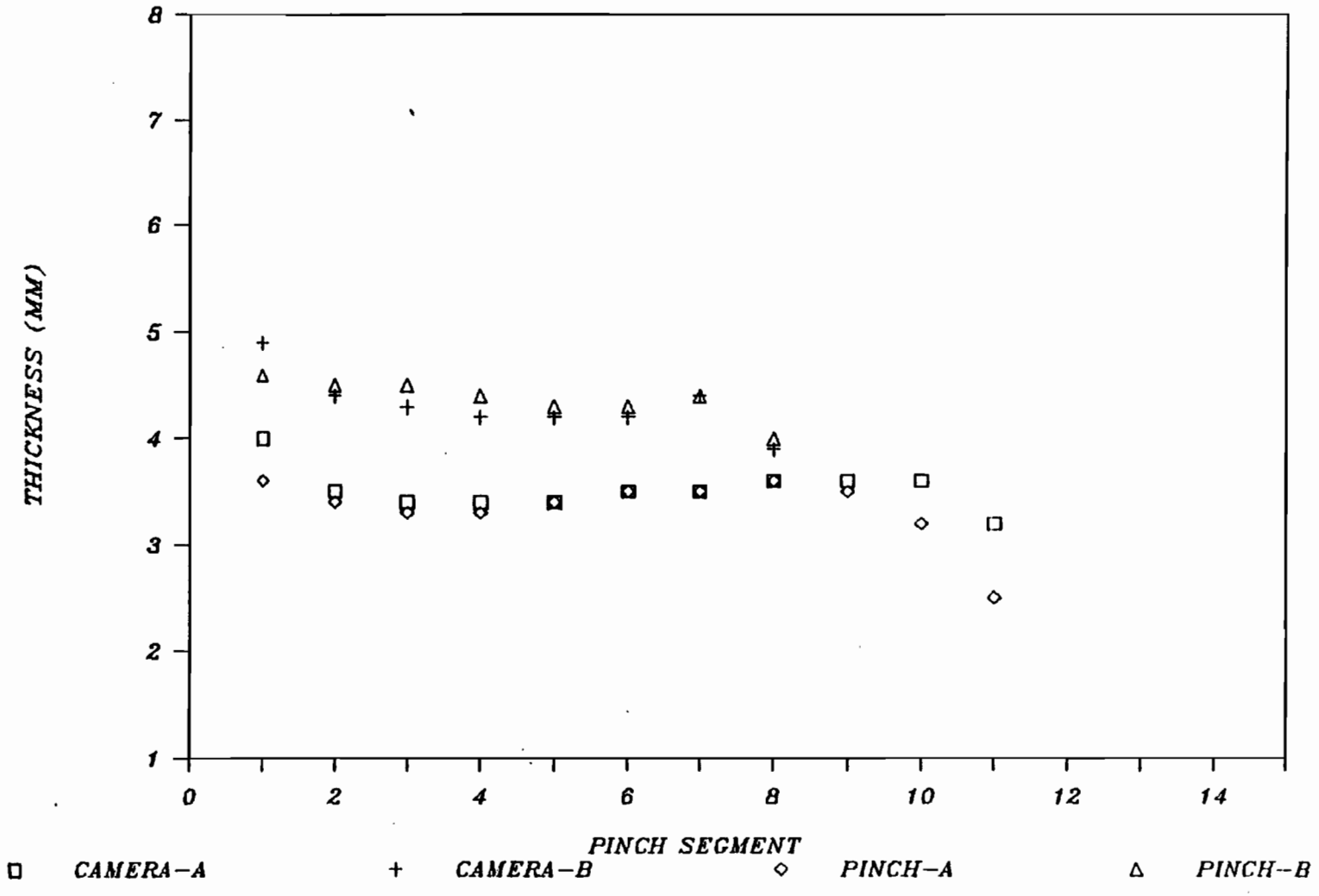

Figure 5.33: Parison Thickness Profiles, Measured with Pinch-Off Mold and Video Camera at 190°C.

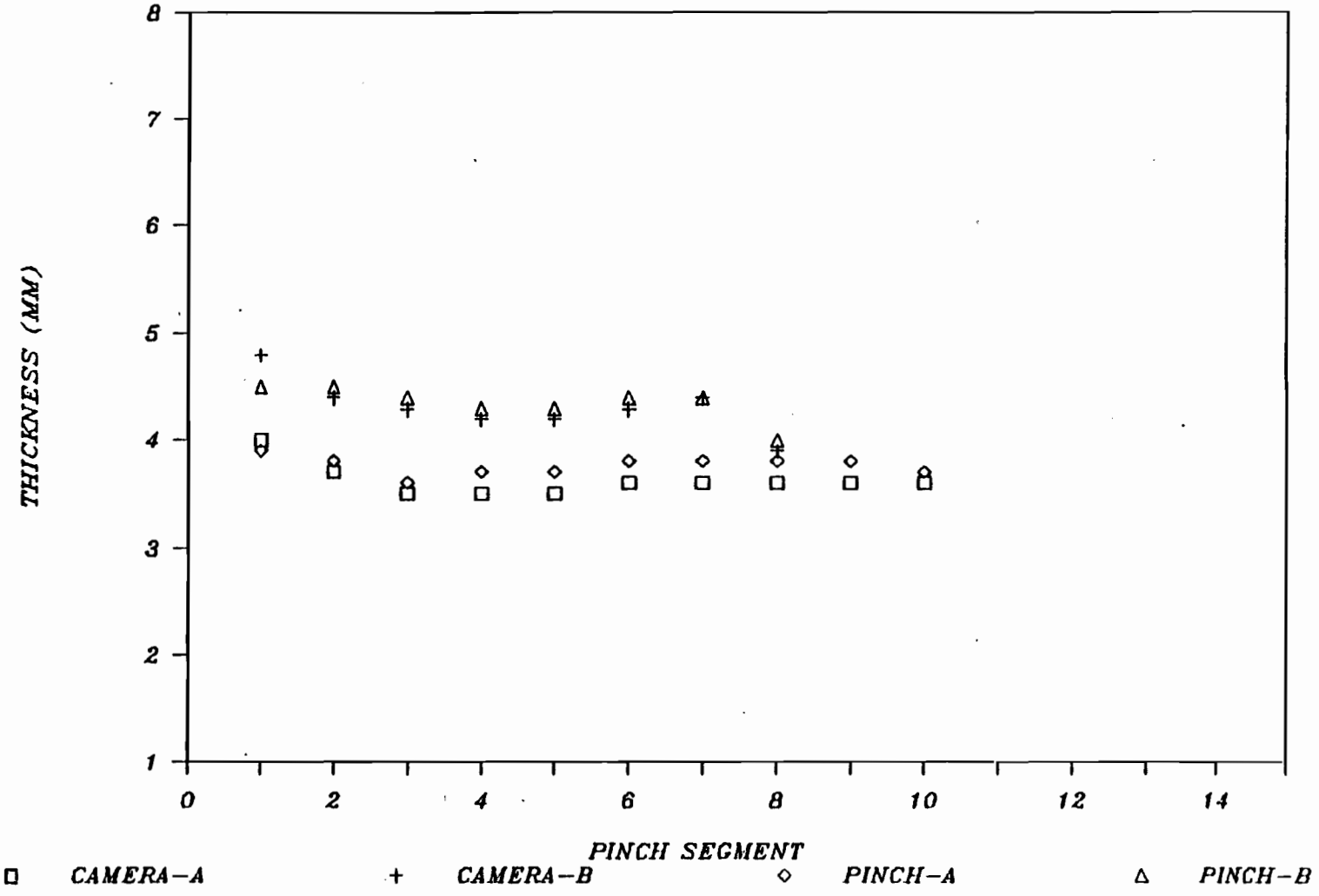

Figure 5.34: Parison Thickness Profiles, Meassured with Pinch-Off Mold and Video Camera at 210°C.

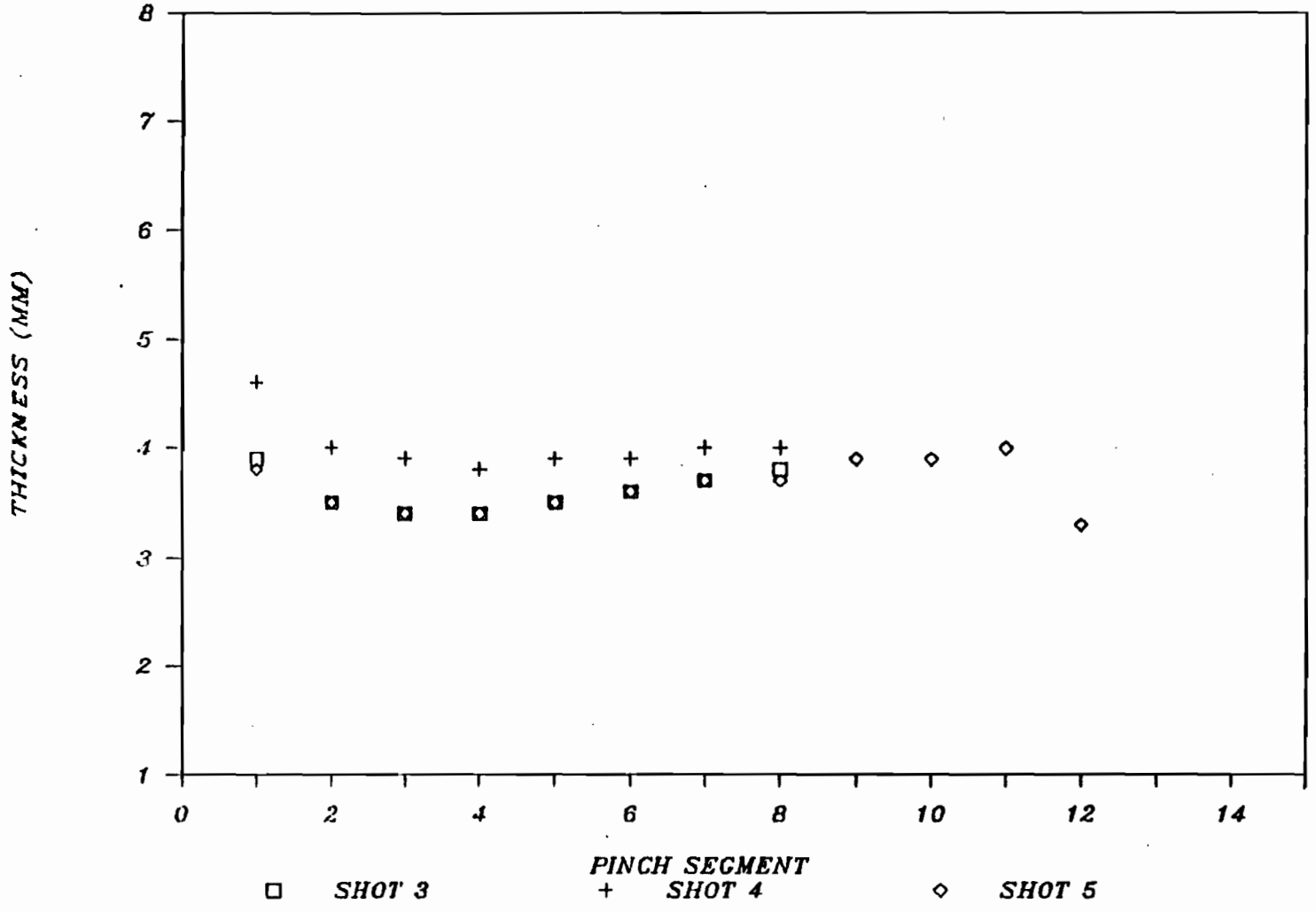

Figure 5.35: Effect of Shot Number on Parison Thickness Profile, for Resin A.

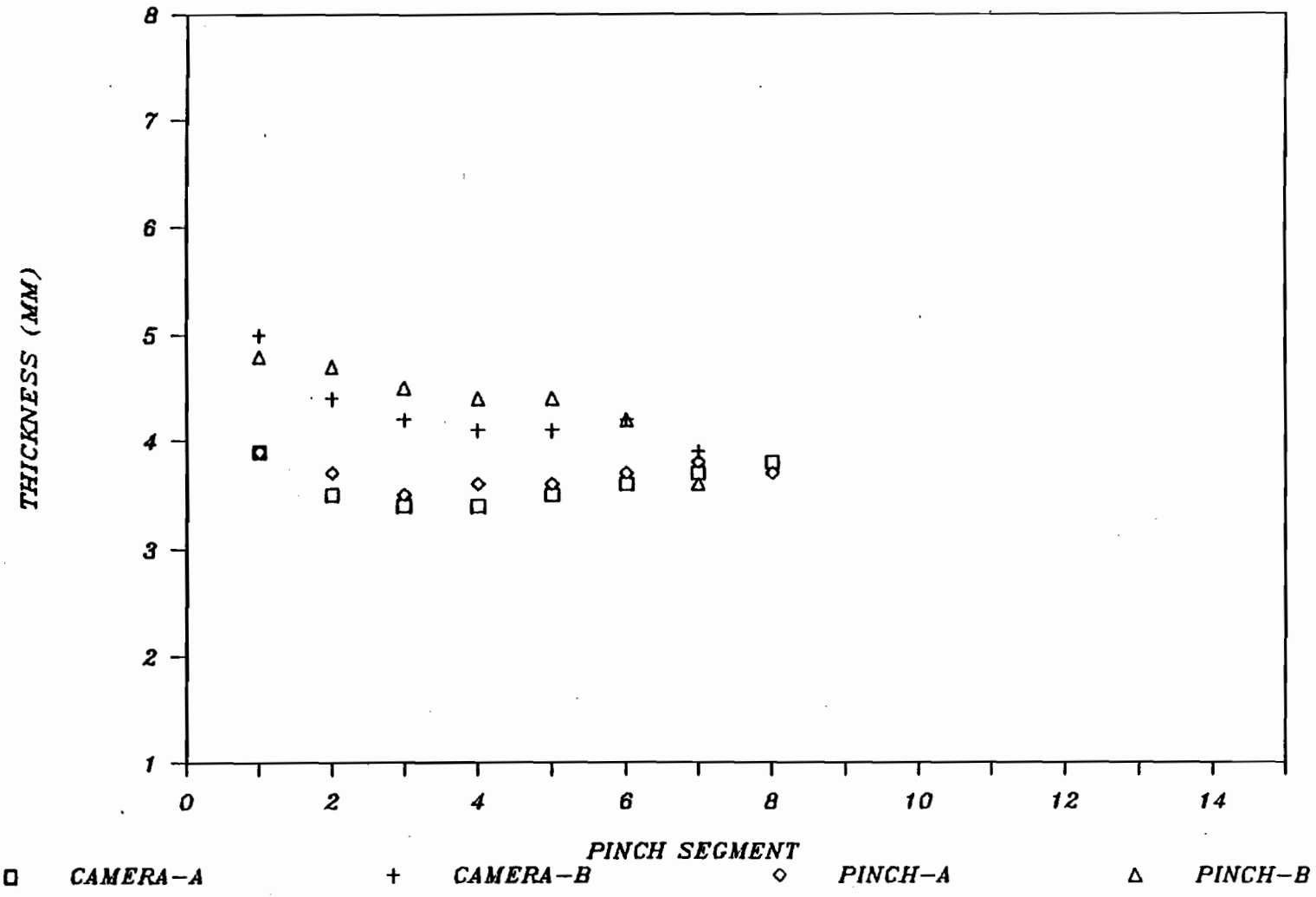

Figure 5.36: Parison Thickness Profiles, Measured with Pinch-Off Mold and Video Camera at Shot Number 3.

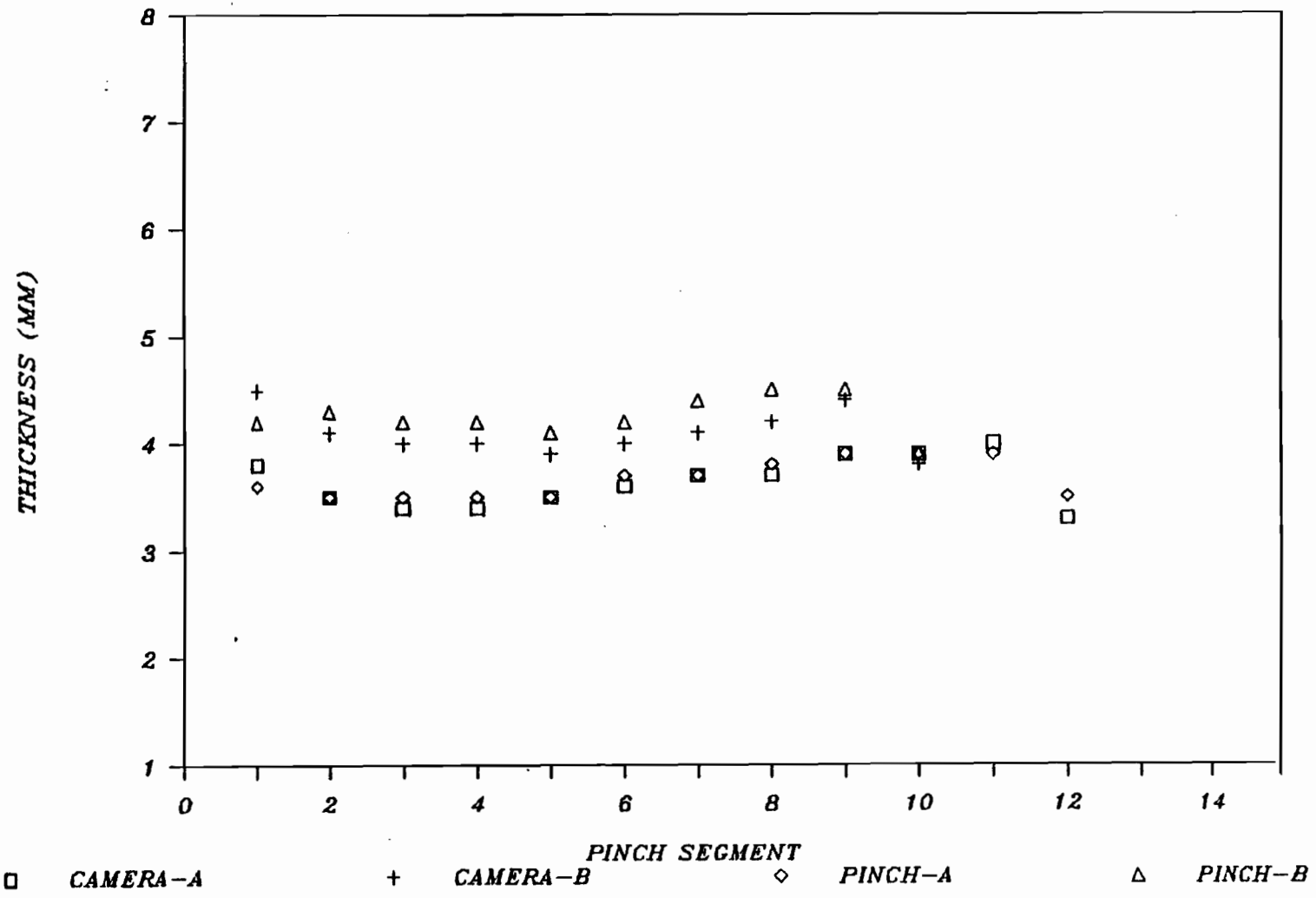

Figure 5.37: Parison Thickness Profile, Measured with Pinch-Off Mold and Video Camera at Shot Number 5.

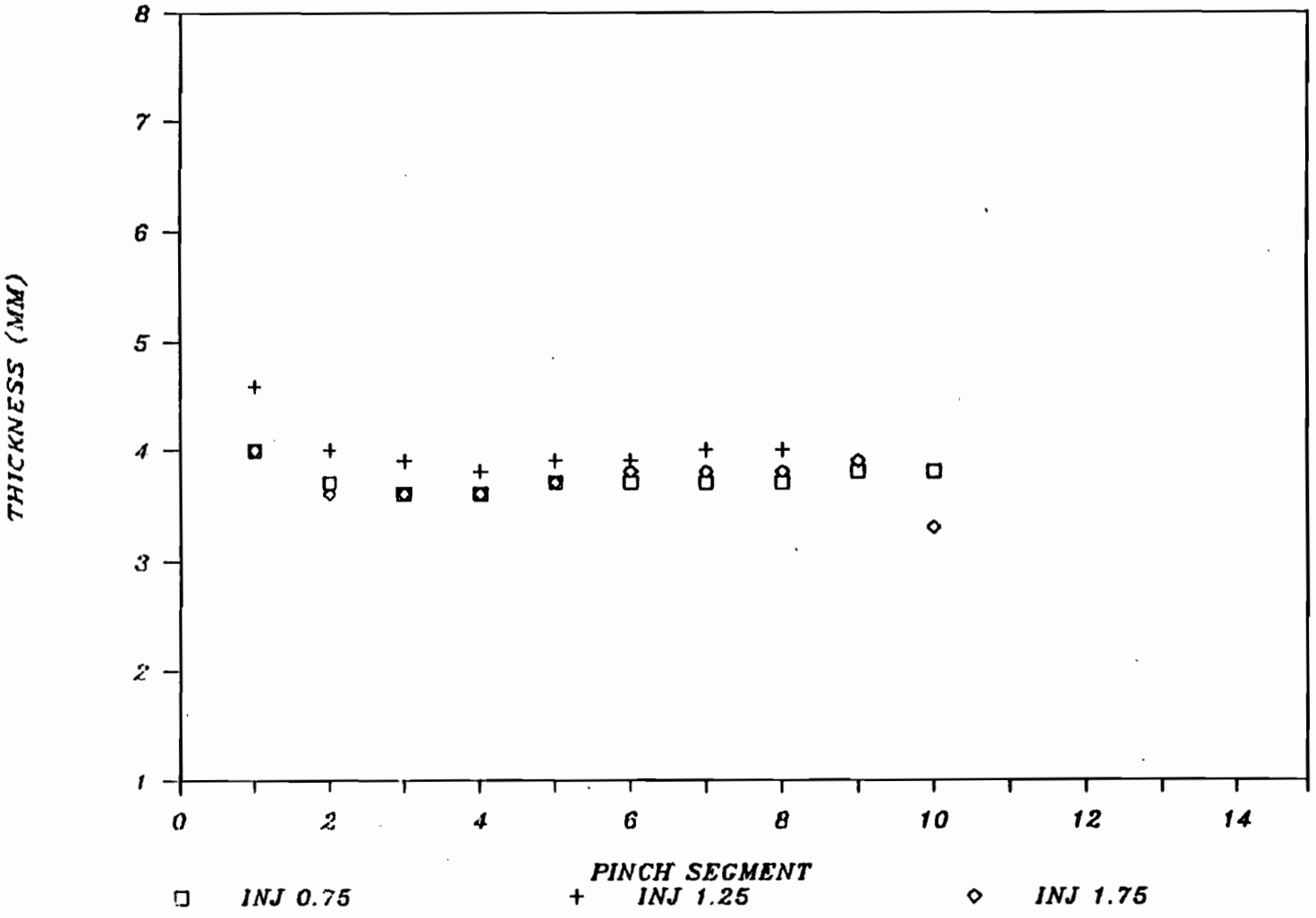

Figure 5.38: Effect of Injection Valve Setting on Parison Thickness Profile, for Resin A.

injection rate on the thickness profile. It is important to realize that the decrease in injection rate causes two balancing effects to occur. The decreased shear rate, and subsequently swell, is offset by the increase in swell due to the increased extrusion time.

It is also important to realize that the swell obtained from a blow molding machine is not equivalent to the swell obtained from a laboratory isothermal oil bath experiment. The swelling in blow molding is limited by the parison extrusion time and the mold close time.

The agreement between the pinch-off mold and the on-line measurement is shown in Figures 5.39 and 5.40 for injection valve settings of 0.75 and 1.75 respectively.

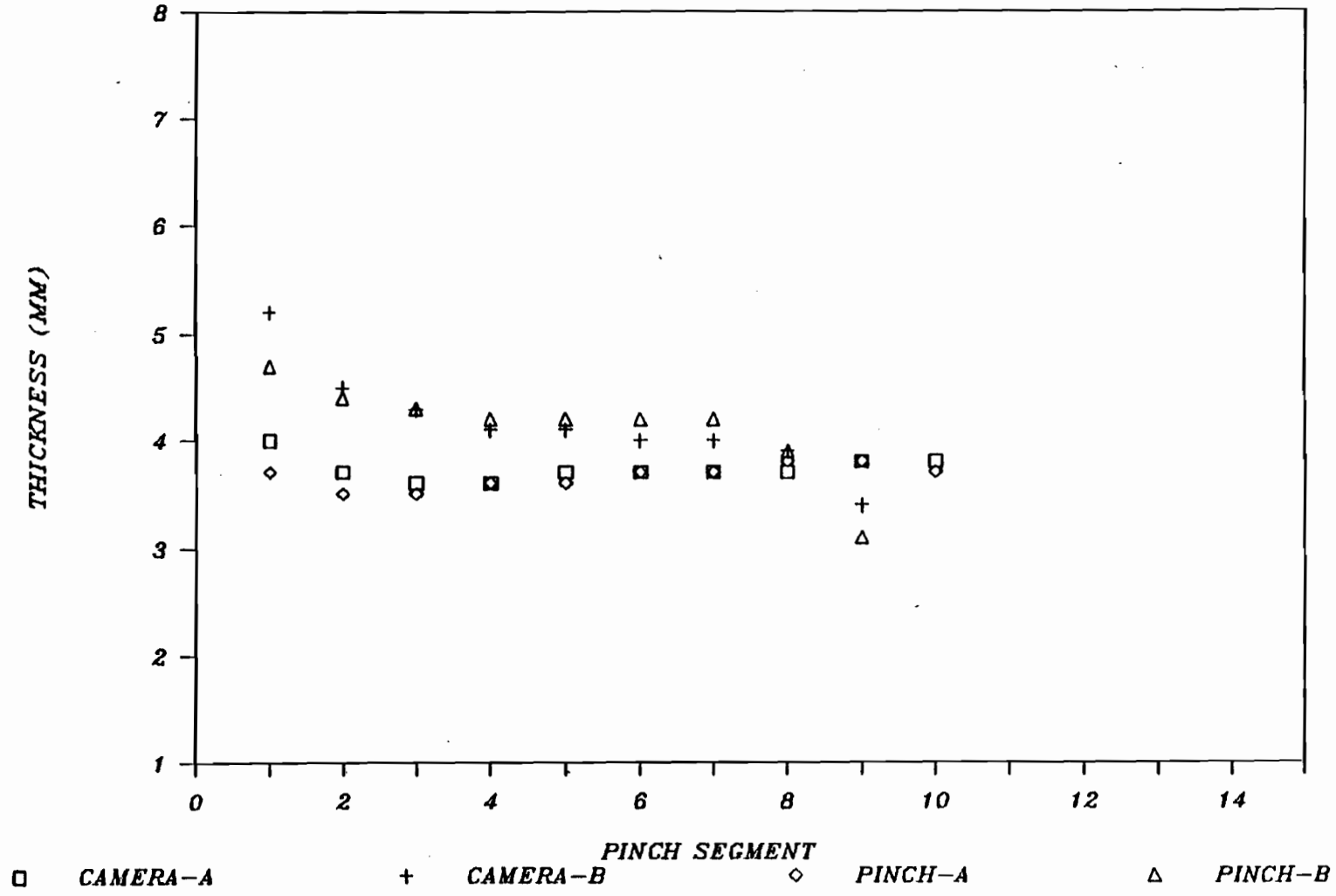

Figure 5.39: Parison Thickness Profiles, Measured with Pinch-Off Mold and Video Camera at Injection Valve Setting 0.75.

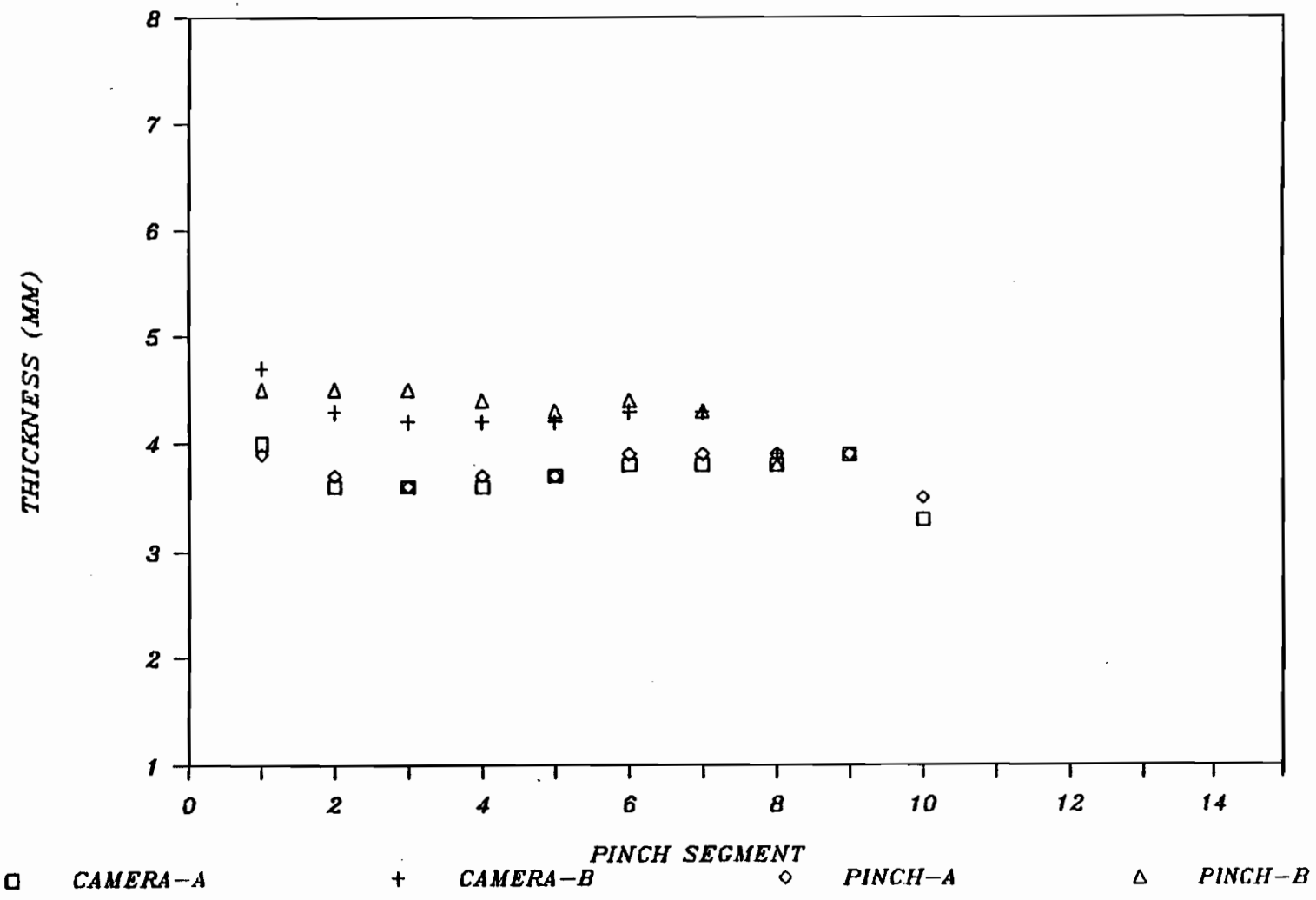

Figure 5.40: Parison Thickness Profiles, Measured with Pinch-Off Mold and Video Camera at Injection Valve Setting 1.75.

5.2 DYNAMICS AND ON-LINE CONTROL OF PARISON THICKNESS PROFILES

5.2.1 DYNAMIC RESPONSES

A process model is necessary for developing a control system. Processes can be simulated by solving the appropriate transport equations with initial and boundary conditions. The differential equations associating the variables and parameters are then usually solved with considerable computing effort. These models are not suitable for on-line real time applications. Empirical models utilizing the transfer function approach are more appropriate.

$$G(t) = Y'(t) / X'(t) \qquad (5.1)$$

G(t) is the process transfer function, Y'(t) is the output response and X'(t) is the input variable.

The transfer function scheme of closed loop parison thickness profile control is shown in Figure 5.41. The various transfer functions and variables are identified in Table 5.2. A practical scheme for the direct measurement of parison thickness profiles was not found and therefore, an inferential scheme was a logical alternative (81). The parison thickness profile can be estimated, as shown in Chapter 4, from the parison diameter profile, parison length versus time measurements and the melt flowrate during extrusion.

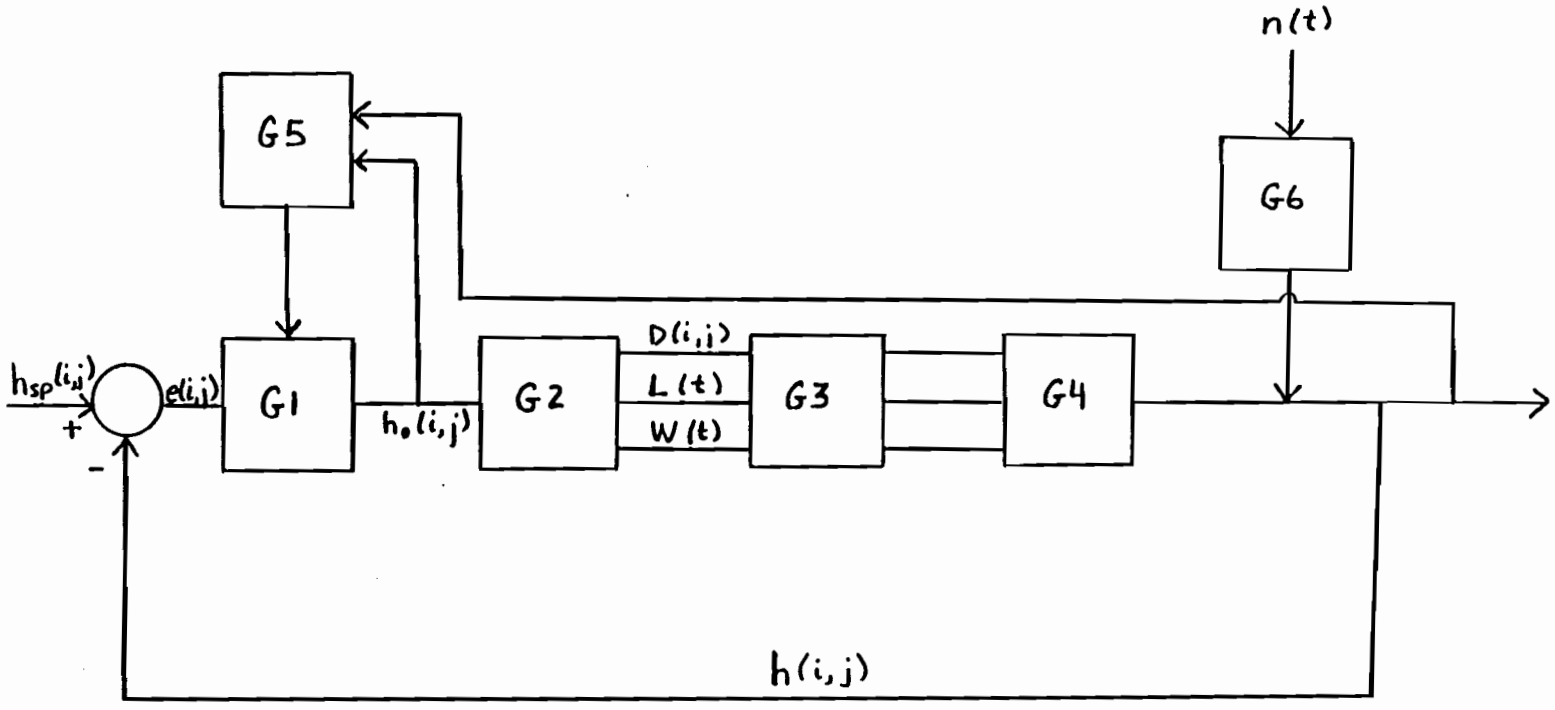

Figure 5.41: Overall Transfer Function Scheme for Control of Parison Thickness Profiles.

TABLE 5.2

TRANSFER FUNCTION NOMENCLATURE

VARIABLE	DEFINITION
G1	Controller Transfer Function
G2	Process Transfer Function
G3	Measurement Transfer Function
G4	Estimation Model Transfer Function
G5	Controller Adjustment Transfer Function
G6	Noise Transfer Function
i	Parison Profile Point Location
j	Cycle Location
$h_{SP}(i,j)$	Programmed Set Point
h(i,j)	Measured Thickness Profile
$h_O(i,j)$	Die Gap Profile
e(i,j)	Error Profile
D(i,j)	Diameter Profile
L(t)	Length Versus Time Measurements
W(i,j)	Flowrate
n(t)	White Noise

The transfer function, G4, is the estimator model. The direct measurement is represented by G3 and the process by G2. The controller transfer function is represented by G1.

5.2.1.1 IN-CYCLE VERSUS CYCLE TO CYCLE CONTROL

It is important to define the time scale, for the specific case of parison thickness profile control, in which the control is to be enacted. The dynamic studies necessary for the control model development are performed in the corresponding time frame. In-cycle control incorporates absolute time during the parison extrusion as the time scale. It can be discrete or continuous. Cycle-to-cycle control incorporates the cycle number as the corresponding discrete time scale. The relative advantages and disadvantages of the in-cycle and cycle-to-cycle control should be examined.

5.2.1.1.1 IN-CYCLE CONTROL

In-cycle control involves corrective adjustments to the die gap during one extrusion cycle. Thus, it is necessary to obtain a sufficient number of data points of the controlled variable of interest in order to properly characterize the response. Typically, to obtain an adequate in-cycle stochastic model, a minimum of 32 changes in the manipulated variable must be enacted during the cycle.

during the cycle.

It was ascertained, for the blow molding machine used in this study (Section 5.1.2.2.1), that a change in the gap requires 0.05 seconds, for any magnitude and direction of change. Consequently, for a typical one second extrusion cycle, the number of possible gap transitions is limited to twenty. This limitation means that an in-cycle stochastic response determination would not be accurate.

A deterministic model would also require a minimum of three data points during the gap transition, for proper characterization. The number of transition thickness profile points is directly dependent on the number of gap values available during the transition. The number of gaps available, in the transition region, is limited to the initial gap, the final gap and one transition value, by a timing restriction associated with the data acquisition section of the system. These values are only useful for a crude estimate of a first order deterministic response. The speed of the computer and the camera resolution are the causes of this limitation, as thickness measurements cannot be obtained during the extrusion, with reasonable accuracy. A limitation associated with in-cycle control is that once a segment has been extruded, any error in the thickness of that segment cannot be corrected in that cycle.

For the above reasons, in-cycle control is deemed not feasible, for the case of closed loop parison thickness profile control, at least in relation to the blow molding machine and

5.2.1.1.2 CYCLE-TO-CYCLE CONTROL

Cycle-to-cycle control has the changes in the manipulated variables enacted between parison extrusions. This is the control of choice, because of the limitations associated with in-cycle control.

5.2.1.2 THICKNESS PROFILE BEHAVIOR TO GAP STEPS DURING EXTRUSION

In-cycle disturbances, in the form of a step in the gap during the extrusion, are essential for the determination of the interaction response of the thickness profile. Cycle-to-cycle disturbances were examined as part of the stochastic study of Section 5.2.1.3. From this point onwards in the work, the thickness profile was measured at the end of extrusion, instead of at the point of mold closing, as the end of extrusion is more universally acceptable.

The top, first segment or last extruded segment and the bottom, last segment or first extruded segment, were neglected in further aspects of this work. Both segments are generally pinched by the mold closing process. The dimensions of the first segment cannot be measured adequately. The last segment exhibited an irregular shape produced during the early stages of extrusion.

The diameter scan location is now at the halfway point of each individual equiweight segment. The software SWELL was

each individual equiweight segment. The software SWELL was employed to obtain the swell factors, B_{12} and ϵ. The software DYN was utilized for the thickness profile estimation. Steps in the gap were input during the extrusion, with emphasis being placed on determining the effect of step magnitude, direction and location during the extrusion, as well as initial gap.

5.2.1.2.1 CONSTANT GAP EXTRUSIONS The response of the thickness profile to constant gap extrusions at gaps of 0.75, 1.0, 1.25, 1.5 and 1.75 mm, for Resins A and B, is presented in Figures 5.42 and 5.43, respectively. The thickness decreases to a steady value, along the length of the parison. Resin B exhibits higher thicknesses than Resin A.

5.2.1.2.2 FINAL AND INITIAL GAP The effect of step magnitude and direction, is illustrated in Figures 5.44 and 5.45. The initial gap is 1.25 mm. Five final gaps were studied. The effect of initial gap is shown in Figures 5.46 and 5.47. The final gap is 1.25 mm. Five initial gaps were considered. The response to a gap step change was instantaneous, requiring only one transition segment, to achieve the ultimate level.

5.2.1.2.3 STEP LOCATION The effect of step location during the extrusion is shown in Figures 5.48 and 5.49, for a step

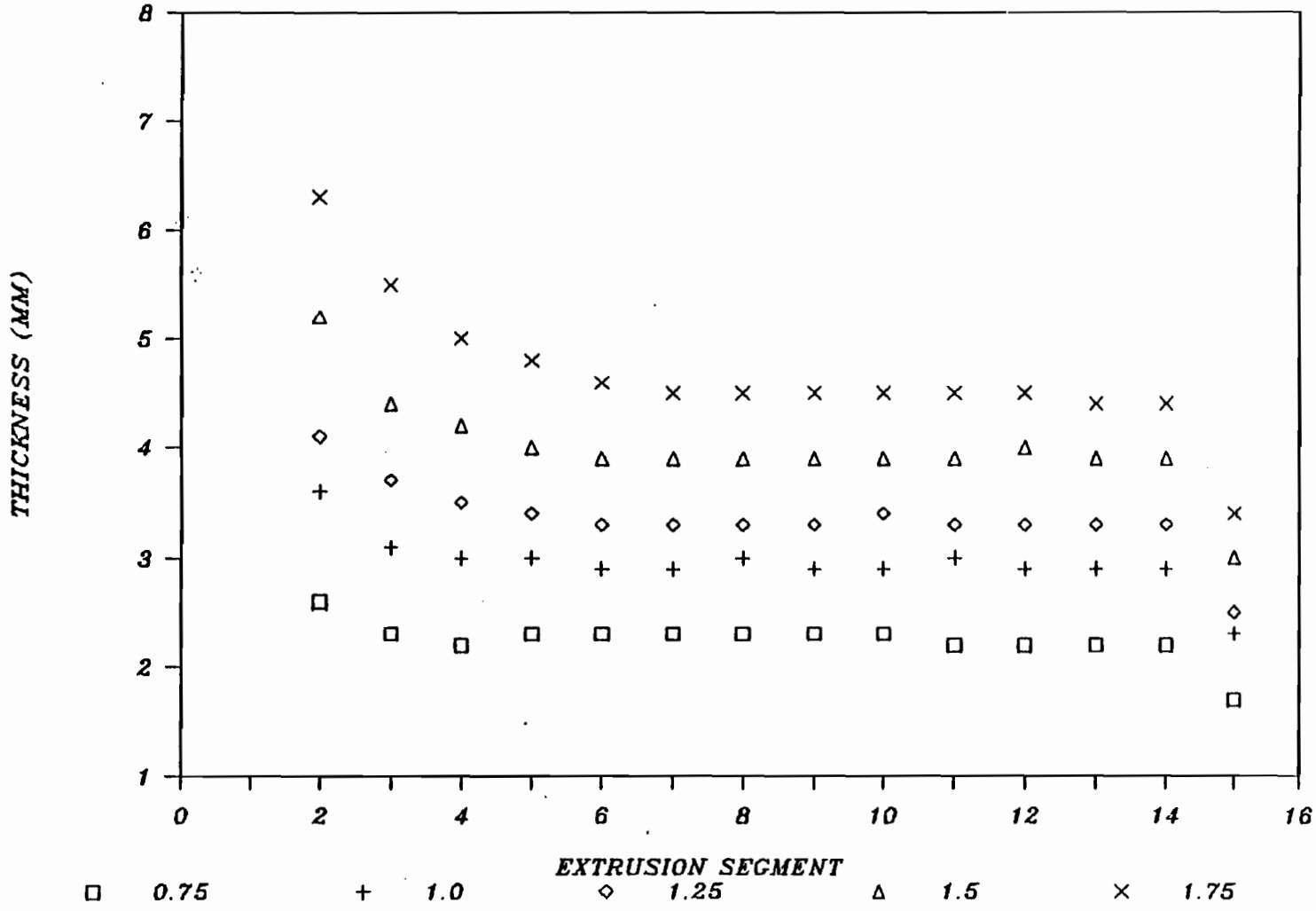

Figure 5.42: Parison Thickness Profile Response, for Resin A, to Constant Gap Extrusions of 0.75, 1.0, 1.25, 1.5 and 1.75 mm Gap.

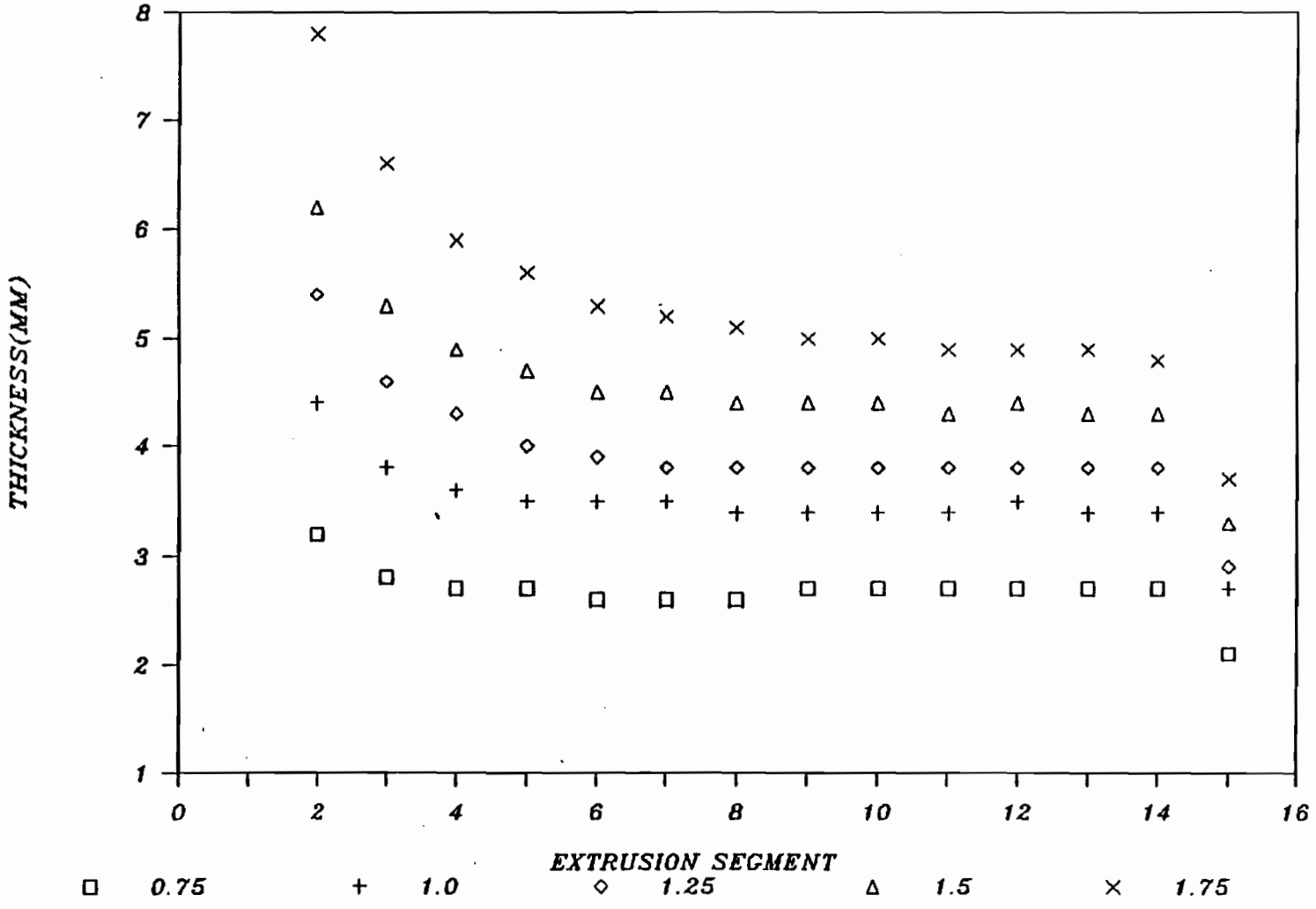

Figure 5.43: Parison Thickness Profile Response, for Resin B, to Constant Gap Extrusions of 0.75, 1.0, 1.25, 1.5, 1.75 mm Gap.

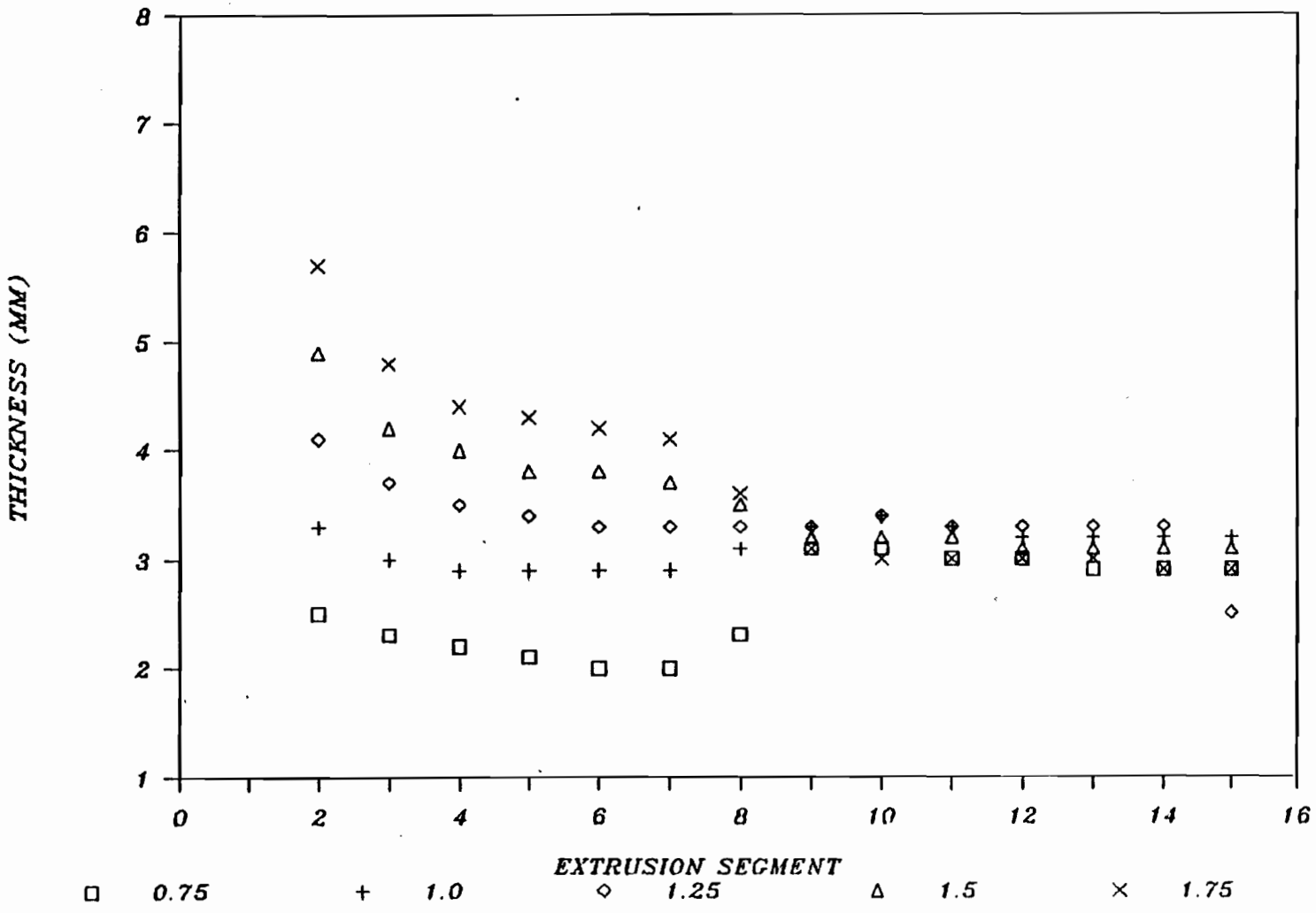

Figure 5.44: Parison Thickness Profile Response, for Resin A, to Final Gaps of 0.75, 1.0, 1.25, 1.5 and 1.75 mm Gap.

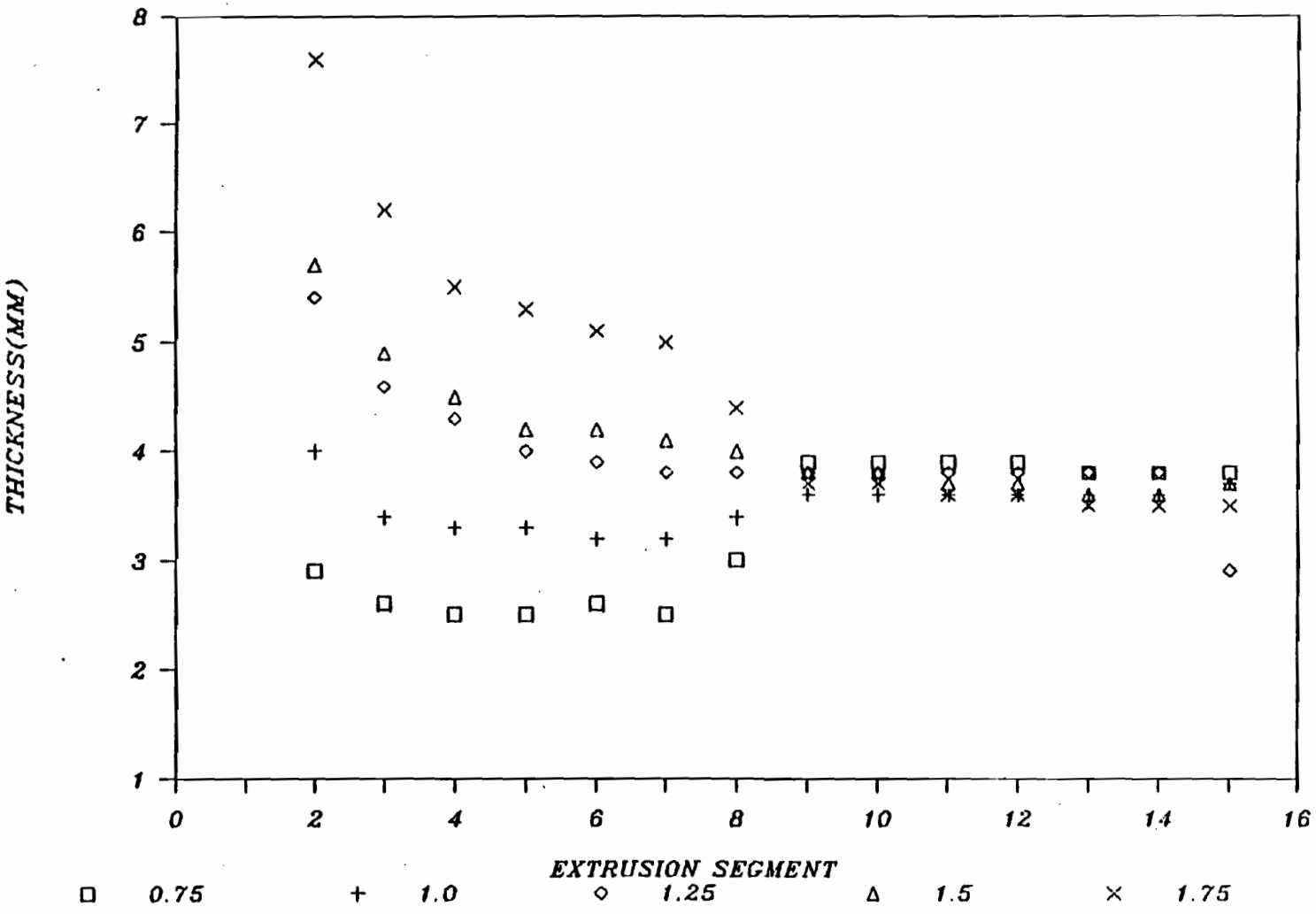

Figure 5.45: Parison Thickness Profile Response, for Resin B, to Final Gaps of 0.75, 1.0, 1.25, 1.5 and 1.75 mm Gap.

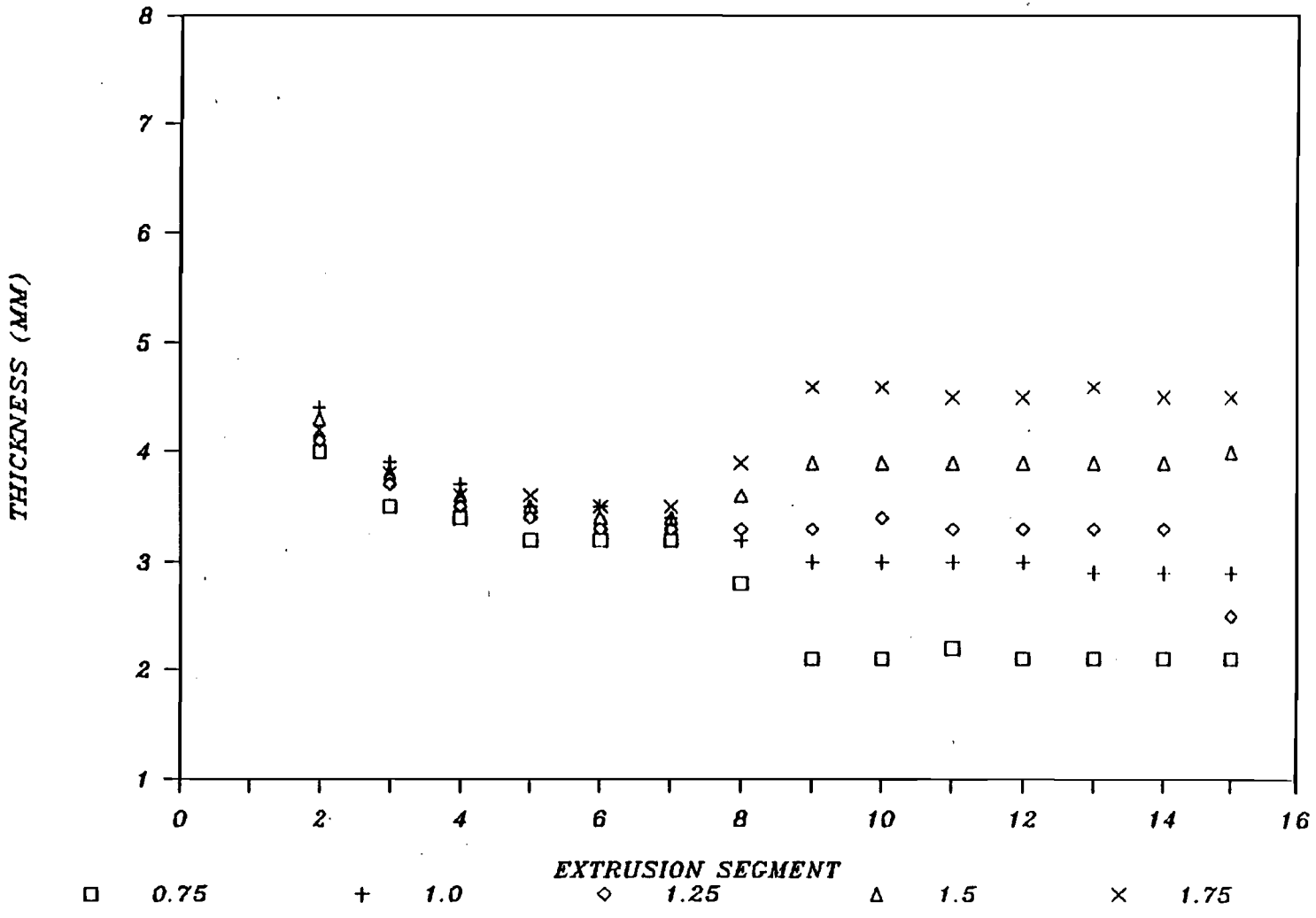

Figure 5.46: Parison Thickness Profile Response, for Resin A, to Initial Gaps of 0.75, 1.0, 1.25, 1.5, 1.75 mm Gap.

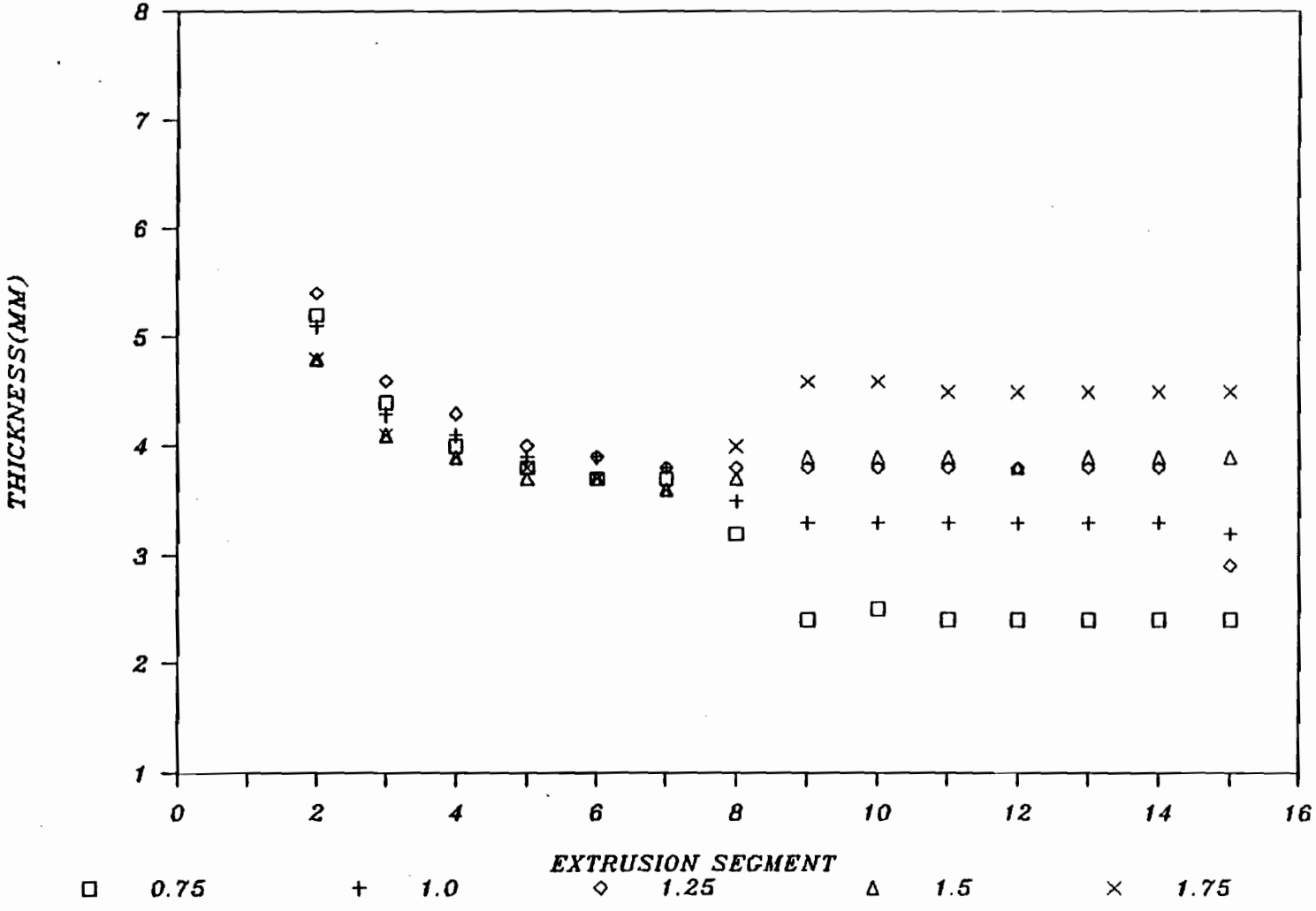

Figure 5.47: Parison Thickness Profile Response, for Resin B, to Initial Gaps of 0.75, 1.0, 1.25, 1.5 and 1.75 mm Gap.

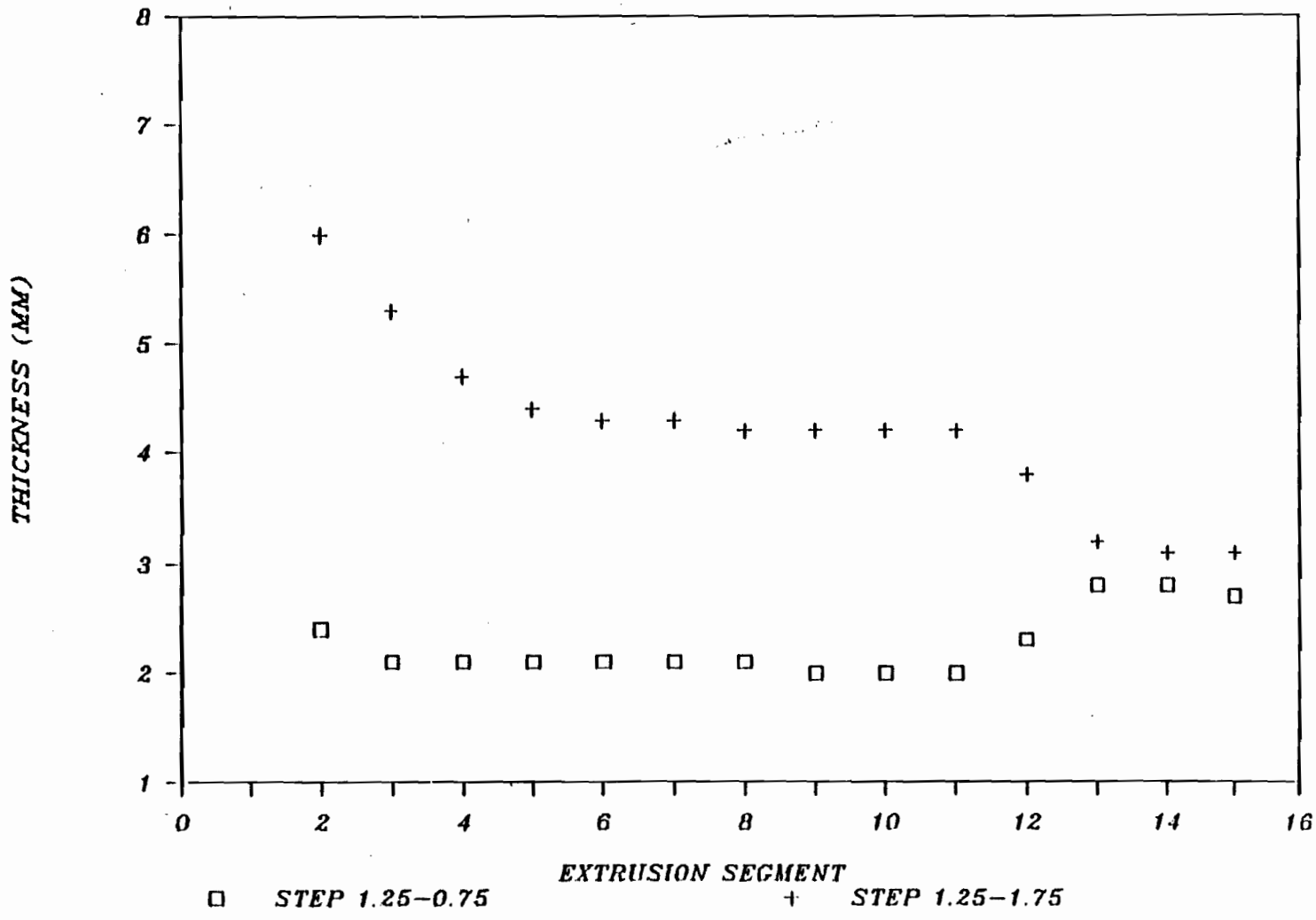

Figure 5.48: Parison Thickness Profile Response, for Resin A, to Step Location of 4/16 of a Stroke.

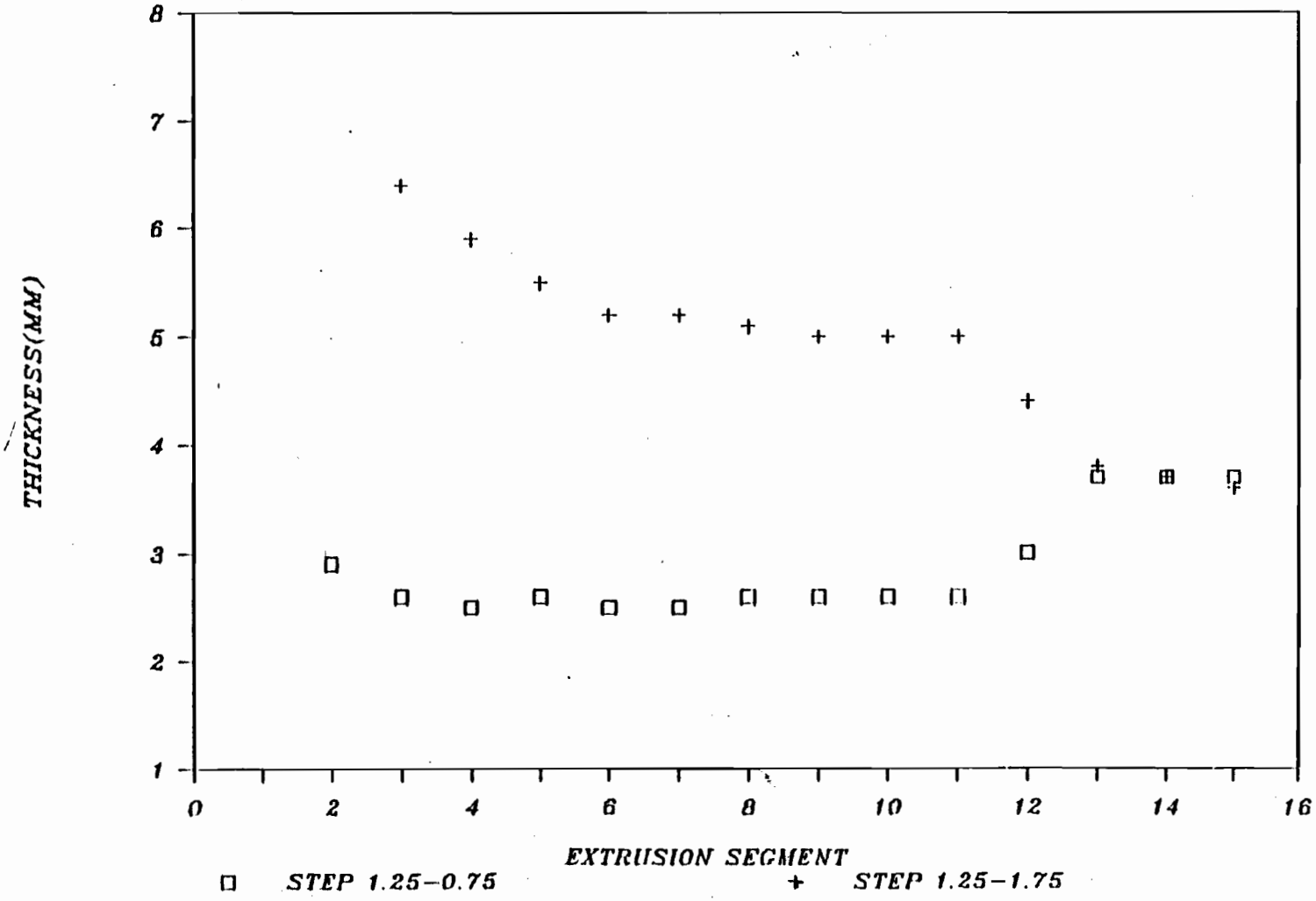

Figure 5.49: Parison Thickness Profile Response, for Resin B,Step Location of 4/16 of a Stroke.

location of 4 sixteenths of a stroke, and Figures 5.50 and 5.51, for a step location of 12 sixteenths of a stroke. A step location of 8 sixteenths of a stroke is shown in Figures 5.44 and 5.45.

The gain tends to increase with increasing delay in the step application during the stroke, for a step up in the gap. The reverse is true for a step down in the gap. This is expected because of the inherent decrease in the thickness along the length of the parison, for a constant gap extrusion.

5.2.1.3 STOCHASTIC RESPONSES

Measurements of process variables contain random disturbances or noise, which cannot be characterized solely by deterministic modelling. This noise can have a prominent effect on the output variable. Stochastic identification techniques can supply both a noise and a process model for the system under study. The output of the transfer function, G6(i,j), represents the correlation of the white noise input, n(t), (Figure 5.41). A random white noise process would be represented by a value of unity for G6(i,j) (82).

In the present work, PC Matlab software was used in an interactive iterative fashion to determine statistically adequate models based on examination of the cross correlation and autocorrelation functions. This procedure is discussed in detail elsewhere (82,83).

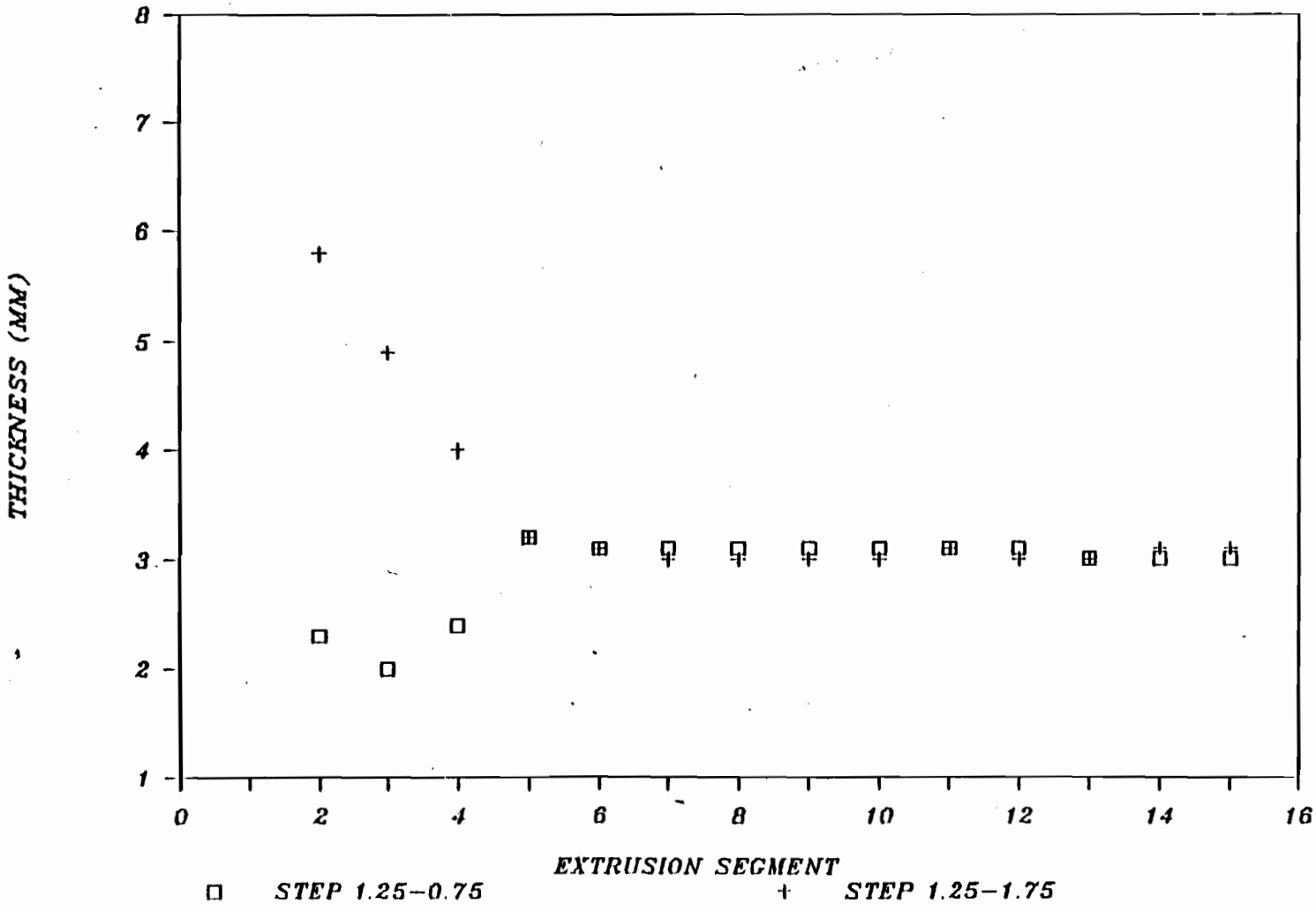

Figure 5.50: Parison Thickness Profile Response, for Resin A, to Step Location of 12/16 of a Stroke.

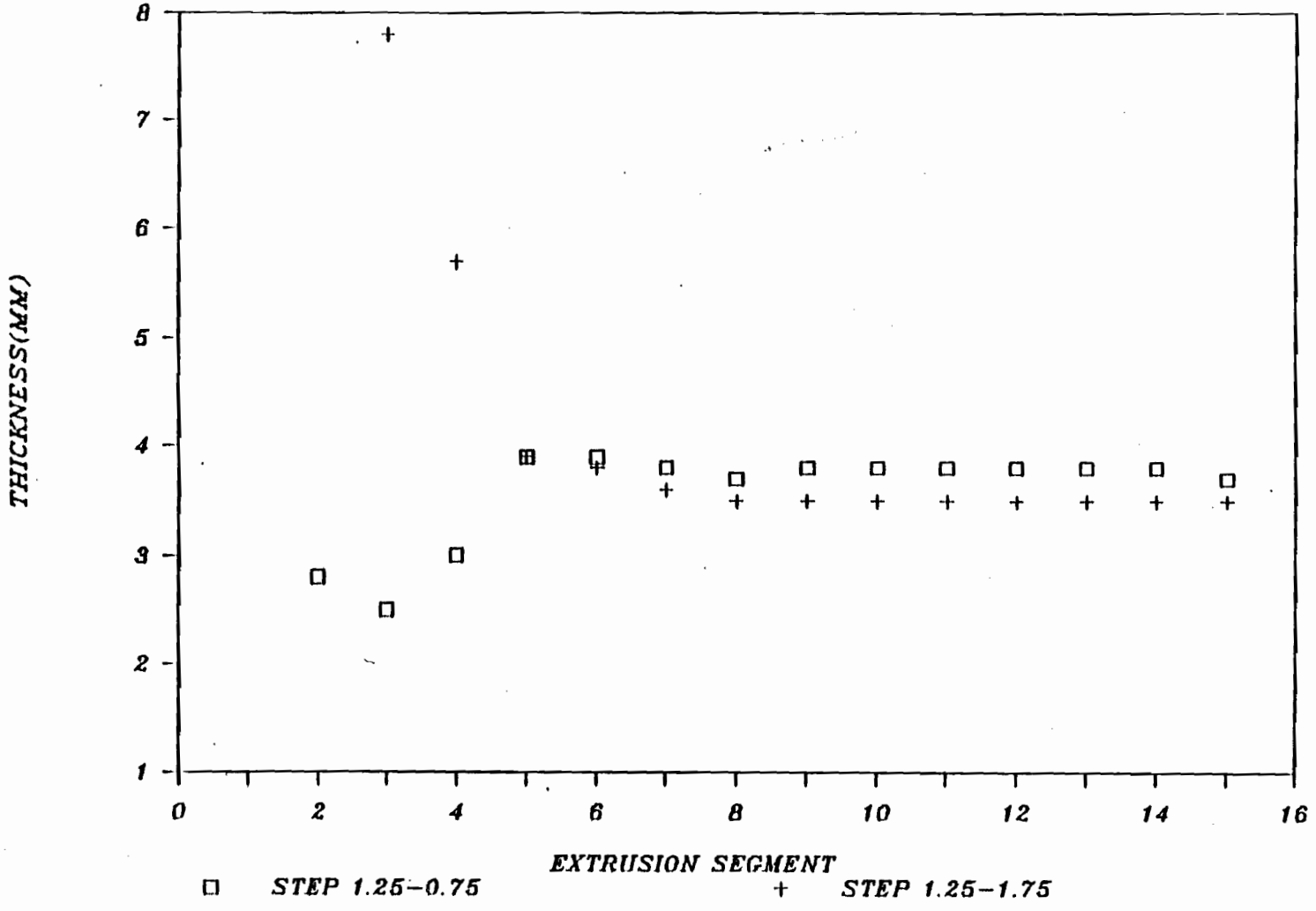

Figure 5.51: Parison Thickness Profile Response, for Resin B, to Step Location of 12/16 of a Stroke.

5.2.1.3.1 CYCLE-TO CYCLE RESPONSE

A system identification routine was carried out in order to determine if the process noise, cycle-to-cycle, is white, autocorrelated or cross-correlated. The stochastic study was conducted by applying a pseudo-random binary sequence (PRBS) disturbance to the gap, in a series of cycle-to-cycle constant gap extrusions. The sequence generated by a shift register of length, "2^n - 1", in the software PSEUDO is shown in Figure 5.52.

The measured output to this PRBS disturbance is the thickness of the middle segment of the parison in every cycle. This thickness is measured with the software DYN. The response is presented in Figure 5.53.

5.2.1.3.2 NOISE MODEL DETERMINATION

The data were fit to the following Box-Jenkins models.

$$h(t) = \frac{H(q)}{U(q)} h_o(t-ak) + n(t) \qquad (5.2)$$

$$h(t) = \frac{H(q)}{U(q)} h_o(t-ak) + \frac{C(q)}{J(q)} n(t) \qquad (5.3)$$

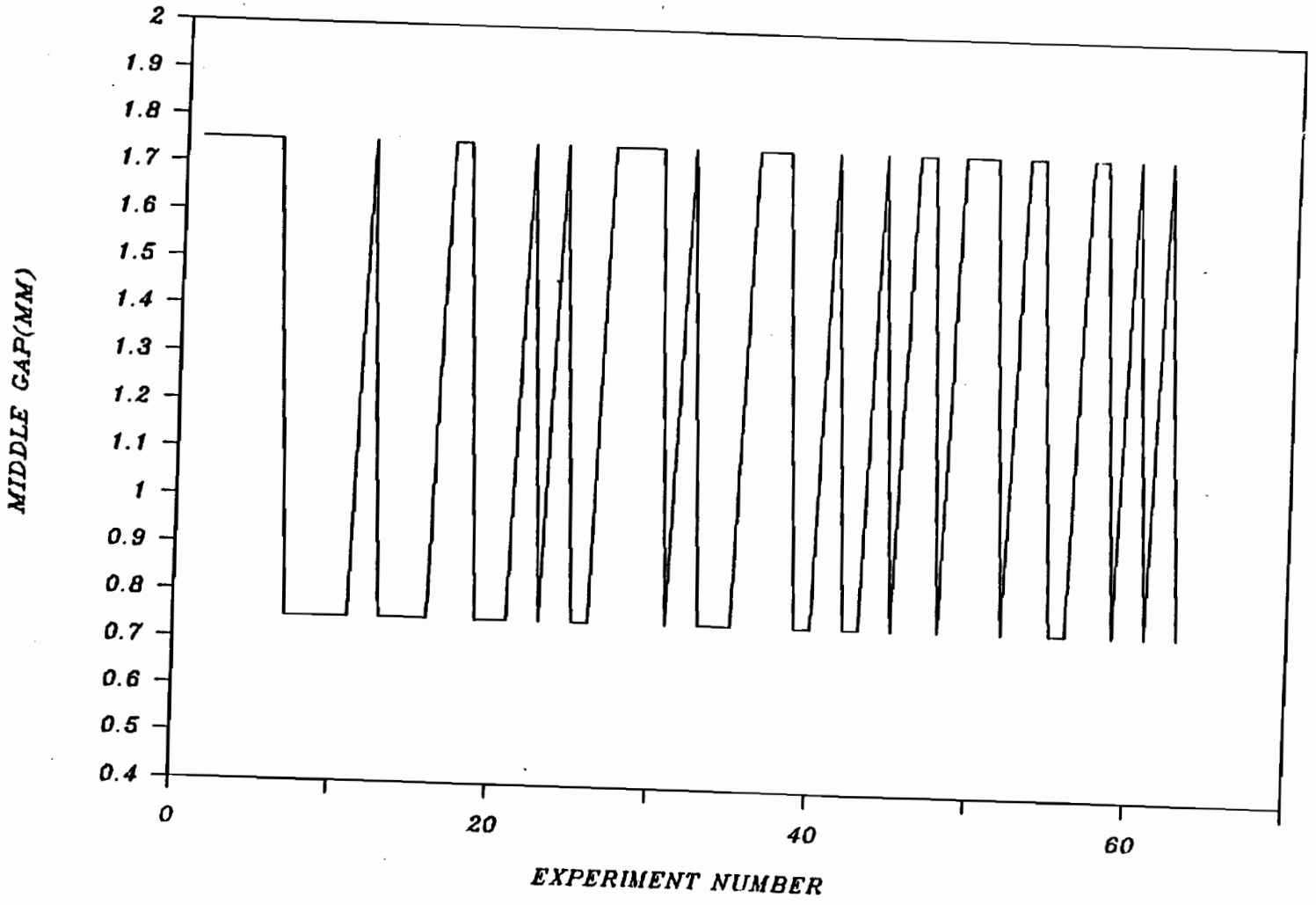

Figure 5.52: Cycle-to-Cycle Pseudo Random Binary Sequence Variation of Die Gap in Constant Gap Extrusions.

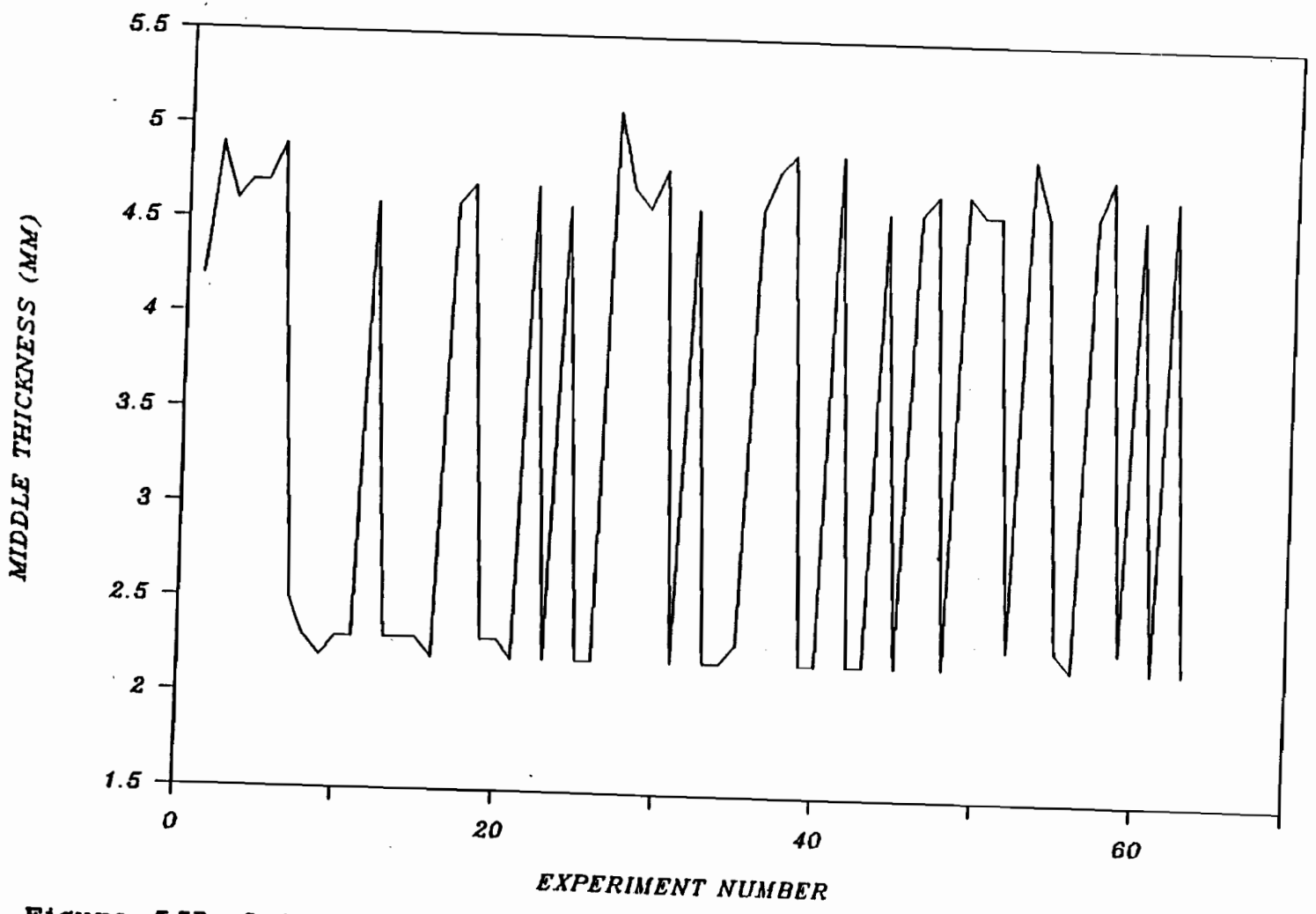

Figure 5.53: Output Response to Input of Figure 5.52 (Thickness of Segment 8).

where H(q) and U(q) are the process transfer functions and C(q) and J(q) are the noise transfer functions, with q representing the time series backward operator. The cycle response delay is represented by a, k depicts the lag and n(t) is the white random noise.

The quality of the models is tested for statistical adequacy by determining if the residuals are within specified limits. Figure 5.54 represents the noise autocorrelation for a zero order moving average model of Equation (5.2). Figure 5.55 shows the cross correlation of the residuals with the input, for Equation (5.2). The model of Equation (5.2) is statistically adequate, because the autocorrelation is not significant after lag 1 and the cross correlation is within interval limits.

Figures 5.56 and 5.57 show the residual autocorrelation and cross correlation, respectively, for a first order moving average model of Equation (5.3). There is no significant advantage, for a first order model over a zero order model, in decreasing the values of the correlations within the limits. The same conclusion holds for higher order and different form models.

The ratio C(q)/J(q) is found to be " 1 + 0.072q ", where q represents the backward operator. The first order term, 0.072 (standard deviation = 0.0167), is close to zero, and it is much less than the zero order term, 1. This again indicates that the system is of zero order, or white random noise.

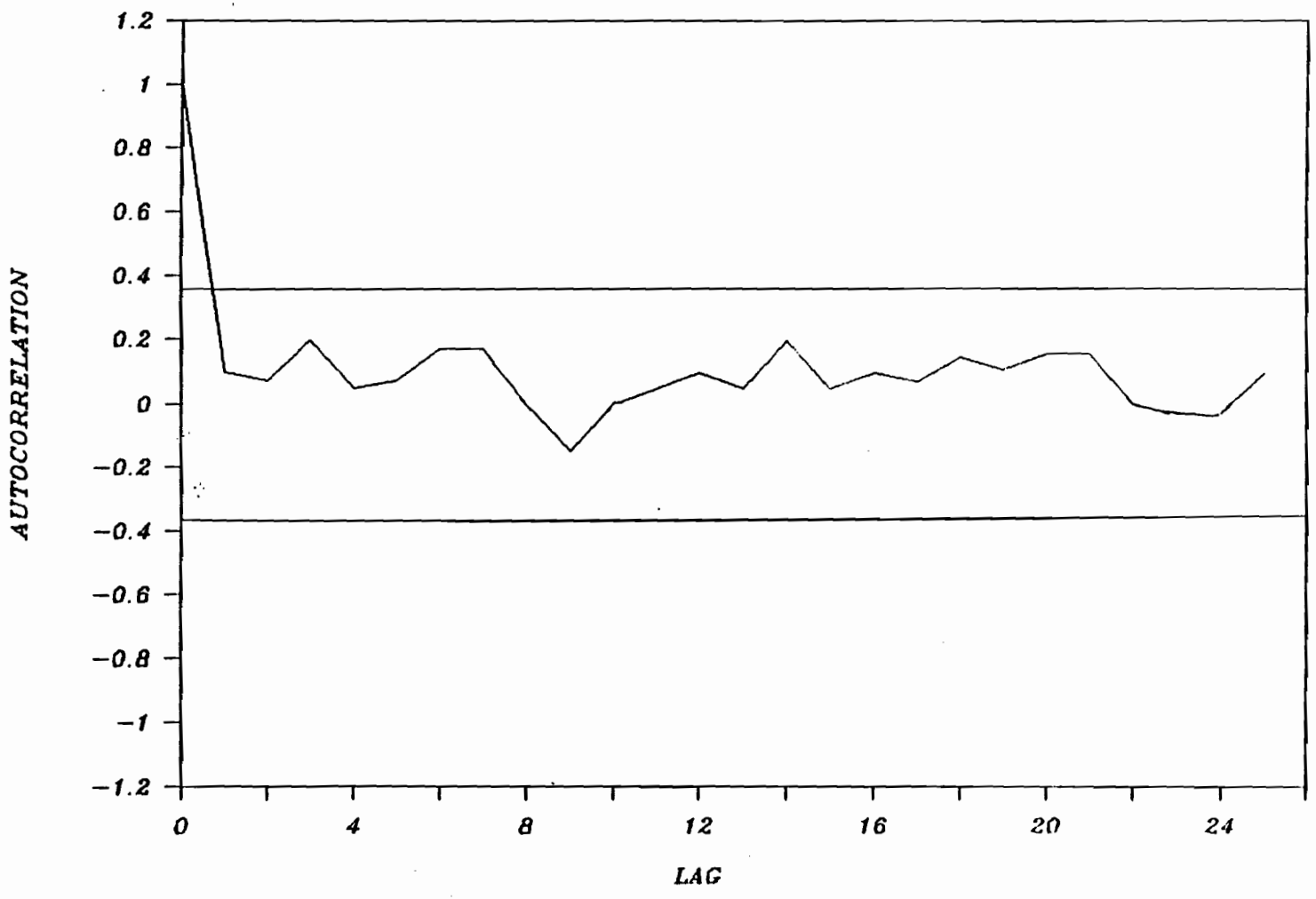

Figure 5.54: Noise Autocorrelation for a Zero Order Model of Equation 5.2.

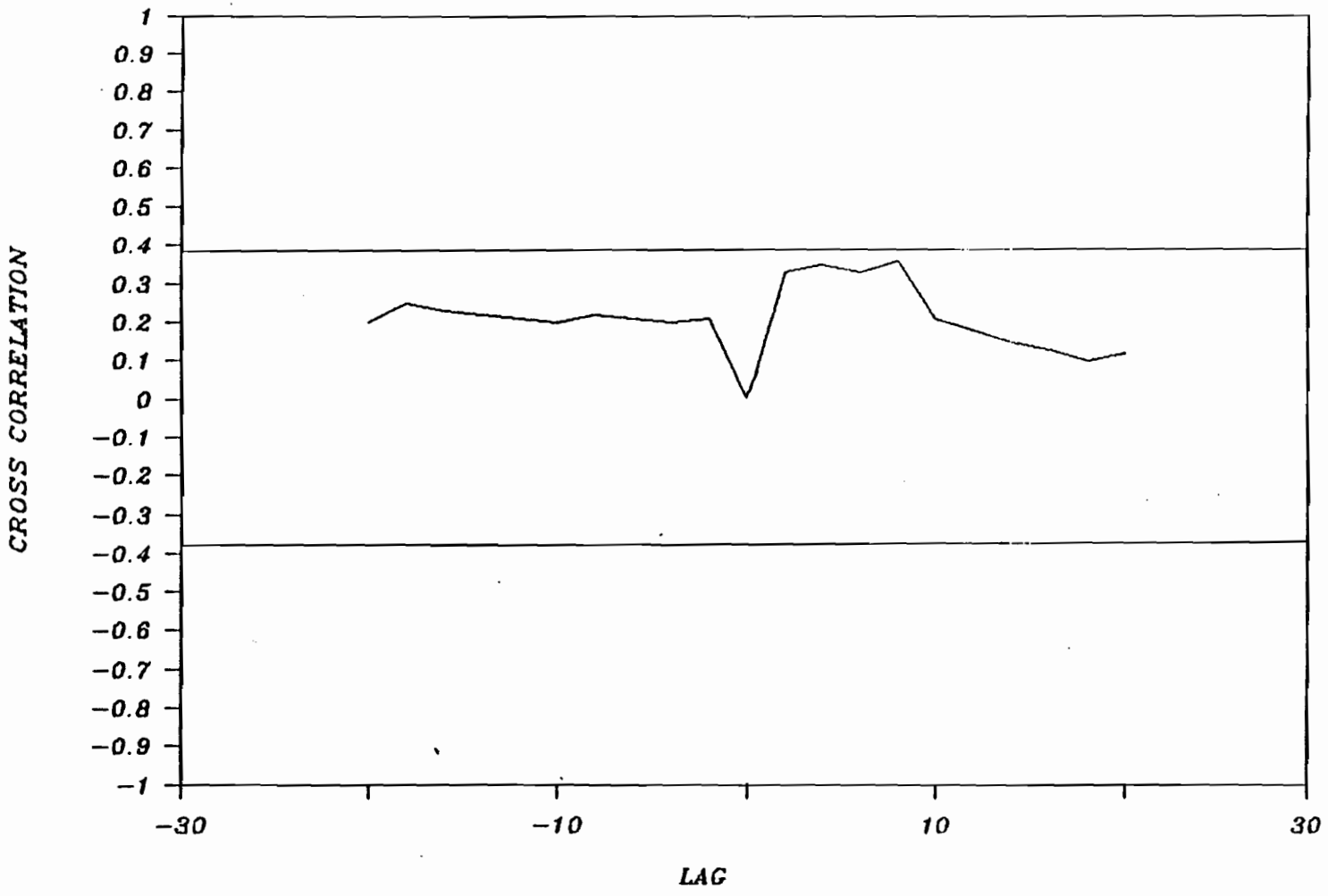

Figure 5.55: Cross Correlation of Residuals for a Zero Order Model of Equation 5.2

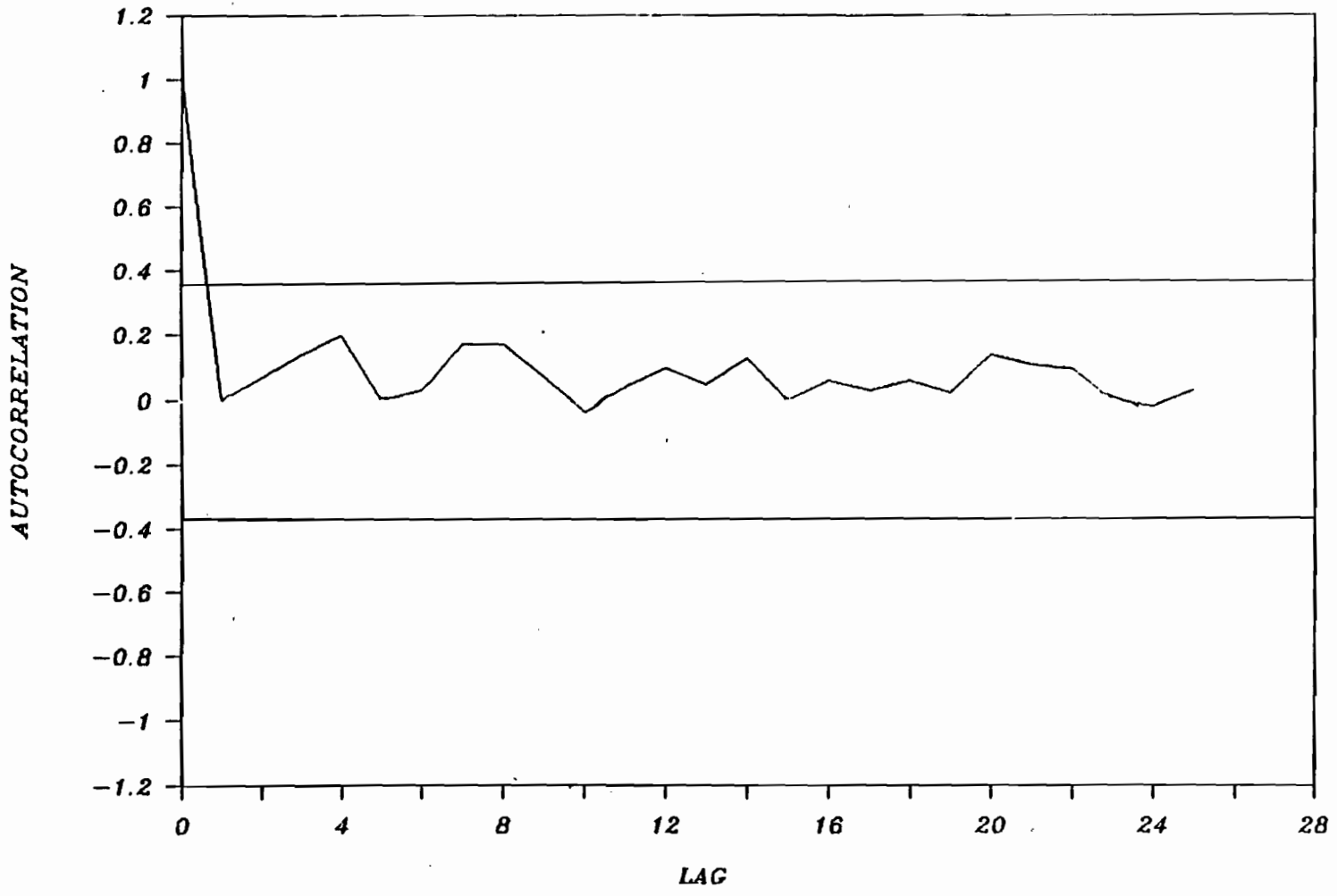

Figure 5.56: Noise Autocorrelation for a First Order Model of Equation 5.3.

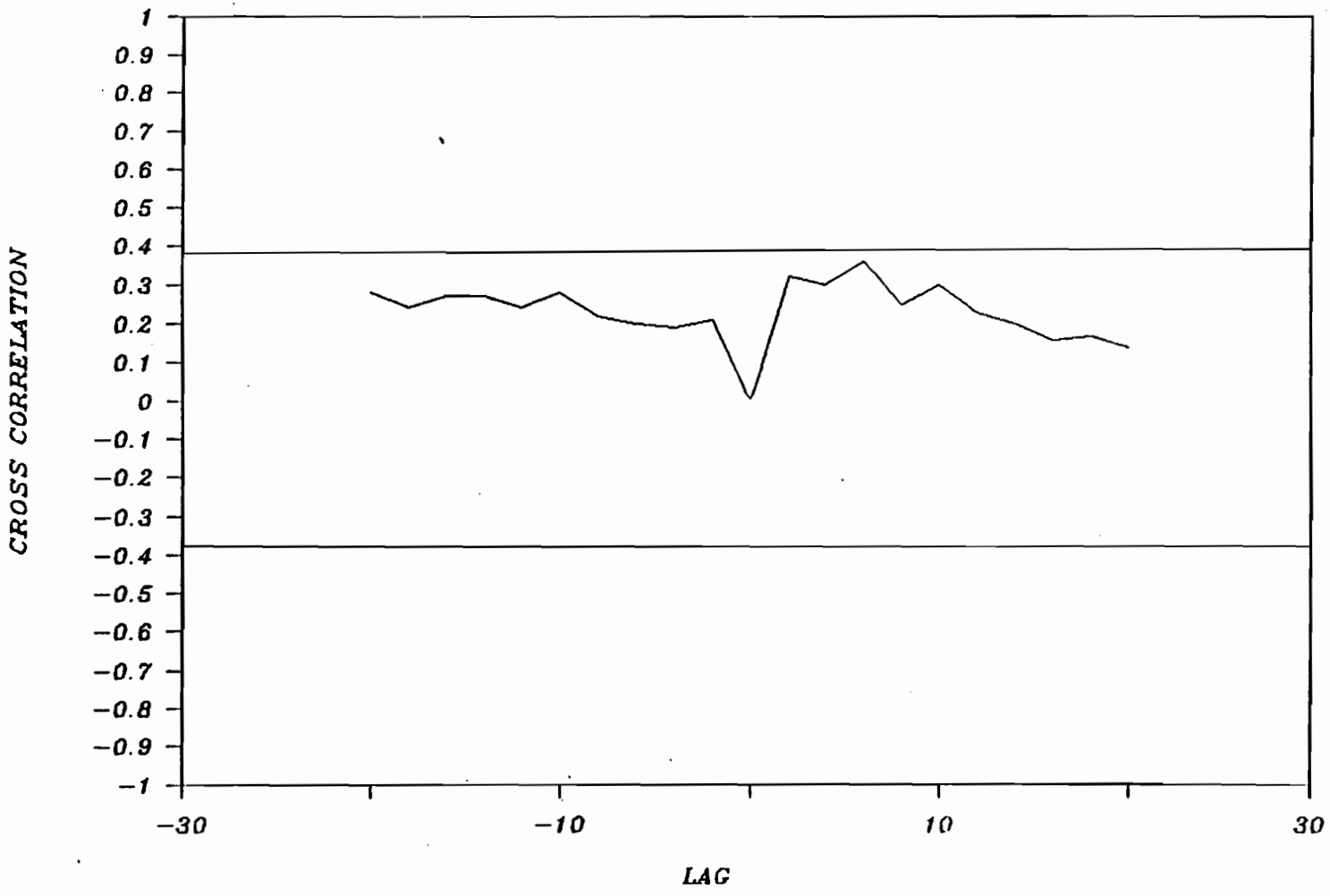

Figure 5.57: Cross Correlation of Residuals for a First Order Model of Equation 5.3.

5.2.1.3.3 DETERMINISTIC RESPONSE

The ratio of the process transfer functions, H(q) and U(q), can be used to resolve the form of the cycle-to-cycle deterministic response to a step change. H(q)/U(q) has a constant value of 2.73 (standard deviation = 0.0004), in the case of both Equations (5.2) and (5.3). The value of the delay, a, is zero. The fact that the transfer function has a constant value confirms that the cycle-to-cycle response to an input disturbance is completely accomplished within the cycle time. The response can therefore be considered proportional, requiring only one tuning parameter, gain.

5.2.2 ON-LINE CONTROL

5.2.2.1 CONTROL SCHEME

Control of parison thickness profiles, is a special case of multivariable control. A multivariable process entails several inputs and outputs to the system. Each individual thickness value along the length of the profile represents a controllable variable, h(i,j), in a cycle-to-cycle loop (Figure 5.41). The subscripts i and j correspond to the parison segment along the length and the cycle number, respectively. The corresponding manipulated gap profile is represented by $h_o(i,j)$. The programmed set point, representing the thickness set point along

the length of the parison, is designated by $h_{SP}(i,j)$. The individual transfer functions are represented by $GK(i,j)$, where K is the specific block in the control loop.

Interactive cross transfer functions, portraying the effect of a gap change on the thicknesses, along the parison length, different from that corresponding gap's thickness, were found to be minimal (Section 5.2.1.2). The result of this absence of coupling was that each individual output has only one corresponding input, gain and command signal associated with it.

The control strategy chosen is a cycle-to-cycle adaptive control scheme, in which the individual process gains, together with the profile, are updated and monitored for each extrusion. The controller is adjusted in transfer block $G5(i,j)$ (Figure 5.41). These gains, $m(i,j)$, are given by

$$m(i,j) = \frac{h(i,j) - h(i,j-1)}{h_o(i,j) - h_o(i,j-1)} \qquad (5.4)$$

The initial estimates for $h(i,0)$ and $h_o(i,0)$ are obtained, as a first estimate, from a thickness distribution of a constant gap extrusion. The value of the gain, $m(i,j)$, takes on a value of three, should Equation 5.4 yield an indeterminate result.

The error profile is obtained, for each individual i, according to

$$e(i,j) = h_{SP}(i) - h(i,j) \qquad (5.5)$$

The command signal for the next extrusion is then calculated according to

$$h_o(i,j+i) = h_o(i,j) + m(i,j)e(i,j) \qquad (5.6)$$

The cycle number is subsequently updated to j+i, and the following extrusion takes place.

This scheme is chosen, for control over many cycles, in order to account for slow process drifts. The adaptive strategy, which measures the tuning parameters on-line, corrects these drifts.

A better control strategy would have been to determine the gains as functions of the process parameters, such as magnitude, direction, location of the step along the profile, melt temperature, shot size, injection rate and resin. This is a deterministic approach as opposed to the on-line determination which is the case in this work. This approach was not utilized because of time and machine limitations. However, a simulation employing this approach, is presented in Appendix 5.

The extrusion blow molding machine was operated in the intermittent, cycle-to-cycle mode for the on-line control experiments of this work. This was necessary, in order to simulate actual process conditions. The process itself was monitored and controlled with the software CONTROL. The algorithm for CONTROL is presented in Figure 5.58.

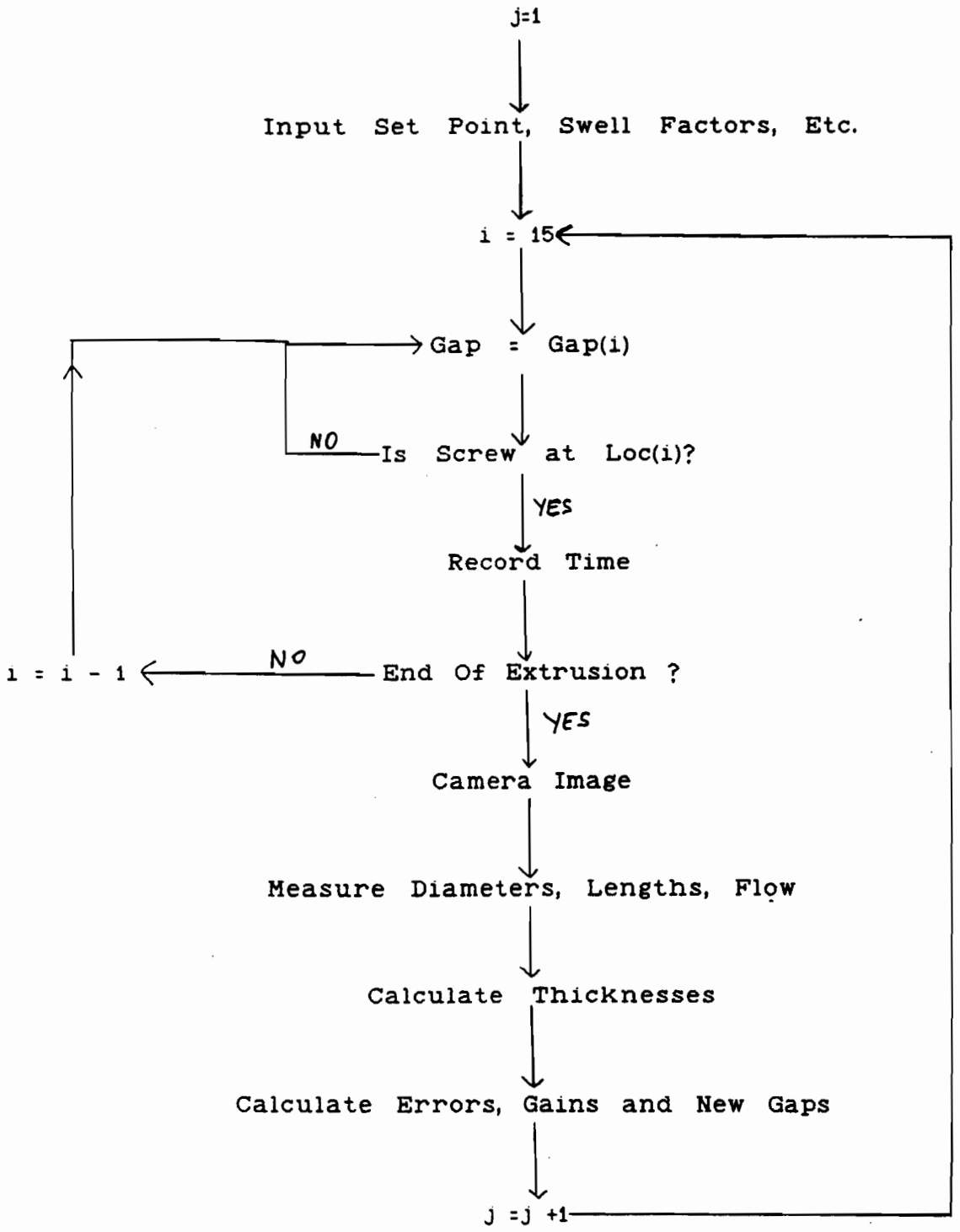

Figure 5.58: Algorithm for the Software CONTROL.

The percent error, monitored cycle-to-cycle, is defined as

$$P_E = \frac{\Sigma \text{ abs}[h(i) - h_{SP}(i)]}{\Sigma h_{SP}(i)} \times 100 \qquad (5.7)$$

with summation over i. It indicates the quality of the control action. The swell factors were obtained with the software SWELL. During the course of the process, whenever the factor, α,

$$\alpha = L_E / \Sigma L(i) \qquad (4.68)$$

deviated outside the specified limits, the gap scan, was repeated to determine new swell factors. This occured infrequently during the course of the work.

5.2.2.2 CONTROL WITH PROGRAMMED SET POINTS

The results of control experiments for various programmed set points are now discussed. In the figures that follow, the solid lines represent the set point profiles, whereas the symbols represent individual replicate experimental profiles. The first thickness profile employed in the on-line gain calculations was based on the constant gap data of Section 5.2.1.2.1. In the first part of the following discussion, all experiments were carried out with Resin A.

5.2.2.2.1 THICKNESS RESPONSE TO SET POINT CHANGE The control action response of the thickness of segments 4, 8 and 12, representing the top, middle and bottom of the parison, is shown in Figures 5.59, 5.60 and 5.61 respectively. The initial gap profile, of the first cycle, was that obtained with the constant gap of 1.25 mm. It was subsequently adjusted, in order to minimize the error. The control action was instantaneous, in that the set point is attained after the first or second cycle.

5.2.2.2.2 CONSTANT THICKNESS AND STEP SET POINTS Results obtained with constant thickness set point profiles of 2, 3 and 4 mm are shown in Figures 5.62, 5.63 and 5.64, respectively. The results for set points of 3 and 4 mm show good control action.

The set point of 2 mm, exhibits an offset. This offset was caused by the limits placed on the gap. The gap could not be less than 0.70 mm or greater than 1.75 mm, for the reasons discussed in Section 3.2.3.2.4. A gap less than 0.70 mm would be required to eliminate the offset with the 2 mm set point. However, it is important to note that this limitation was not a function of the parison programmer employed. Figure 5.65 and 5.66 show typical die gap profiles during extrusion for the programmed set point profiles of 2 and 3 mm, respectively. The die gap goes to the lower limit for the set point profile of 2 mm.

Figures 5.67 and 5.68 relate to set points with a step up and down, of magnitude 1 mm, respectively. Figure 5.69 shows a

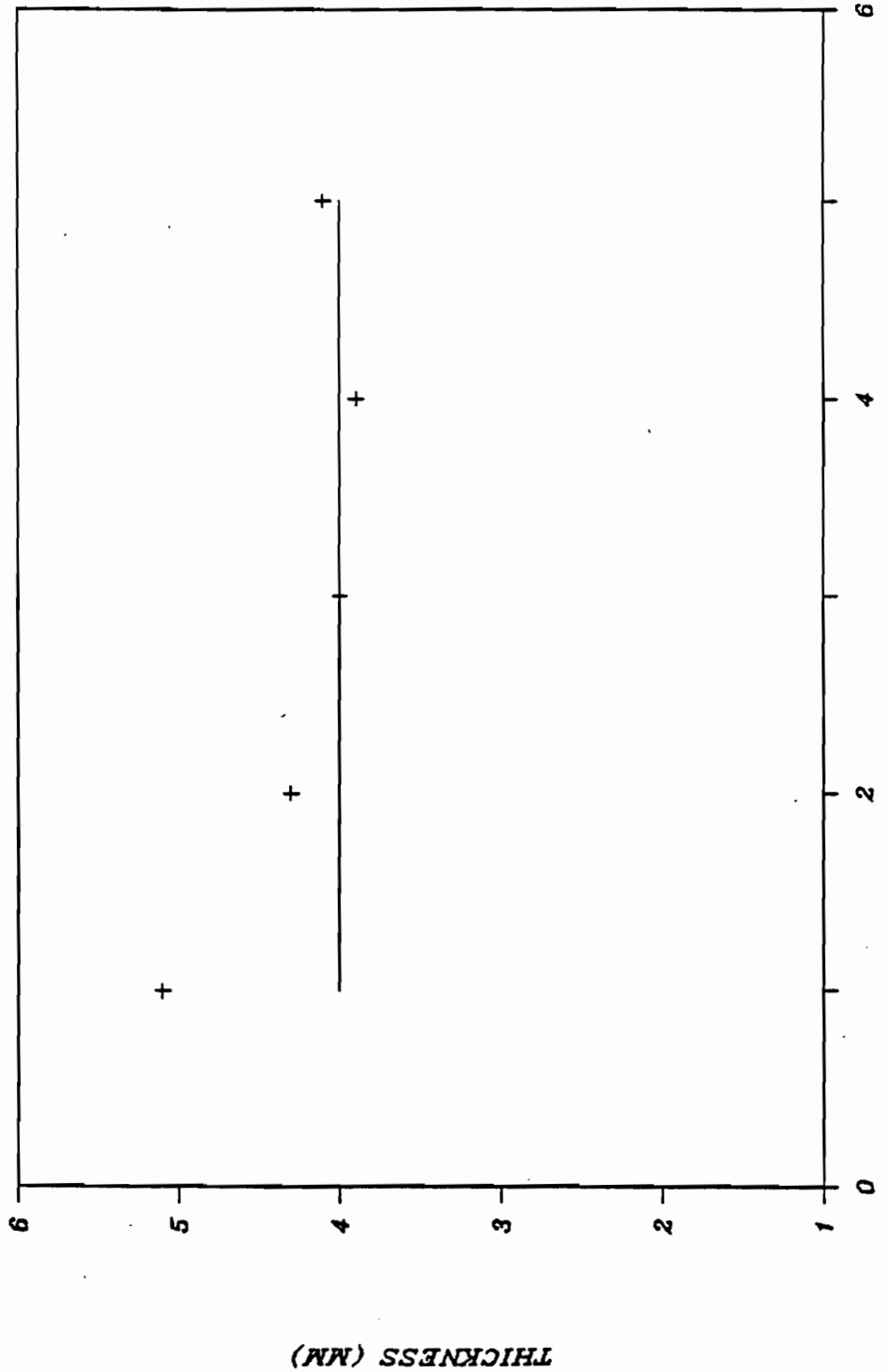

Figure 5.59: Control Action Response of Thickness Segment 4.

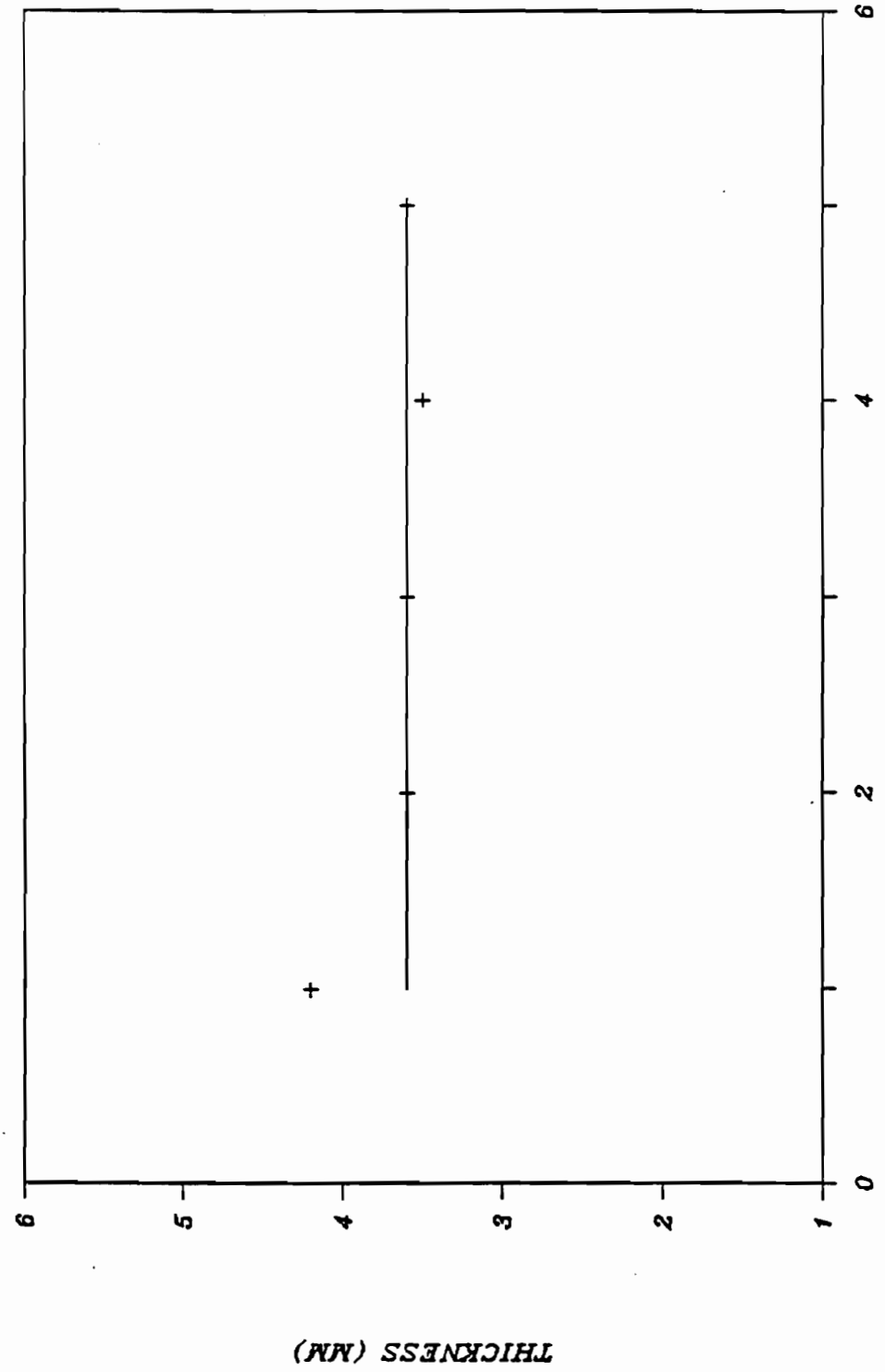

Figure 5.60: Control Action Response of Thickness Segment 8.

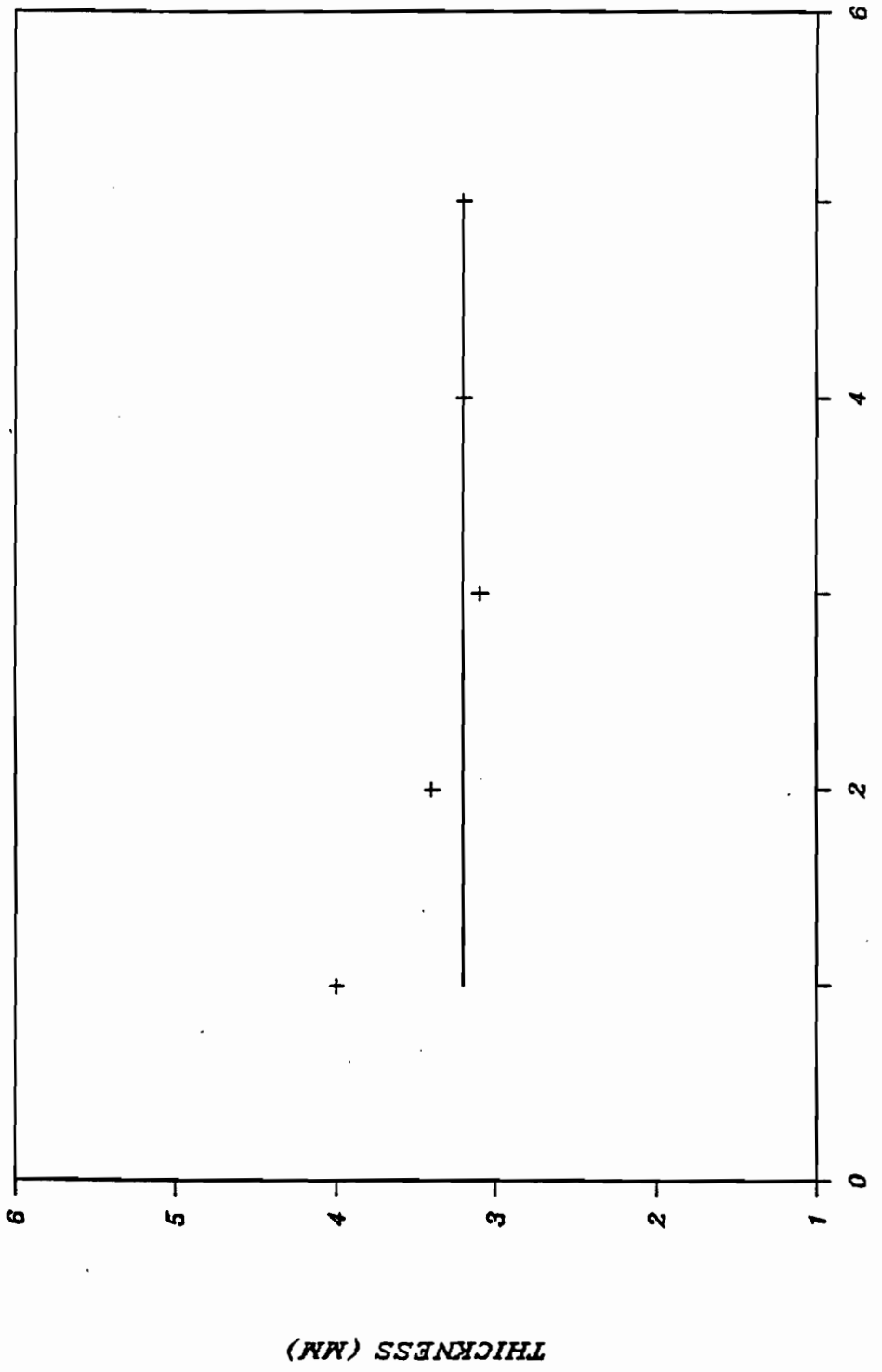

Figure 5.61: Control Action Response of Thickness Segment 12.

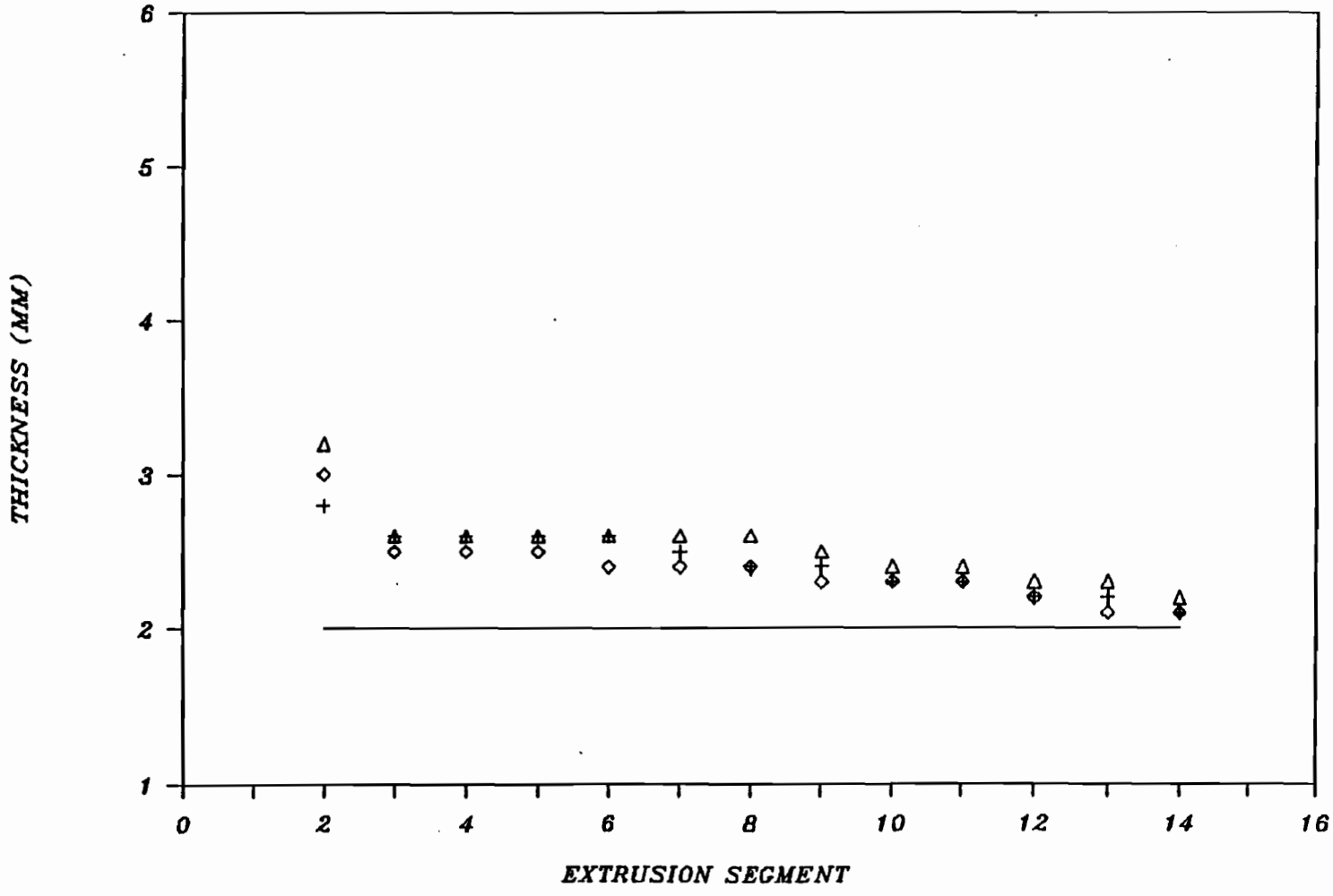

Figure 5.62: On-Line Control of Constant Thickness Set Point Profile 2mm.

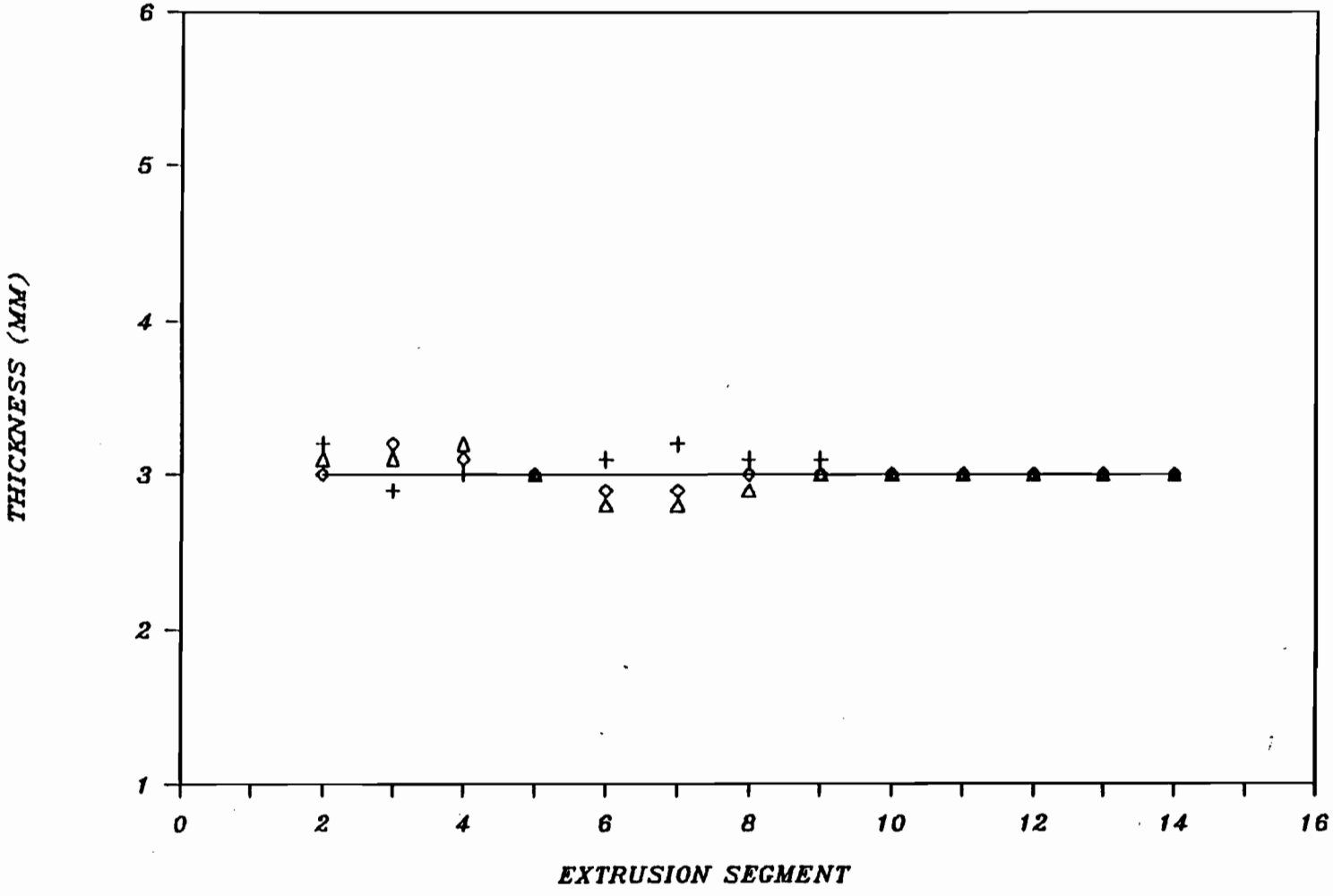

Figure 5.63: On-Line Control of Constant Thickness Set Point Profile 3mm.

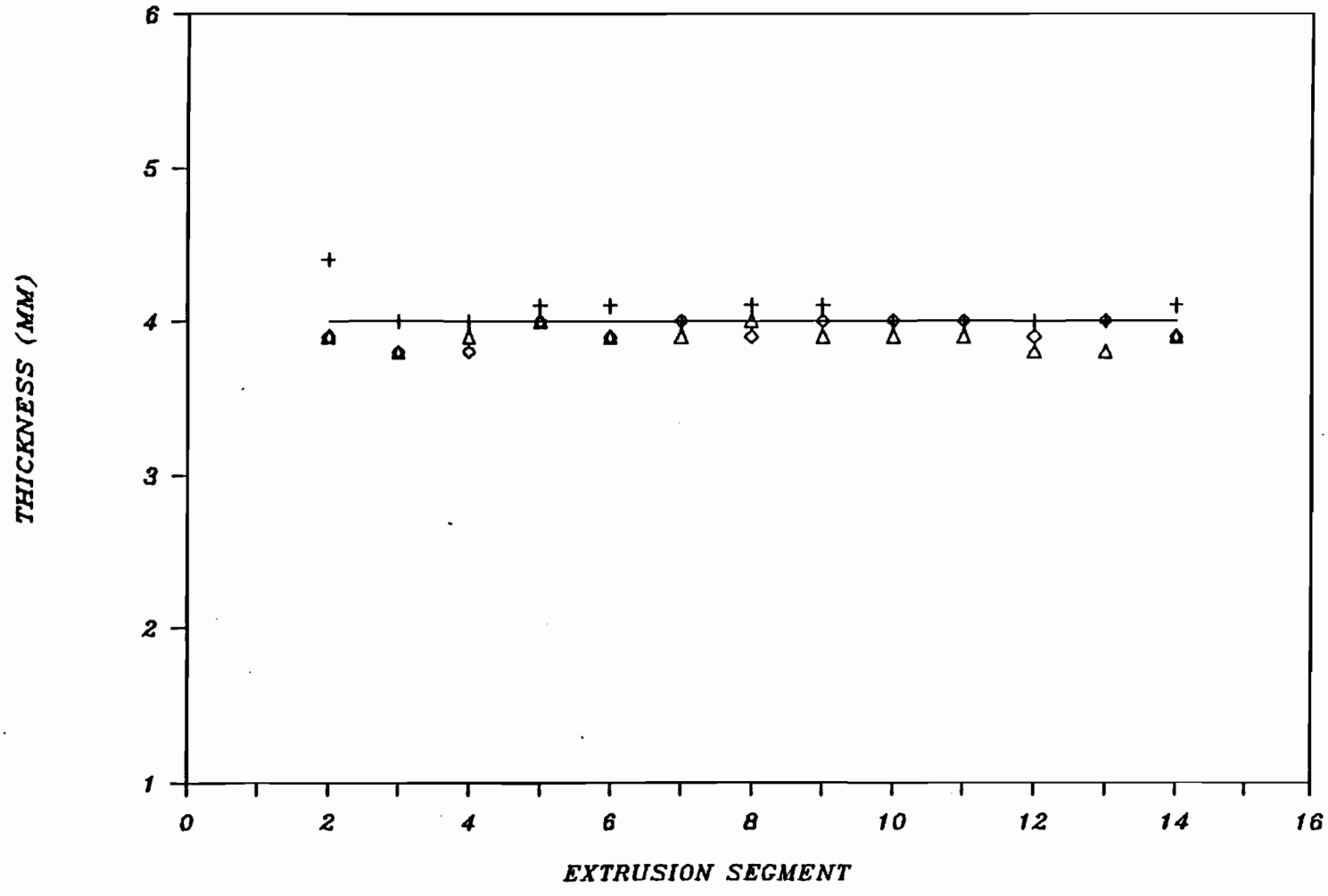

Figure 5.64: On-Line Control of Constant Thickness Set Point Profile 4mm.

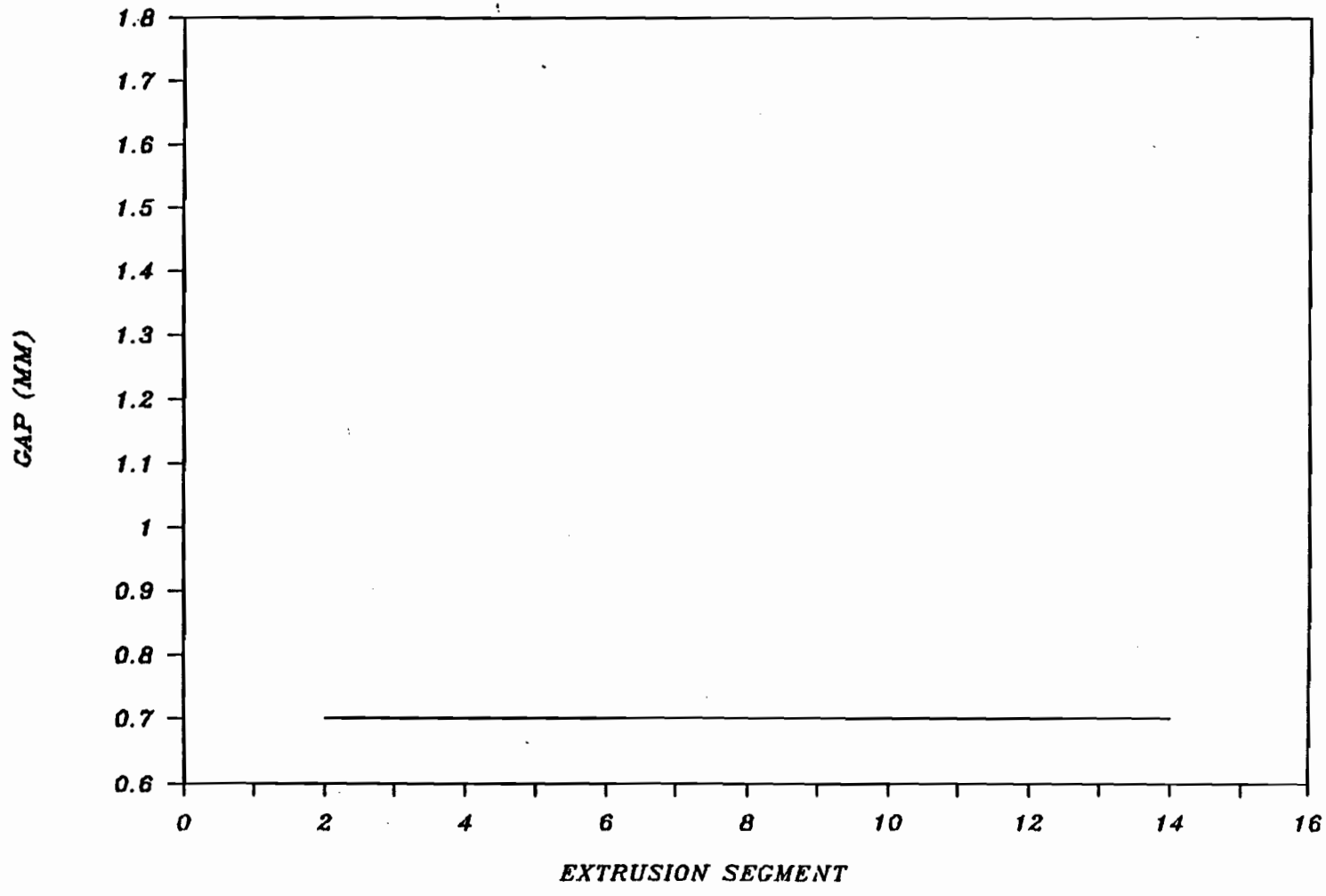

Figure 5.65: Typical Die Gap Profile for Constant Thickness Set Point Profile of 2mm.

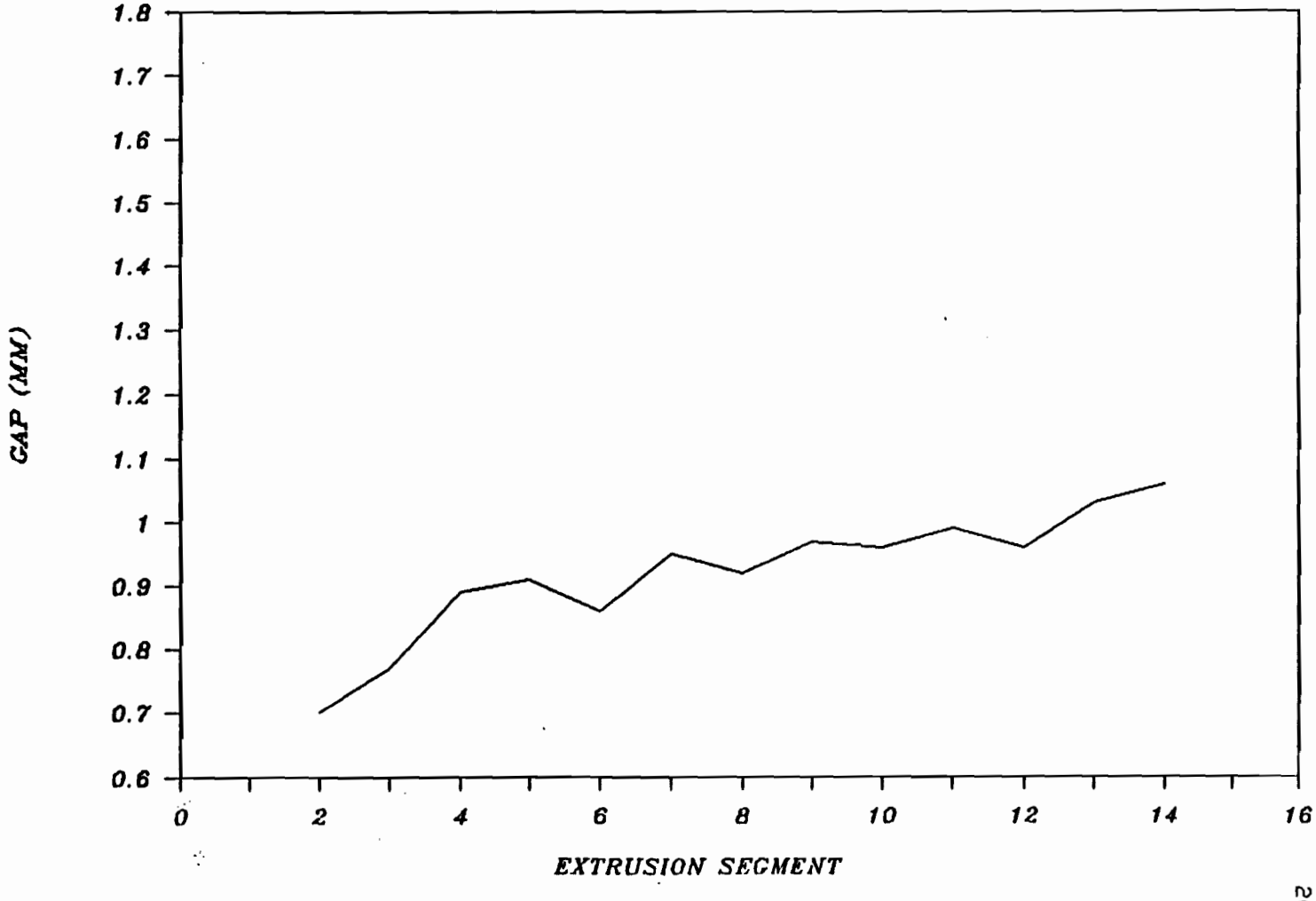

Figure 5.66: Typical Die Gap Profile for Constant Thickness Set Point Profile of 3mm.

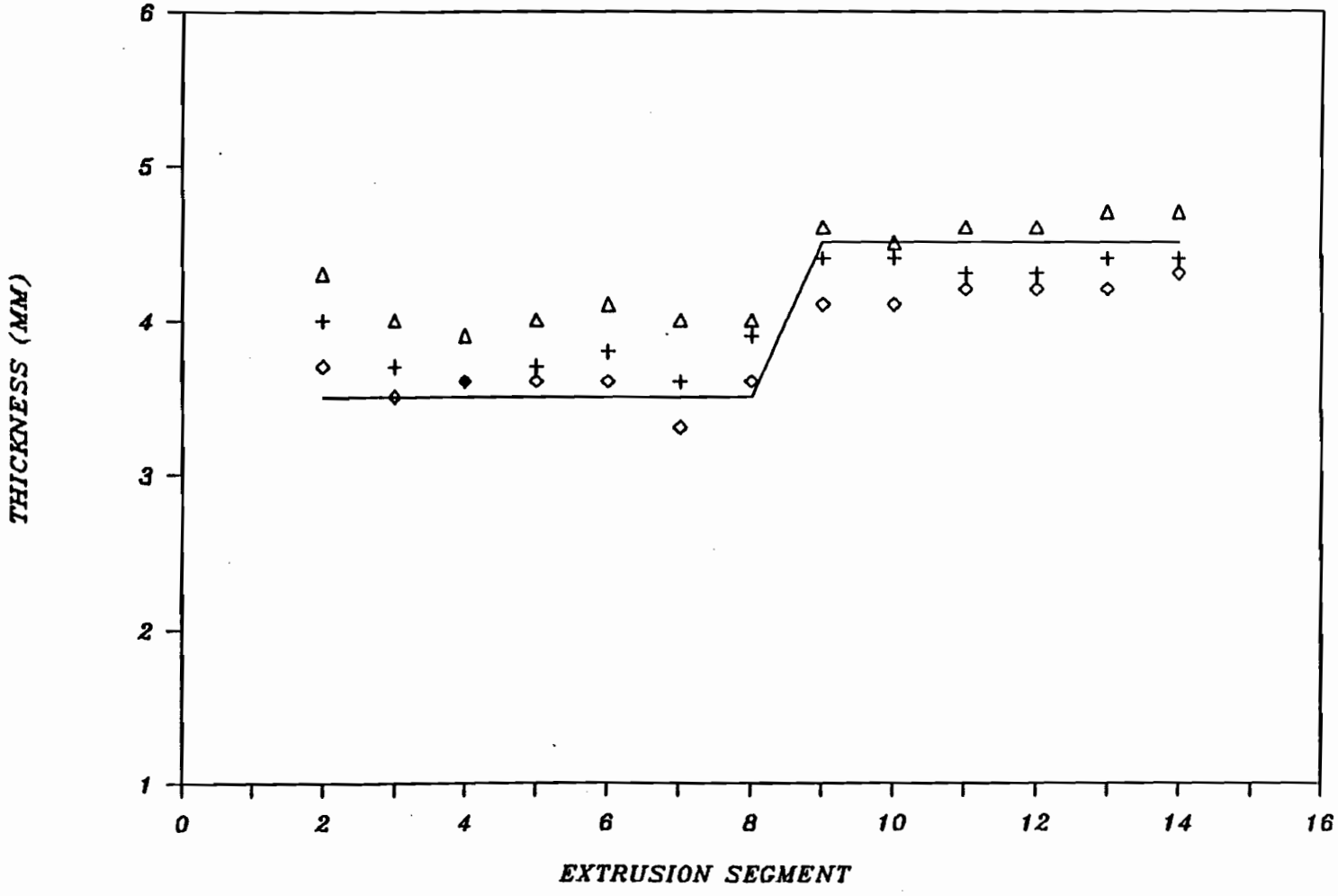

Figure 5.67: On-Line Control of Step Up Set Point Profile, Step Magnitude 1 mm.

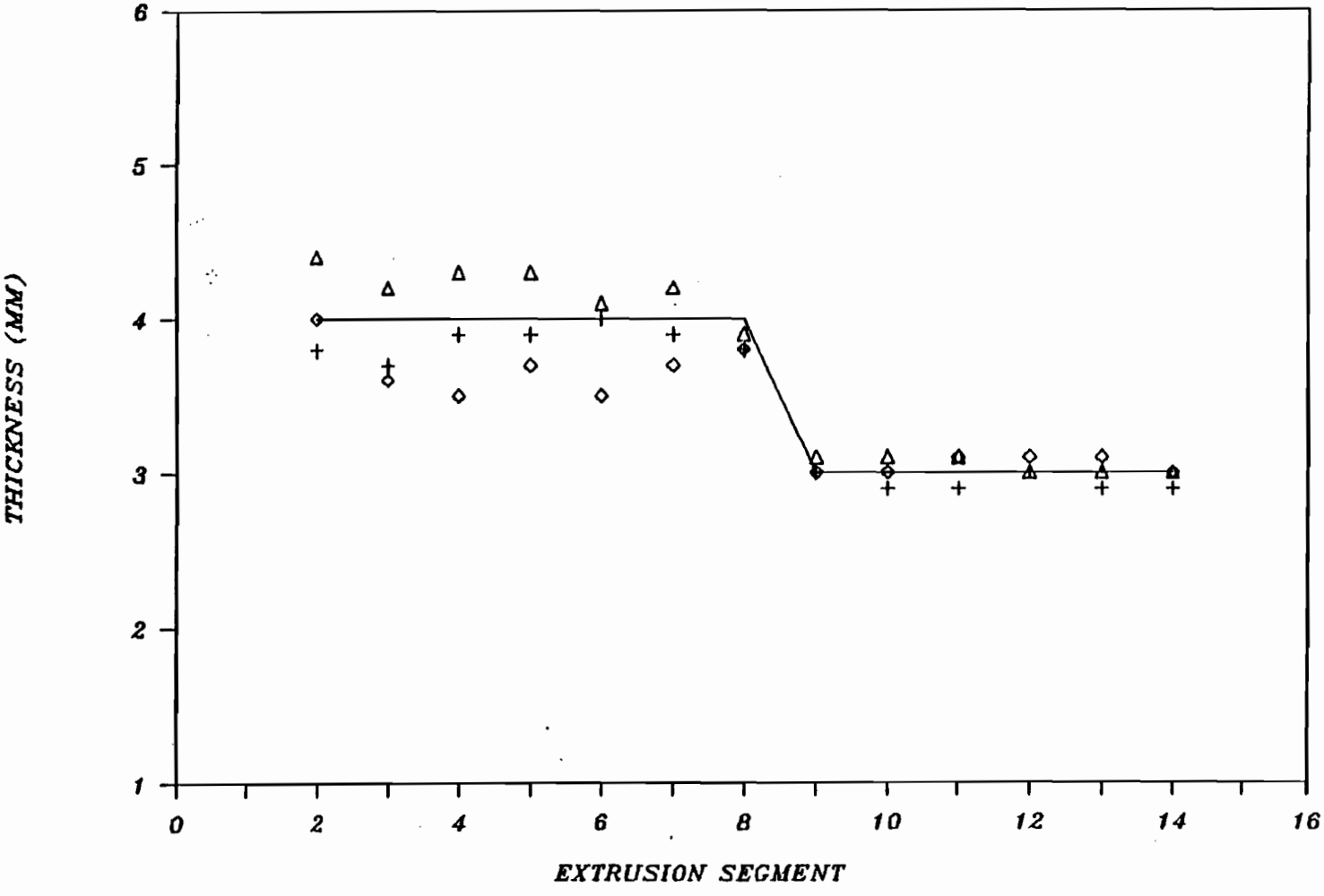

Figure 5.68: On-Line Control of Step Down Set Point Profile, Step Magnitude 1 mm.

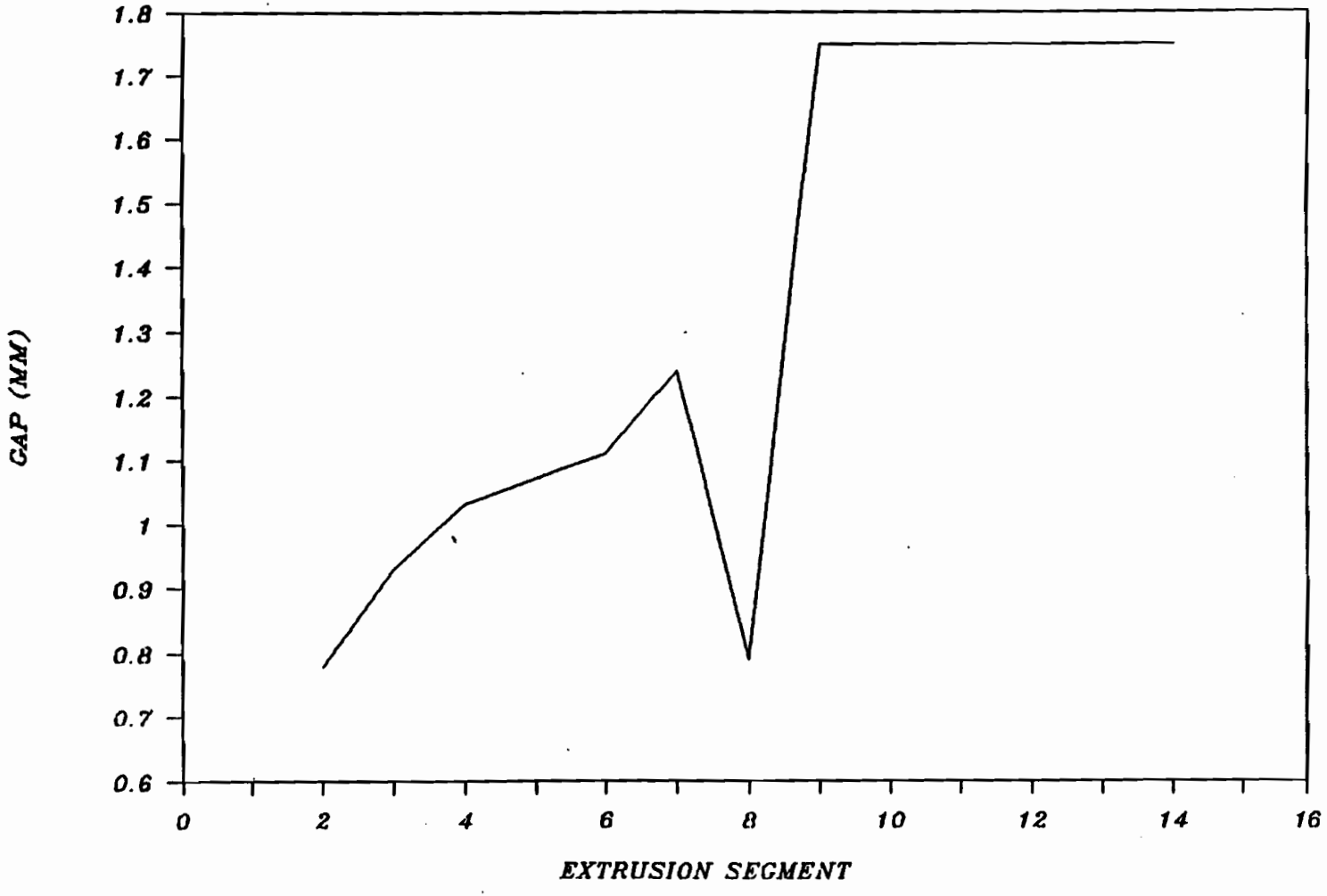

Figure 5.69: Typical Die Gap Profile for Step Up Set Point Profile, Step Magnitude 1.0 mm.

typical die gap profile during extrusion for the step up profile. There is a difficulty at the end of extrusion, or top of the parison, with these programmed set point profiles, since the gap was changed drastically. The programmer-servoamp combination could not produce the control action required once the step has been applied. The offset is caused by a gap overshoot resulting from the inertia of the machine in the gap change.

Control at the start of extrusion was not adequate for the step up, because of the gap limit situation. However, the control at the start of extrusion is adequate for the step down, as the required gap profile for the set point profile was within the equipment limits.

Other ranges of set points were evaluated but the results obtained were similar, for this magnitude of step change. Figures 5.70 and 5.71 illustrate the effect of decreasing the step magnitude. The control action is much better, as the step magnitude was reduced sufficiently (e.g. to 0.4 mm), to allow the programmer to follow the set point profile.

5.2.2.2.3 LINEAR AND STAIRCASE SET POINT VARIATIONS This group of programmed set points is controlled very well, with the control scheme employed. Figures 5.72 and 5.73 illustrate the control over linear declining set point profiles, of slopes 0.1 and 0.2, respectively. Figure 5.74 illustrates the control of a linear increasing set point profile. Control of parisons with higher order polynomial set point profiles was not sufficiently

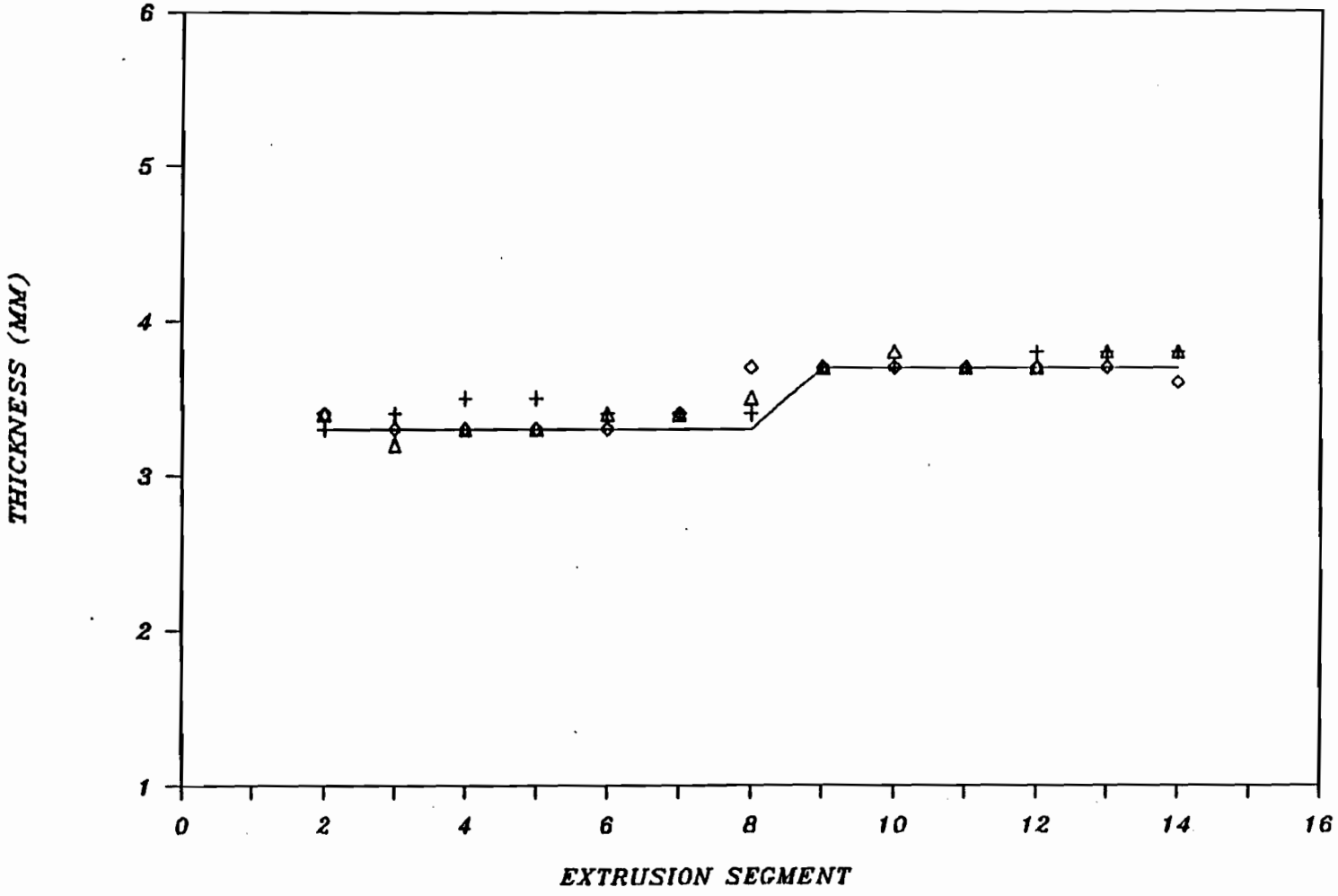

Figure 5.70: On-Line Control of Step Up Set Point Profile, Step Magnitude 0.4 mm.

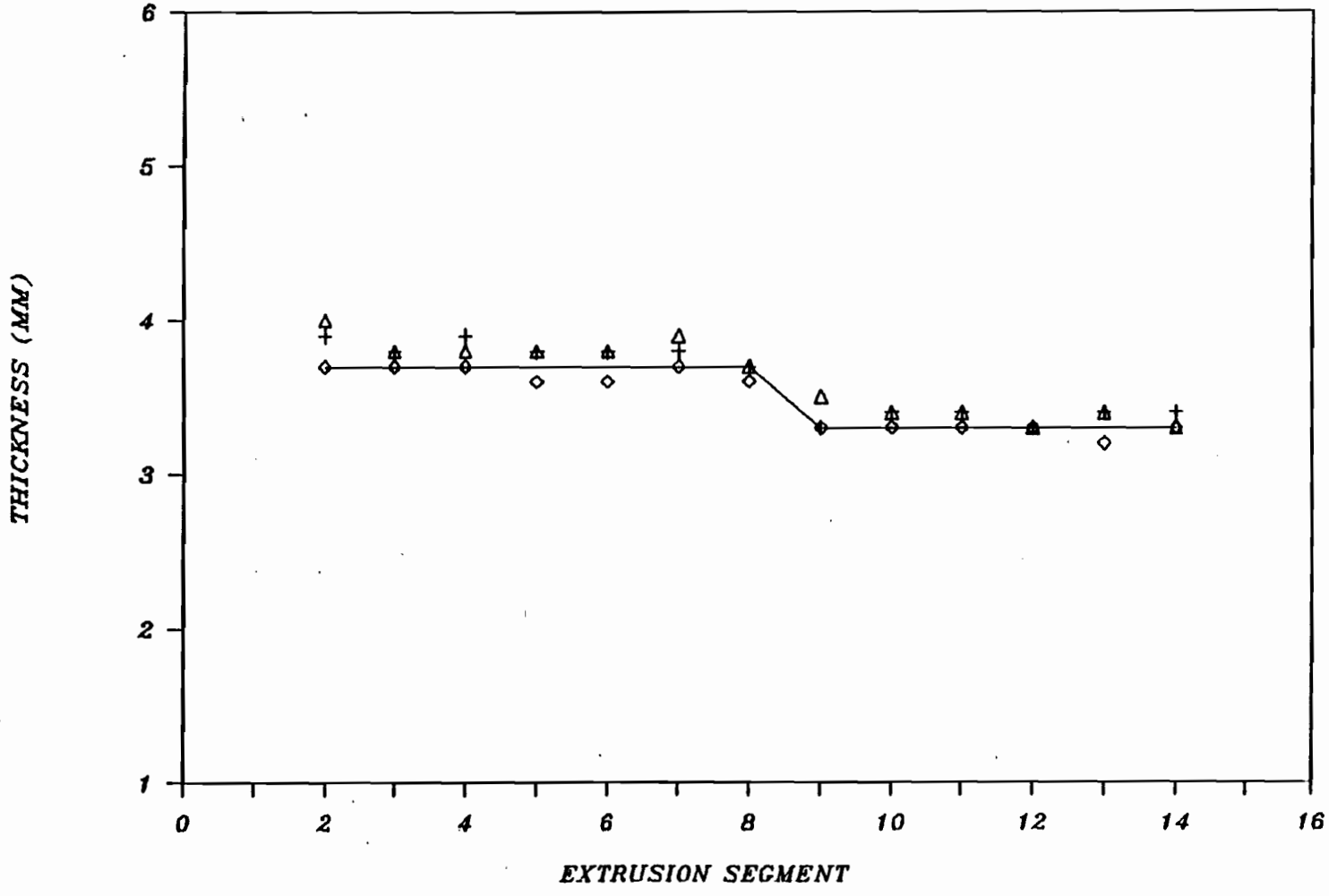

Figure 5.71: On-Line Control of Step Down Set Point Profile, Step Magnitude 0.4 mm.

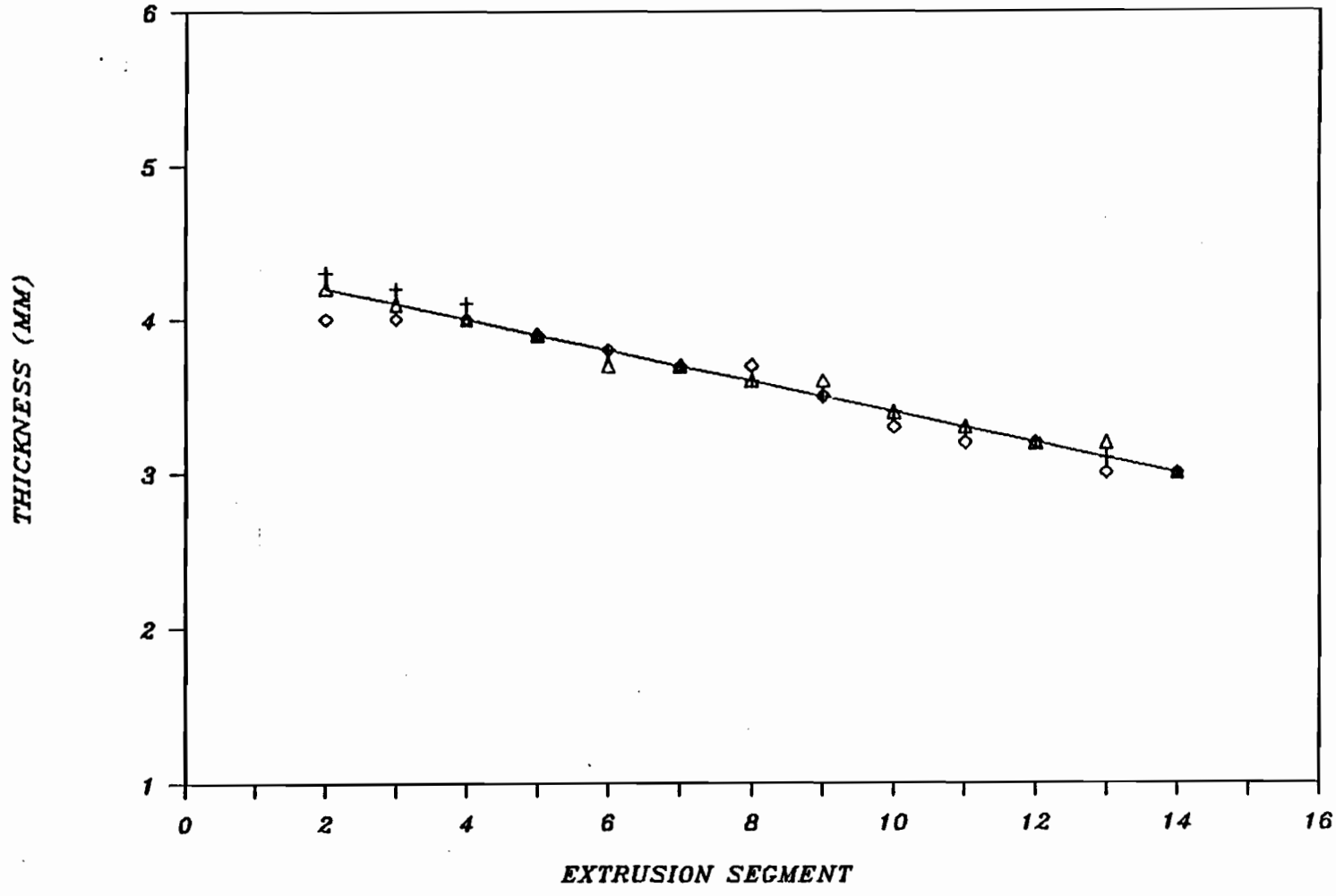

Figure 5.72: On-Line Control of Linear Declining Set Point Profile, Slope 0.1 mm/segment.

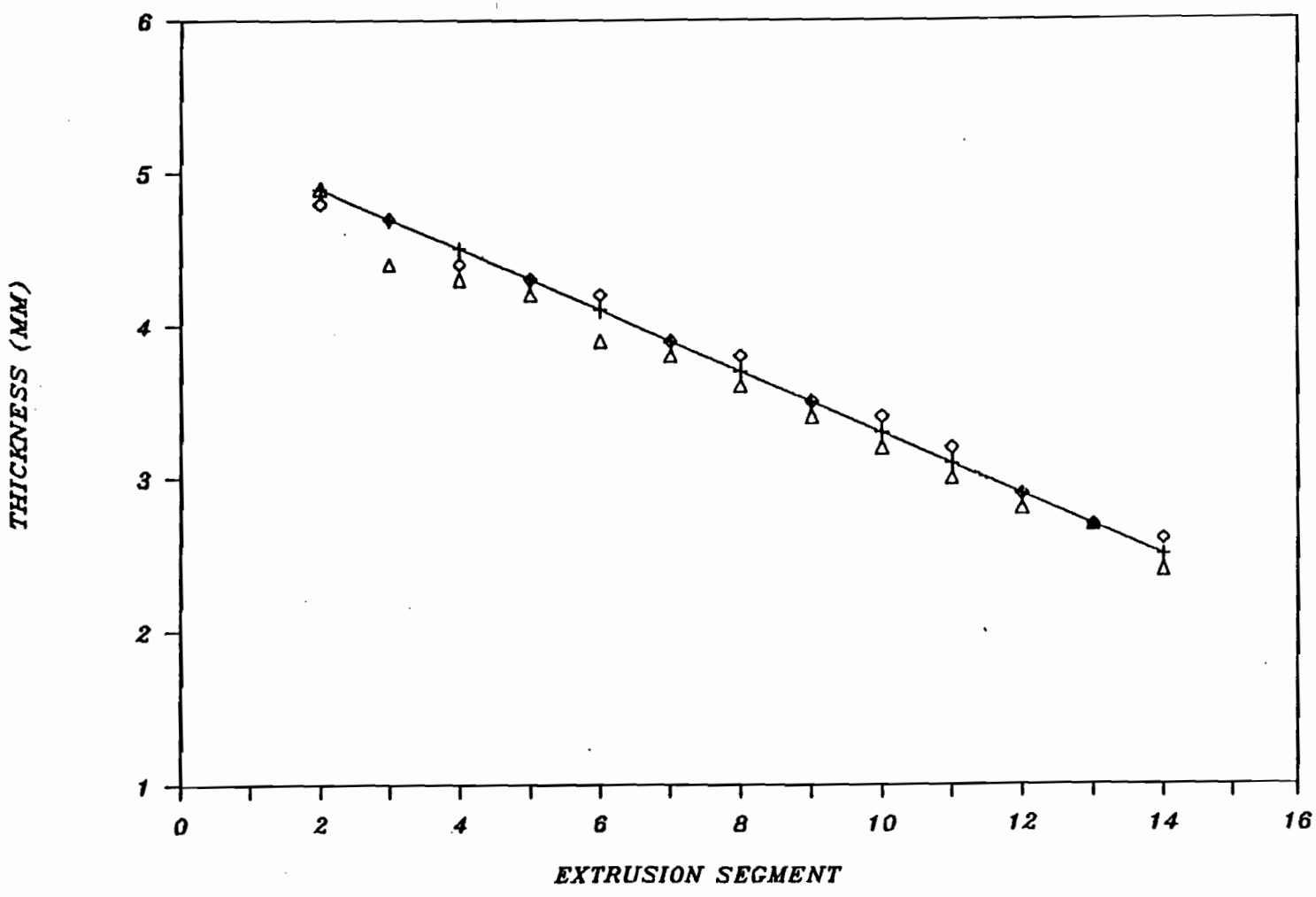

Figure 5.73: On-Line Control of Linear Declining Set Point Profile, Slope 0.2 mm/segment.

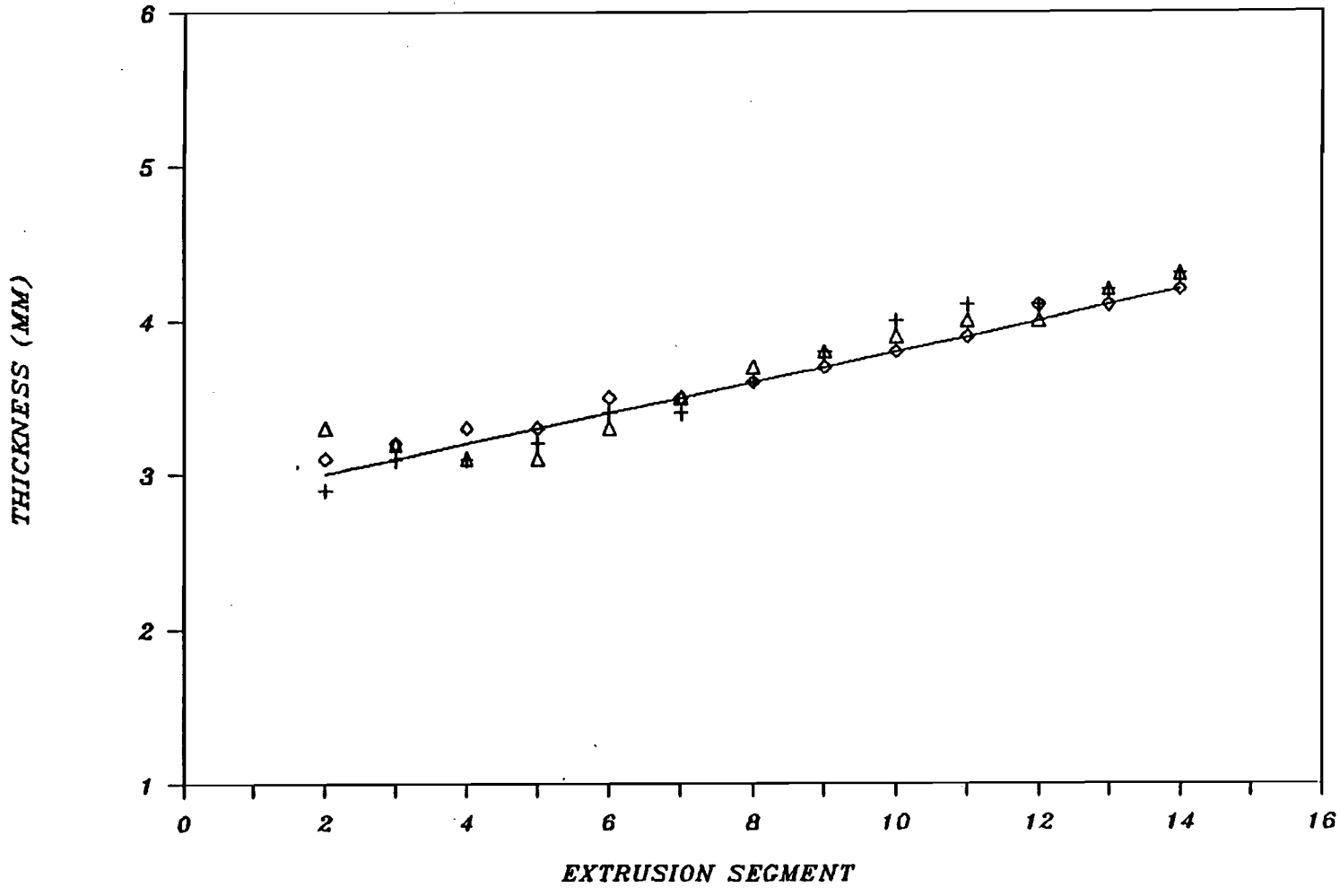

Figure 5.74: On-Line Control of Linear Increasing Set Point Profile, Slope 0.1 mm/segment.

different from the action with a linear set point profile, to warrant an independent evaluation.

Figures 5.75 and 5.76 refer to staircase increasing and declining set point profiles, respectively. Figures 5.77 and 5.78 illustrate constant-declining set point profiles with a halfway and late transition, respectively. Figures 5.79 and 5.80 deal with declining-constant set point profiles with halfway and early transitions, respectively. These set point profiles are typical for parisons utilized in bottle formation. The linear portion is employed to simulate bottle neck and handle formation in regular and upside down inflation.

5.2.2.2.4 INVERTED V AND V-SHAPED SET POINTS As mentioned in Chapter 2, there is a trend towards the blow molding of complicated shapes, such as automobile parts. For this reason, it is desirable to evaluate the feasibility of reproducing complicated set point profiles, such as inverted V and V-shapes, as well as oscillatory set point profiles.

Figure 5.81 illustrates the control action on an inverted V-shaped profile. The reverse programmed set point profile, V-shaped, is shown in Figure 5.82. The control scheme had difficulty in attaining adequate control with the inverted V shaped profile, because of the gap limits. The thickness at the peak required a gap greater than the upper limit. This tended to set the entire gap profile into a continuous cycle-to-cycle oscillation, with no apparent damping. The V-shaped set point

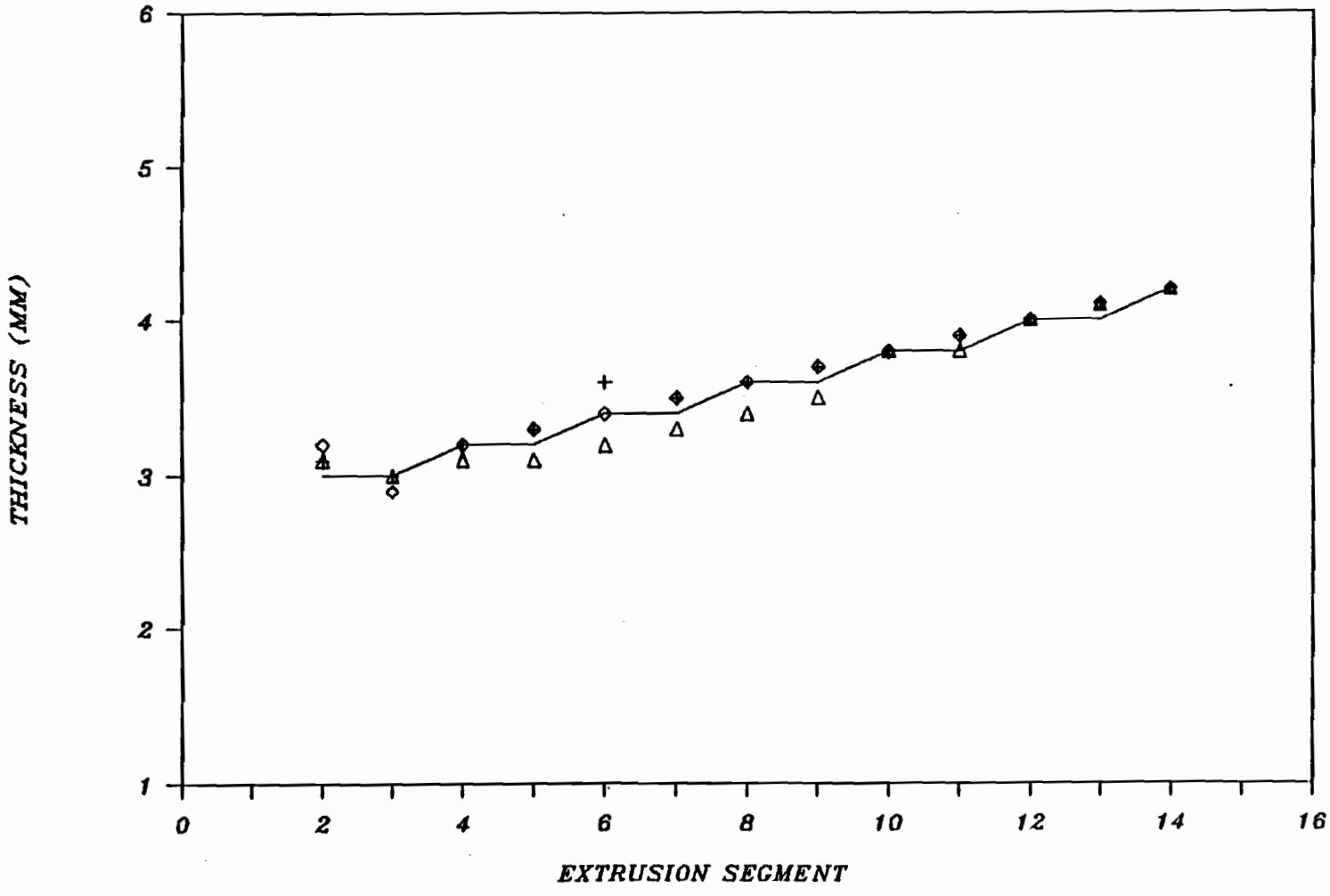

Figure 5.75: On-Line Control of Staircase Increasing Set Point Profile.

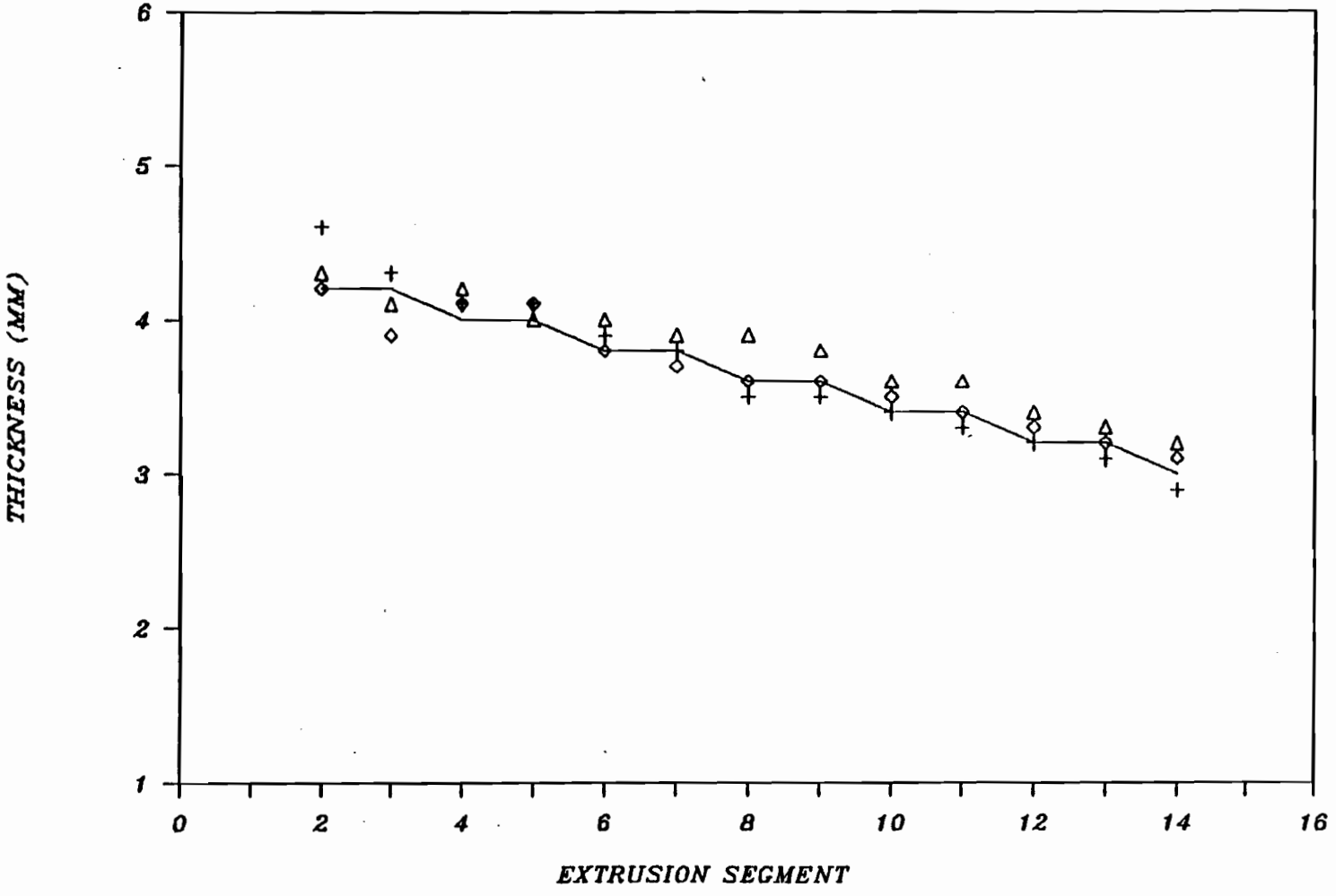

Figure 5.76: On-Line Control of Staircase Declining Set Point Profile.

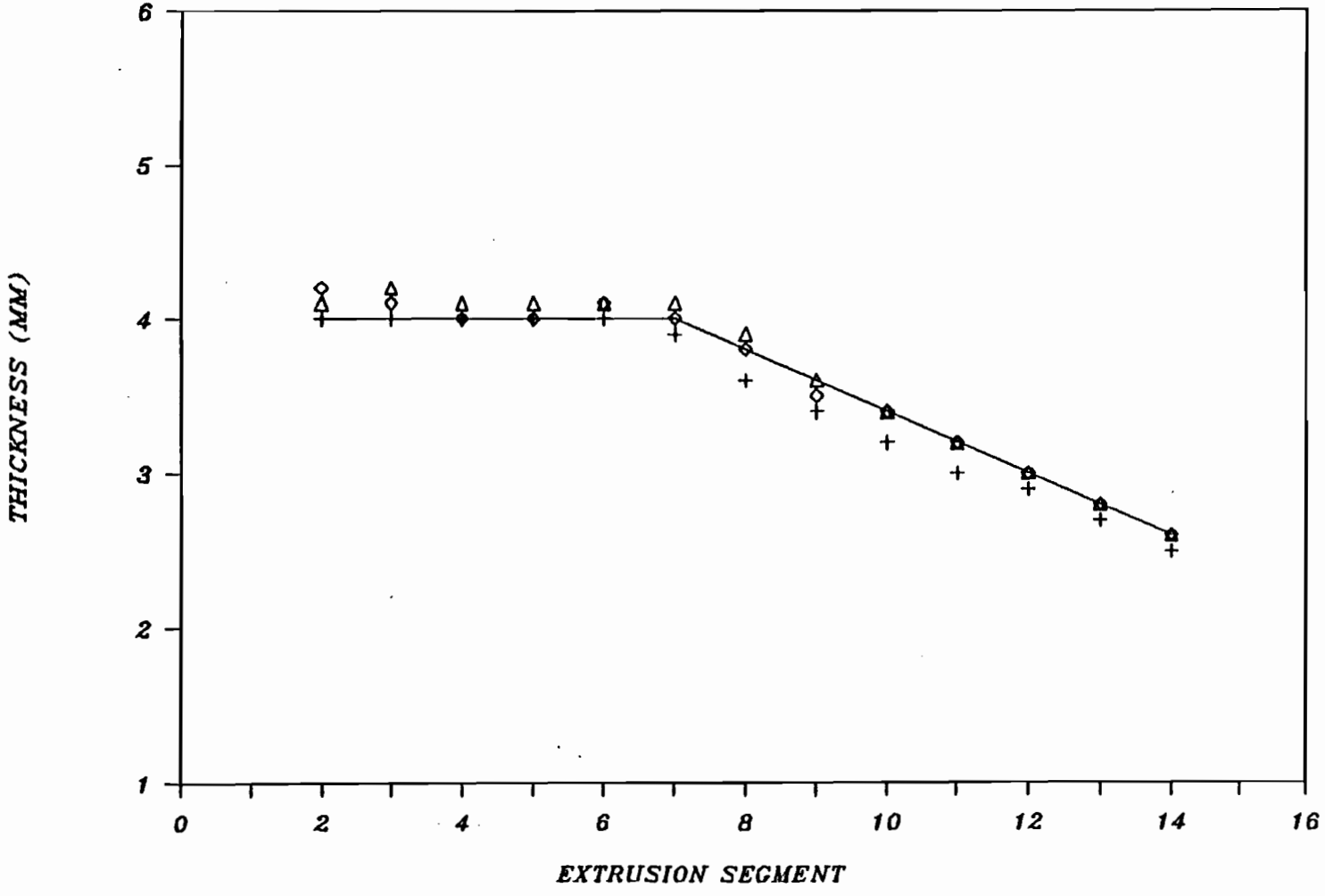

Figure 5.77: On-Line Control of Constant-Declining Set Point Profile, Halfway Transition.

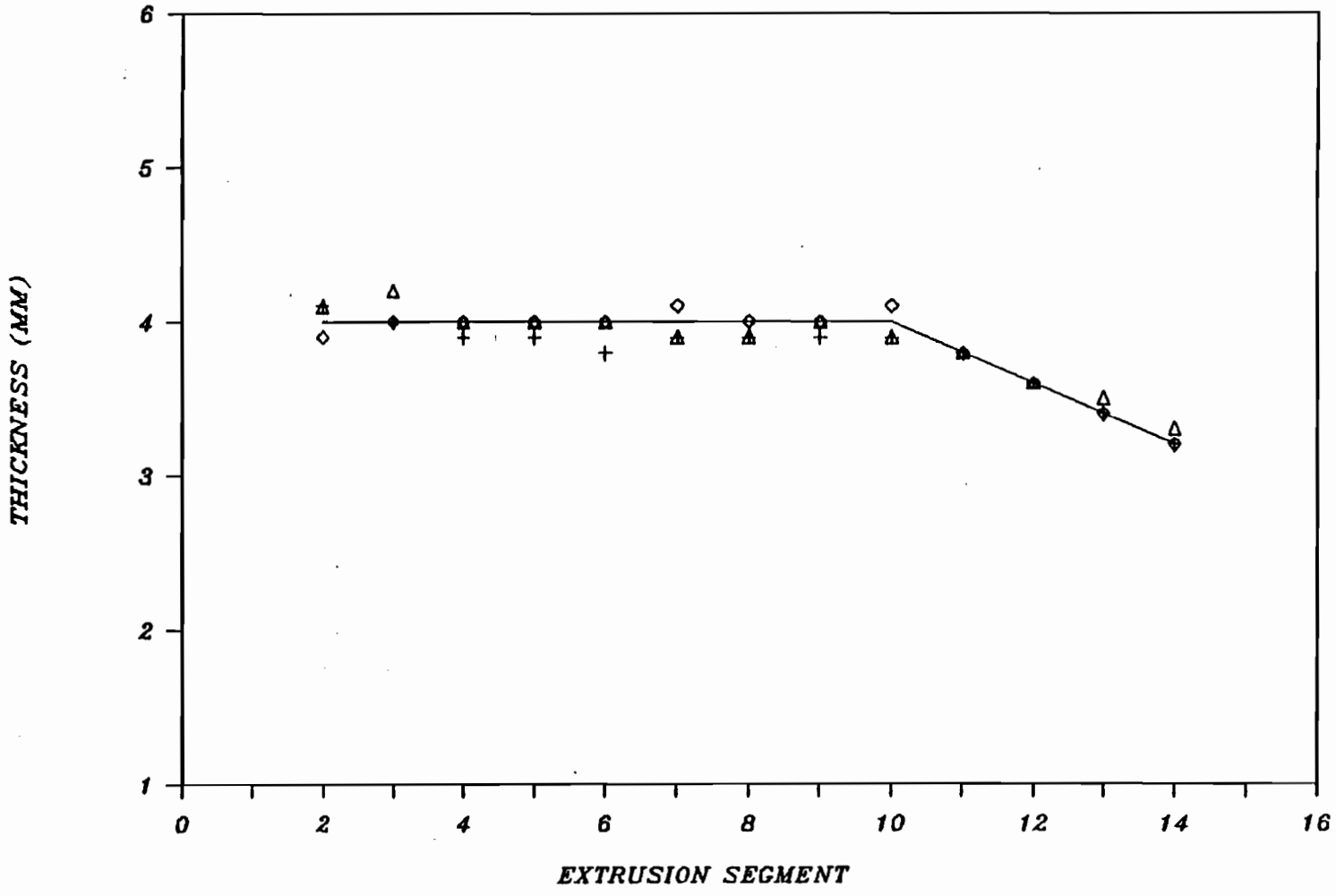

Figure 5.78: On-Line Control of Constant-Declining Set Point Profile, Late Transition.

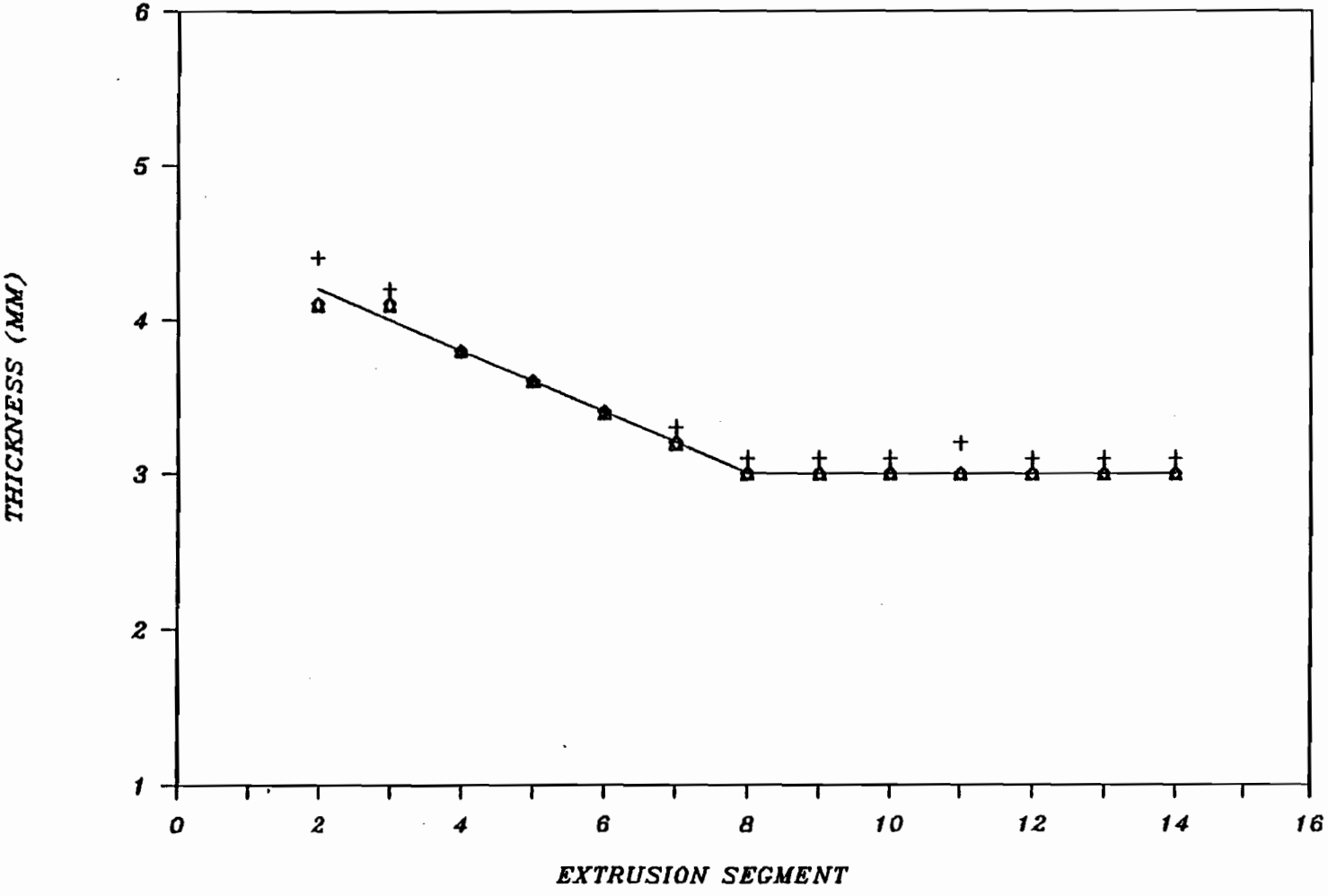

Figure 5.79: On-Line Control of Declining-Constant Set Point Profile, Halfway Transition.

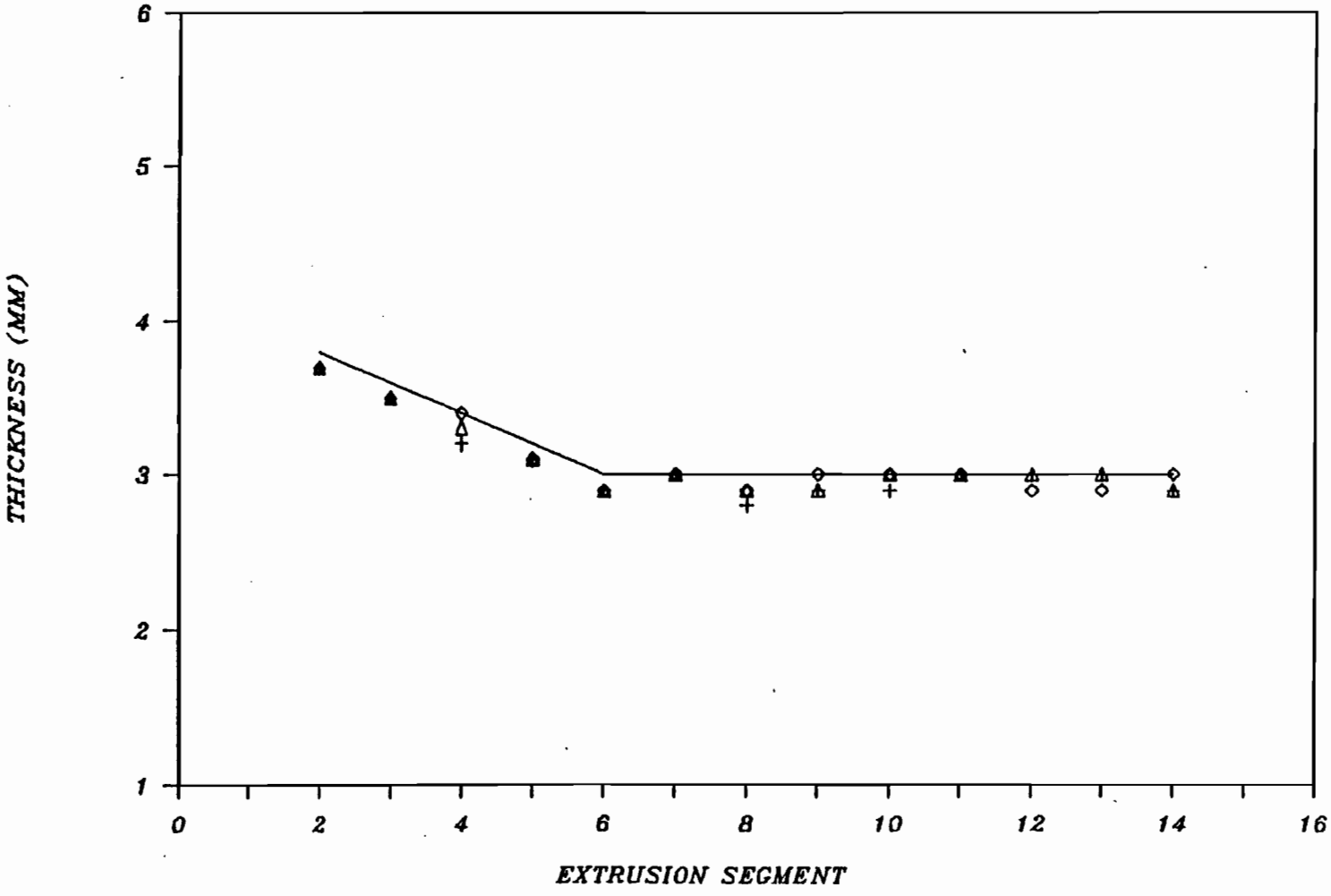

Figure 5.80: On-Line Control of Declining-Constant Set Point Profile, Early Transition.

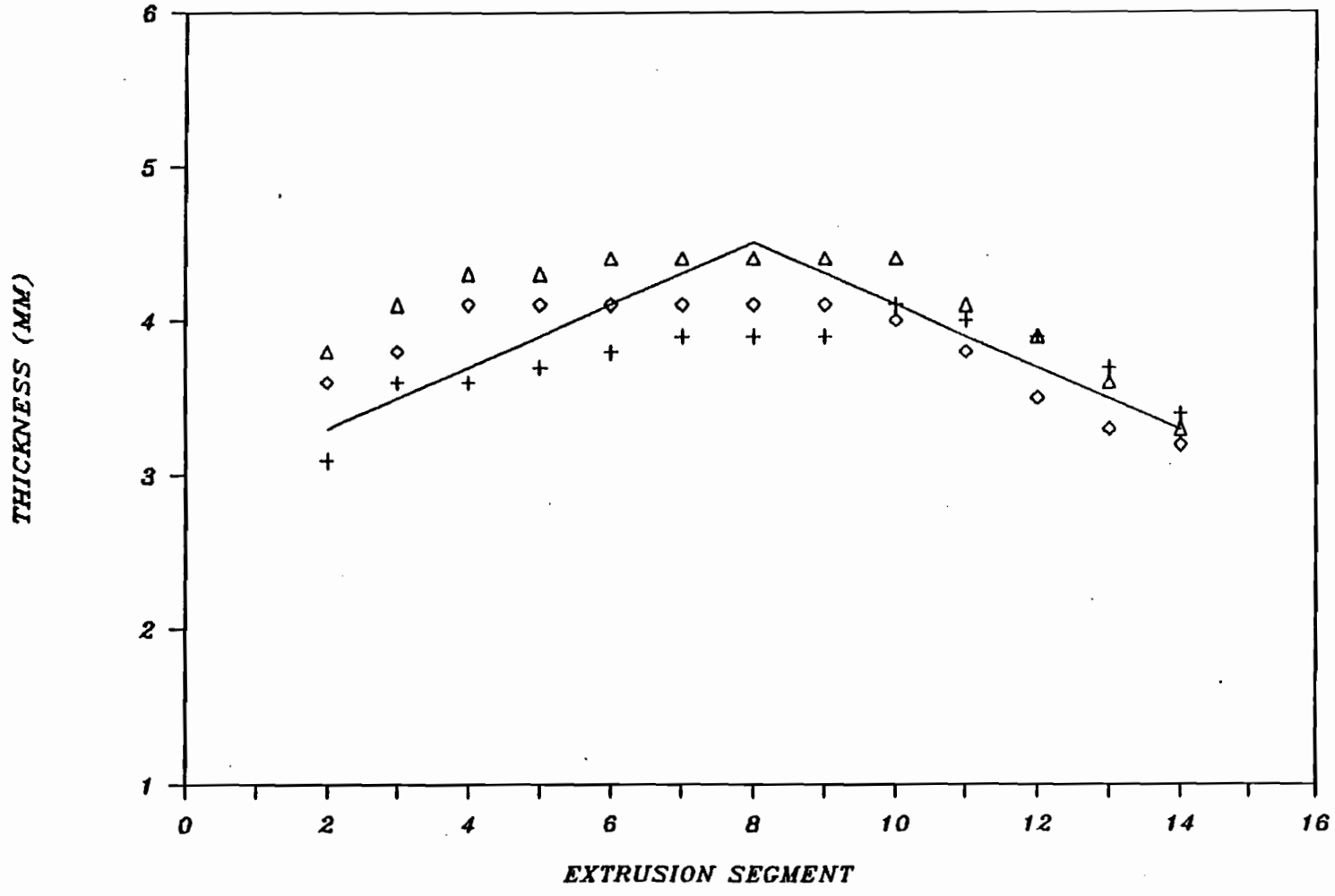

Figure 5.81: On-Line Control of Inverted V-Shaped Set Point Profile.

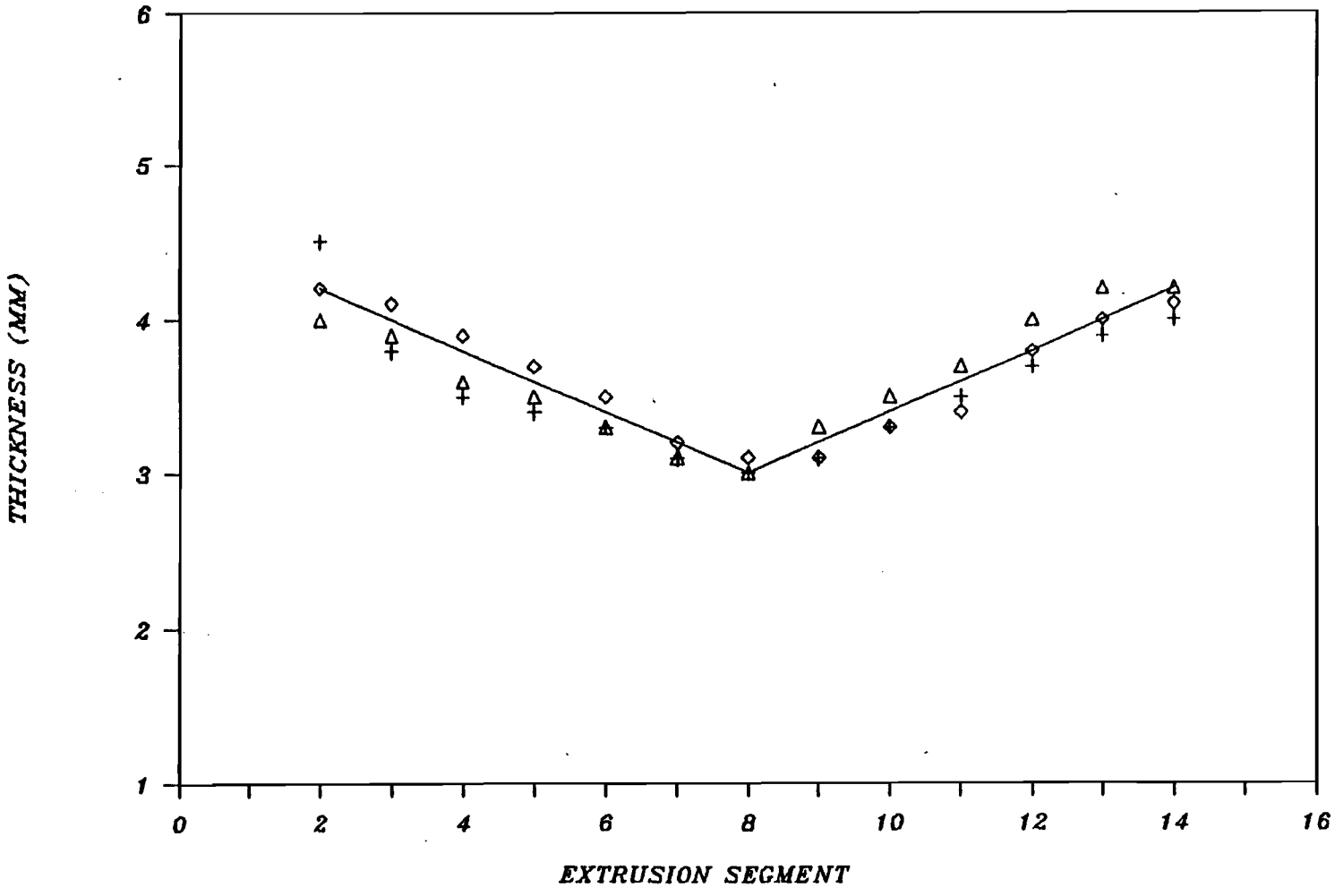

Figure 5.82: On-Line Control of V-Shaped Set Point Profile.

profile was controlled well. Again, it is important to realize that controllability of the set point is dependent on the upper and lower limits of the gaps.

5.2.2.2.5 OSCILLLATORY SET POINTS Figures 5.83 and 5.84 illustrate the control action on four and eight point set point profiles, respectively. The four point profile was controlled well, whereas difficulties arose in the control of the eight point profile. Apparently, the high frequency and rapid changes from an established thickness cannot be handled by the control scheme. Medium and high frequency oscillation set point profiles are evaluated in Figures 5.85 and 5.86, respectively. The control was adequate for the medium frequency case. The high frequency set point profile was not controlled well, as the number of up and down changes in the gap was too great to be handled by the control scheme.

5.2.2.3 RESIN B

Resin B was tested with selected profiles. The selected profiles were: step up, linear declining, declining-constant, inverted V-shape and medium frequency oscillating, as shown in Figures 5.87-91, respectively. As is the case with Resin A, control of the sharp step up and inverted V-shape set point profiles was not adequate. Control of the linear down, linear down-steady and medium frequency oscillating set points was good.

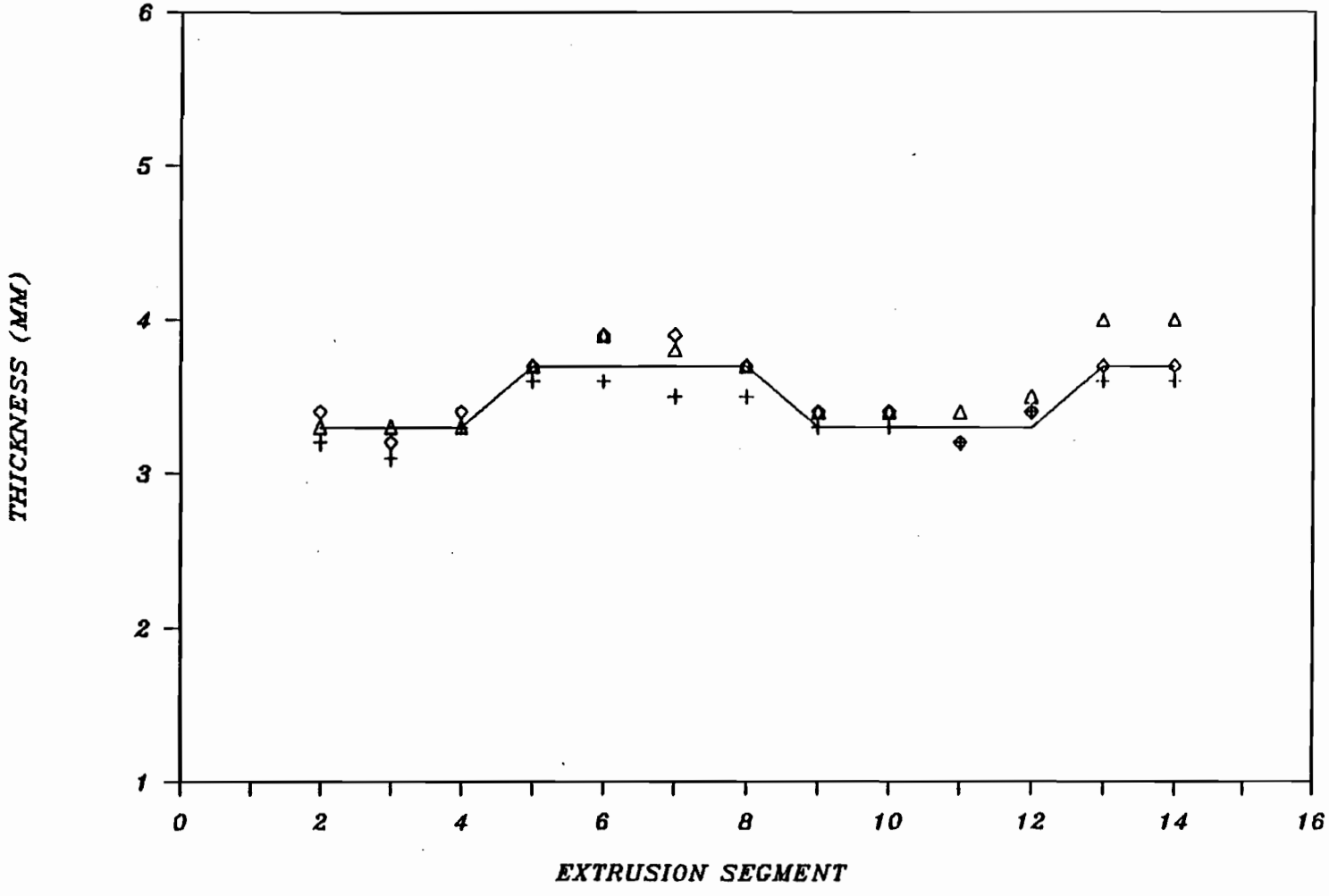

Figure 5.83: On-Line Control of Four Point Set Point Profile.

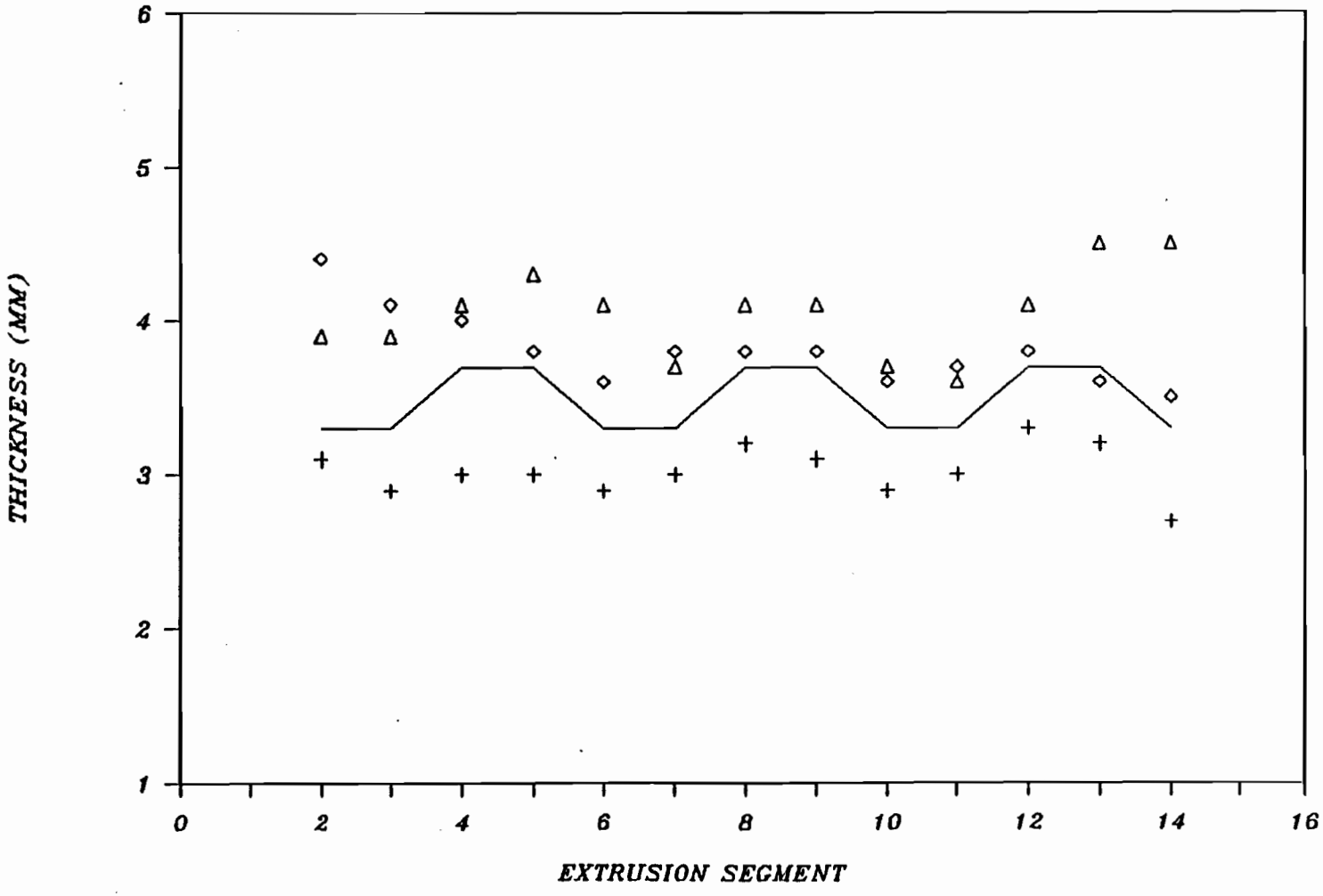

Figure 5.84: On-Line Control of Eight Point Set Point Profile.

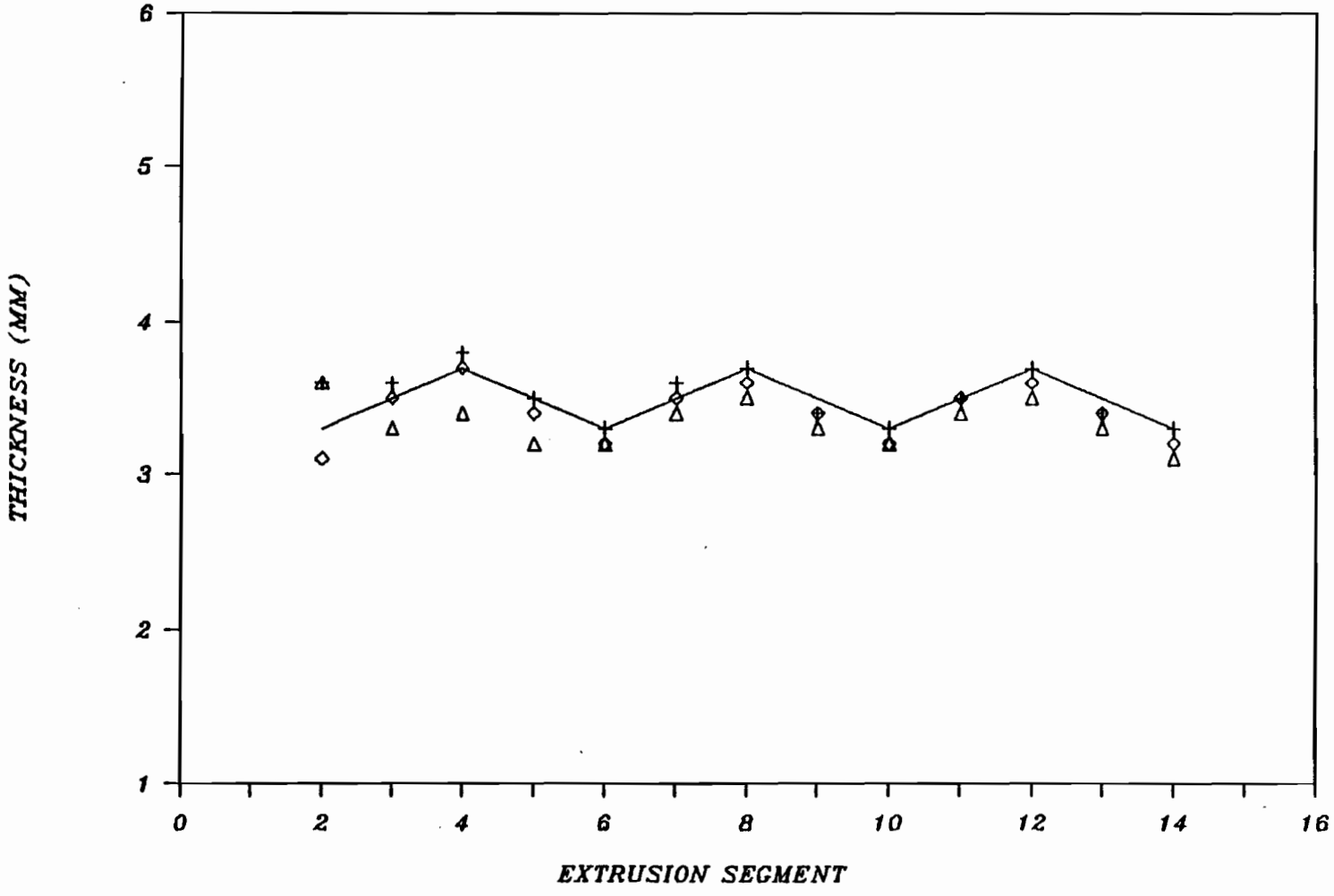

Figure 5.65: On-Line Control of Medium Frequency Oscillation Set Point Profile.

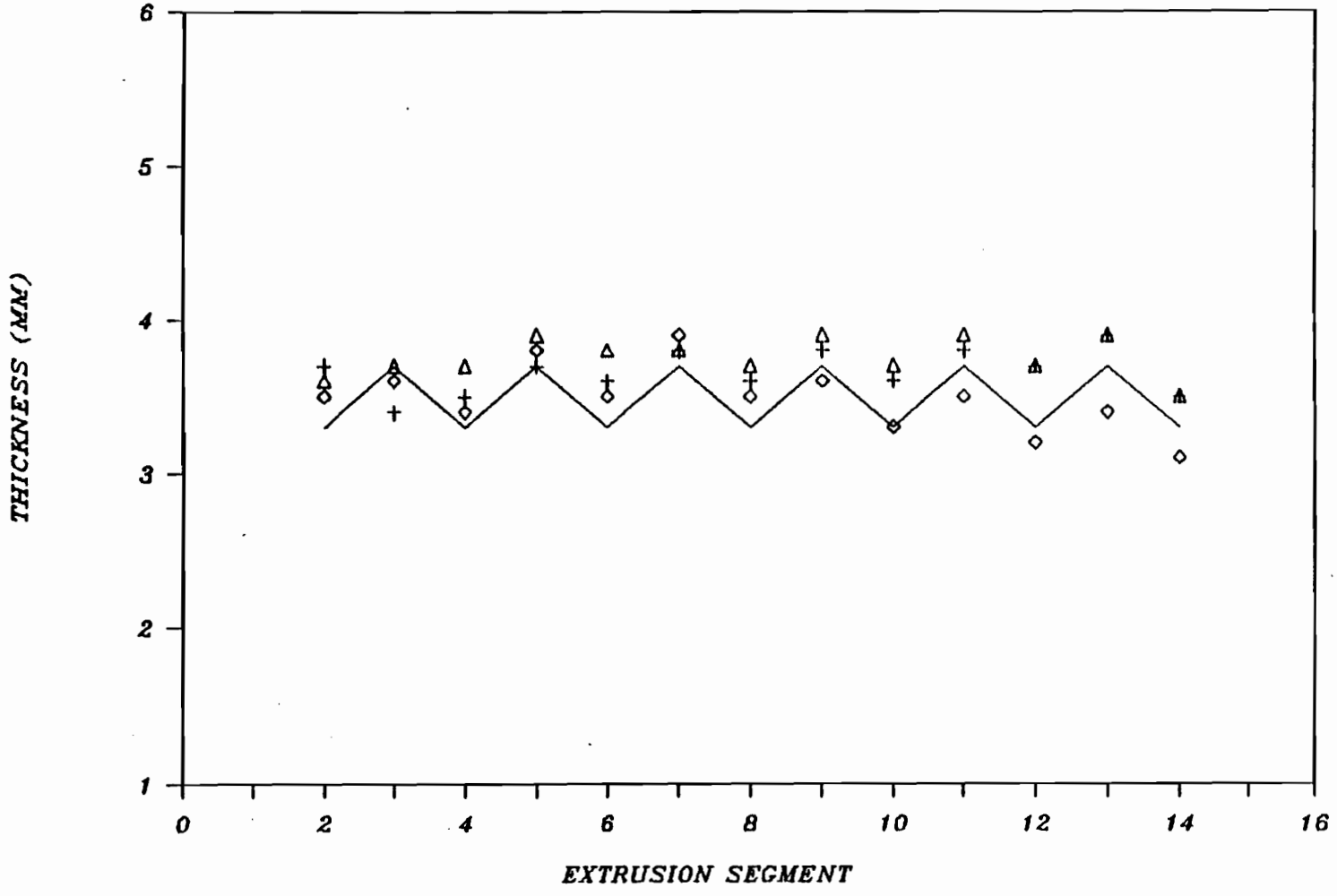

Figure 5.86: On-Line Control of High Frequency Oscillation Set Point Profile.

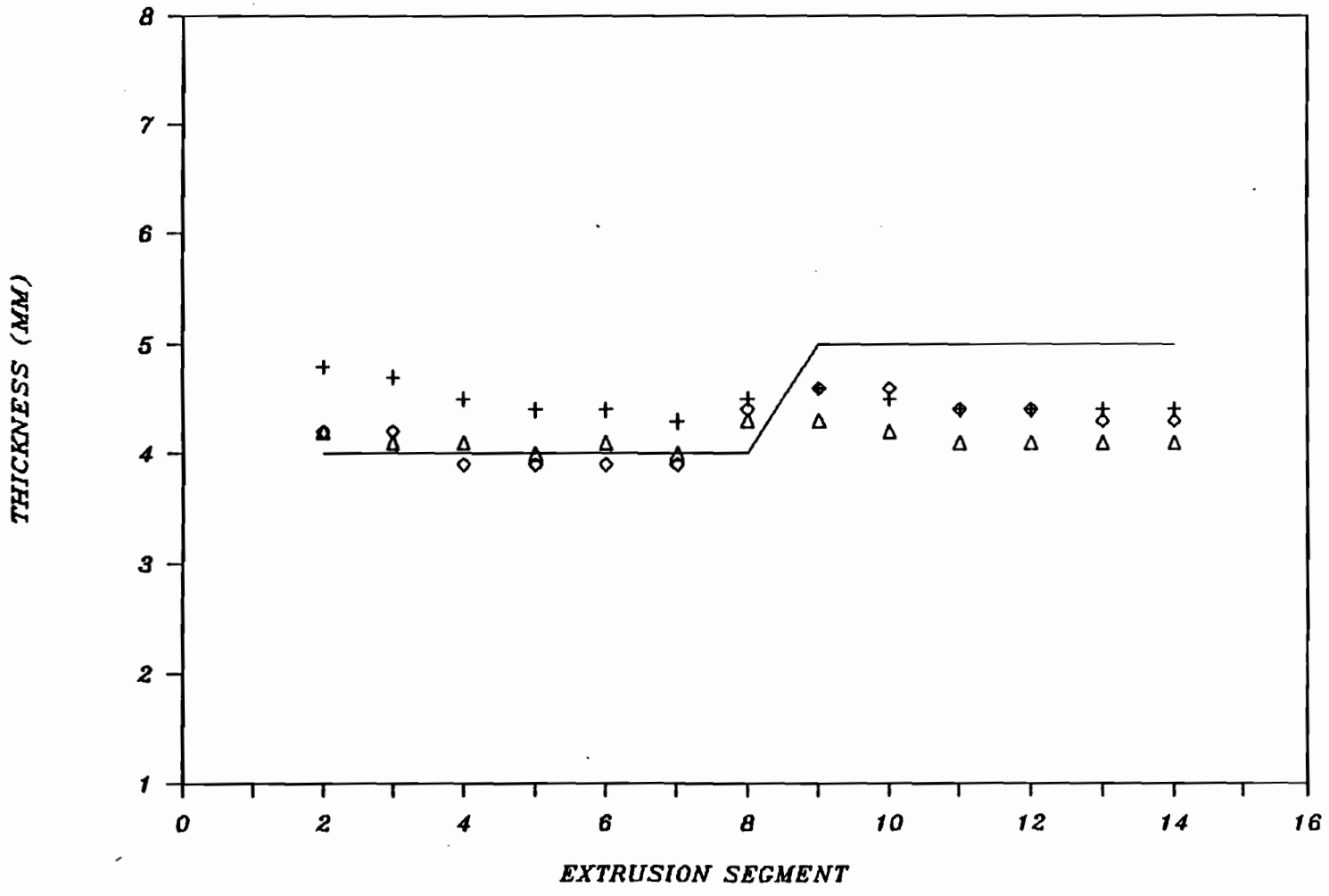

Figure 5.87: On-Line Control, for Resin B, of Step Up Set Point Profile, Step Magnitude 1 mm.

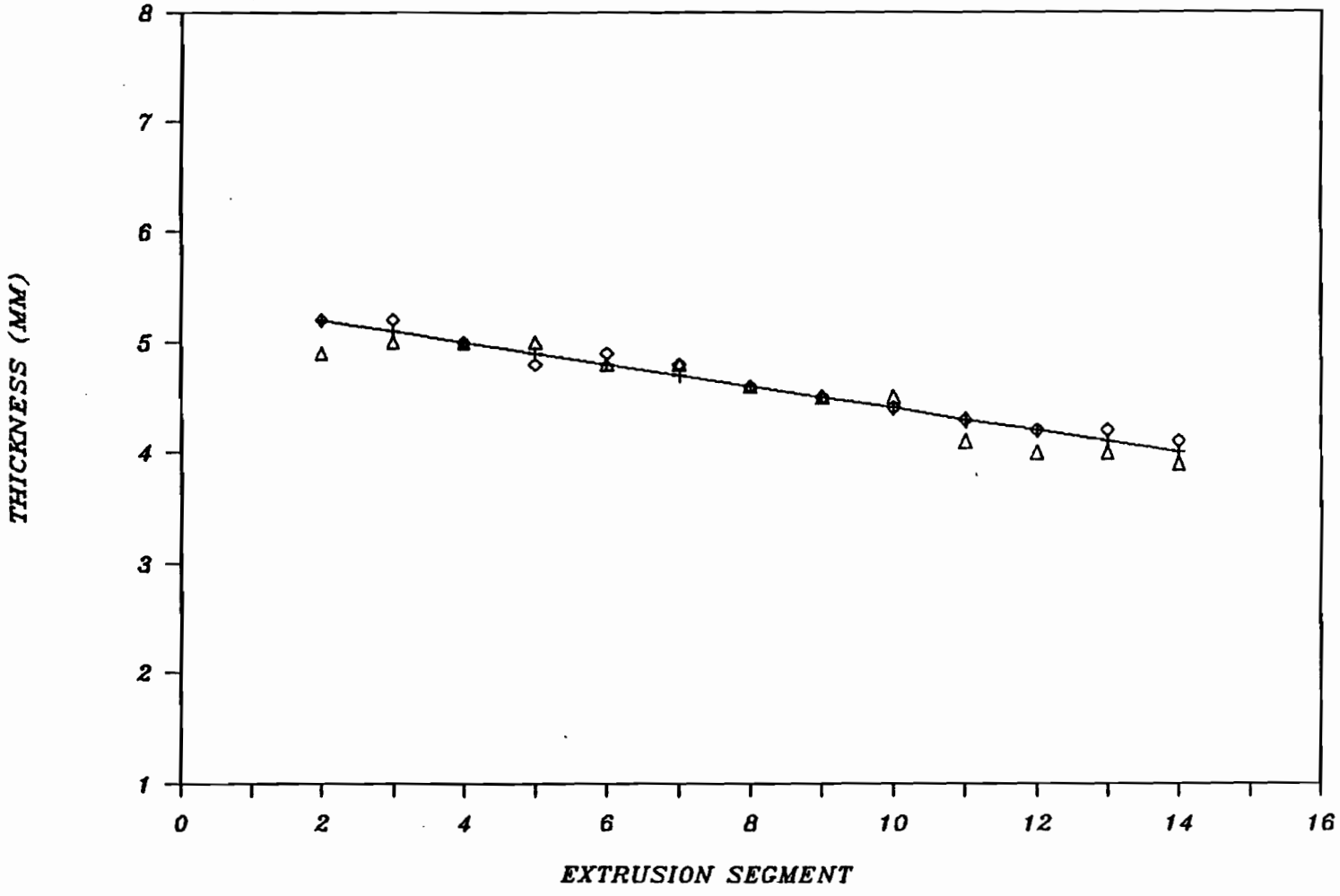

Figure 5.88: On-Line Control, for Resin B, of Linear Declining Set Point Profile, Slope 0.1 mm/segment.

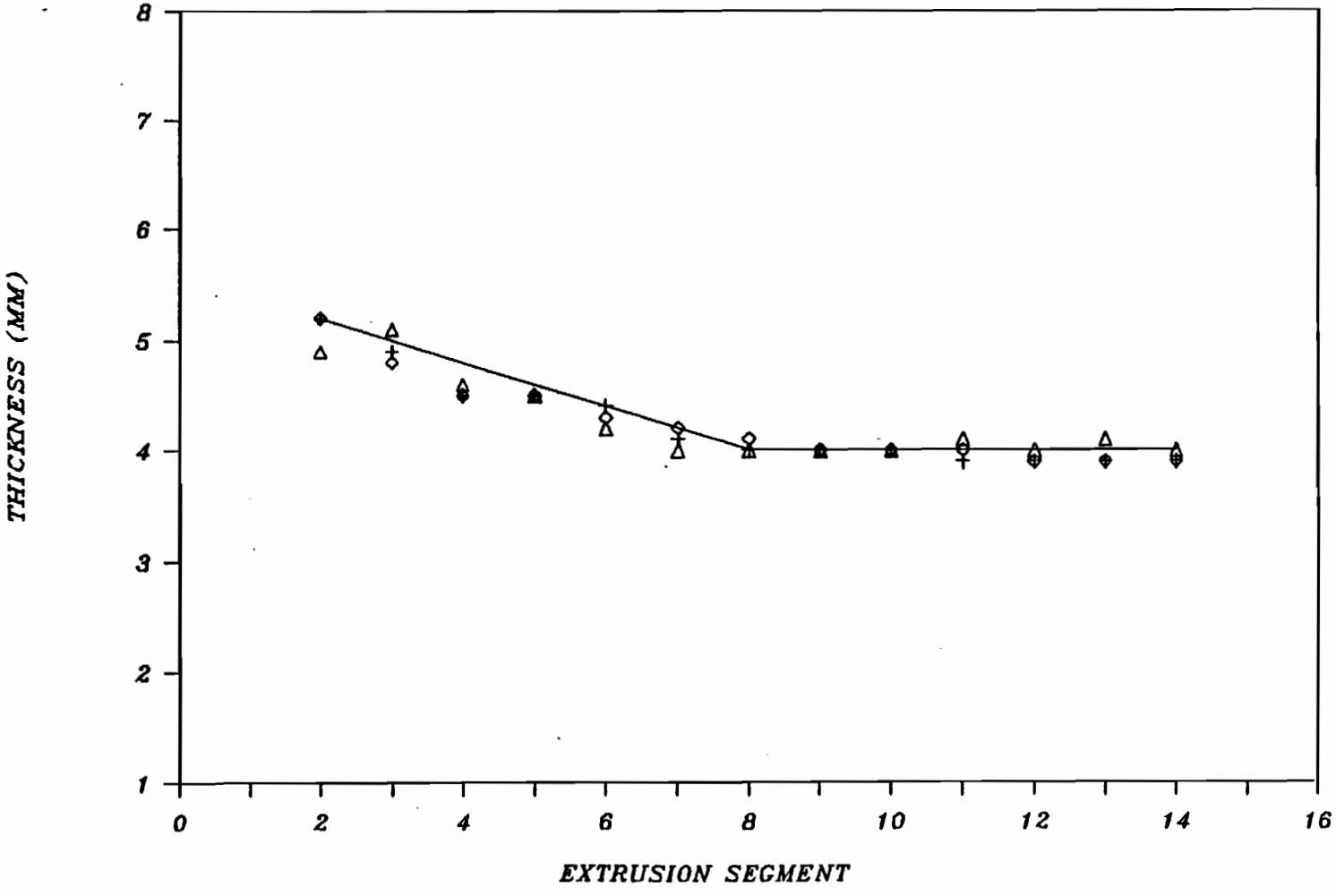

Figure 5.89: On-Line Control, for Resin B, of Declining-Constant Set Point Profile, Halfway Transition.

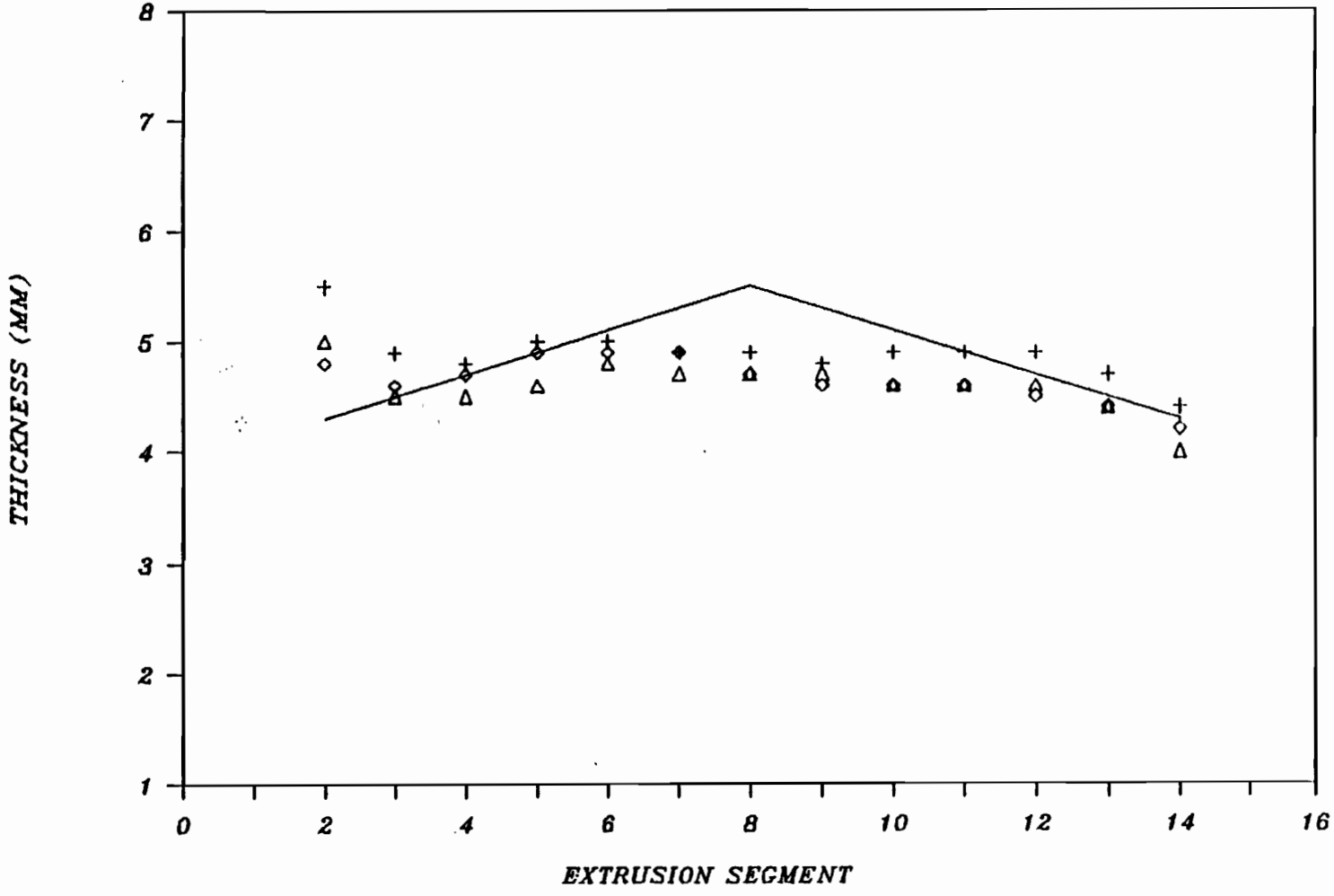

Figure 5.90: On-Line Control, for Resin B, of Inverted V-Shaped Set Point Profile.

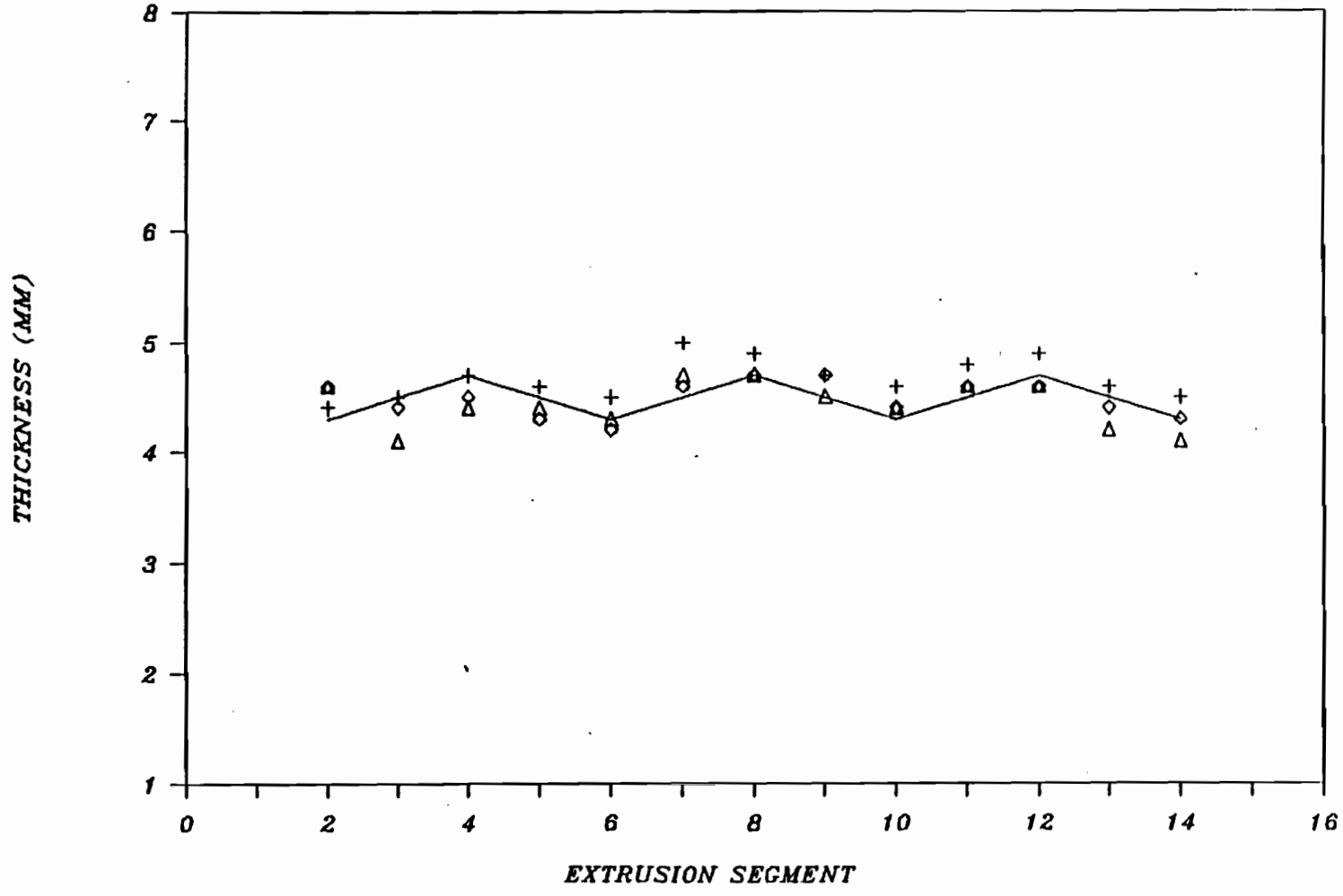

Figure 5.91: On-Line Control, for Resin B, of Medium Frequency Oscillation Set Point Profile.

5.2.2.4 CYCLE TO CYCLE CONTROL

The percent error was monitored over a large number of cycles. The results are presented in Figure 5.92. The programmed set point evaluated was the linear declining form. System noise, in the form of an increased percent error, appears in the process, at times during the cycle-to-cycle monitoring. The noise is rectified instantaneously in the subsequent cycle. At cycle 48, the parison broke before the image was captured. This disturbance is also corrected quickly by the algorithm.

5.2.2.5 DISTURBANCE CORRECTION

Large disturbances were introduced into the system suddenly at a specified cycle number. It was felt that if the control system could handle such sudden disturbances, then the more typical gradual disturbances would also be handled. It was not possible to introduce specified gradual disturbances, as they could not be differentiated from inherent system noise.

The set point profile studied in this section was the linear declining type. The percent error was monitored until the disturbance was corrected. The individual disturbances were introduced at cycle number 4.

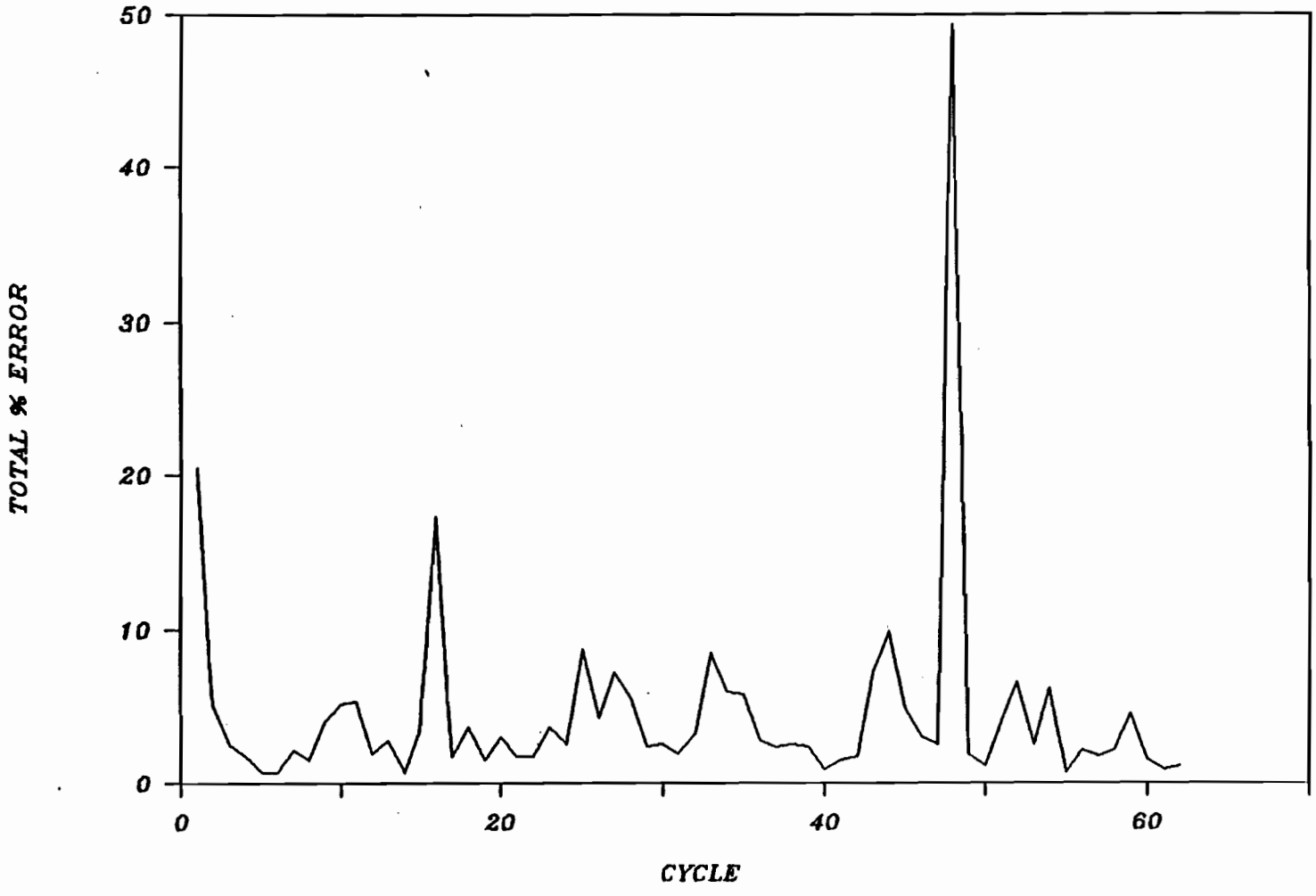

Figure 5.92: Cycle-to-Cycle Control Monitoring of Percent Error.

5.2.2.5.1 THICKNESS RESPONSE TO DISTURBANCE Figures 5.93, 5.94 and 5.95 show the thickness response of the segments 4, 8 and 12 respectively, to an input disturbance of -10°C. In all three cases, the response was of the damped oscillation type, reaching steady state, three cycles into the disturbance. This behaviour is associated with the movement of the process to a different operating point of gain settings.

5.2.2.5.2 PARISON BREAK Figure 5.96 shows the percent error response to the break in the parison discussed in the previous cycle-to-cycle control section. The disturbance was corrected instantaneously.

5.2.2.5.3 TEMPERATURE Figures 5.97 and 5.98 illustrate the response to disturbances of -10°C and +10°C, respectively. In both cases, it took several cycles to bring the percent error within acceptable limits.

5.2.2.5.4 INJECTION RATE Figures 5.99 and 5.100 illustrate the response to disturbances of -0.25 and +0.25 in injection valve setting, respectively. In the case of a decrease in injection rate, the disturbance was rectified within a few cycles. In the case of an increase in injection rate, the disturbance was not large enough to be visualized in the percent error. There seems to be an error increase at cycle 7. However, this is

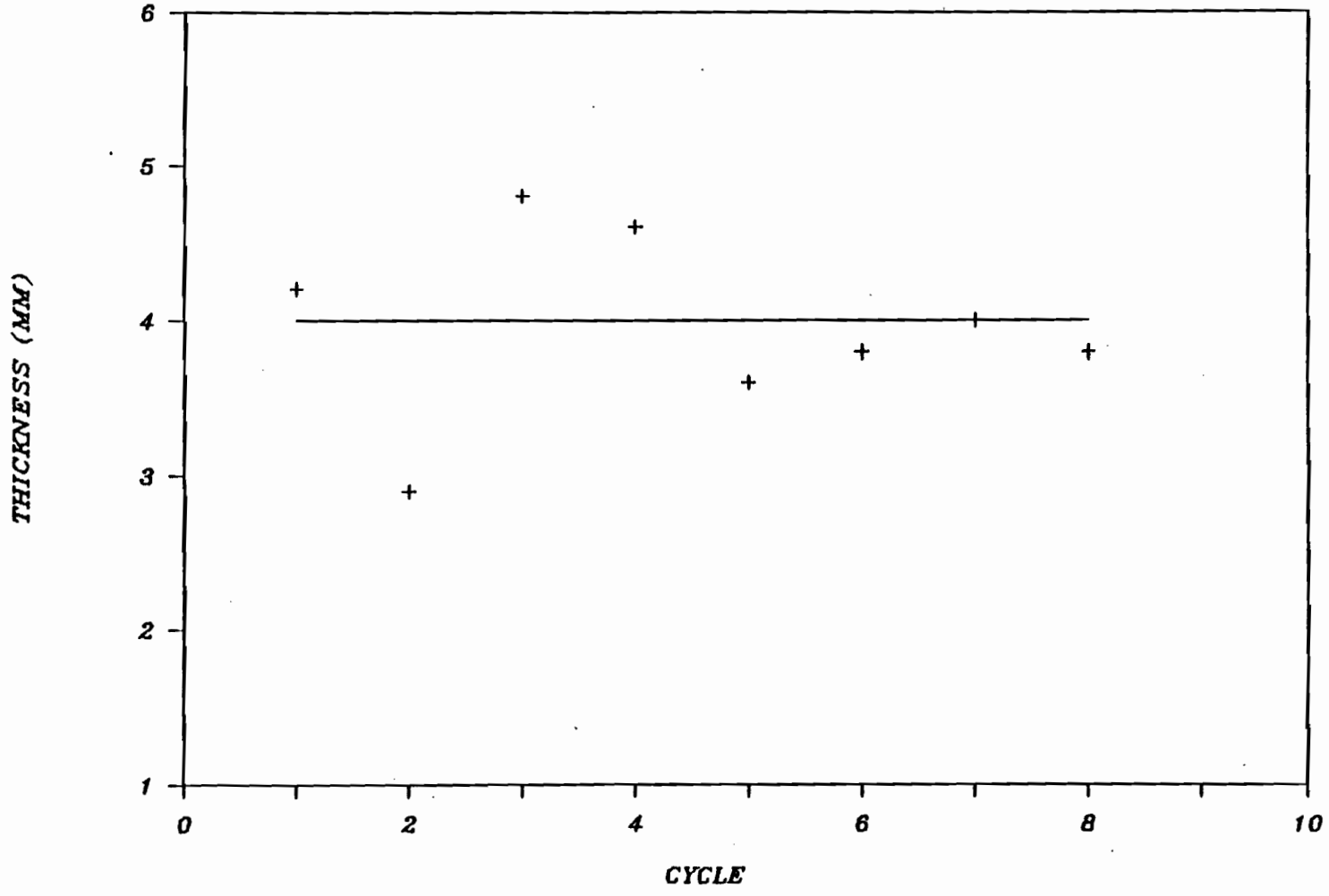

Figure 5.93: Control Action Response to Disturbance of -10 ^{o}C, of the Thickness Segment 4.

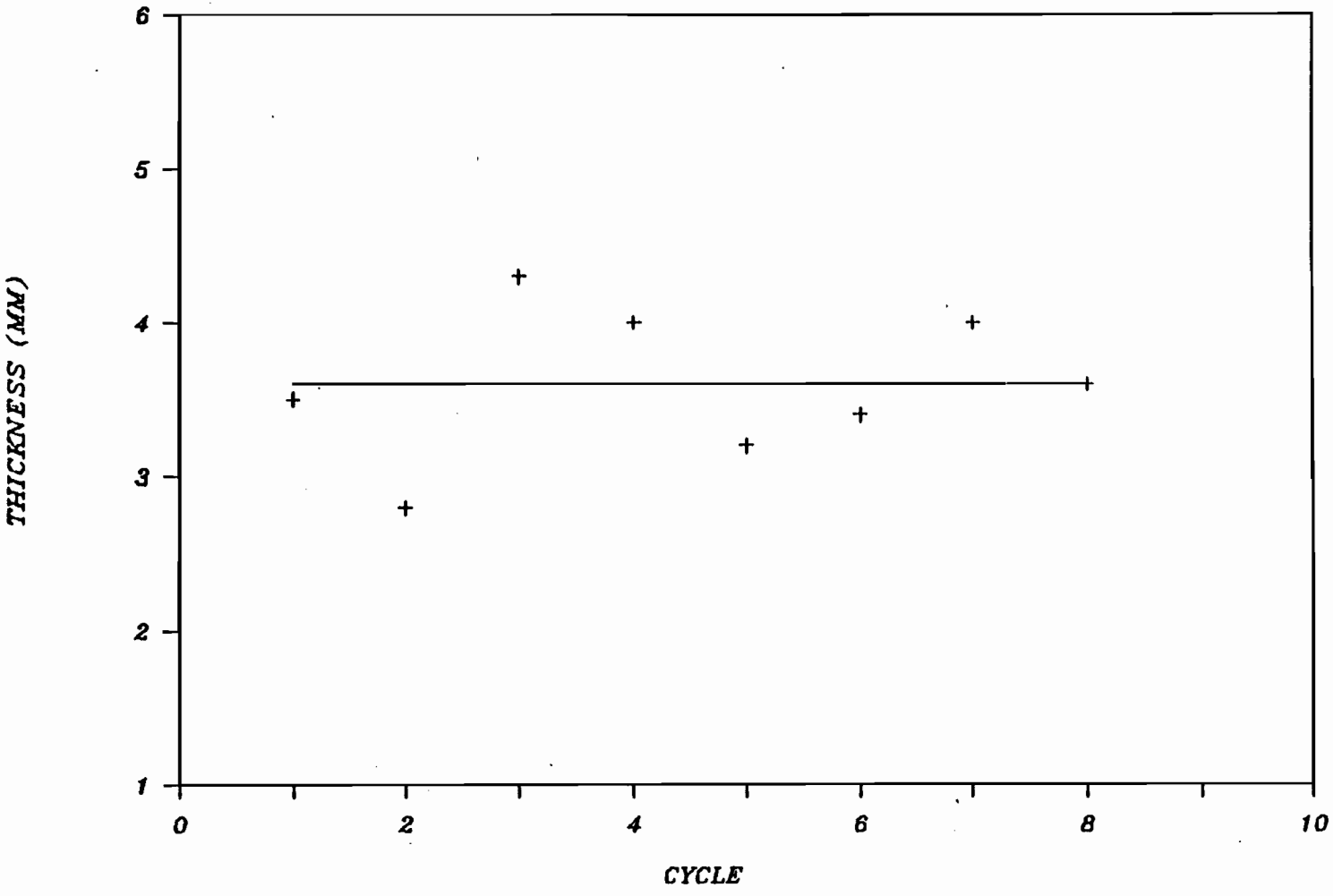

Figure 5.94: Control Action Response to Disturbance of -10 °C, of the Thickness of Segment 8.

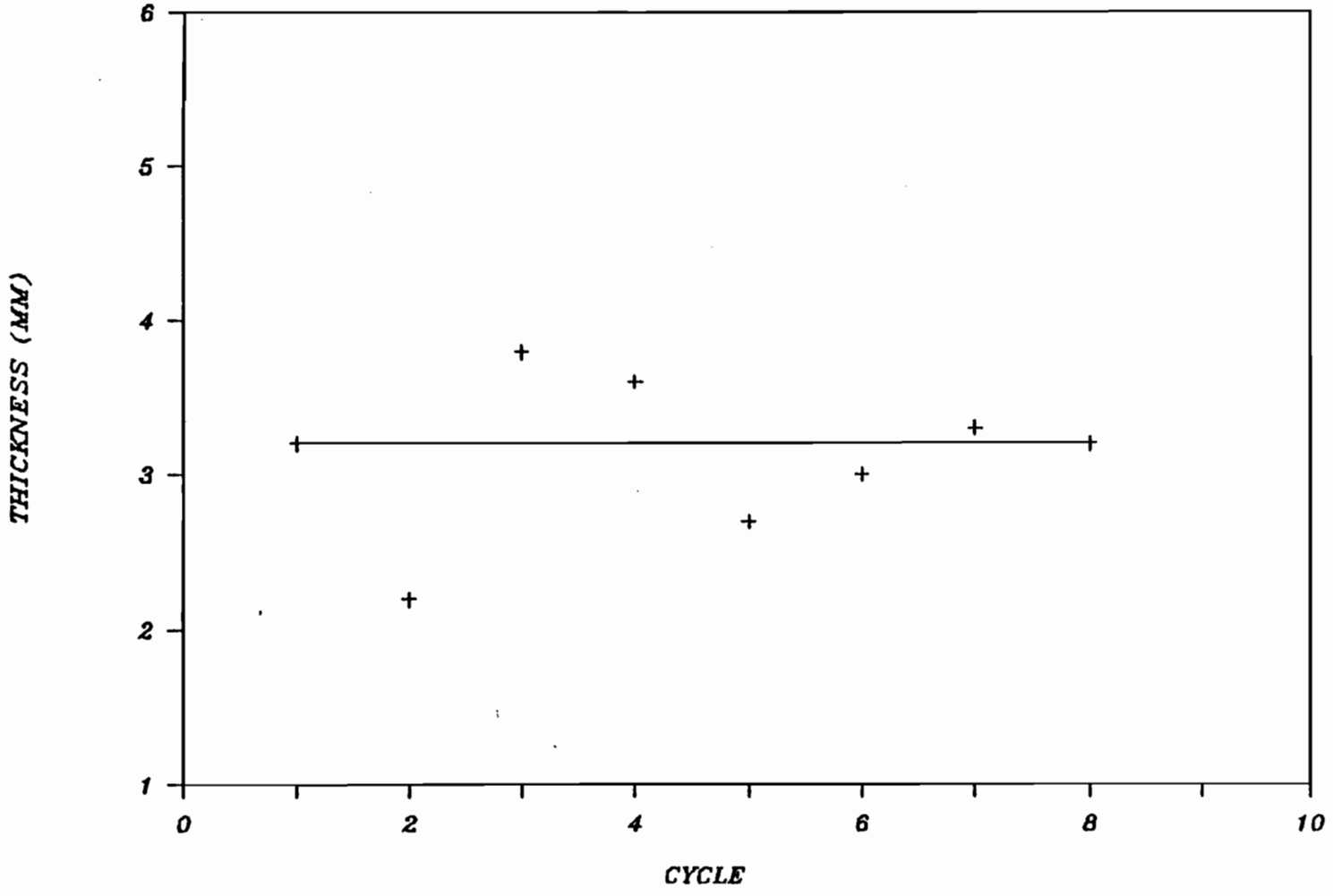

Figure 5.95: Control Action Response to Disturbance of -10°C, of the Thickness Segment 12.

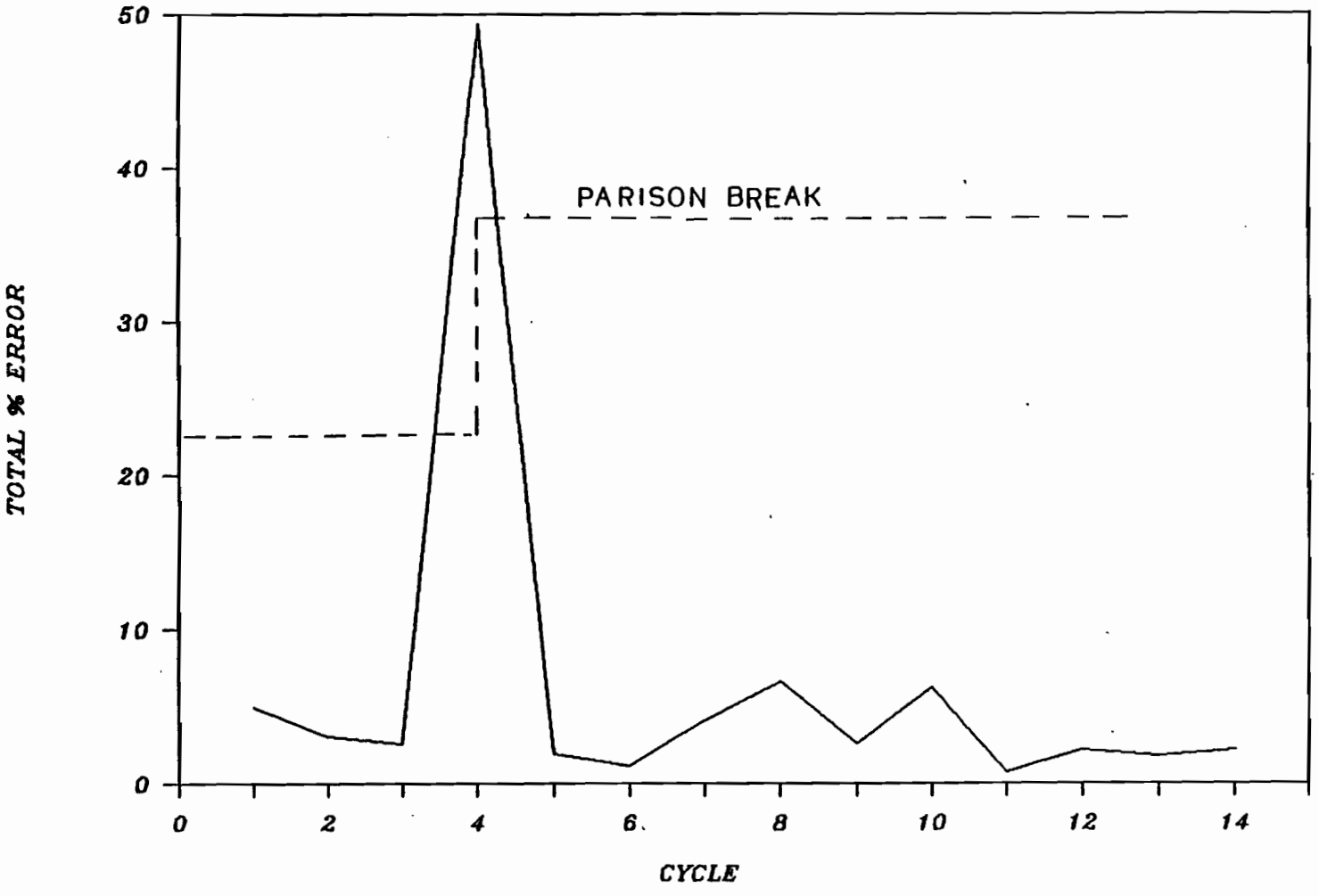

Figure 5.96: Control Action Response to Parison Break Disturbance at Cycle 4.

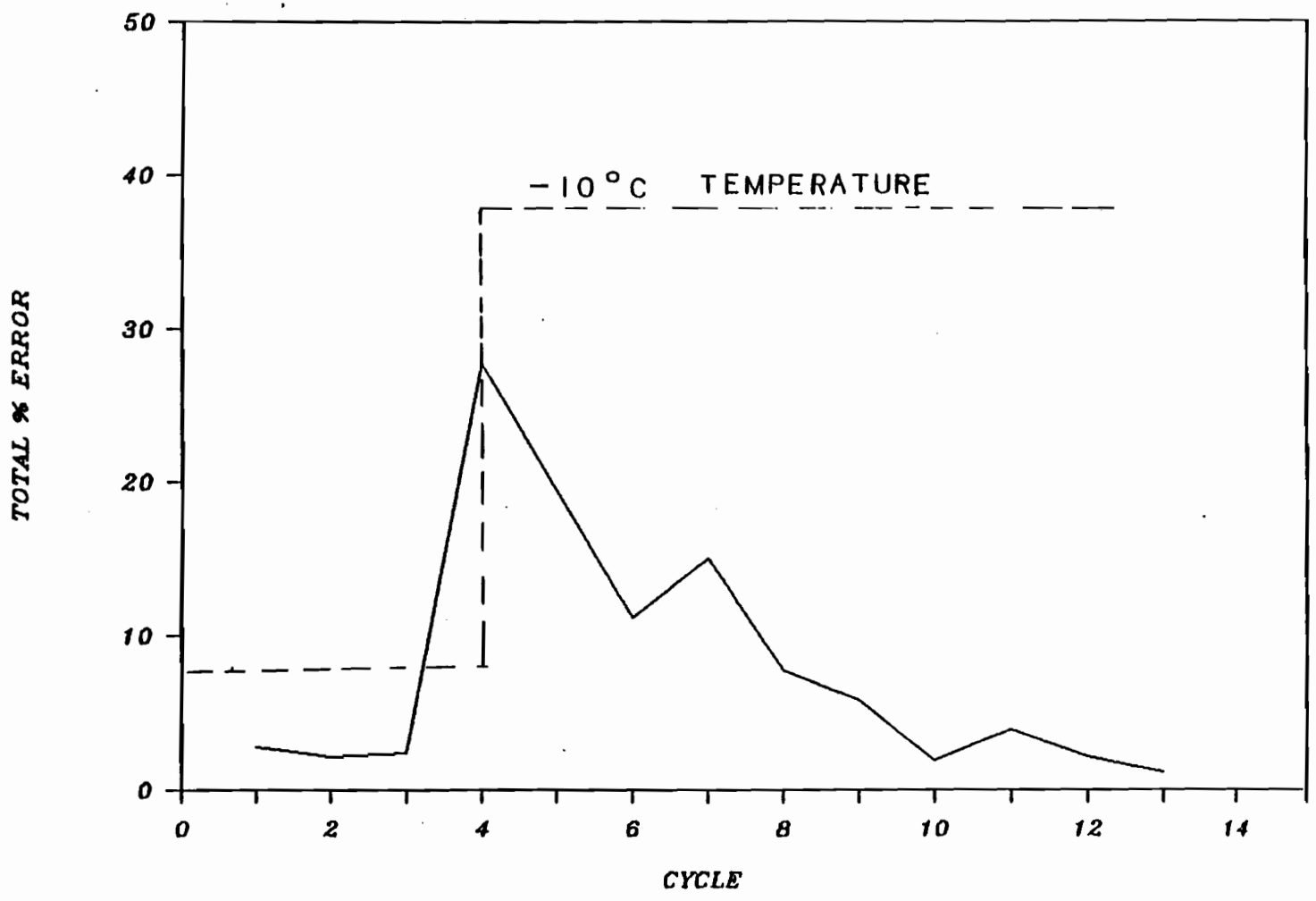

Figure 5.97: Control Action Response to Disturbance of -10°C, at Cycle 4.

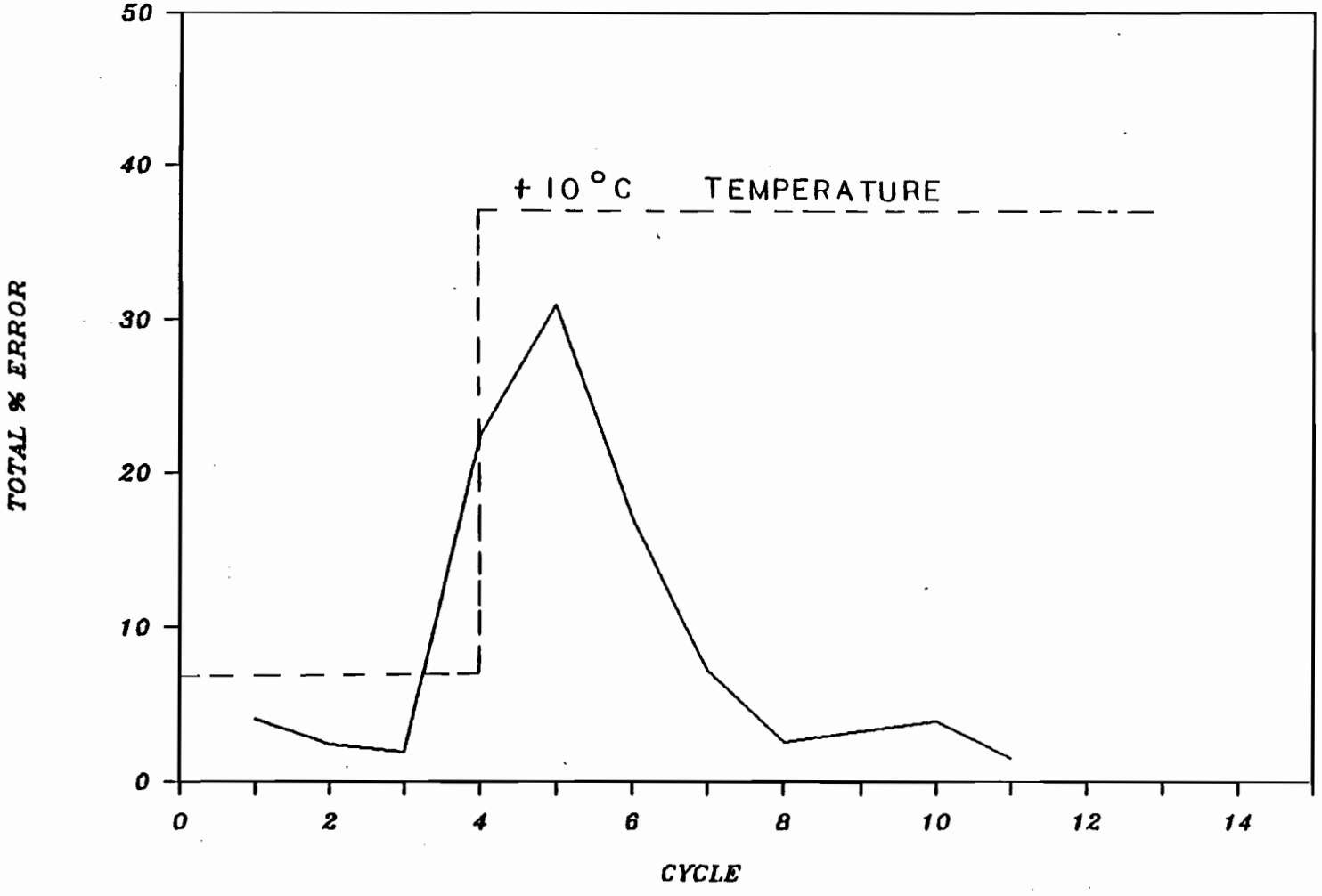

Figure 5.98: Control Action Response to Disturbance of +10°C, at Cycle 4.

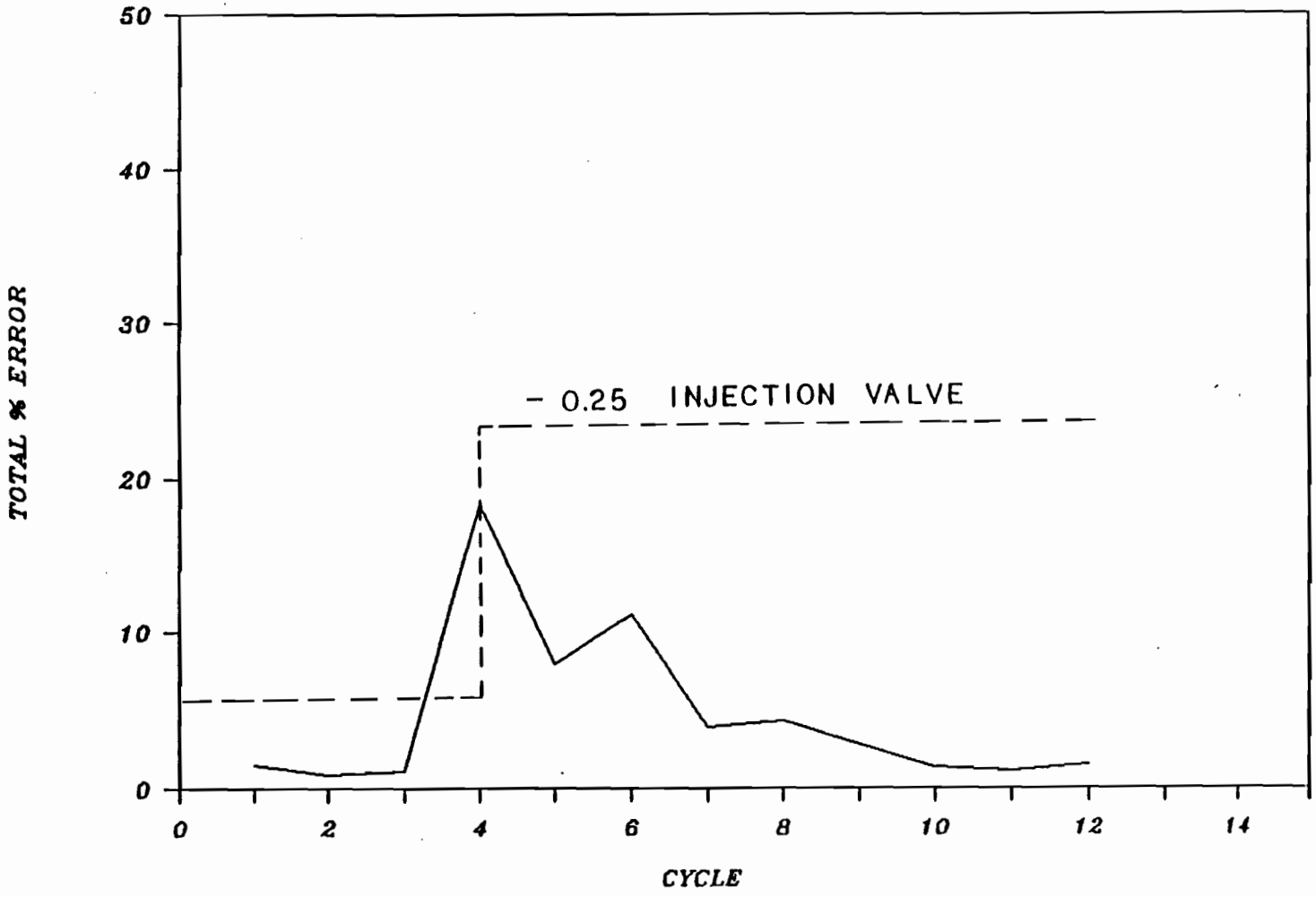

Figure 5.99: Control Action Response to Disturbance of -0.25 Injection Valve Setting, at Cycle 4.

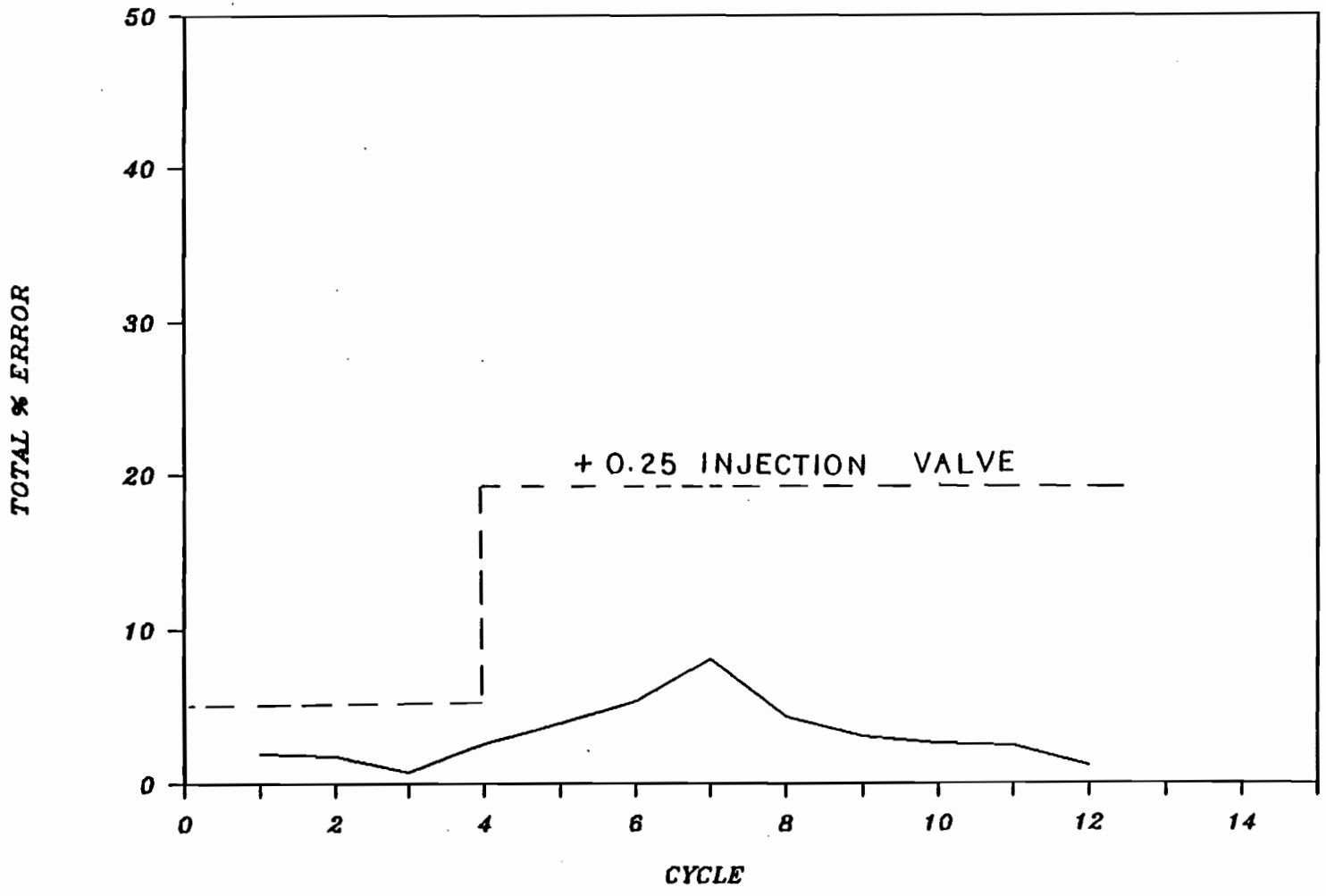

Figure 5.100: Control Action Response to Disturbance of +0.25 Injection Valve Setting, at Cycle 4.

probably attributable to system noise rather than to the injection rate increase.

5.2.2.5.5 RESIN A 20 % blend of LLDPE and RESIN A was introduced into the system at cycle number 4. The LLDPE had a melt index of 1.0 g/10 min and a density of 918 Kg/m^3. The response to the disturbance is shown in Figure 5.101. A number of cycles were required to rectify the disturbance, in this case. An oscillatory percent error response followed by eventual damping after 10 cycles, was observed.

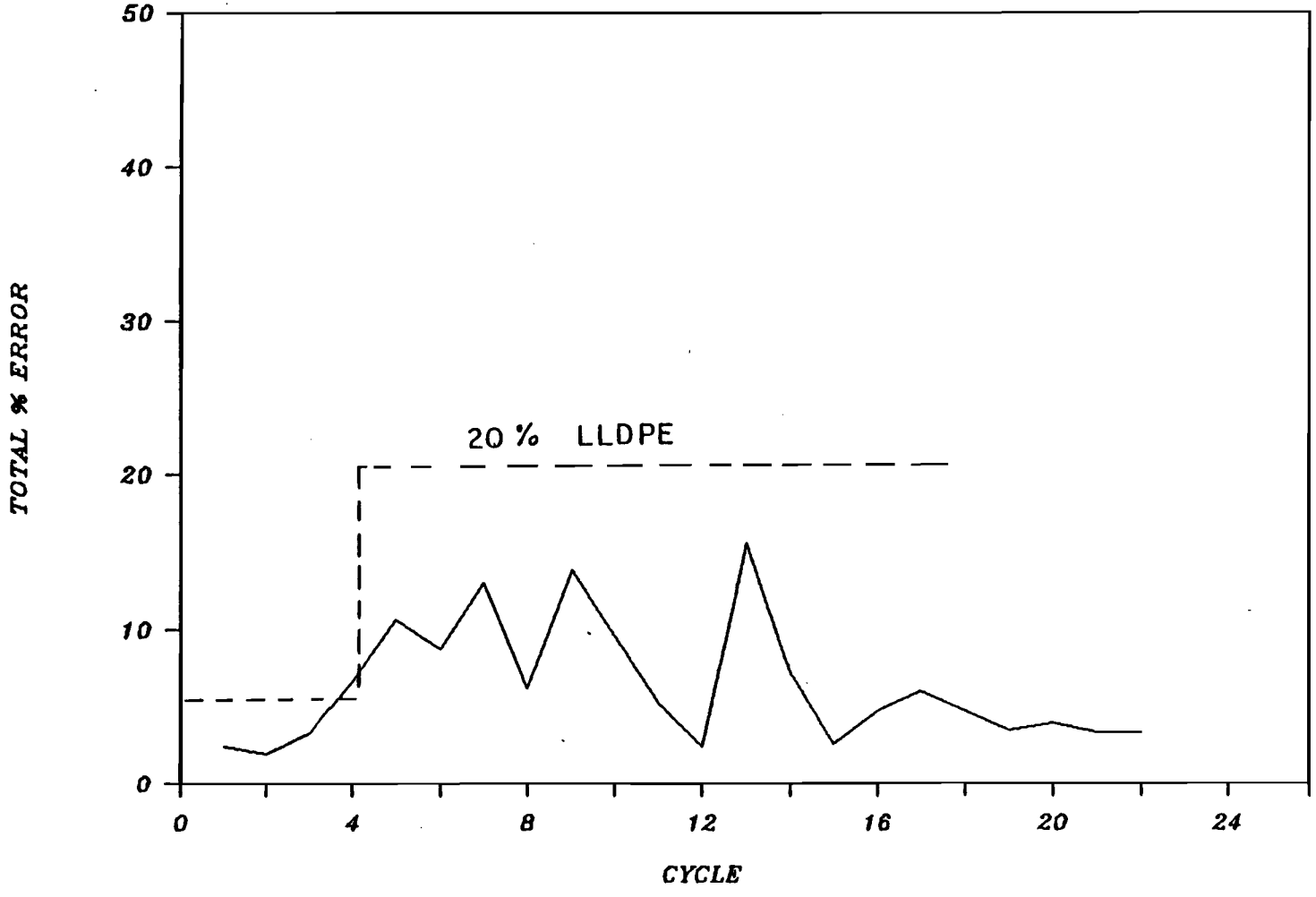

Figure 5.101: Control Action Response to Disturbance of 20 % LLDPE, at Cycle 4.

CHAPTER 6

CONCLUSIONS

6.1 CONTRIBUTION TO KNOWLEDGE

An on-line computerized non-contact parison thickness profile estimation technique has been developed and verified in conjunction with parison formation in extrusion blow molding. Control of various programmed parison thickness profile set points, as well the correction of unexpected disturbances entering the process, was achieved. The proposed closed loop control scheme provides significant improvement over the present commercially available open loop parison programmers.

6.1.1 SUMMARY OF FINDINGS

The parison thickness profile measurement utilized a video image processing scheme interfaced with a data acquisition system. The method incorporated relationships describing the relaxation of the polymer as well as optical relationships describing the field of view. The thickness profiles estimated by this technique compared well with thickness profile data obtained from the established pinch-off mold technique.

The response of the process to step changes in the gap was instantaneous, requiring only one or two transition segments.

The cycle-to-cycle system noise could be characterized by white noise.

The proposed measurement and control system was employed to control various forms of set point parison thickness profiles, such as constant, linear and oscillatory. Problems were encountered in controlling profiles with a high frequency changes in the thickness along the extrusion, and with profiles requiring gaps above or below the upper and lower gap limits, respectively. However, these were problems inherent with the blow molding machine and were not caused by the control strategy.

The proposed scheme was successful in obtaining control in the presence of unexpected disturbances entering the process, by utilizing an on-line adaptive control technique.

6.2 RECOMMENDATIONS

Several aspects can be investigated to further improve the thickness estimation approach.

The thickness resolution of the estimation scheme is ±0.05 mm. This limits the measurement of very thin parisons. Very thick parisons cause the assumption of Equation (4.58) to become invalid, thereby affecting the accuracy of the estimation technique. The resolutions of parison length and diameter measurements with the video camera are ±0.3 cm and ±0.1 cm, respectively. These levels of resolution directly affect the

thickness resolution. The relatively low resolution for length prevents the measurement of short parisons. Higher pixel resolution, attainable with a larger array and lower pixel spacing, results in improved length, diameter and thickness resolution. This would permit the measurement of short parison lengths and improve thickness measurement.

The total number of thickness measurements along the length of the parison is limited by the total number of possible gap changes during an extrusion. The servovalve responds at a rate of 20 times in a one second extrusion. This limits the number of controllable thickness segments to 20. A faster servovalve would allow for improved thickness control along the parison length and a smaller transition segment to the new gap. This causes an increase in the number of parison programming points.

In-cycle control was not considered as the extrusion is after the fact, that is, once a segment has been extruded, its thickness cannot be controlled by implementing changes in the extrusion process alone. However, some form of in-cycle control would be achievable if smaller segments are employed in conjunction with better video camera resolution and faster data processing facility.

The first and last segments along the length of the parison are ignored in this work, as their estimation is considered undependable. The relaxation assumptions of Chapter 4 and the high diameter gradient prevent an accurate thickness measurement in the first segment. The last segment comprises the unsteady

onset of extrusion flow, yielding an incomplete segment with unknown relaxation characteristics. However, both these segments are subsequently pinched by the mold in a typical blow molding process.

Long parison suspension times and resins with low melt strength introduce significant sag into the system, leading to the loss of dependability of the models developed in Chapter 4. Long suspension times also produce large temperature gradients in the parison. A thickness estimation model that would account for the effect of sag would be useful in the case of long parison extrusion times and resins with low melt strength.

Segments with variable thickness along the perimeter were not considered. A model that accounts for this ovalized tooling would be of use in complex shape parisons, such as those employed in the production of automobile parts.

An inner control loop, controlling the total parison length by manipulating the shot size, would also be useful. The addition of a servovalve and modification of the hydraulic and electrical circuitry of the blow molding machine would be required for this purpose.

REFERENCES

1. J. Agranoff, Ed. Modern Plastics Encyclopedia, 65, McGraw-Hill, NY (1988).
2. M.E. Ryan, Advances in Transport Processes, Eds. M.R. Kamal, R.A. Mashelkar and A.S. Mujumdar, 6, In press 1989
3. P. Junk, SPE Technical Papers, 34, 775 (1988).
4. Z. Tadmor and C.Gogos, " Principles of Polymer Processing ", J. Wiley and Sons, NY (1979).
5. GE Bulletin, Canadian Plastics, 12, 17 (1986).
6. D. Kalyon, PhD Thesis, McGill University (1981).
7. D.L. Peters and J.R. Rothman, Plastics Eng, 3, 59 (1985).
8. J. Higgins, SPE Technical Papers, 34, 763, (1988).
9. G.R. Smoluk, Modern Plastics, 2, 43, (1983).
10. T.L. Strojinc, SPE Technical Papers, 31, 890 (1985).
11. Trade Bulletin "Model 320 Microprogrammer", Hunkar Laboratories, Cincinnati, Ohio (1985).
12. Trade Bulletin "HACO VI", Barber-Colman Co., Rockford, Ill. (1985).
13. Trade Bulletin "Parison Programmer", Moog Inc., Aurora, NY (1984).
14. D.V. Voelz and G.A. Gleason, SPE Technical Papers, 31, 898 (1985).
15. S. Middleman, " Fundamentals of Polymer Processing ", McGraw-Hill, NY (1977).

16. J. Vlachopoulos, Reviews on the Deformation Behaviour of Materials, III, 4, 219 (1981).

17. G.R. Cotten, Rubber Chem. Tech., 54, 61 (1981).

18. G.R. Cotten, Rubber Chem. Tech., 52, 187 (1979).

19. M. Samara, Masters Thesis, McGill University (1985).

20. E.B. Bagley and H.J. Duffey, Trans. Soc. Rheol., 14, 545 (1970).

21. C.D. Han and M. Charles, Trans. Soc. Rheol., 14, 213 (1970).

22. C.D. Han, " Rheology in Polymer Processing ", Academic Press, N.Y. (1976).

23. L.L. Chapoy and S. Pedersen, Polym. Eng. Sci., 17, 724 (1977).

24. W. Graessley, S.D. Glasscock and R.L. Crawley, Trans. Soc. Rheol., 14, 519 (1970)

25. A.S. Anand and I.S. Bhardwaj, Rheol. Acta., 19, 614, (1980).

26. R. Racin and D.C. Bogue, Trans. Soc. Rheol., 23, 263 (1979)

27. F.P. LaMantia, A. Valenxa and D. Acierno, Rheol. Acta, 22, 308 (1983).

28. D. Romanini and G. Pezzin, Rheol. Acta, 21, 699 (1982).

29. N. Alle, F.E. Andersen and J. Lyngaae-Jorgensen, Rheol. Acta, 20, 222 (1981).

30. G. Pezzin, " Proc. Second World Congr. Chem. Eng. ", Montreal, 6, 273 (1981).

31. N. Orbey, PhD Thesis, McGill University (1984).

32. M. Fleissner, Angew. Makromol. Chem., 33, 75 (1973).

33. R.N. Shroff and M. Shida, SPE Technical Papers, 23, 285 (1977).

34. R.A. Mendelson and F.L. Finger, J. Appl. Polym. Sci., 19, 1061 (1975).

35. N. Sheptak and C. Beyer, SPE J., 21, 2, 190 (1965).

36. J. Vlachopoulos, M. Horie and S. Lidorikis, Trans. Soc. Rheol., 16, 669 (1972).

37. L. Utracki, Z. Bakerdjian and M.R. Kamal, J. Appl. Polym. Sci., 19, 481 (1975).

38. A. Garcia-Rejon, PhD Thesis, McGill University (1980).

39. Trade Bulletin "Extrusion Blow Molding Resins", Dupont Plastics, Kingston, Ont.

40. N. Wilson, M. Bentley and B. Morgan, SPE J., 26, 2, 34 (1970).

41. E. Henze and W. Wu, Polym. Eng. Sci., 13, 2,153 (1973).

42. K. Chao and W. Wu, SPE J., 27, 7, 37 (1971).

43. Verpackungs Rundschau, 24, 4, 345, (1973).

44. K. Blower and N. Standish, Polym. Eng. Sci., 13, 3, 222 (1973).

45. G. Ajroldi, Polym. Eng. Sci., 18, 10, 743 (1978).

46. F. Cogswell, Plast. and Polym., 38, 391 (1970).

47. F. Cogswell, P. Webb, J. Weeks, S. Maskell and P. Rice, Plasts. and Polym., 39, 340 (1971).

48. D. Kalyon, V. Tan and M.R. Kamal, Polym. Eng. Sci., 20, 773, (1980).

49. M.R. Kamal, V. Tan and D. Kalyon, Polym. Eng. Sci., 21, 331

(1981).

50. D. Kalyon and M.R. Kamal, Polym. Eng. Sci., 26, 508 (1986).

51. A. Dutta and M.E. Ryan, J. Non-Newt. Fluid Mech., 10, 235 (1982).

52. S. Basu and C.Rauwendaal, SPE Technical Papers, 28, 720 (1982).

53. T.A. Huang and G.A. Campbell, Adv. Polym. Tech., 5 , 3, 181 (1985).

54. J.M. Dealy, " Rheometers for Molten Polymers ", Van Nostrand Reinhold Co., NY (1982).

55. J. Leblanc, Rheol. Acta, 20, 95, (1981).

56. "Trade Bulletin", C.W. Brabender Instruments, Inc., NJ

57. "Trade Bulletin", Optikon Corp. Ltd. , Waterloo,Ont.

58. "Trade Bulletin", Metrelic Sarl., Paris France.

59. W.I. Patterson and T. deKerf, SPE Technical Papers, 24, 483, (1978).

60. D. Dennis-Germuska, P.A.Taylor and J.D. Wright, Cdn. J. Chem. Eng., 62, 790 (1984).

61. J.F. Stevenson, SPE Technical Papers, 30, 93 (1984).

62. J.F. Stevenson, L.J. Lee and R.M. Griffith, SPE Technical Papers, 31, 118, (1985).

63. J. Sneller, Modern Plastics, 3, 48, (1983).

64. S. Tormola, SPE Technical Papers, 30, 909 (1984).

65. E. Galli, Plastics Mach. and Equip., 11, 17, (1983).

66. K.W. Buchscheidt, Ettligen and D. Walter, Plasts. Proc. Ind.

and Prod. Eng., 28 (1988).

67. "Capillary Rheometer Model 3211 Operation Manual", Instron, Canton, Ma.

68. "System Four Operation Manual", Rheometrics, Union, NJ.

69. "Extensional RER 9000 Operation Manual", Rheometrics, Union, NJ

70. P.W. Fry, SPIE, "Industrial Applications of Solid State Image Scanners", 145, 2 (1978).

71. "XC-38 Camera Module Operation Manual", Sony, NJ.

72. F. Baxes, "Digital Image Processing", Prentice-Hall, NJ (1984).

73. H.E. Schroeder, "EG & G Reticon Trade Bulletin", Sunnyvale, Calif.

74. R.Nevatia, "Machine Perception", Prentice-Hall, NJ, (1982).

75. "PIP 1024 Operation Manual", Matrox Inc., Montreal, Que.

76. "Impco B-13 Operation Manual", Ingersoll Rand Plastics Machinery, NH.

77. "Trade Bulletin" Dynisco Pressure Transducers, Westwood, Mass.

78. "Trade Bulletin", Trans-Tek Series 100 Linear Velocity Transducers, Ellington, Conn.

79. "Trade Bulletin" Data Translation DT2801 Series Data Acquisition Boards, Malborough, Mass.

80. R. Resnick and D. Halliday, "Physics-Combined Edition", J. Wiley and Sons, NY (1966).

81. G. Stephanopoulos, " Chemical Process Control", Prentice-

Hall, Englewood Cliffs, NJ (1984).

82. G. Box and G. Jenkins, " Time Series Analysis-Forecasting and Control", Holden Day, Oakland, (1972).

83. "System Identification Toolbox Instructions", PC MATLAB, Sherborn, Ma., (1986).

84. Ding T. and E. Garmine, Applied Optics, 22, (20) 3177 (1983).

NOMENCLATURE

A	Side of triangle in Figure 4.7
a_0	Coefficient of Equation (4.29)
a_1	Coefficient of Equation (4.39)
a_2	Coefficient of Equation (4.47)
a_3	Coefficient of Equation (4.56)
B	Swell
B_1	Diameter swell
B_{12}	Swell factor defined in Equation (4.64)
B_2	Thickness swell
B_3	Weight swell
B_C	Capillary swell
b_0	Coefficient of Equation (4.29)
b_1	Coefficient of Equation (4.39)
b_2	Coefficient of Equation (4.47)
b_3	Coefficient of Equation (4.56)
C	Noise transfer function of Equation (5.3)
c	Constant in Equation (A2.1)
c_0	Coefficient of Equation (4.29)
c_1	Coefficient of Equation (4.39)
c_2	Coefficient of Equation (4.47)
c_3	Coefficient of Equation (4.56)
D	Diameter
D_1	Side of triangle of Figure 4.8
D_2	Side of triangle of Figure 4.8

D_C	Capillary diameter
D_E	Capillary extrudate diameter
D_i	Die inner diameter
D_{max}	Droop effect parison bottom maximum diameter
D_o	Die outer diameter (3.3 cm)
D_P	Parison outer diameter
d_1	Coefficient of Equation (4.39)
d_2	Coefficient of Equation (4.47)
d_3	Coefficient of Equation (4.56)
E	Pixel element spacing
e	Error deviation from set point
e_1	Coefficient of Equation (4.39)
F	Trigonometric factor in Equation (4.13)
F'	Trigonometric factor of Equation (4.34)
f	Camera lens focal length (1.6 cm)
f_1	Coefficient of Equation (4.39)
G	Transfer function of Equation (5.1)
G'	Storage modulus
G''	Loss modulus
G_1	Controller transfer function
G_2	Process transfer function
G_3	Measurement transfer function
G_4	Model transfer function
G_5	Controller adjustment transfer function
G_6	Noise model transfer function
g	Acceleration due to gravity

H	Process transfer function of Equation (5.2)
h	Parison thickness
h_o	Die gap
h_{SP}	Thickness set point
I	Image dimension
I_1	Side of triangle in Figure 4.5
I_2	Side of triangle in Figure 4.5
i	Array image height
i_v	Injection Valve Setting
J	Noise transfer function of Equation (5.3)
J_E	Steady state shear compliance
K	Constant in Equation (A2.1)
L	Parison length
L'	Mirror length of parison droop effect
L_D	Total parison length with a one second delay after extrusion end
L_E	Total parison length at end of extrusion
L_S	Length increase due to sag
M	Demagnification
M_N	Number average molecular weight
M_W	Weight average molecular weight
M_W/M_N	Polydispersity
M_Z	Z average molecular weight
m	Controller gain
mag	Magnitude of step change
N	Number of illuminated pixels

N_1	First normal stress difference
N_t	Total number of illuminated pixels in the length direction
n	White noise
O	Distance from object to lens
P	Axis dimension
P'	Axis dimension on mirror
P''	Side of triangle in Figure 4.4
P_1	Side of triangle in Figure 4.4
P_2	Side of triangle in Figure 4.4
P_E	Percent error set point deviation of controller action
R	Array resolution
R'	Distance from die to mirror
S	Side of triangle in Figure 4.4
S_R	Recoverable strain
T	Side of triangle in Figure 4.7
t	Time
t_s	Parison segment suspension time
U	Process transfer function of Equation (5.2)
V	Time weighted transition average of ϵ, B_{12} or h_o
V'	Distance in Figure 4.2 (120 cm)
V_1	Value of ϵ, B_{12} or h_o at initial gap of step
V_2	Value of ϵ, B_{12} or h_o at final gap of step
W	Segment weight
W'	Distance in Figure 4.2 (20 cm)

w	Pinch-off segment width
X	Pixel scan location
X'	Input variable to transfer function in Equation (5.1)
Y'	Output response of transfer function in Equation (5.1)

GREEK LETTERS

α	Noise factor of Equation (4.69)
β	Curl inward factor of Equation (4.47)
Γ^+	Growth extensional viscosity
δ	Relaxation time
ϵ	Relaxation time defined in Equation (4.63)
θ	Mirror angle of tilt with vertical
ρ	Melt density (0.76 g/cc)
ρ_s	Solid extrudate density (0.955 g/cc)
Σ	Summation
τ	Applied stress
ϕ	Angle of reflection

ELEMENTS

a	Cycle reponse delay
i	Equiweigth parison segment
j	Control cycle
k	Lags in Equations (5.2) and (5.3)

l	Equilength parison segment
q	Time series backward operator
t	Time

SUBSCRIPTS

B	Relating to the bottom of Figure 4.9
b	Relating to the droop effect
C	Relating to capillary flow
c	Individual distances to camera lens
k	Individual transfer function
o	Instantaneous value at the die gap
s	Individual diameter or thickness swell
T	Relating to the top of Figure 4.9
x	Diameter-x axis
y	Length-y axis
∞	Long time equilibrium value

APPENDIX 1

SOFTWARE

Software has been written for the following aspects of this work :

1. Field of View Alignment - CONT
2. Parison Length Versus Time During the Extrusion - LEN
3. Data Acquisition - SAMP
4. Camera Pinch-off Mold Thickness Comparison - PINCH
5. Swell Factor Determination (ϵ,B_{12}) - SWELL
6. Thickness Dynamic Responses to a Step During Extrusion - DYN
7. PRBS Sequence Generation - PSEUDO
8. Control Experiments - CONTROL
9. Simulation - SIMUL

The software for the experimental sets is not presented, for sake of brevity, but it is available from the author upon request. All programs are written in FORTRAN. FORTRAN was chosen because of its speed, simplicity and compatiblity with the vision, data acquisition and clock software systems.

APPENDIX 2:

THICKNESS MEASUREMENT ALTERNATIVES

There are three basic requirements for the thickness measurement technique needed in this system.

(1) The measurement must be on-line and non-contact and must supply the necessary feedback signal at a rate adequate for enacting closed loop control on the process.
(2) The sensor chosen must be easily adaptable to the extrusion blow molding process, without interfering with the cycle.
(3) The sensor chosen must be affordable.

Several sensors for dimension measurement are available. They can be divided into various categories, depending on the mode of operation.

A.2.1 OPTICAL TECHNIQUES

A.2.1.1 PHOTOGRAPHIC METHODS Photographic techniques for parison dimension measurement employ a 35 mm camera equipped with a motor drive mounted on a tripod. Photographs are taken at predetermined time intervals to obtain the parison dimensions as a function of time. The negatives of the pictures are analyzed with a microscope to obtain the measurement. A ruler is placed

next to the die, so that the dimensions can be obtained as a function of distance from the die. A parison retains its transparency, if it is extruded into an oil bath of the same temperature. The parison thickness can be measured in this way (31). This method is not applicable for this work, as the measurement is not on-line and no feedback signal is available.

A.2.1.2 SHADOW CASTING Diameter and length measurements can be obtained by the shadow casting technique. An illumination source is projected onto the parison and the shadow cast is demagnified onto a linear photodiode array. Another alternative would be to illuminate the parison and maintain a matte black background, as was effected in this work. This alternative is preferable since it is not necessary to incorporate collimated light. Edge detecting, counting the number of pixels and multiplying by the corresponding expansion factor allows for length and diameter measurements. The measurement allows a feedback, since the sensor is interfaced to a computer (19).

Thickness measurements cannot be made directly with this method since molten polyethylene is opaque in air, preventing the inner surface from being visible. Indirect thickness measurement utilizing this mode is employed in this work.

A.2.1.3 LASER REFRACTION PATTERNS Ding and Garmine (84) employ laser beam deflection, caused by a thin film, to simultaneously determine the refractive index and thickness of the film.

Aluminum and silicon oxide films on silicon substrate films were utilized. The measurable thickness range was less than 0.0025 mm.

The presence of an object interrupts the path of a laser beam. The amount of the deflection is measured and detected with a linear photodiode array. The degree of the interference is related to the thickness and the refractive index of the material.

This method is not applicable to polymer melts, because the parison is too thick, signal attenuation or scattering will occur, and polymers tend to have a varying refractive index dependent on the direction and stress applied.

A.2.2 ABSORBANCE TECHNIQUES

A.2.2.1 NUCLEAR BACKSCATTER Sneller (63) proposes using a beta backscatter gage for film thickness measurement. Gamma and/or beta rays are emmited by a sensor and travel to a polymer film. The amount of radiation scattered back to the sensor is a function of the polymer thickness.

The sensor must be positioned in very close proximity to the melt. Therefore, it is essential to know the exact location of parison extrusion. This is inconceivable, as a result of parison sway and swell from one point to the next. The gages would have to be removed during the cycle so as to not interfere with mold closing. This would entail elaborate changes to the hydraulic

system of the blow molding machine.

The speed of response is not fast enough for processing and closed loop control purposes. Cost is also a problem with this alternative as the list price of the gages is approximately $50000. An element of hazard also exists because of the exposure to nuclear radiation.

A.2.2.2 INFRA-RED ABSORBANCE Tormola (64) discusses the measurement of bottle thicknesses by employing infra-red gages. As infra-red passes through an object, it is absorbed as a function of layer thickness and material properties. The infra-red radiation output by the hot parison will tend to swamp the gage, making measurement impossible. The gage would also have to be positioned in close proximity to the parison making removal during the cycle a necessity.

A.2.2.3 CAPACITANCE TECHNIQUES The change in capacitance induced by the presence of an object between two charged plates can be used to determine the object's thickness (Electromatic components). The overall dielectric constant is composed of a intermediate value between that for air and molten polymer. The value of the plate separation should be of the same order of magnitude as the value of the measured thickness. This value of plate separation is too narrow for use in parison formation. The positioning of the parison would have to be known apriori so as to locate the charged plates accordingly.

A.2.3 SIGNAL REFLECTION

Signal reflection determination of thickness involves simultaneous measurement of parison inner and outer diameter. Therefore, sensors would have to be placed on the parison interior and exterior.

A.2.3.1 ULTRASONIC TECHNIQUES Ultrasonic techniques (66) measure material thicknesses by evaluating the time required for a sonic wave, that is sent through a medium, to be reflected at the air interface and return to the sensor. A piezoelectric transducer is used as the sensor by electronically switching the two functions. A liquid couplant in conjunction with a flush contact between the sensor and the surface is required for measurement. The reason for this is that sound waves tend to attenuate greatly in any air gap. Attenuation in air, prevents utilizing this alternative as a measurement technique.

A.2.3.2 RADAR Radar (Automation Concepts) involves sending a signal, at the speed of light, to an object. The signal reflects and returns to the sensor. However the time required for this reflection is too miniscule in the application of parison formation to be detected by present technology.

A.2.3.3 EDDY CURRENTS An electromagnetic field generated by an oscillator circuit exists in the area of the object to be

detected (Omron Electronics). An eddy current is set up in the object, upon entering of the object into the electromagnetic field. This current is related to the distance from the sensor to the object. However, eddy currents are limited to conductors. Therefore, they are not applicable for polymer melts.

A.2.3.4 PNEUMATIC This method involves sending a pneumatic jet onto the parison and measuring the recoil deflection of the jet (61,62). This device would have to be removed during the blow molding cycle. Also, there is not enough space inside the parison for determining the inner diameter.

A.2.4 INDIRECT TECHNIQUES

A.2.4.1 THICKNESS MEASUREMENT FROM DIAMETER MEASUREMENT Orbey (31) demonstrated that thickness swell could be related to diameter swell by

$$B_2 = KB_1^C \qquad (A2.1)$$

where K and c are empirical constants. However, this technique is highly empirical and dependent on the resin. Pinch-off mold calibrations would have to be performed at various shear rates, temperatures and die gaps. The logarithmic type relationship also limits the accuracy of the measurement.

A.2.4.2 FLOW METER PUMP The thickness profile of a parison can be determined indirectly by the use of a flow metering pump. This pump fits directly into the die of the blow molding machine. The pump measures exact volumes of polymer melt flowing through in specific time intervals.

Further information on the operation of such pumps is unavailable. However the technique likely employs parison length and diameter measurements to obtain a value for thickness.

APPENDIX 3

VALIDATION OF NEGLIGIBLE SAG

Garcia-Rejon (38) developed a model for predicting the effect of sag on an extruded parison. The assumption of constant growth extensional viscosity yields the following relationship for the length increase as a result of sag, during the extrusion and the mold close time.

$$L_S = L_E \left\{ \frac{\Gamma^+}{\Gamma^+ - \rho g L_E t_s} - 1 \right\} \qquad (A.3.1)$$

The assumption of constant growth extensional viscosity is acceptable since only an indication of the effect of sag is being sought. Growth extensional viscosity values are obtained from a Rheometrics RER 9000 extensional Rheometer (74). The total length of the parison is represented by L_E, the length increase due to sag by L_S, the growth extensional viscosity by Γ^+, the melt density by ρ and the suspension time by t_S.

The effect of the sag would then be determined from the deviation of L_S from L_E. Substitution into the equation yields a value of less than a 2 % effect of sag, for a typical one second extrusion of Resin A, with a length of 30 cm at extrusion end.

APPENDIX 4

TRANSDUCER-DATA ACQUISITION BOARD INTERFACING DIAGRAMS

The interface of the computer data acquisition system to the extrusion blow molding machine was designed as part of this work, as mentioned in Chapter 3. The analog to digital interface is presented in Figure A4.1. The digital to analog interface is shown in Figure A4.2.

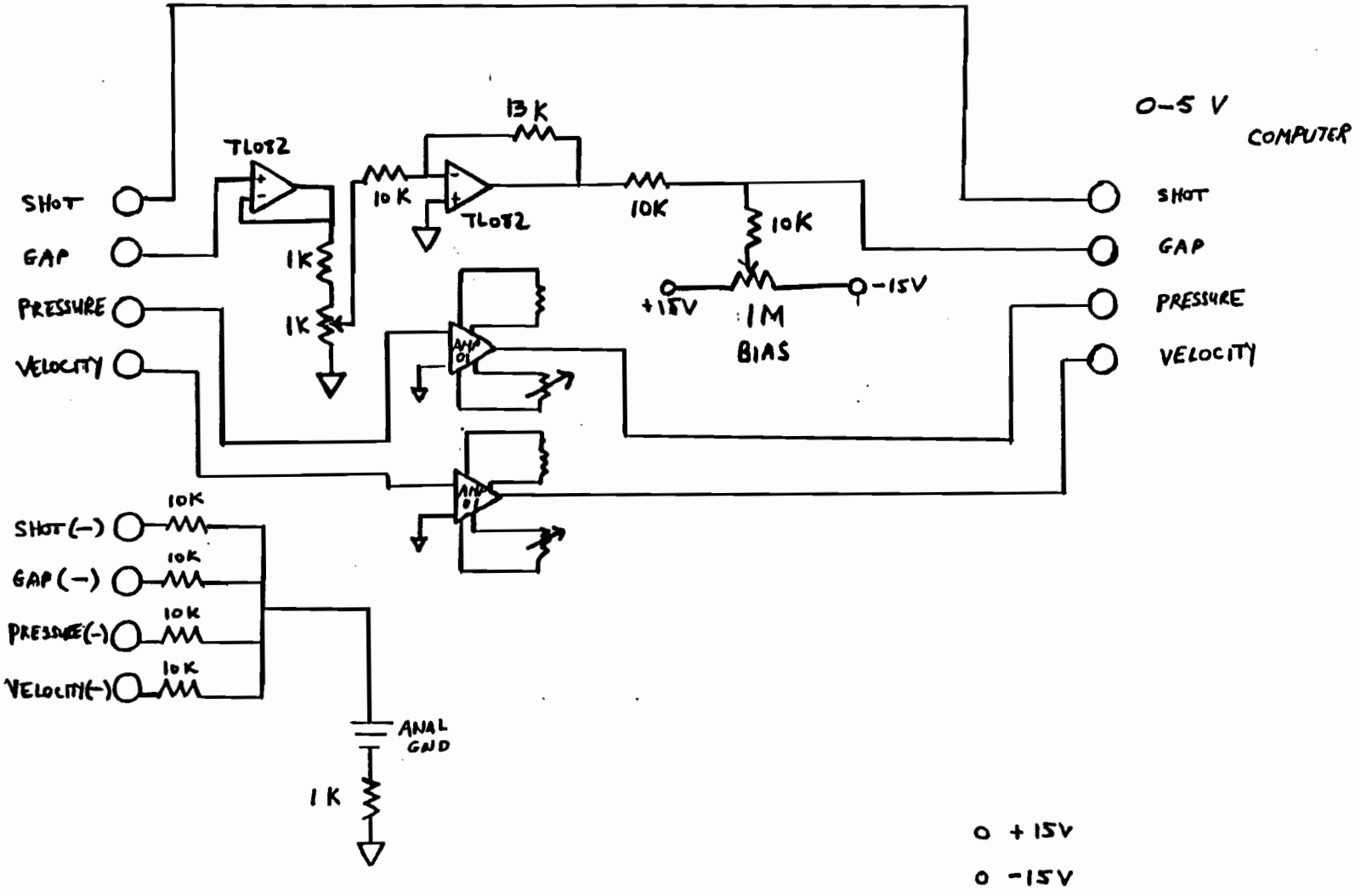

Figure A4.1: Analog to Digital Interface of the Blow Molding Machine to the Computer.

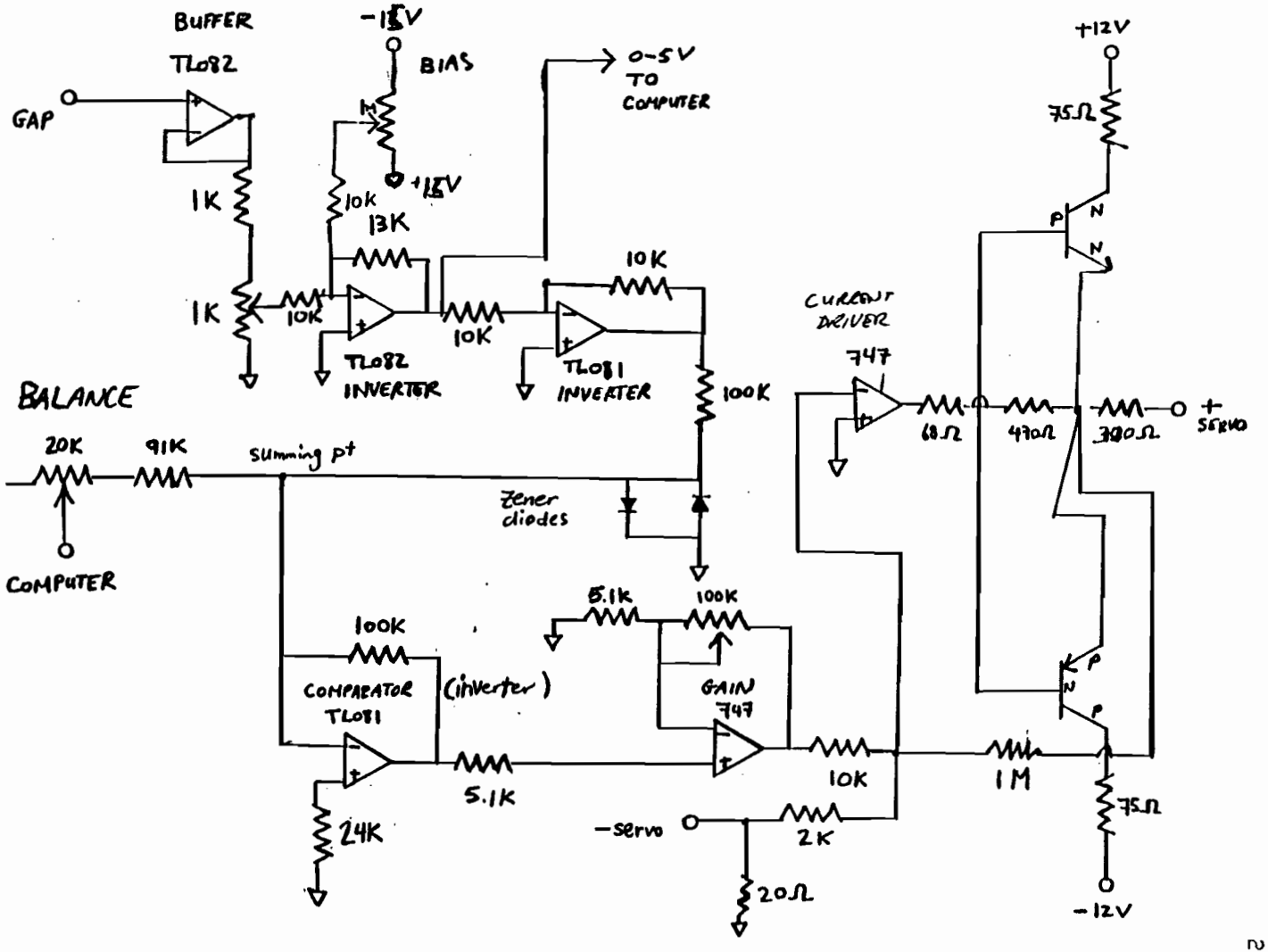

Figure A4.2: Digital to Analog Interface of the Blow Molding Machine to the Computer.

APPENDIX 5

CONTROL SIMULATION

A better alternative than the control scheme chosen in Section 5.2.2.1 would have been to determine the gain as a function of the process parameters. These process parameters include magnitude, direction and location of step along the profile, melt temperature, shot size and injection valve setting. A simulation, employing this approach, is described in this chapter.

The control simulation was performed in the software SIMUL. The thickness profile, for a simulation based on Resin A, was estimated by employing the following equations. The thickness was obtained, for segment locations i = 2 to 6, from

$$h = p_1(3.6h_o + 0.1)\exp[i/(p_2(14.8h_o - 40))] \qquad (A5.1)$$

The thickness for segments 7 to 14 was obtained from

$$h = 2.7p_3h_o \qquad (A5.2)$$

where the factors p_1, p_2 and p_3 are unity for an extrusion at a melt temperature of 200°C and an injection valve setting 1.25 and empirically fit for other conditions. These two equations are obtained by fitting the experimental data of Section 5.2.1.2.1.

The relationship between gain and the process parameters was obtained by fitting the data of Section 5.2.1.2. Several forms of the final equation were proposed. The equation with the best fit, determined by the highest correlation coefficient (0.96), was found to be

$$m(i) = -1.08i_v - 0.50i + 0.025i^2 + 8.48mag(i) - 1.07i_v mag(i) - 0.247imag(i) \quad (A5.3)$$

where the gains are m(i,j), the injection valve setting is i_v and the magnitude of the step change, mag(i), is

$$mag(i) = h_o(i) - h_o(i+i) \quad (A5.4)$$

The melt temperature and shot size were found to have little effect on the gain.

The control then follows the form described in Chapter 5, with the exception that the gains were obtained from Equation A5.3.

A5.1 PROGRAMMED SET POINTS

Five programmed set point profiles were evaluated in the simulation. These included three that were studied previously in the work; a constant thickness set point profile in Figure A5.1, a linear declining set point profile in Figure A5.2 and an

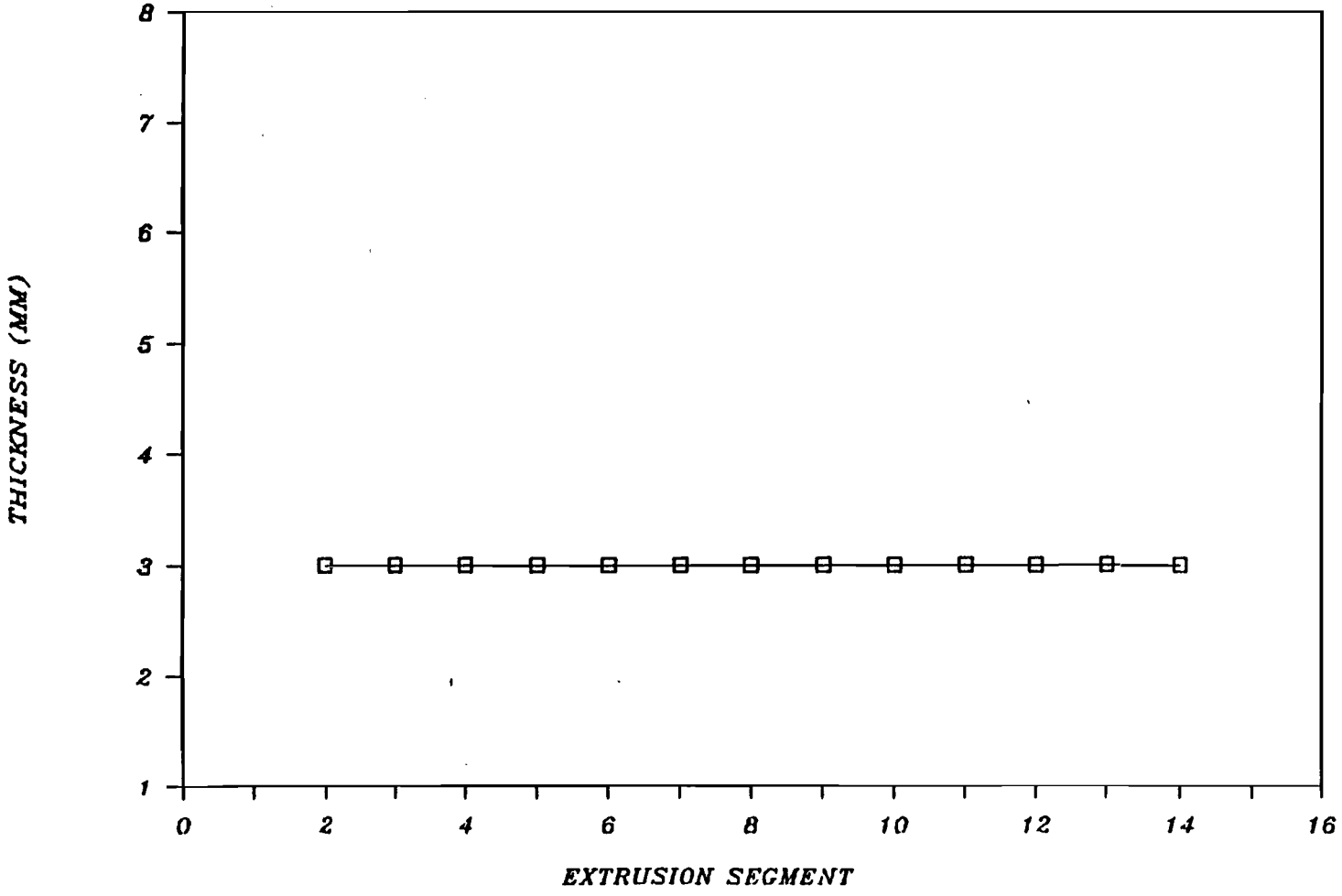

Figure A5.1: Simulation of On-Line Control of Constant Thickness Set Point Profile of 3 mm.

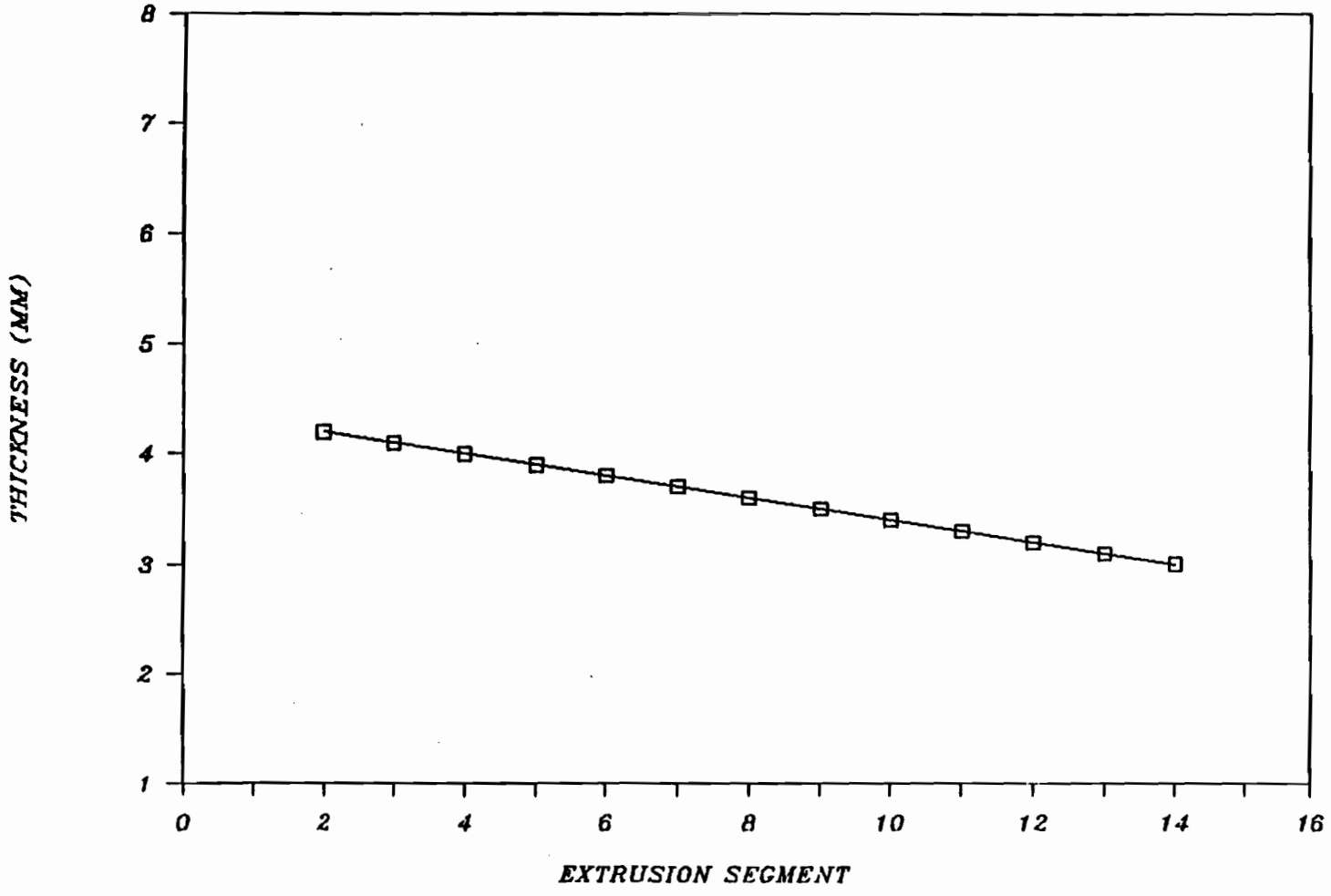

Figure A5.2: Simulation of On-Line Control of Linear Declining Set Point Profile.

oscillating set point profile in Figure A5.3. Two new set points were also considered; an inverted-V staircase set point profile in Figure A5.4 and a wave set point profile in Figure A5.5. The set point profiles are represented by the solid lines and the simulation results are depicted by the data points.

The control is excellent and stable for all these cases. This is not unexpected as a simulation is different from actual processing conditions. The percent error was reduced to acceptable limits within three cycles.

A5.2 DISTURBANCE CORRECTION

Two inputted disturbances were considered; a melt temperature drop of 10°C (Figure A5.6) and an injection valve setting drop of 0.50 (Figure A5.7). The disturbances were inputted at cycle number 4. The percent error is reduced to acceptable limits within two cycles.

The factors p_1, p_2 and p_3 in Equations A5.1 and A5.2 changed accordingly for each of these cases, and were determined from constant gap extrusion data in Section 5.1.4.2. In the case of the first disturbance, (-10°C), p_1 = 1.05, p_2 = 0.70 and p_3 = 0.98. The second disturbance (-0.50 injection valve setting) values are p_1 = 1.18, p_2 = 0.79 and p_3 = 1.06.

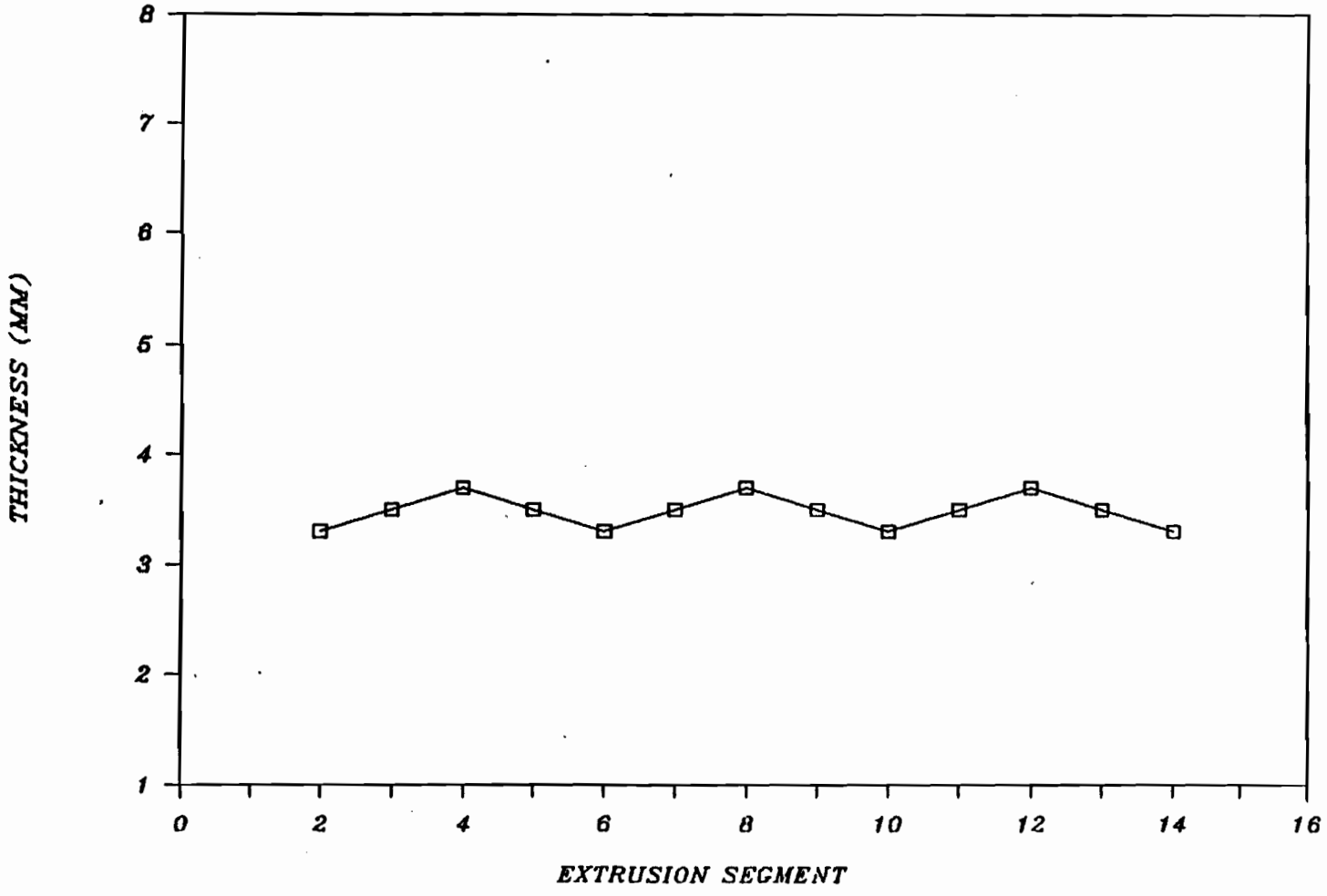

Figure A5.3: Simulation of On-Line Control of Medium Frequency Oscillating Set Point Profile.

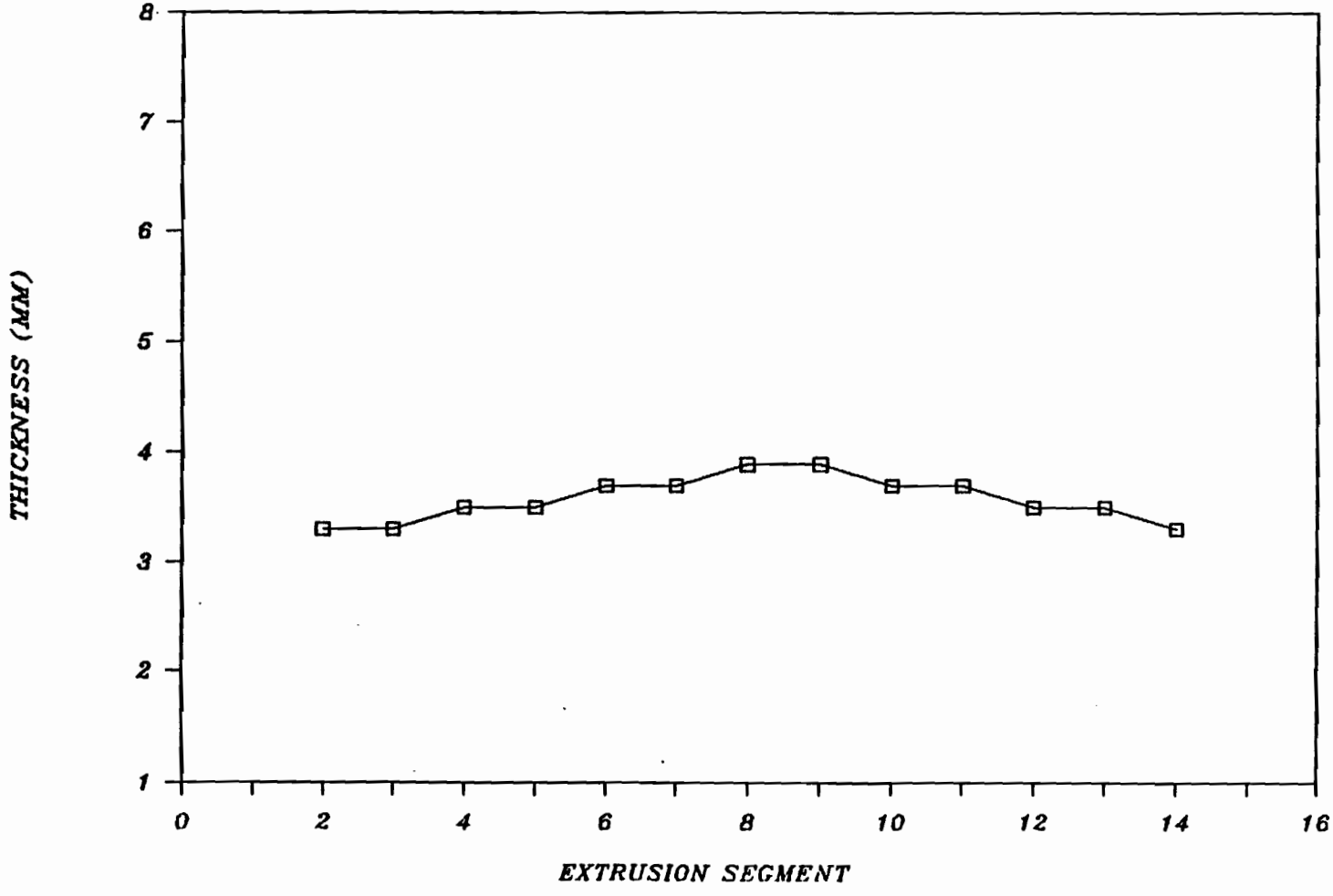

Figure A5.4: Simulation of On-Line Control of Inverted V Staircase Set Point Profile.

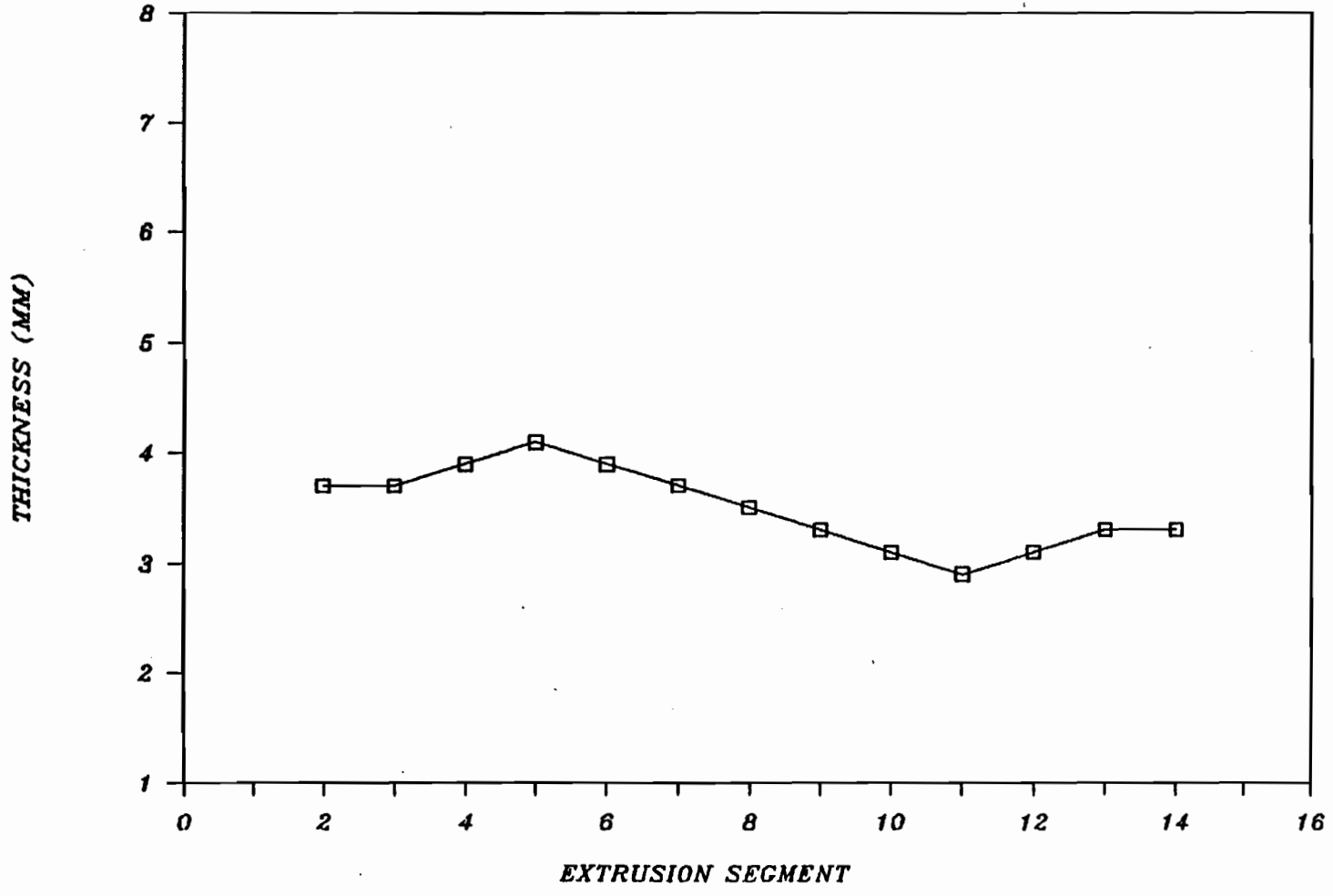

Figure A5.5: Simulation of On-Line Control of Wave Set Point Profile.

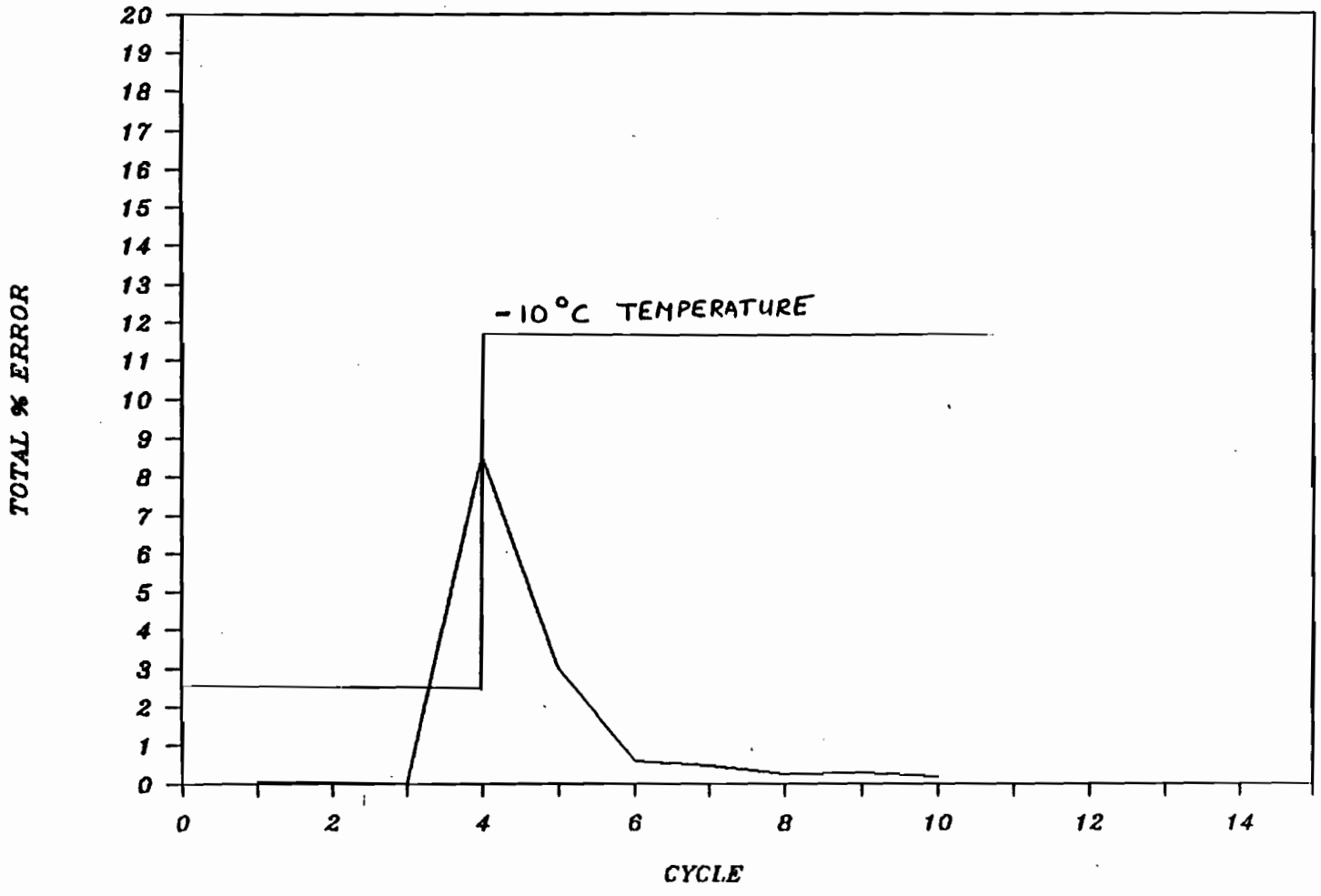

Figure A5.6: Simulation of Control Action Response, to Disturbance of -10°C, at Cycle 4.

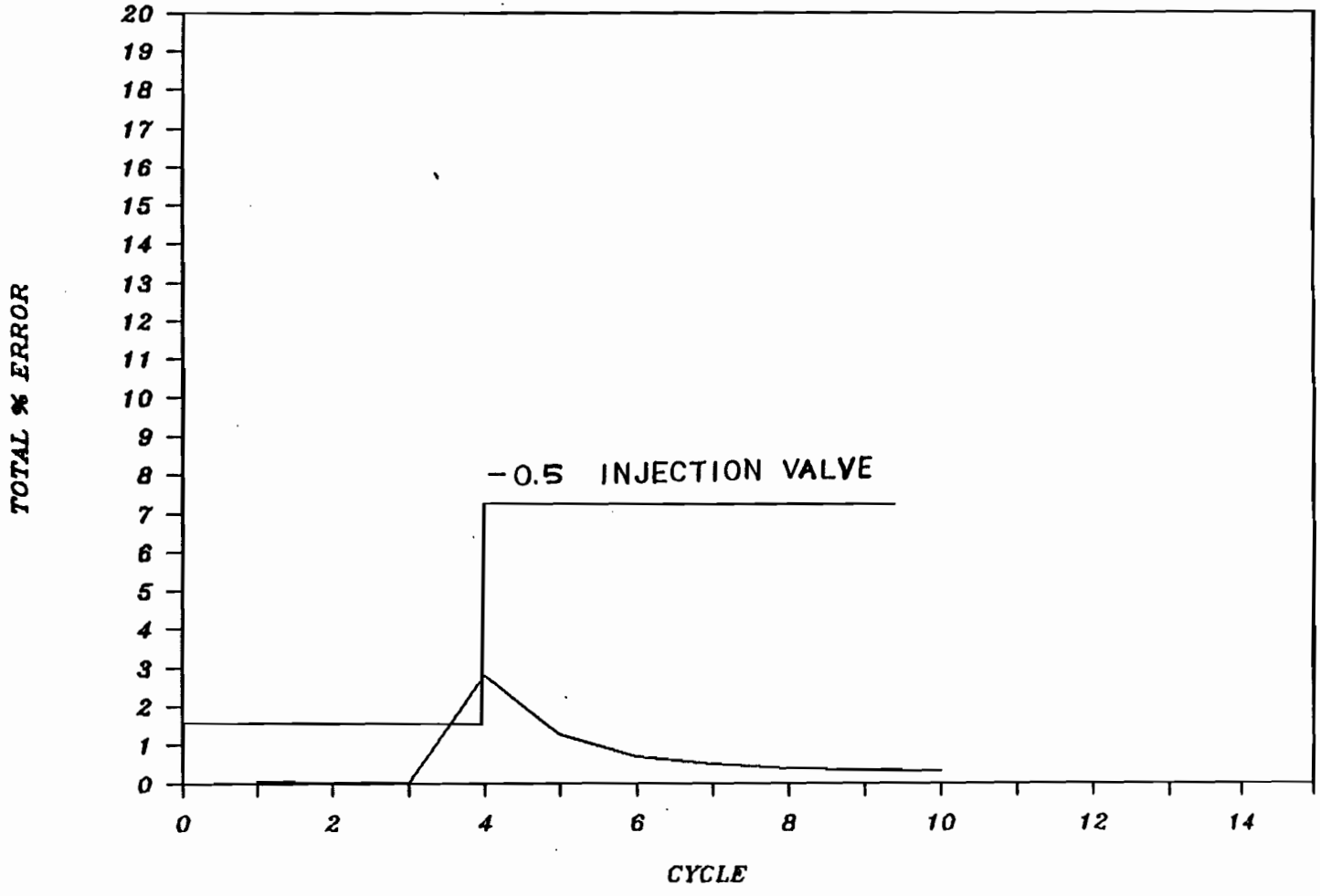

Figure A5.7: Simulation of Control Action Response to Disturbance of -0.50 Injection Valve Setting, at Cycle 4.